The functions of Beaten path II and Sidestep IV in the migration and differentiation of *Drosophila* longitudinal visceral muscle precursor cells

Inaugural-Dissertation

zur Erlangung des Doktorgrades
der Mathematisch-Naturwissenschaftlichen Fakultät
der Heinrich-Heine-Universität Düsseldorf

vorgelegt von

Na Huang

aus Shimian

Düsseldorf, 10/2024

aus dem Institut für Funktionelle Zellmorphologie
der Heinrich-Heine-Universität Düsseldorf

Gedruckt mit der Genehmigung
der Mathematisch-Naturwissenschaftlichen Fakultät
der Heinrich-Heine-Universität Düsseldorf

Referent: Prof. Dr. Hermann Aberle
Korreferentin: Prof. Dr. Christine R. Rose

Tag der mündlichen Prüfung: 03/12/2024

Abstract

The proper formation of tissues and organs relies on precisely regulated cell migration and differentiation events. In *Drosophila* embryos, the development of the midgut visceral musculature requires coordinated migrations from the caudal and trunk visceral mesoderm cells to form longitudinal and circular visceral muscles. This thesis focused on the migration and differentiation processes of the caudal visceral mesoderm (CVM) and the CVM-derived longitudinal visceral muscle precursor (LVMP) cells. It is the first to reveal that Beaten path II (Beat II) and Sidestep IV (Side IV) exert critical roles in these processes.

Both Beat II and Side IV belong to the *Drosophila* immunoglobulin superfamily. The Beat family contains fourteen members, most prominently expressed in subsets of neurons in the central nervous system. The Side family includes eight transmembrane proteins, which are dynamically expressed in neurons and specific peripheral tissues. Beat and Side family members often function as ligand-receptor pairs to facilitate neurogenesis. It has been demonstrated that Beat Ia-expressing motor axons follow the Side-expressing cellular substrates to reach their target areas; expression of Side II and Beat VI in pre- and postsynaptic partners promotes synaptic specificity and inhibits miswiring.

Notably, Beat II proteins (Beat IIa and Beat IIb) are found not only in neurons but also in migrating CVM and LVMP cells. At the same time, Side IV is present in the trunk visceral mesoderm (TVM), which serves as the migration substrate for the CVM and LVMP cells. Similar migration defects are present in both the *beat II* and *side IV* mutants, characterized as irregular migration patterns combined with abnormal cell morphologies and distributions. CVM and LVMP cells that have lost contact with the TVM show signs of apoptosis. The midgut contains areas lacking longitudinal muscles at the end of embryogenesis, resulting in fewer longitudinal muscle fibers at the larval stage. In a cell-cell aggregation assay using transiently transfected S2 cells, Beat II has been shown to specifically interact with Side IV *in trans*. Moreover, the ectopic expression of Side IV in the trachea misguides the migrating LVMP cells toward and closely attaches to the visceral tracheal branches.

Altogether, these findings suggest that Beat II and Side IV likely act as a ligand-receptor pair, providing guidance signals to assist the migration of CVM and LVMP cells on their intended substrate.

Zusammenfassung

Die ordnungsgemäße Bildung von Geweben und Organen hängt von genau regulierten Zellmigrations- und Differenzierungsvorgängen ab. Die Entwicklung der viszeralen Muskulatur des Mitteldarms von *Drosophila* erfordert die koordinierte Migration von Zellen des viszeralen Mesoderms, um longitudinale und zirkuläre viszerale Muskeln zu bilden. Diese Forschungsarbeit konzentriert sich auf die Migrations- und Differenzierungsprozesse des kaudalen viszeralen Mesoderms (CVM) und der sich aus den CVM Zellen entwickelnden Vorläuferzellen, den sogenannten longitudinalen viszeralen Muskelvorläufern (LVMP). Die Arbeit zeigt, dass die Proteine Beaten path II (Beat II) und Sidestep IV (Side IV) eine entscheidende Rolle bei diesen Entwicklungsprozessen spielen.

Sowohl Beat II als auch Side IV gehören zur Superfamilie der Immunglobuline von *Drosophila*. Die Beat-Familie hat vierzehn Mitglieder, von denen die meisten in Untergruppen von Neuronen im zentralen Nervensystem exprimiert werden. Die Side-Familie umfasst acht Transmembranproteine, die in Neuronen oder bestimmten peripheren Geweben sehr dynamisch exprimiert werden. Beats und Sides fungieren häufig als Ligand/Rezeptor-Paare, um die Neurogenese zu fördern. Es wurde nachgewiesen, dass Beat Ia-exprimierende motorische Axone Side-exprimierenden Zelloberflächen folgen, um in ihre Zielgebiete einzuwachsen. Die Expression von Side II/Beat VI in prä- und postsynaptischen Partnern fördert die Synapsenbildung und beugt somit Fehlverschaltungen vor.

Interessanterweise werden Beat-II-Proteine nicht nur in Neuronen, sondern auch in migrierenden CVM- und LVMP-Zellen gefunden. Gleichzeitig existiert Side IV im viszeralen Rumpfmesoderm (TVM), das als Substrat für die Migration der CVM- und LVMP-Zellen dient. Interessanterweise werden sowohl bei den Beat-II- als auch bei den Side-IV-Mutanten ähnliche Migrationsdefekte festgestellt, die durch unregelmäßige Migrationsmuster und abnormalen Zellmorphologien und -orientierungen gekennzeichnet sind. In mutanten CVM- und LVMP-Zellen, die den Kontakt mit dem TVM verloren haben, wird Apoptose beobachtet. Am Ende der Embryogenese weist der Mitteldarm Bereiche auf, denen die Längsmuskeln fehlen. Infolgedessen werden im Larvenstadium weniger Längsmuskelfasern im Mitteldarm nachgewiesen. Im Zell-Zell-Aggregationstest mit transient transfizierten S2-Zellen kann Beat II mit Side IV *in trans* interagieren. Darüber hinaus führt die Fehlexpression von Side IV in Tracheen dazu, dass die migrierenden LVMP-Zellen in Richtung der viszeralen Tracheenäste gelenkt werden und sich eng an diese anlagern. Diese Ergebnisse deuten darauf hin, dass Beat II und Side IV wahrscheinlich als Ligand/Rezeptor-Paar fungieren und Orientierungssignale liefern, um CVM- und LVMP-Zellen bei ihrer Wanderung um und entlang des sich entwickelnden Mitteldarm zu unterstützen.

Table of Contents

1 Introduction

Cell migration is the directional movement of cells over various substrates and through diverse terrains. It is a fundamental process that plays a key role throughout life. During embryogenesis, cell migration ensures that cells meet their specific locations and are appropriately arranged to support cell differentiation and organogenesis. In adult organisms, it remains prominent in normal and pathological conditions. Under normal situations, cell migration is involved in processes like wound healing, immune response, tissue homeostasis, and bone remodeling. However, dysregulated cell migration can be the basis for many pathological situations and a major cause of human diseases (Badolato 2013; Xu et al. 2013; Lauffenburger and Horwitz 1996). Thus, cell migration mechanisms have garnered considerable attention in the fields of biology and pathobiology.

1.1 The basics of cell migration

To migrate, cells must acquire a polarized morphology, facilitating the conversion of forces generated within the cell into net cell body translocation. One manifestation of polarization is the growth of protrusions at the actin-rich leading edge, including filopodia and lamellipodia. Filopodia are thin, needle-like projections, as opposed to lamellipodia, which are flat and sheet-like structures (**Fig. 1**). Actin and actin-associated proteins are abundant in those protrusions, while cytoplasmic organelles are excluded. Filopodia and lamellipodia formation primarily take place around the cell front. They can extend reversibly into three dimensions around the cell and adhere to the substrate (Lauffenburger and Horwitz 1996; Pocha and Montell 2014).

Different types of forces are involved in migrating (**Fig. 1**). The first protrusive force to extend protrusions is generated by actin polymerization. Once these protrusions are attached to the substrate, translocation of the cell body forward may occur via the myosin-actin filaments interactions, where the myosin catalyzes the hydrolysis of ATP to ADP, utilizing this chemical energy to perform mechanical work on an actin filament (Ananthakrishnan and Ehrlicher 2007). Meanwhile, the detachment of the cell is enabled by disassembling the cell-substrate adhesion complexes at the rear of the cell. This process is repeated, resulting in a contractile force which is crucial in driving the cell forward (Ananthakrishnan and Ehrlicher 2007).

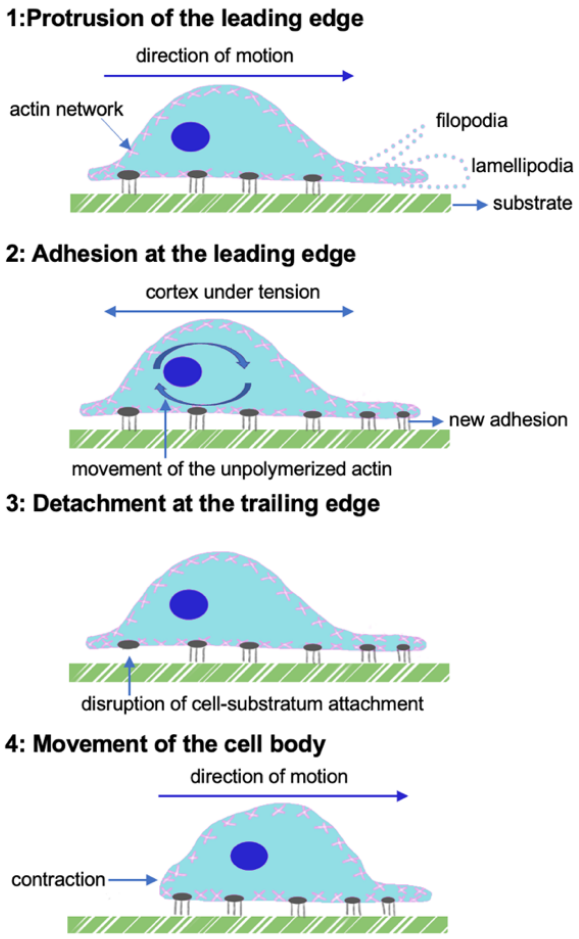

Fig. 1: General scheme of cell movement.
(1) The cell uses actin polymerization at the leading edge to expand membrane protrusions, which can be long and thin filopodia or lobular lamellipodia. (2) It then adheres its front edge to the substrate by adhesion molecules and (3) detaches at the trailing edge of the cell body via disassembling pre-existing cell-substrate attachments. (4) Eventually, it generates contractive force at the rear, which pulls the entire cell body forward. Adapted from Ananthakrishnan and Ehrlicher 2007.

In living organisms, cells may migrate as individuals or groups of different sizes, ranging from a few to hundreds of cells. The environments through which they migrate are quite diverse. They have been found to migrate on a basement membrane secreted by another cell layer, a loose matrix of extracellular matrix (ECM) proteins, or directly on the cellular surface. Interestingly, environmental composition has the potential to influence migratory mechanisms. Contrary to cell-cell interactions, which are dominated by adhesion and connection mediated by cadherin, cell-matrix interactions are regulated by integrin. Migratory guidance molecules can be distinguished into different subtypes: chemical or physical; diffusible or non-diffusible; attractive or repellent. Examples of molecules include proteins or small molecules like hydrogen peroxide (Pocha and Montell 2014; Moreira et al. 2010; Alberts et al. 2002).

1.2 Cell migration in human diseases

Cell migration is not only an essential process in development; it can also be the basis for many human diseases. For example, dysregulated cell migration is a hallmark of cancer metastasis. Malignant tumor cells increase their migration capacity by reprogramming gene expression to form invasive and metastatic tumors (Gupta et al. 2005; Nguyen and Massagué 2007). Furthermore, a subset of autoimmune diseases, such as multiple sclerosis, is also caused by the up-regulated migration ability of lymphocytes (Engelhardt and Ransohoff 2012; Norman and Hickey 2005). Conversely, the decreased migration capacity can cause many other diseases, such as Hirschsprung's disease(Mowat et al. 1998), impaired wound healing (Xu et al. 2013), and immunodeficiencies (Badolato 2013). Understanding the migration mechanism would thus benefit many modern medical branches in developing novel treatments for these diseases. However, studies in humans or human tissues could only provide limited insights into this complicated process due to the limitation of clinical samples and ethical unjustifiability. Thus, using a model organism could be beneficial in elucidating the underlying mechanism.

1.3 *Drosophila* as a model organism for cell migration

Over decades, *Drosophila melanogaster* has proved an excellent model organism for acquiring knowledge of complex biological phenomena like cell migration due to its short generation time, low cost, and numerous well-established tools. Various types of migrating cells are present in the *Drosophila* embryo, and their migration patterns vary in trajectory, timing, and cellular composition.

1.3.1 Single-cell migration

Single-cell migration refers to the movement of individual cells within a tissue or organism. In *Drosophila* embryos, cell types like primordial germ cells and hemocytes migrate in this manner.

Primordial germ cell migration

The primordial germ cells (PGCs), precursors of gamete-producing cells in the gonad, are specialized at the posterior pole of blastoderm-stage embryos. Shortly after specialization, PGCs acquire a polarized morphology by remodeling their actin cytoskeleton and extending

pseudopodia in different directions (Jaglarz and Howard 1995). Their initial migration from the outside of the blastoderm into the posterior midgut primordium (PMG) is largely passive, as they are carried with the invaginating PMG, and they exhibit reduced protrusive activity and increasingly uniform cortical actin (Kunwar et al. 2008). Once inside the PMG, they cluster tightly together, extending protrusions to the midgut from their outward-facing leading edges (Kunwar et al. 2008). Following this, PGCs undergo dispersion, migrate into the mesoderm as single cells between cells of the midgut epithelium, and subsequently sort bilaterally along the sides of the embryo and associate with the two distinct groups of somatic gonad precursors (SGP) that are localized at dorsolateral segments of the mesoderm.

Multiple regulating genes are involved in this process. For instance, *wunen (wun)* and *wun2*, which encode the lipid phosphate phosphatases, are required to orient PGC migration out of the PMG and toward the SGP. Their midline expression in the central nervous system facilitates the bilateral sorting of PGCs. In *wun* mutants, germ cells are lost, and one or several PGCs are often located outside the PMG and fail to migrate onto the PMG (Renault et al. 2010; Renault et al. 2004; Stepanik et al. 2016). A study also suggests that the migrations of PGCs and caudal visceral mesoderm cells are interdependent, as both migration patterns are disorganized when Wun is absent. In *wun* mutants, caudal visceral mesoderm cells are mis-migrating over the lateral sides of the PMG instead of moving over the top of the PMG, and more cells are found around the mislocalized PGCs (Stepanik et al. 2016).

Hemocyte migration

Hemocytes, which are embryonic immune cells of *Drosophila* and are comparable to macrophages in mammals, originate from the procephalic mesoderm. During development, hemocytes migrate as individuals along highly reproducible paths to reach their sentinel positions. Once uniformly distributed throughout the embryo, they remain motile, monitoring for dead or infected cells (Tepass et al. 1994). The directional migration of hemocytes is regulated by chemotaxis. For example, H_2O_2 released by dying cells is a major attractant for hemocytes to wound sites (Moreira et al. 2010). Meanwhile, the basis of a mechanism called contact inhibition of locomotion response seems important in distributing hemocytes evenly throughout the embryo (Davis et al. 2012; Stramer et al. 2010).

1.3.2 Collective migration

Collective cell migration refers to the coordinated directional movement of groups of cells. A significant difference between single-cell and collective migration is how they interact with their environment and detect guidance cues (**Fig. 2**). When cells migrate individually, the directional cues come from the environment (Aman and Piotrowski 2010). For instance, when PGCs migrate, Cxcr7b (a Cxcl12a sink) is dynamically expressed in non-migrating cells surrounding the PGCs to sharpen a broad Cxcl12a gradient (Badolato 2013). However, during collective migration, cells move together, have contact for at least some time, and exert influence on one another. Collectively migrating cells thus sense directional information not only from the environment but also from the collective itself (Aman and Piotrowski 2010).

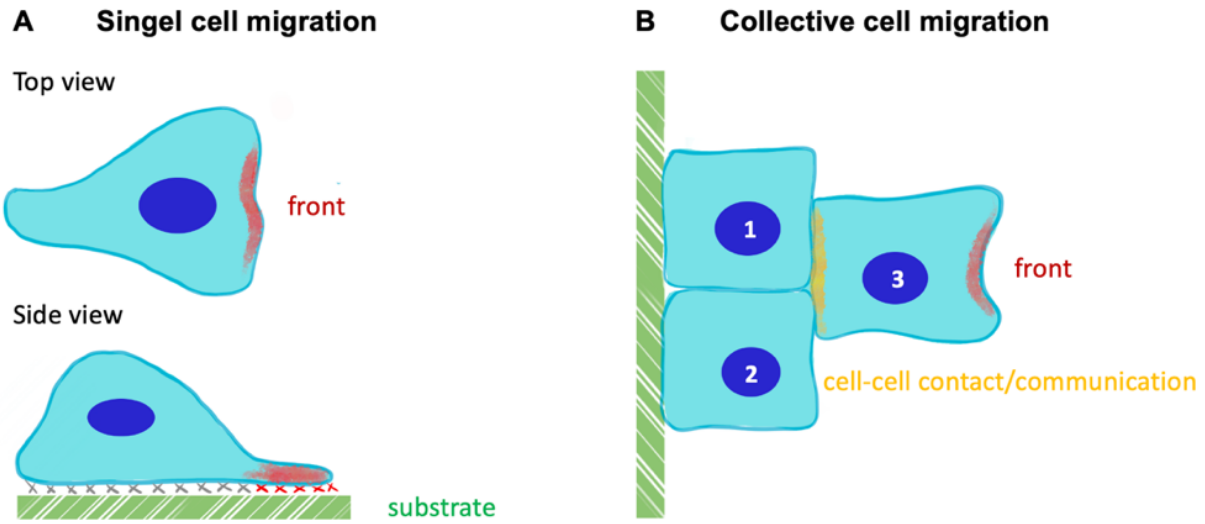

Fig. 2: Basics in individual and collective cell migration.
(A) An individual cell moving on a flat 2D surface is observed from both top and side views. When cells migrate individually, they sense the guidance cues from the environment. The red shading highlights the front membrane with increased actin-protrusion activity. The lower panel shows contact with the substrate that provides traction. This polarization provides the basis for cell movement. （B） In collective migration, cells migrate as a group, and the motion of cells is dependent not only on the environment but also on other co-migrating cells. For instance, the movement of cell 3 can be affected by the actions of cells 1 and 2. Enhanced forward migration of cell 3 may occur if cells 1 and 2 stretch, migrate forward, intercalate, or multiply. However, if cells 1 and 2 are stiff and immotile, the mobility of cell 3 will be hindered. Furthermore, cells can induce nonautonomous polarisation effects: the front of cell 3 (red) can be described as the side not in contact with other cells (yellow). Adapted from Rørth 2009.

Sheet migration

A characteristic of sheet migration is a clear front of the migrating sheet and a directional movement provided by the free space (Rørth 2009). In the embryonic development of *Drosophila*, the dorsal closure is an excellent illustration of sheet migration (**Fig. 3**). In contrast to border cells, which depart the epithelium in clusters, the epidermal epithelium in its entirety migrates across the underlying amnioserosa to close the hole in the dorsal epidermis. While many cell migrations take place over substrates that passively offer traction, the amnioserosa cells actively engage in this particular process by contracting apically. This contraction reduces the surface area to which epithelial cells adhere via adherens-type junctions and over which they are required to migrate (Gorfinkiel and Arias 2007).

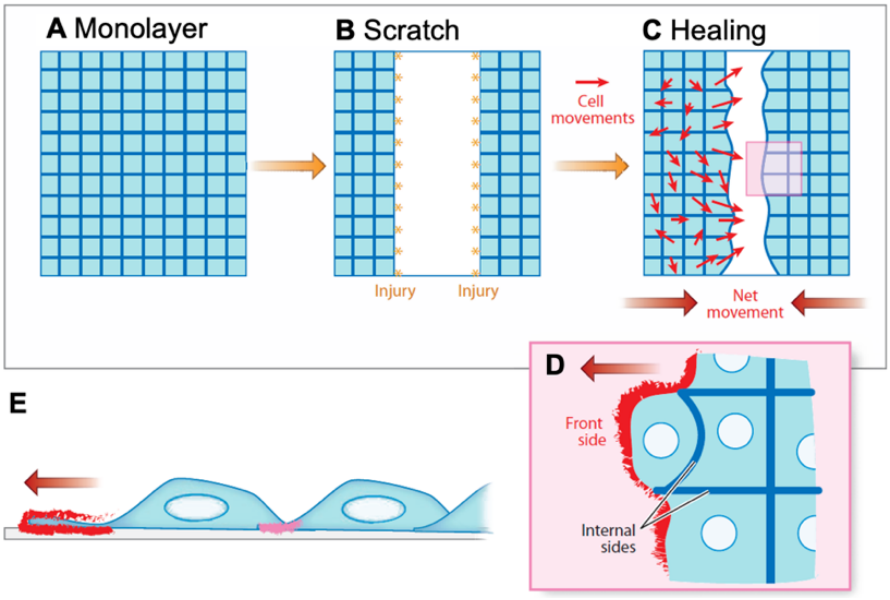

Fig. 3: Sheet migration in 2D.
(A) An undisturbed, continuous layer of epithelial cells, viewed from above. (B)When one sector of cells is mechanically scratched away, edge cells may be harmed and become next to a gap (white). (C) The cell sheets migrate to fill the space. Small red arrows represent displacement vectors for individual cells at a specific time point. (D) Higher magnification of the area from (C). The front cell inherently possesses polarity, with a front (red) surface facing the free space. Internal cells lack an inherent front orientation. (E) Side view of cells migrating to fill the gap, with the leading cell's free surface expansion highlighted in red. Cells located behind the leading cell may also create straight extensions (pink). Redrawn from Rørth 2009.

Stream migration

When cells migrate in a stream, the stream can be dense (as shown in **Fig. 4**) or loose. For example, in *Drosophila* embryos, the caudal visceral mesoderm cells move in a loose stream-

type manner. While migrating, the CVM cells are more loosely connected than other collective migration types, like *Drosophila* border cells or neural crest cells in vertebrates. Nevertheless, they are more tightly than individually migrating cells like *Drosophila* PGCs (Aman and Piotrowski 2010; Pocha and Montell 2014). The subsequent section will provide a comprehensive description of the CVM cell migration.

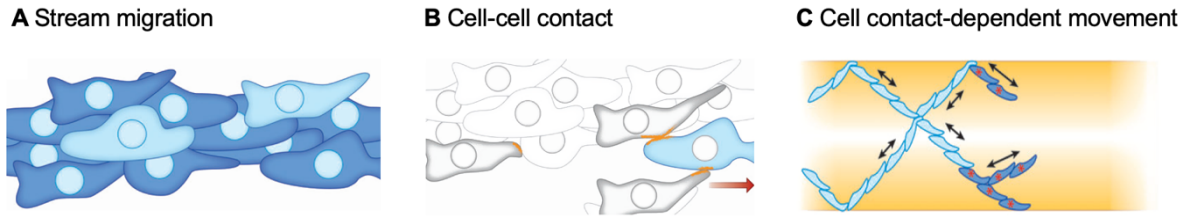

Fig. 4*:* Illustration of stream migration.
(A) Cells migrate in a dense stream. (B) Cell-cell contact between migratory cells can influence the cytoskeleton and assist in cell polarisation. If a contact in the immediate vicinity hinders front actions, the blue cell will shift to the right. (C) Cell contact-dependent effects can influence cell motions and proliferation (only cells that have free space will divide, red asterisks), resulting in an organized spreading network of cells. Redrawn from Rørth 2009.

Free group migration

The border cell cluster of the *Drosophila* ovary is a well-studied collective migration as a free group. This cell group consists of four to eight motile border cells and two nonmotile cells called polar cells in the center (**Fig. 5**). These cells initially originate from the epithelial layer of somatic follicle cells. Once they start migrating, they form a free migrating group with no fixed front or back orientation relative to the tissue (Montell 2003; Rørth 2009).

During the migration, they use the adhesion molecule E-cadherin to get proper adhesion from the giant germ line cells (nurse cells), which serve as their migrating track (Niewiadomska et al. 1999). As there is no space and no ECM, border cells must use the traction force they get from adhering to the substrate to squeeze between these giant cells to migrate toward the oocyte. This migration process is guided by the attractant information provided by the oocyte, perceived by a PDGF/VEGF-related receptor and epidermal growth factor receptor in the border cells.

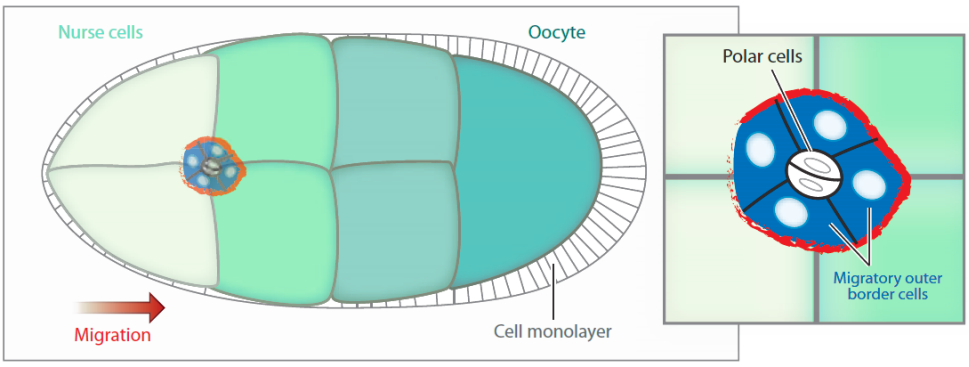

Fig. 5: Schematic of border cell migration.
Border cells migrate as an independent group. Germ line cells are depicted in various colors of cyan. The border cells detach from an epithelium encircling the germ line cluster and go towards the egg by passing through the giant nurse cells. The nurse cells also function as a substrate for migration. Within the migrating cluster are two stationary polar cells at the core, encircled by mobile outer border cells shown in blue. The migratory group has no inherent orientation relative to the tissue, and the motion is influenced by attractant signals from the oocyte. These signals are detected by certain receptors in the border cells, including PDGF/VEGF-related receptors and epidermal growth factor receptors. Each outer border cell within the cluster has inherent polarity due to intracluster connections on the inner surface (black) vs substrate contacts on the outer surface (red). Redrawn from Rørth 2009.

1.4 Mesoderm-derived visceral muscles

A hallmark of development in the *Drosophila* embryo is the specialization of three germ layers: endoderm, mesoderm, and ectoderm. Different cells and tissues originate from these three layers. For example, gastrointestinal epithelia develop from the endoderm, the mesoderm gives rise to visceral muscles and other cell types, and the trachea and nervous system arise from the ectoderm.

Mesoderm migration in the *Drosophila* embryo is a complex and highly conserved process essential in developing specialized organs and tissues. It provides an excellent model for dissecting the migration mechanism. This introduction will first introduce the mesoderm-derived visceral muscles and then focus on the migration and differentiation of the caudal visceral mesoderm-derived muscle progenitors, which use the trunk visceral mesoderm as their migrating track.

1.4.1 *Drosophila* visceral muscles are derived from the mesoderm

The *Drosophila* embryonic visceral musculature consists of two cell types arising from the mesoderm. The first is the circular visceral muscles (CirVM), arising from the trunk visceral

mesoderm (TVM). The second is the longitudinal visceral muscles (LVM), originating from the caudal visceral mesoderm (CVM) (Azpiazu and Frasch 1993; Martin et al. 2001). CirVM cells are oriented dorsoventrally, whereas LVM cells are elongated in the anterior and posterior direction of the midgut. These two types of muscles are interwoven, with LVM cells on top of the CirVM cells, ensheathing the entire midgut. Once the embryos are developed to the larval stage, these muscles are responsible for transporting food through the gut tube by their peristaltic movement.

1.4.2 TVM-derived circular visceral muscles

The first visceral muscle type, the CirVM, is derived from TVM (**Fig. 6**). These cells originate at the most dorsal positions of the mesoderm after the mesoderm spreading. They are specialized by the expression of Biniou (Bin) and the homeodomain transcription factor Bagpipe (Bap) (Azpiazu and Frasch 1993; Zaffran et al. 2001).

TVM cells are initially seeded as 11 segmental clusters by ectodermal patterning signals along the dorsal mesoderm of the trunk region (Azpiazu and Frasch 1993). Along with the germ band retraction, these 11 clusters merge, forming a continuous narrow band on each side of the trunk beneath the somatic mesoderm. This band will then be a migrating track for CVM cells moving along. While CVM cells are migrating, the fate of the CirVM founder cell is determined by the Delta/Notch signaling and Ras/MAPK signaling through the ALK receptor tyrosine kinase and its ligand Jelly Belly (Lee et al. 2003; Englund et al. 2003; Popichenko et al. 2013; Stute et al. 2004). Each founder cell fuses with one fusion-competent cell, also derived from the TVM, forming a binucleated CirVM precursor. Once the fusion is completed, CirVM precursors extend dorsoventrally and arrange next to each other in a palisade-like manner. They collectively encircle the endodermal tube by forming semicircles on each side of the midgut connected to their contra-lateral equivalents along the dorsal and ventral midlines (Martin et al. 2001; Frasch et al. 2023).

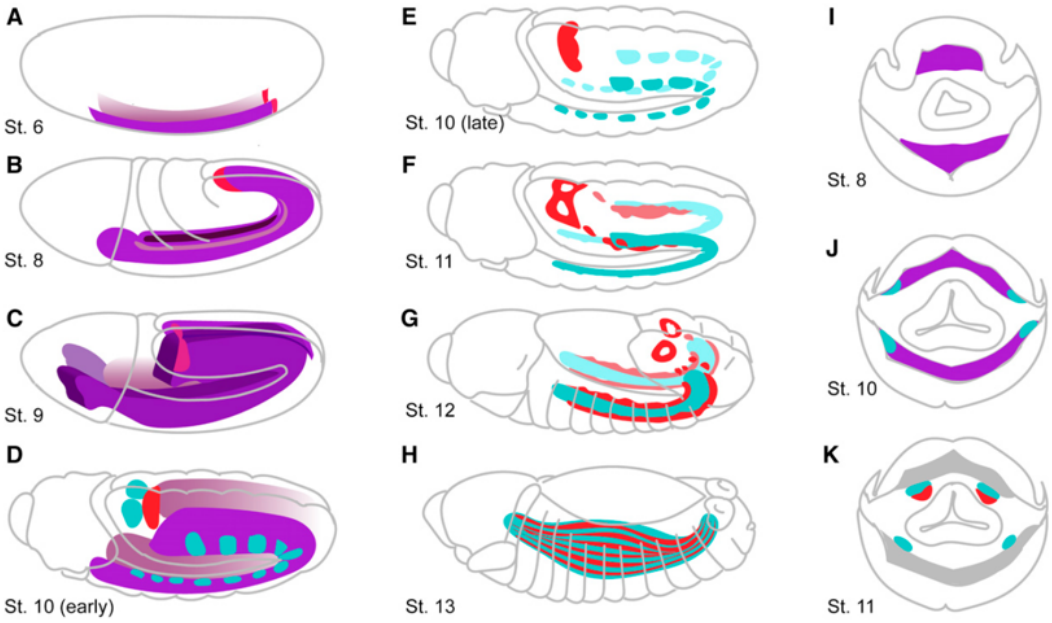

Fig. 6: Domains in the *Drosophila* embryo relating to trunk and caudal mesoderm cell lineages.
(A-H) Steps of presumptive mesoderm specialization during gastrulation, ventral furrow creation, and dorsolateral spreading occurring simultaneously with germband extension in stage 6–13 embryos. CVM cells are initially located as a stripe at the posterior tip of the presumptive mesoderm before transitioning into a migratory state. Eventually, they merge with TVM cells to cover the whole length of the gut. (I-K) Transverse cross sections illustrate the spreading and differentiation of mesoderm into several subtypes, with a focus on the positioning of TVM and CVM in relation to somatic mesoderm at three specific phases. Somatic mesoderm was excluded from E–H for clarity. TVM (cyan), CVM (red), somatic mesoderm (grey). Taken from Sun et al. 2020.

1.4.3 CVM-derived longitudinal visceral muscels

In contrast with CirVM formation in which both the founder cell and fusion-competent cell are from the TVM, the founder cell of LVM is derived from CVM cells, which are specialized at the most posterior tip of the mesoderm during the cellular blastoderm stage (**Fig. 6**). Although the specialization of most presumptive mesoderms relies on inputs from both *snail (sna)* and *twist (twi)*, CVM cells appear to mainly require *sna* for their differentiation (Kusch and Reuter 1999; Nguyen and Xu 1998). Additionally, CVM specialization is regulated by the basic helix-loop-helix transcription factor HLH54F. In *HLH54F* mutants, there is a complete loss of CVM cells, resulting in gut integrity and morphology defects (Ismat et al. 2010). During several migratory events, discussed in the following sections, these cells become founder cells and fuse with four to five fusion-competent cells from the TVM to form LVM precursor (LVMP) cells. Then, the LVMP cells, containing around six nuclei, are longitudinally elongated and evenly spaced around the midgut tube (Martin et al. 2001; Frasch et al. 2023). Together with CirVM, they form the visceral musculature to ensheath the entire midgut.

1.5 Migration of CVM cells

As mentioned above, this work focuses on the migration and differentiation of the CVM-derived LVMP cells. First, the anterior migration of CVM cells will be discussed, followed by the subsequent migration and differentiation events of the LVMP cells.

1.5.1 The anterior migration of CVM cells

Shortly after specialization, CVM cells undergo a proliferation. At stage 10, they separate from the remaining mesoderm and divide into bilateral streams. These two cell streams collectively move in a loosely-contacted manner. Initially, they migrate between the posterior midgut primordium and the TVM (Ismat et al. 2010). This initial migration is actively and independent from the germ band retraction, as the CVM cells can continue the migration in the *u-shaped* mutants where the germ band retraction does not occur (Kadam et al. 2012). By the end of stage 11, after the continuous TVM band is formed, CVM cells migrate at both the dorsal and ventral margins of the band. Around stage 13, the CVM cells at the front reach their destination, the foregut-midgut transition, and the anterior migration ends (**Fig. 7**, from A to E) (Urbano et al. 2011; Sun et al. 2020; Frasch et al. 2023).

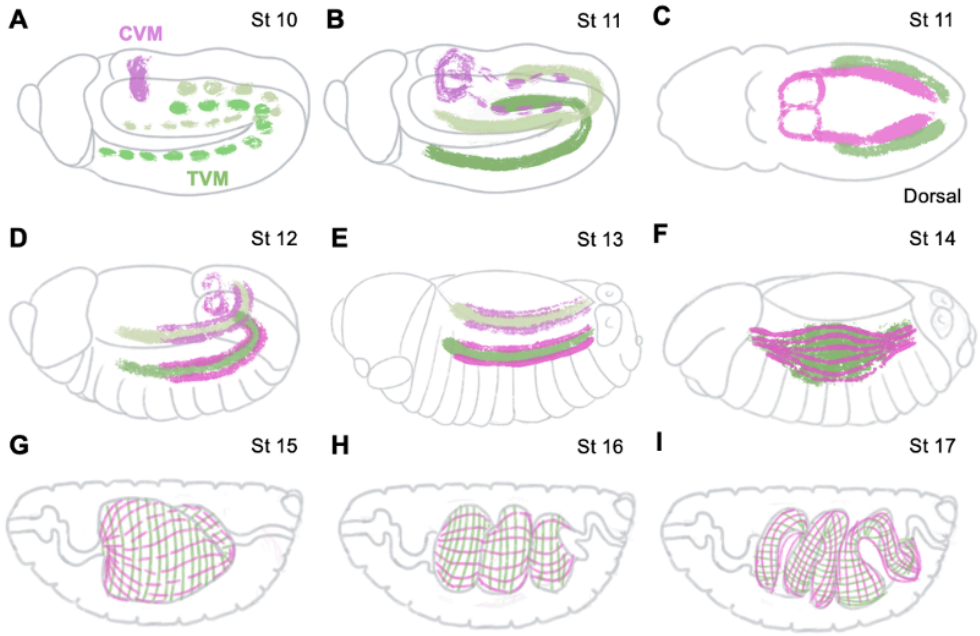

Fig. 7: Illustration of CVM and LVMP cell migration.
(A-E) CVM cells initiate the anterior migration at stage 10. They are arranged in two bilateral streams and migrate migration simultaneously. At stage 13, when the front cells arrive at the foregut and midgut transition, the anterior

migration is ended. During the migration, CVM cells are specialized into founder cells and fuse with TVM-derived FCMs to form LVMP cells. (F-I) LVMP cells migrate ventrally and dorsally along the expanding midgut. Meanwhile, they continue to fuse with more FCM cells and have highly dynamic filopodia activity to detect guidance cues. At stage 15, most cells own up to 6 nuclei and fully cover the whole midgut. Afterward, the anterior-posterior neighboring LVMP cells connect and extend into long, thin fibers along the midgut. At late stage 16, the filopodia activity stops and the LVM fibers are eventually developed. CVM, LVMP, and LVM cells are drawn in magenta. TVM and CirVM cells are depicted in green. A+B, D-I: lateral view, C: dorsal view.

1.5.2 CVM cell migration signaling

Directional cell migration is regulated by a complex network of signal transduction pathways. Cells interact dynamically with extracellular guidance cues to accomplish forward movement, which may involve a coupled remodeling of adhesion and polarity complexes.

FGF signaling

The fibroblast growth factor (FGF) signaling pathway exerts functions in cell migration in different biological contexts in various species (Tulin and Stathopoulos 2010; Dorey and Amaya 2010). In *Drosophila*, there are three FGF ligands: Thisbe (Ths), Pyramus (Pyr), and Branchless (Bnl); and two FGF receptors: Heartless (Htl) and Breathless (Btl). The ligand/receptor pair, Bnl/Btl, is crucial in the development of the tracheal system (Cabernard et al. 2004). By contrast, the Pry/Ths/Htl complex is known to regulate early embryonic and pupal mesodermal cell specialization and migration (Beiman et al. 1996; Stathopoulos et al. 2004).

Htl, is a membrane tyrosine kinase that regulates gene expression through the mitogen-activated protein kinase pathway. In *Drosophila* embryos, it is expressed in CVM cells before and during the migration (Mandal et al. 2004). Interestingly, its ligands, Pyr and Ths, are found in TVM cells, which serve as the migrating track for the CVM cells (Kadam et al. 2012; Reim et al. 2012).

In *htl* mutants, as well as a deficiency line lacking both *ths* and *pyr*, comparable phenotypes are detected (Kadam et al. 2012; Reim et al. 2012; Mandal et al. 2004), which can be characterized as defects in the CVM cell survival and migration pattern. In detail, more cells cross the midline instead of getting separated as two distinct bilateral streams followed by an extensive cell death at stage 13. In either the *ths* or *pyr* single mutant, a similar but less severe phenotype can be detected, suggesting both ligands play a role in this process (Kadam et al. 2012; Reim et al. 2012). Meanwhile, when apoptosis of CVM cells is avoided by expressing p35, a caspase

inhibitor, the surviving CVM cells regain a high migration ability, but the CVM migration path is less regular, and fewer cells can reach the anterior end compared with the wild-type. Together with the fact that the ectopic expression of either Ths or Pyr can support the CVM survival as well as misdirect the migrating CVM cells, FGF signals are found to be crucial for the survival and pathfinding for the synchronous and symmetric CVM migration (Reim et al. 2012; Kadam et al. 2012).

Integrin signaling

To perform a forward movement, migrating cells must break the existing adhesive bonds with the surroundings and establish new adhesion, the traction point. Among the various adhesion receptors, integrins, which are heterodimeric receptors consisting of α and β chains, are found to be important in promoting cell migration. They serve as connections between the ECM and the actin cytoskeleton, enabling cells to adhere to the substratum and perform forward movements. Meanwhile, they regulate intracellular signaling components, including Rho family GTPases and other adhesion kinases, to mediate cell migration (Bökel and Brown 2002).

In *Drosophila* embryos, there are two βs (βPS and βv) and five αs (α1- α5) are characterized, and different integrins are involved in different migrating cell types. When maternal and zygotic βPS1 are absent (referred to as $\beta PS1^{-}$), the initial migration of CVM cells over the posterior midgut primordium to the TVM is unaffected. However, most embryos show defects in the later migration process (Urbano et al. 2011). In wild-type embryos, only 12.5% show a mild delay for CVM cells reaching the foregut and midgut transition (corresponding to thoracic segments T1/T2). However, in the $\beta PS1^{-}$ mutant, 60.4% show a mild delay, and 25.8% have a strong delay. At later stages, the distribution and spreading of the LVMP cells among the TVM are also affected in the $\beta PS1^{-}$ mutants, in which a less efficient movement of extending and retracting protrusions is detected. Because a loss of βPS1 results in a complete loss of PS1 integrin function (as only αβ heterodimers are transported to the cell membrane), these results suggest that PS1 integrin may function in the proper adhesion of protrusions to the substrate to promote directional cell migration (Urbano et al. 2011).

ECM proteins

The ECM is a network of extracellular macromolecules and minerals that provide structural and biochemical support to surrounding cells. Examples of ECM components include collagen, laminins, and perlecan. As mentioned, migrating CVM cells use TVM as their migration substratum. However, it is still unclear whether CVM cells are migrating directly over the cell surface of TVM cells or the ECM present on the TVM. To get more insights into this question, a previous work performed by Urbano and colleagues has checked several mutants lacking different ECM components (Urbano et al. 2011).

Firstly, they checked *laminin*, as its mRNA had been detected in the visceral mesoderm at the time of CVM migration (Martin et al. 1999). While the embryos lacking LamininA do not show any migration defects, more than 80% of the embryos lacking LamininW exhibit abnormal CVM migration. Interestingly, these phenocopied defects are also detectable in the Lamβ^- mutants, which lack both LaminA and LaminW (Urbano et al. 2011). However, when both Laminins are absent, the deposition and assembly of other ECM components, such as Collagen IV and Perlecan, are also severely impaired (Urbano et al. 2009). Therefore, LamininW may play a direct or indirect role in this process. To test this, Collagen IV and Perlecan in the LamW mutant were analyzed. There, the distribution of Collagen IV and Perlecan is normal. Additionally, in neither the *collagen IV* nor *perlecan* mutant embryos, no CVM migration defects are detected. Together, these results suggest that LamininW, not LamininA, is one of the migrating substrates for CVM cells (Urbano et al. 2011). Moreover, they found another ECM component, Nidogen is aberrantly accumulated around the TVM in the $\alpha PS2^-$-integrin mutant, where the TVM morphology and CVM migration are affected (Urbano et al. 2011).

Taken together, these findings indicate that a proper ECM substrate, which may be assembled by integrin, is likely required for CVM migration. Thus, the model in which CVM cells are migrating over the ECM present on TVM is preferable.

Other signaling pathways

The focus of recent research has been identifying the molecular cues responsible for the distinctive behavior displayed by CVM cells. One is AdamTS-A, the *Drosophila* ortholog of human ADAMTS9 and ADAMTS20, which belongs to the secreted metalloproteases.

AdamTS-A is expressed in CVM cells, and a loss of this metalloprotease results in an increase (up to 40%) in embryos with mismigrated CVM cells (Ismat et al. 2013). A recent comparison of experimental results with mathematical simulations indicates that the site of the AdamTS-A function in CVM cells is mainly at the CVM-ECM interface, not on the cell surfaces in contact with TVM. In the absence of AdamTS-A, CVM cells migrate in all directions along the TVM substrate instead of migrating along the dorsal and ventral margins of TVM. These results suggest that AdamTS-A cleaves connections between CVM cells and the ECM on all sides not attached to the TVM (see **Fig. 8**), thus promoting CVM cells migrating as a loose collective (Hamilton et al. 2022).

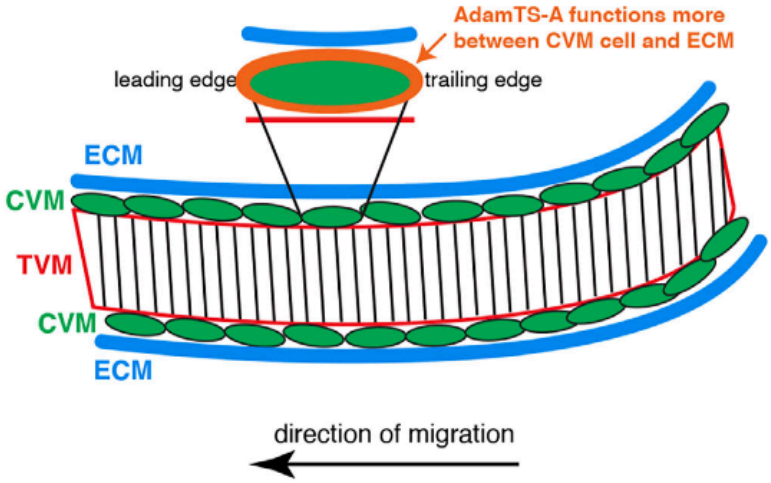

Fig. 8: Model of Adam TS-A function in CVM migration.
AdamTS-A (orange) appears to be functioning at the necessary time and location to break connections between the migrating cell (green) and the ECM (blue). AdamTS-A is more active at the CVM-ECM contact than at the CVM-TVM interface. Taken from Hamilton et al. 2022.

As the elimination of abnormal cells is crucial to avoid compromised function and patterning and to achieve tissue homeostasis, the anoikis mechanism of migrating CVM cells is also an important topic. It is demonstrated that *Drosophila* CVM cells utilize signaling pathways involving bone morphogenetic protein (BMP) and FGF to maintain homeostasis through anoikis, a type of cell death induced by substrate de-adhesion. CVM anoikis is caused by disruptions in the expression of the cell death gene *head involution defective (hid)* regulated by the cell cycle. Through a visceral mesoderm-specific cdc25/string enhancer, the secreted BMP ligand coordinates both collective proliferation and apoptosis of cells that have no longer access to substrate-derived FGF, thereby driving cell-cycle progression (Macabenta et al. 2022).

1.6 Migration and differentiation of LVMP cells

By the end of stage 13, when CVM cells have reached their destination, they become founder cells (FCs). After their fusion with the fusion-competent myoblasts (FCMs) developed from the TVM, they are differentiated into LVMP cells, which undergo subsequent events of migration and differentiation until they become LVM fibers.

1.6.1 The dorsal-ventral migration of LVMP cells

LVMP cells are formed upon the fusion of CVM-derived FCs with FCMs. Afterward, at early stage 14, when the CirVM precursors expand in the dorsoventral direction, LVMP cells elongate in the anteroposterior direction. Nevertheless, LVMP cells migrate dorsally and ventrally to cover most of the expanded CirVM precursors. By the termination of stage 14, LVMP cells are largely extended and arranged in parallel to their neighbors. Along with the dorsal and ventral closure of the midgut at stage 15, LVMP cells have been distributed evenly throughout the midgut. During early stage 16, the elongated LVMP cells formed long, thin rows along the midgut by contacting their anterior and posterior neighbors. In the remainder of stage 16, this arrangement matures, resulting in the differentiated LVM fibers, which are evenly arranged around the midgut, and each of them extends over much of the length of the midgut (the dorsal-ventral migration process is shown in **Fig. 7**F-I).

Notably, the migratory LVMP syncytia are covered by filopodia, which extend toward the neighboring LVMP cells and the underlying CirVM precursors. They are highly dynamic and efficient in extending and retracting, possibly detecting the guidance signals from the migration substrate and the neighboring cells. Finally, only until late stage 16, when the morphogenetic processes are completed, do these dynamic activities begin to fade (Frasch et al. 2023).

1.6.2 LVMP cell migration signaling

Compared with the anterior migration of CVM cells, the subsequent dorsal-ventral migration and their coordinated alignment along the midgut have yet to be researched extensively. Teyrha-Meyrha (Tey), a diverged member of the RNF220 family, is proven to play a role in the dorsoventral migration and proper morphogenesis of LVMP cells (Frasch et al. 2023). In *tey* mutants, instead of being precisely aligned in anteroposterior orientations and uniformly

distributed along the dorsoventral axis, LVMP cells exhibit irregular distances and frequently assume oblique or transverse orientations. Moreover, the morphology of the precursors is abnormal, predominantly adopting squat or triangular forms rather than their original elongated spindle-like shape. Additionally, their nuclei are more often clustered rather than individually distributed (but the number of the nuclei is not affected). Although LVMP cell migration in the *tey* mutants reaches the dorsal and ventral regions of the developing midgut tube, it appears to be extremely uncoordinated due to the random orientation of the cells. Furthermore, while certain areas of the midgut contain an abundance of LVMP cells, others remain devoid of them. This mutant phenotype persists until the larval and adult stages, where abnormal morphologies and differentiation of LVM fibers are detected (Frasch et al. 2023).

1.6.3 Longitudinal visceral myoblast fusion

Like other muscle fibers, the embryonic *Drosophila* LVM cells are multinucleated and arise from the fusion of mononucleated myoblasts during embryogenesis. The myoblast fusion process is a special fusion of the lipid bilayers, after which two membranes merge to become one (Kozlov and Chernomordik 2015). To initiate the fusion, fusion-competent myoblasts (FCMs) extend their filopodia to the founder cells (FC) to which they attach. They align and come into close contact, forming finger-like protrusions and fusion pores, which lead to the final fusion (Rout et al. 2022).

As mentioned, *Drosophila* LVM cells contain six nuclei fused from the CVM-derived FC and the TVM-derived FCMs. Firstly, during the anterior migration, the CVM cells become FCs and fuse 1-2 times with the FCMs to form the LVMP cells. During the following dorsal-ventral migration, LVMP cells undergo several more rounds of fusion (Frasch et al. 2023). At early stage 14, most migrating LVM precursors consist of two to four nuclei. By late stage 14, three to five nuclei are detected, and six nuclei are seen by the end of stage 15 (Frasch et al. 2023).

1.6.4 Signaling in longitudinal visceral myoblast fusion

The myoblast fusion of LVM shares similarities with somatic myoblast fusion, such as the same cell-adhesion molecules. However, there are also distinctions between the two processes (Rudolf et al. 2014; Rout et al. 2022). During the myoblast fusion *of Drosophila* somatic muscles, Wip and WASp, which form a complex and can activate the Arp2/3, are required. In

comparison, LVM myoblast fusion depends on SCAR/Wave and Kette but not on WASp-dependent Asp2/3 activation. In either *wip* or *wasp* mutant, the migration and myoblast fusion of the LVMP cells is unaffected (Rout et al. 2022; Rudolf et al. 2014). Although more LVMP cells fail to migrate along TVM when the WASp-dependent Asp2/3 is abolished, this phenotype is mainly due to migration defects instead of fusion defects (Rout et al. 2022).

Another difference between these two processes is the need for Rolling Pebbles 7 (Rols7). During the LVM myogenesis, Dumbfounded/Kin-of-irre (Duf/Kirre), Blown fuse (Blow), and Rols7 are accumulated at fusion sites. The Duf/Kirre and Rols accumulation is comparable with the FuRMAS (fusion-restricted myogenic-adhesive structure) observed in the somatic mesoderm fusion. However, Rols7 and Duf/Kirre are not in a ring-like structure as they are in the somatic mesoderm but appear as foci. In the *rols7* mutant, LVM fusion is affected, which can be characterized as more unfused FCMs are found between the somatic and visceral mesoderm (Rudolf et al. 2014). The model of longitudinal myoblast fusion is shown in the scheme below (**Fig. 9**)

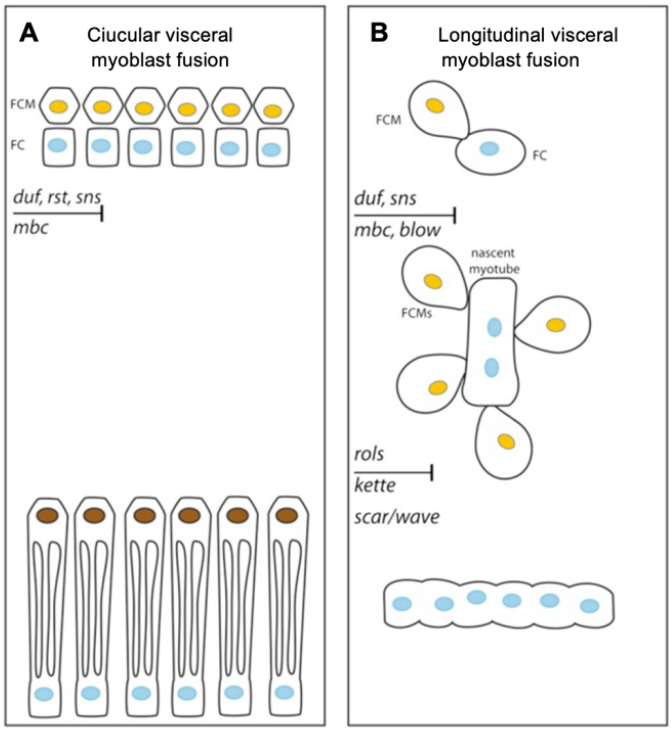

Fig. 9: *Drosophila* CirVM and LVM myoblast fusion model.
(A) Each CirVM cell is derived from one FC fused with one FCM. The blue nuclei represent FCs and the yellow (after fusion in brown) nuclei represent FCMs. The process is regulated by Rst, Duf, Mbc, and Sns. (B) Longitudinal fusion of visceral myoblasts results in syncytia, typically containing six nuclei. Duf is expressed in blue nuclei, while Sns yellow nuclei are Sns-positive. Without Mbc, fusion does not happen; a lack of Blow and Rols results in a restricted number of fusions. Taken from Rudolf et al. 2014.

1.7 CVM and LVMP cells migrate over TVM

When cells migrate, they need adhesion to and traction on a substrate. The substratum is diverse; it can be basal lamina, ECM, or the surface of other cells (Rørth 2009). Both the anterior migration of CVM cells and the dorsal-ventral migration of LVMP cells use TVM as their substratum (Zaffran et al. 2001; Reim et al. 2012; Frasch et al. 2023). Although it is still unclear if the migrating CVM or LVMP cells directly move over the TVM cell surface or the ECM covering the TVM, the interactions between the CVM and LVMP cells with the TVM are more interdependent than previously believed (Macabenta and Stathopoulos 2019; Sun et al. 2020).

Accordingly, when the TVM formation is disrupted, CVM and LVMP cells can not migrate properly (Reim et al. 2012; Zaffran et al. 2001). In the *bap* or *bin* mutants, which lack TVM, initial CVM migration is regular, but after stage 12, CVM cells start to migrate irregularly. At the end of stage 13, no CVM cells reach the border between the foregut and midgut, which usually is their anterior destination. At the end of the embryogenesis, a strong reduction of LVM cells is found (Reim et al. 2012; Zaffran et al. 2001). During the migration, most cells appear in a shrunken and roundish cell shape and eventually disappear, indicating they undergo apoptosis. However, when the over-expressing caspase inhibitor p35 blocks their apoptosis, the movement of the surviving cells is still less regular compared with controls (Reim et al. 2012; Zaffran et al. 2001).

Interestingly, the migrating CVM cells can also control the morphogenesis of TVM cells (Macabenta and Stathopoulos 2019). In the *htl* mutant, at stage 11, when many CVM cells cross the midline instead of being separated as two bilateral streams, TVM also shows a contralateral merging defect. By restoring the FGF signal in CVM, the CVM immigration and the TVM contralateral merging are both rescued. In addition, a loss of CVM induces TVM morphological defects. In the absence of CVM cells, TVM cells exhibit a convoluted, looping morphology instead of a relatively linear shape (Macabenta and Stathopoulos 2019).

These results, together with other observations, including the migrating LVMP cells dynamically extending and retracting filopodia toward and away from the TVM (Frasch et al. 2023), suggest that TVM serves as a substratum for CVM and LVMP cells and that the migratory cell-substratum interaction is interdependent.

1.8 Beaten path and Sidestep proteins

Recent research has increasingly concentrated on understanding the specific signals that CVM and LVMP cells rely on to navigate their migratory process successfully within the developing embryo. Still, there are open questions left in this delicate process. For instance, when FGF signaling is absent, CVM cells can still migrate anteriorly, even though misguided and slow, indicating that additional guidance cues are involved (Reim et al. 2012; Kadam et al. 2012).

Most interestingly, the expression of other families of guidance molecules, e.g. Beaten path II, has been detected in CVM cells (Pipes et al. 2001; Ismat et al. 2010; Bae et al. 2017). To gain more insights, this research focuses on the two protein families, Beaten path and Sidestep, which have yet to be studied in the migration and differentiation of CVM and LVMP cells.

1.8.1 Beaten path protein family and Beat II

The Beaten path (Beat) family belongs to the immunoglobulin superfamily (IgSF). In *Drosophila* species, fourteen members in the Beat family are characterized, and both secreted and membrane-bound isoforms are predicted. These 14 Beats are divided into seven clusters according to their phylogenetic relationships (Pipes et al. 2001; Li et al. 2017). Beats that resemble each other are grouped (**Fig. 10**), and the grouped Beats, like Beat IIa and Beat IIb, have similar divergence rates after the first duplications. Embryonic expression patterns for the grouped Beats are similar but not the same. For example, Beat Ia is expressed in all motor neurons, while Beat Ib and Beat Ic can be detected only in certain subtypes (Pipes et al. 2001; Fambrough and Goodman 1996). These findings suggest that Beats have become more specialized at two different levels: first, they became functionally specialized after being duplicated and the seven major Beat branches formed; second, they became specific in their expression patterns and binding preferences for members of the four subclusters (I, II, III, V) (Li et al. 2017).

In *Drosophila* embryos, most *beats,* like *beat Ia, Ib, Ic, Va, Vb, Vc,* and *VI*, were only found in the central nervous system (CNS) using *in situ* hybridization (Pipes et al. 2001). Among them, Beat Ia has been studied the most. It is constantly expressed in motor neurons and works with Side as a ligand/receptor pair to guide motor axons (Fambrough and Goodman 1996; Siebert et

al. 2009). Thus, it is interesting to note that two paralogues, Beat IIa and IIb, are found not only in the CNS but also in CVM cells (Pipes et al. 2001; Bae et al. 2017; Ismat et al. 2010).

As mentioned, Beat IIa and Beat IIb are closely related. They have similar divergence rates and exhibit similar embryonic expression patterns. Recent studies have found that Beat II interacts with Side IV to regulate the synaptic formation in the *Drosophila* visual system (Osaka et al. 2024; Carrier et al. 2023; Yoo et al. 2023). It is suggested that Beat IIb-Side IV works in a key-lock manner, which can establish synapses by forming a complex with a co-receptor Kirre or through cytoplasmic signaling via Dsyd-1/Liprin-α in the R7 photoreceptor (Osaka et al. 2024). Nevertheless, the specific expression and function of Beat II in the *Drosophila* embryonic visceral muscles have not been investigated yet. Therefore, it is still an open question whether Beat II plays a role in the migration and differentiation of these muscle precursors.

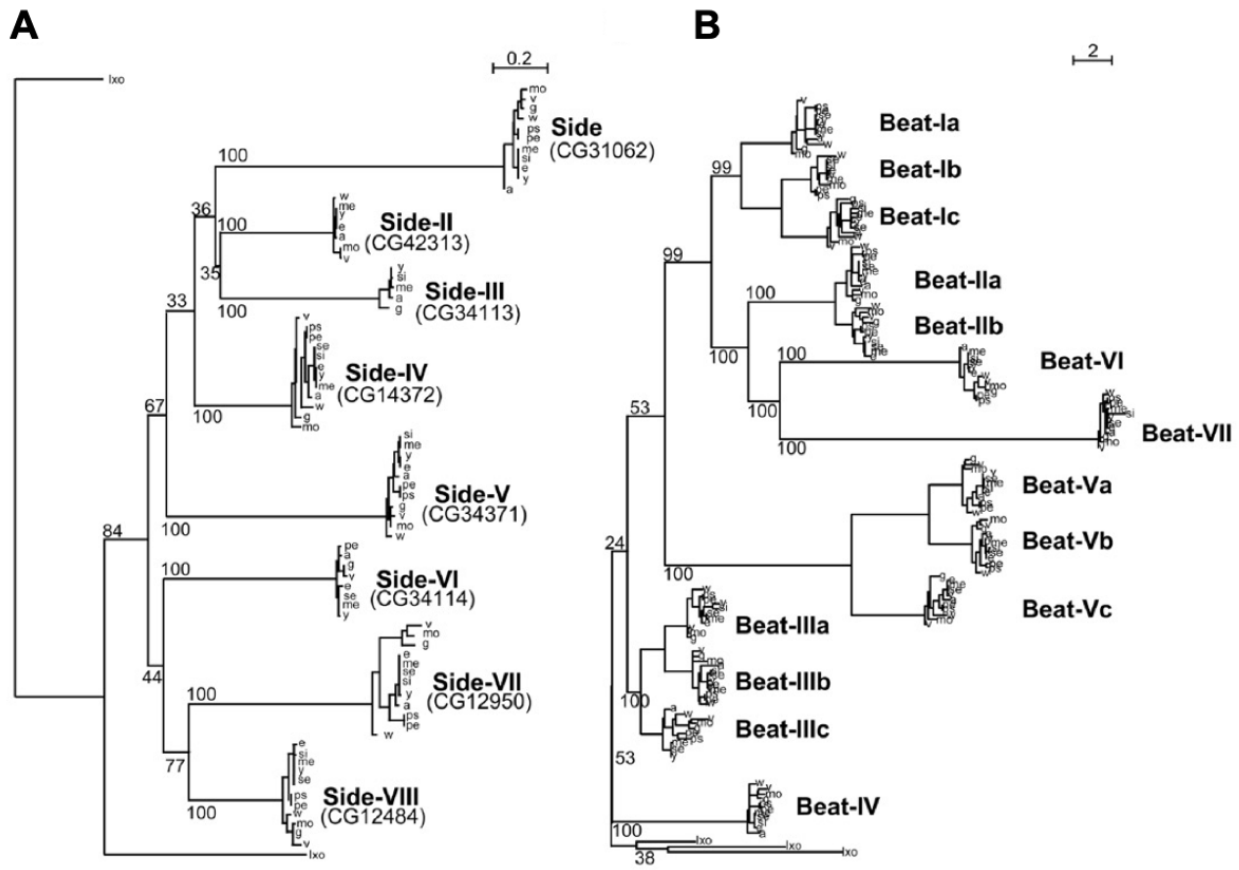

Fig. 10: Phylogenetic analysis of Sidestep and Beaten path paralogs.
(A) Phylogeny of the Side family based on similar IgSF proteins predicted in the tick *Ixoides scapularis* (Ixo). Paralogs are named based on their evolutionary distance from Sidestep, with their CG Flybase identities provided in brackets. (B) Phylogeny of the Beat family based on the tick *Ixoides scapularis* (Ixo) Beats as the root. *melanogaster (me), pasilla (ps), sechellia (se), simulans (si), yakuba (y), erecta (e), ananassae (a), persimilis(pe), willistoni (w), mojavensis (mo), virilis (v),* and *grimshawi (g)*. Taken from Li et al. 2017.

1.8.2 Sidestep protein family and Side IV

Sidestep (Side) family also belongs to an IgSF subfamily. Eight Sides are characterized in *Drosophila* species, and all are transmembrane proteins (Aberle 2009; Sink et al. 2001). In contrast to Beats, which are clustered according to their phylogenetic relationships, no Sides are coded by clustered genes (**Fig. 10**). The embryonic expression patterns of *side* genes have been identified using *in situ* hybridization and immunohistochemistry staining methods. The expression of Side (referred to as Side I) is spatial and temporal dynamic, as its expression changes along with the axon growth. It is detected in the cells over which growth cones travel during embryogenesis. This expression pattern fits its function, acting as an attractant for Beat-expressing motor axons (Sink et al. 2001; Siebert et al. 2009). All the other *side* genes, except for *side VIII*, are found in peripheral tissues transversed by motor and sensory axons (Li et al. 2017).

Among all the Sides, this research focuses on Side IV, which interacts with Beat IIa and IIb (Osaka et al. 2024; Li et al. 2017; Özkan et al. 2013). During *Drosophila* embryogenesis, *side IV* has been found in ventral muscle precursors at stage 12, some ventral and lateral muscles (muscles 5, 8, 15,16, and 17) after stage 14 (Li et al. 2017), and also in lateral-adult muscle precursors (Lavergne et al. 2020). In *Drosophila* adults, *side IV* has been detected in neurons in the visual system, where it interacts with Beat II to regulate the establishment of synapses (Osaka et al. 2024; Carrier et al. 2023).

1.8.3 Interactions between Side and Beat proteins

Based on the findings that Side and Beat Ia recognize and interact with each other to regulate axon growth (Siebert et al. 2009; Sink et al. 2001), more investigations have been done to check the interactions between Sides and Beats (Osaka et al. 2024; Carrier et al. 2023; Li et al. 2017; Özkan et al. 2013; Yoo et al. 2023). According to two independent interactome assays (Özkan et al. 2013; Li et al. 2017), a network of Side-Beat interactions has been established (**Fig. 11**). An interesting observation is that these interactions reflect the evolutionary trees, as Sides that are closer to the root of the tree are more likely to interact with the Beats that are located closely in the tree (compared **Fig. 11** with **Fig. 10**) (Li et al. 2017).

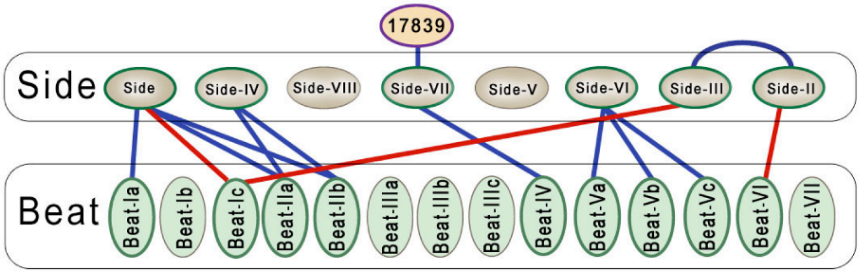

Fig. 11: Network of Side-Beat interactions.
Blue lines depicted interactions previously identified by (Özkan et al. 2013). Red lines indicate novel interactions found by (Li et al. 2017). Interestingly, one Side parolog can interact with different Beat proteins. Taken from Li et al. 2017.

Some of these interactions, which were identified biochemically, have been confirmed in flies or using cultured cells. For instance, when Beat Ia-transfected S2 cells are mixed with Side-transfected S2 cells, after a 2-hour incubation on a shaker, they form large cell-cell aggregates instead of randomly distributing in the medium, indicating Beat Ia can interact *in trans* with Side (Siebert et al. 2009; Heymann et al. 2022). Their *in-trans* interaction is crucial for guiding motor axons to reach the target muscle fields (Siebert et al. 2009).

Recently, a similar cell-cell aggregation experiment verified that Beat II interacts with Side IV *in trans* (Osaka et al. 2024). This Beat II-Side IV interaction has been proven to promote proper synapse formation in the *Drosophila* visual system (Osaka et al. 2024; Carrier et al. 2023). The subcellular location of Side IV depends on the expression of Beat II, and ectopic overexpression of Side IV induces abnormal accumulation of Beat IIb, thus inducing misformed synapses (Osaka et al. 2024). Moreover, Beat VI and Side II, which are expressed in the pre-and postsynaptic partners, interact with each other to regulate wiring specificity in the directional motion detection circuit (Yoo et al. 2023).

These findings suggest that the Beat and Side family members generally work as ligand/receptor pairs to play a guidance role during organogenesis. Thus, it is interesting to investigate whether Beat II, which is expressed in the CVM cells, also plays a guidance role in the migration of these cells.

1.9 Aim of the thesis

In metazoans, precisely regulated cell migration processes and dynamic cell shape modifications are essential for organ development. Typically, these events involve the participation of various cell types whose behaviors must be orchestrated for proper organ function. Despite an abundance of knowledge regarding the regulation of cellular migration and morphogenesis, a comprehensive understanding of these biological phenomena is still lacking in both vertebrates and invertebrates. In *Drosophila*, during the screening of GFP-exon-trap lines of the Beats and Sides for interesting expression patterns, Beat II proteins (Beat IIa and Beat IIb) have been found in the caudal visceral mesoderm (CVM) cells. This work attempts to explore whether Beat II proteins function in the migration and differentiation process of the CVM-derived longitudinal visceral muscle precursor (LVMP) cells.

Methods such as *in situ* hybridization and immunohistochemistry staining will be used to obtain detailed expression patterns of these genes. Because CVM and LVMP cells use the trunk visceral mesoderm (TVM) as their migration track, potential Beat II interaction partners may be expressed in the TVM. Mutations in *beat II* and other genes should then be generated using CRISPR/Cas9 or alternative genetic means. It is important to note that the *beat IIa* and beat *IIb* genes are clustered in the genome, indicating that they have arisen by gene duplication and may exert similar functions. Thus, creating a *beat IIa*/*beat IIb* double mutant is critical to remove potential compensatory functions.

The phenotypes of the mutants will be characterized by immunohistochemistry stainings and morphological analysis. Any detected phenotypes shall be statistically evaluated. Considering that the visceral musculature is responsible for food transport in larvae, behavioral assays, such as food intake measurements, will be used to identify potential behavioral defects at the larval stage. Furthermore, to enable functional analysis *in vivo*, corresponding tagged fusion proteins and transgenic flies will be generated for overexpression and rescue experiments. Together with biochemical methods, such as cell-cell aggregation and apoptosis detection assays, these fusion proteins and flies may assist in elucidating the underlying mechanism of Beat II functions.

In summary, these experiments may reveal a novel function of the Beat and Side families beyond the neuromuscular and visual systems and lead to a more detailed understanding of the regulation of cell migration during intestinal development.

2 Results

2.1 CVM and LVMP cell migration and differentiation

The furthest-distance migration known in *Drosophila* embryos is the migration of caudal visceral mesoderm (CVM) cells and the CVM-derived longitudinal visceral muscle precursor (LVMP) cells. During this process, CVM and LVMP cells use the trunk visceral mesoderm (TVM) as the substrate to reach their destination and eventually differentiate into longitudinal muscles of the midgut.

2.1.1 CVM and LVMP cells migrate over TVM

The CVM and LVMP cell migration process includes the anterior migration of CVM cells and the dorsal-ventral migration of LVMP cells. To visualize these processes, CVM and LVMP cells were marked with *HLH54Fb*-CytoRFP (also known as HLH54F.LVM-RFP; Hollfelder et al. 2014), and visualized by the anti-dsRed (**Fig. 12**A-H). The substate TVM cells were stained by the anti-Fasciclin III (Fas III) (**Fig. 12**A'-H').

At stage 10, CVM cells appear as a group of cells at the most posterior tip of the mesoderm (**Fig. 12**A-A'', arrows). Most CVM cells initiate migration from late stage 10, and a small portion of cells remain in the posterior part of the mesoderm (**Fig. 12**B-B'', circles). Subsequently, the migrating CVM cells arrange into two cell streams on either side of the embryo trunk and collectively migrate towards the anterior (**Fig. 12**C-C''). Meanwhile, TVM cells are specialized as eleven clusters (**Fig. 12**B', arrowhead). Upon the appearance of the TVM, CVM cells have close contact with them and use them as migration substrates (**Fig. 12**B-C''). From late stage 12 onward, when the TVM cells have formed a continuous narrow band (**Fig. 12**D', arrowhead), CVM cells migrate at the dorsal and ventral margins of this band in a loose stream-like manner. Notably, posterior CVM cells that lost contact with the TVM display abnormal cell morphology and undergo apoptosis (**Fig. 12**D-D'', circles; also seen in Video S1 from Macabenta et al. 2022). A group of RFP-positive cells between the migrating streams and amnio serosa is also detected (**Fig. 12**D-D'', empty arrowheads). They probably are off-track CVM cells or unspecific stainings. At stage 13, the anterior migration is completed when the CVM cells at the front reach the foregut-midgut transition (T1 segment).

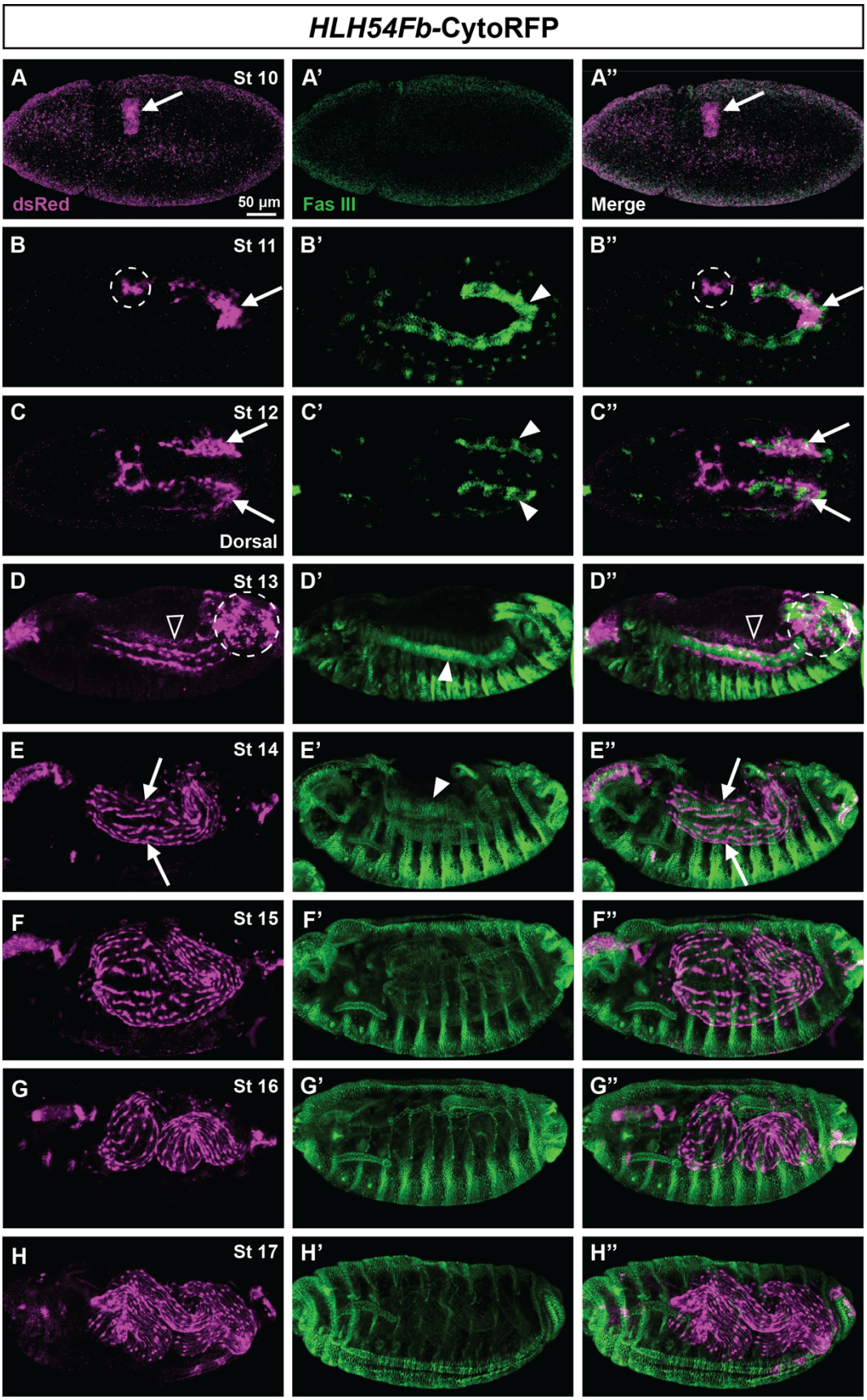

Fig. 12: CVM and LVMP cells migrate over the TVM.
Confocol images of fixed and stained embryos of consecutive stages that express RFP in CVM and LVMP cells (from *HLH54Fb*-CytoRFP). (A-H): Demonstration of normal migration of CVM and LVMP cells marked by anti-dsRed in magenta. CVM cells are detected at early stage 10 at the most posterior tip of the mesoderm (A,arrow).

Afterward, CVM cells are separated into two streams that migrate collectively towards the anterior. A group of cells remain in the posterior part of the mesoderm (circle in B). At early stage 13, cells at the front reach the foregut-midgut transition position, and LVMP cells are derived from the myoblast fusion. From late stage 13 onwards, LVMP cells migrate dorsoventrally and align in parallel to form LVM fibers covering the midgut. The non-migrating cells undergo apoptosis (circle in D). (A'-H'): TVM cells were visualized by anti-Fasciclin III (Fas III) in green. TVM primordia appears at stage 11 (arrowheads in B' and C') and then forms a continuous band. From late stage 13, the TVM-derived circular muscle precursors expand in the dorsal-ventral direction (arrowheads in D' and E'). After stage 14, the Fas III staining decreases in the TVM but increases in the epidermis. (A''-H'') Merged images showing CVM and LVMP cells migrated over the TVM cells. Unless noted otherwise, dorsal is up, anterior is left in this and all the other figures of this thesis. The scale bar in (A) applies to all the images in this figure.

Once CVM cells have reached their destination, they are differentiated into founder cells (FCs). Then, they fuse with the fusion-competent myoblasts (FCMs), resulting in LVMP cells. From stage 14 onwards, the TVM-derived circular muscle precursors expand in the dorsal-ventral direction (**Fig. 12**E', arrowhead). Along with this expansion, LVMP cells migrate dorsal-ventrally (**Fig. 12**E-E''). Additionally, LVMP cells extend in anteroposterior directions and line up in parallel. At stage 15, following the dorsal closure, LVMP cells are distributed evenly and parallelly over the whole midgut (**Fig. 12**F-F''). During stage 16, LVMP cells connect with their anterior and posterior neighbor cells, forming thin, long rows extending along the midgut tube (**Fig. 12**G-G''). This arrangement matures at late stage 16 when the longitudinal visceral muscle (LVM) fibers eventually form. LVM fibers are interwoven with circular visceral muscle fibers to ensheath the midgut and are responsible for intestinal peristaltic movements.

2.1.2 CVM and LVMP migration is disrupted in the absence of TVM

Cell migration can only be understood in relation to its surrounding environment. In most cases, the substrate is essential for the correct migration, as it provides mechanical support, survival cues, and guidance signals to the migrating cells (Rørth 2009; Yamada and Sixt 2019). To acquire more details about the relationship between the migrating cells and their substrate, CVM and LVMP cell migration upon a disrupted TVM was under examination.

As the transcription factor encoding gene *bagpipe (bap)* is critical for the TVM formation (Azpiazu and Frasch 1993; Zaffran et al. 2001), the bap^{208} mutant in which the TVM could not form properly was utilized. Following the cross of bap^{208} with *HLH54Fb*-CytoRFP lines, embryos were immunostained. Anti-Fas III staining showed the TVM in cyan, and anti-dsRed showed the CVM and LVMP cells in magenta (**Fig. 13**).

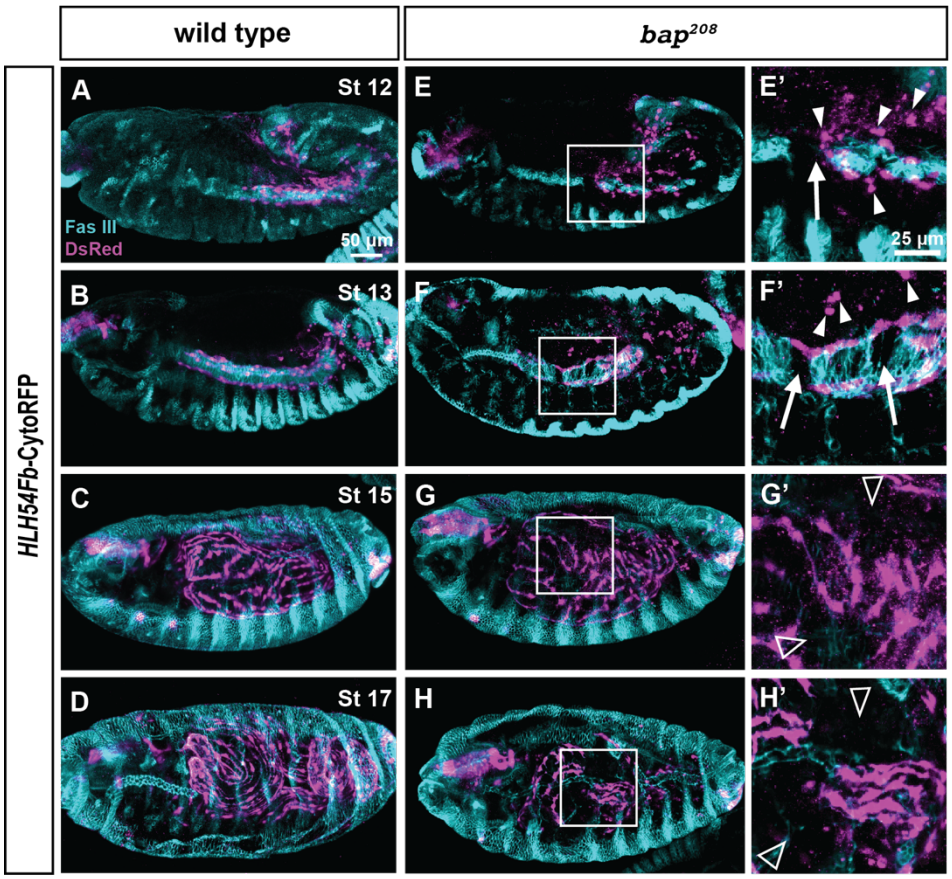

Fig. 13: Disrupted CVM and LVMP cell migration with misformed TVM.
Visulization of CVM and LVMP cells marked with RFP in magenta, and TVM by anti-Fas III in cyan. (A-D): Wild-type embryos showing the regular migration pattern of CVM and LVMP cells. After stage 14, Fas III staining decreases in the TVM (a similar expression pattern was also seen in Klapper et al. 2002. (E-H): Embryos carrying homozygous loss-of-function mutations in *bap*. Squars mark enlarged areas in (E'-H'). The TVM formation is disrupted, and gaps within the TVM are observed (arrows in E' and F'). The CVM and LVMP cell migration is affected after stage 12, as many off-track cells display abnormal cell morphology (arrowheads in E' and F'). Most cells stop migrating before the TVM gaps, and only a few cells can reach their termination. By the end of stage 17, midgut areas devoid of LVM fibers are detected (empty arrowheads in G' and H'). The scale bar in (A) applies to (A-H). The scale bar in (E') applies to (E'-H').

In the control group, TVM cells are specialized as individual clusters at stage 11 (data not shown). Then, the clusters merge and form a continuous band, serving as the migration track for CVM cells (**Fig. 13**A, B). Afterward, they expand in the dorsal-ventral direction and lead to circular visceral muscles of the midgut. However, in the homozygous *bap*^{208} mutant embryos, even at stages 12 and 13, gaps are still present within the TVM band (**Fig. 13**E-F', arrows). Although the CVM migration can initiate similarly to the wild type, the following progress is severely affected. Many migrating CVM cells lose their contact with the TVM and display rounded and shrunken shapes (**Fig. 13**E-F', arrowheads). Most cells stop migrating before the gaps in the TVM and thus can not reach their destination. Only a few are on the correct path and can pass the gaps. By the end of embryogenesis, midgut areas lacking LVM fibers are detected (**Fig. 13**G-H', empty arrowheads; compare H with D).

2.1.3 The formation of syncytia within the longitudinal visceral muscles

Like somatic muscles, the circular and longitudinal visceral muscles around the midgut in *Drosophila* are also identified as syncytia generated by myoblast fusion (Klapper et al. 2002).

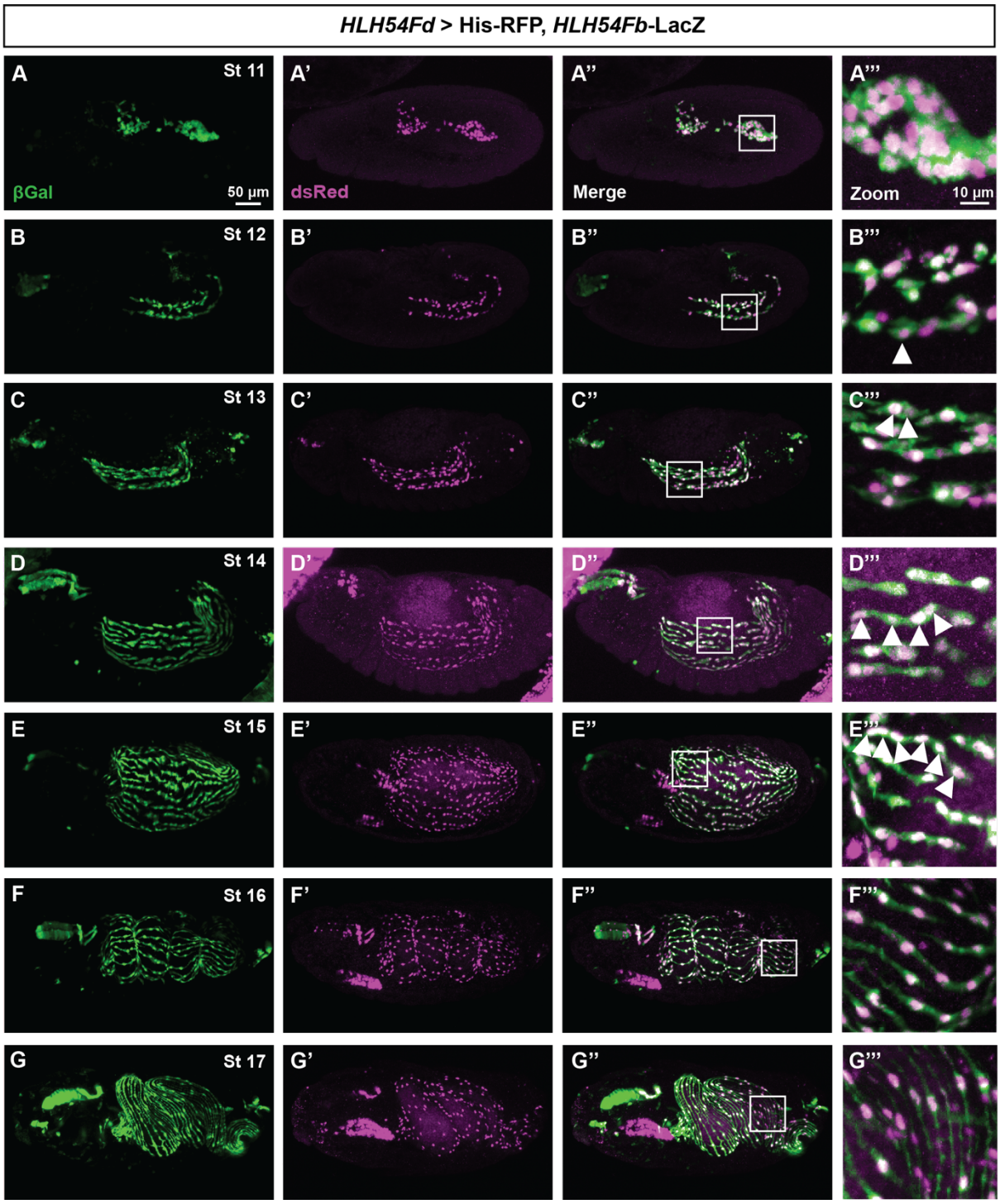

Fig. 14: The formation of syncytia within the developing LVMP cells.
Microscopy of *Drosophila* embryos from consecutive developing stages. (A-G) CVM and LVMP cells were marked in green by HLH54Fb-LazZ expression. (A'-G') Histone-RFP expressed in CVM and LVMP cells were

visualized by anti-dsRed staining in magenta. (A''-G'') Merged images. Until early stage 12, only one nuclea in the migrating CVM cells is detected (arrowhead in B'''). At stage 13, a subset of CVM cells differentiates into founder cells, and each fuses with one FCM from the TVM (binucleate cells are depicted by arrowheads in C'''). During stage 14, two to four nuclei are found in the migrating LVMP cells (arrowheads in D'''). At stage 15, most LVMP cells have five to six nuclei (arrowheads in E'''). At the end of embryogenesis, LVMP cells connect with neighboring cells and are stretched into long fibers (F-G'''). Squares mark the area enlarged in (A'''-G'''). The scale bar in (A) applies to (A-G''). The scale bar in (A''') applies to (A'''-G''').

The circular visceral muscles consist of binucleate syncytia and both FCs and FCMs develop within the TVM. By contrast, the longitudinal visceral muscles have six nuclei, and the myoblast fusion process involves one FC from the CVM and four to five FCMs from the TVM (Rudolf et al. 2014). The CVM-driver line *HLH54Fd*-Gal4 and the UAS-His-RFP, where RFR marks nuclear histones, make it possible to follow the number of nuclei in the differentiation process of the LVMP cells.

As shown in **Fig. 14**, during stage 12, migrating CVM cells are mononucleated (**Fig. 14**B'''). During late stages 12 to 13, upon cells are differentiated into FCs, the fusion step with FCMs is initiated, and the first group of binucleated cells is detectable (**Fig. 14**C'''). At early stage 14, most LVMP cells already have two to three nuclei, while at late stage 14, LVMP cells with three to four nuclei are dominant (**Fig. 14**D'''). At the end of the migration, five or six nuclei are often found in the LVMP cells (**Fig. 14**E'''). From late stage 15 onwards, the multinucleated LVMP cells are stretched. They connect with the anterior and posterior neighboring cells, forming long, thin fibers extending over the most distance of the midgut tube (**Fig. 14**F- G''').

2.2 Beat II expression pattern

Based on previous studies, *beat IIa* and *beat IIb* mRNA were transcribed in CVM cells, making them the only Beat members that show embryonic expression in non-neural tissues (Pipes et al. 2001; Ismat et al. 2010; Bae et al. 2017). To obtain more details about their expression patterns, fluorescence *in situ* hybridization and immunohistochemistry staining methods were utilized.

2.2.1 *beat IIa* is transcribed in CVM and LVMP cells

First, the *in situ* detection of *beat IIa* was performed in the w^{1118} embryos, which showed a promising expression in the CVM and LVMP cells. Thus, *HLH54F*-GFP embryos that express GFP in these cells were used for further *beat IIa in situ* detection (**Fig. 15**).

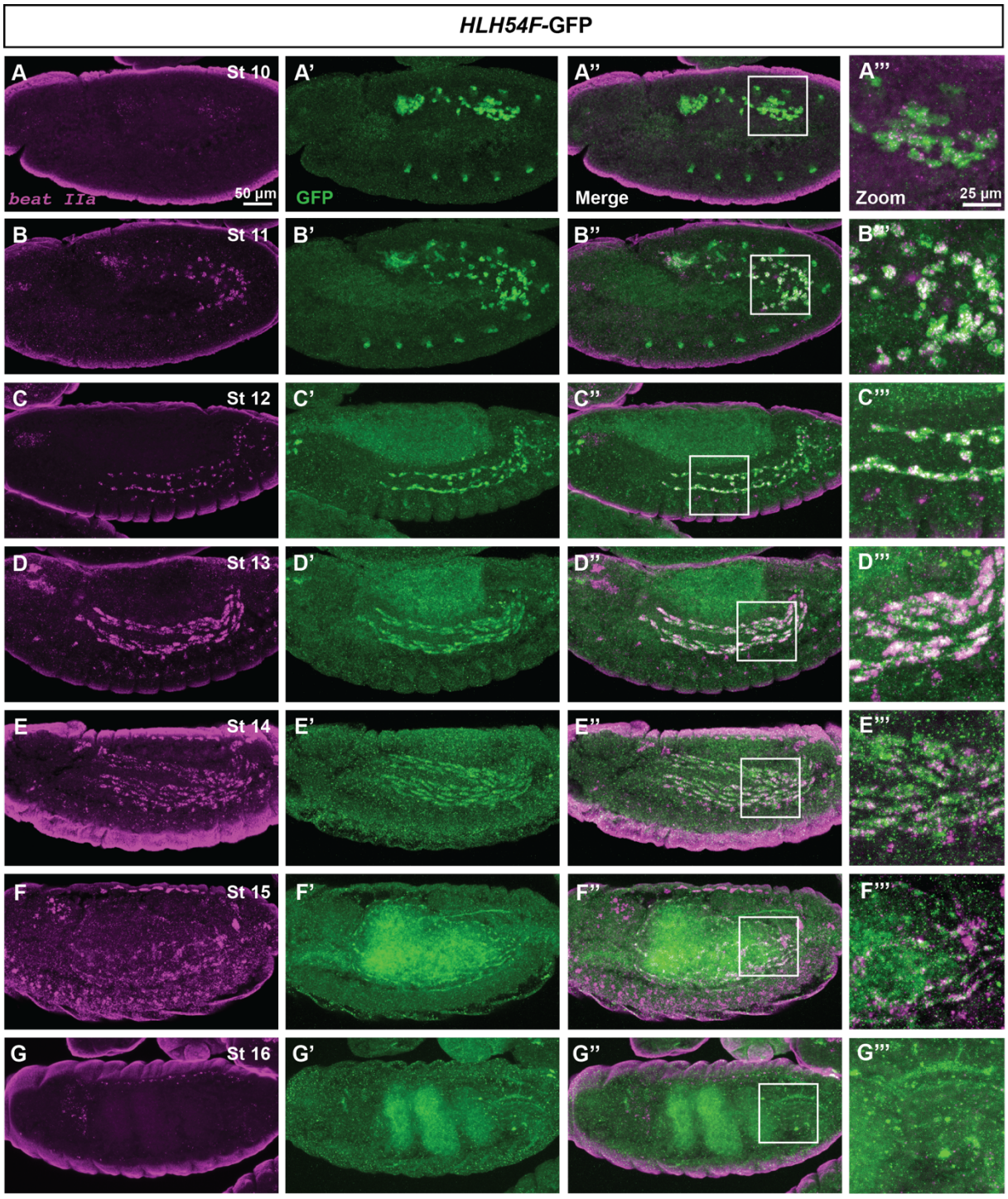

Fig. 15: Expression pattern of *beat IIa* mRNA during embryogenesis.
Images of *HLH54F*-GFP embryos that express GFP in CVM and LVMP cells (green) with *beat IIa in situ* probe (magenta). *beat IIa* mRNA is weakly detected in CVM cells at late stage 10 (A-A'''). The signal increases during the anterior CVM cell migration (B-C'''). At stages 13 and 14, when the LVMP cells are migrating dorsoventrally, the *beat IIa* transcription level is the strongest (D-E'''). After stage 14, the signal in LVMP cells decreases and is no longer detectable in LVM cells at stage 16. Squares mark areas enlarged in (A'''-G'''). The scale bar in (A) applies to (A-G''). The scale bar in (A''') applies to all enlarged images.

At stage 10, when CVM cells appear as a group at the posterior tip of the mesoderm, *beat IIa* mRNA is not detectable (data not shown). Until late stage 10, after the initiation of the CVM migration, *beat IIa* mRNA is weakly observed in a subset of CVM cells (**Fig. 15**A-A’’’). Then, the signal is enhanced in the CVM cells during the anterior migration (**Fig. 15**B-C’’’). From late stage 13 to 14, when the LVMP cells are derived and migrate dorsoventrally, *beat IIa* mRNA is strongly detected in the LVMP cells (**Fig. 15**D-E’’’). Afterward, the signal decreases in these cells and is no longer detectable at stage 16.

Of note, the LVMP and LVM cells after stage 15 are not well-stained by anti-GFP (**Fig. 15**F’, G’), perhaps because the anti-GFP staining was performed after the FISH, and for unknown reasons, the antibody staining was attenuated.

2.2.2 Beat IIa-GFP is detected in CVM and LVMP cells

The embryonic expression pattern of the Beat IIa protein was examined with the Beat IIa-GFP line (also known as Beat IIa::FlpTag; Carrier et al. 2023). The Beat IIa-GFP line was generated using the flippase-depend FlpTag approach. The FlpTag is a protein trap cassette with a GFP tag in the center. Upon insertion into the target gene, the GFP is stably integrated as an artificial exon (Fendl et al. 2020). Thus, the Beat IIa-GFP line can reveal the endogenous expression pattern of the Beat IIa protein.

To check if Beat IIa is expressed in CVM and LVMP cells, Beat IIa-GFP was crossed with *HLH54Fb*-CytoRFP, and their embryos were analyzed. As shown in **Fig. 16**, the GFP signal is detected in a group of cells at stage 11. However, these cells are not CVM cells due to the absence of overlap signals with the reporter line (**Fig. 16**A-A’’’, arrows indicate GFP-positive cells). Based on their localization, they might be pericardial precursors or somatic muscle precursors. From stage 12 on, Beat IIa-GFP signals appear in CVM cells (**Fig. 16**B-B’’’). When the LVMP cells are migrating dorsal-ventrally to cover the midgut, Beat IIa is strongly expressed in these cells (**Fig. 16**D-D’’’). Although its signal decreases later, it is constantly detected in the LVM cells until the end of embryogenesis (**Fig. 16**E- F’’’). In addition, Beat IIa-GFP seems expressed in the CNS (data not shown), some somatic muscles (**Fig. 16**F’, F’’, empty arrowheads), pericardial cells (**Fig. 16**F’, F’’, stars), and other unidentified tissues

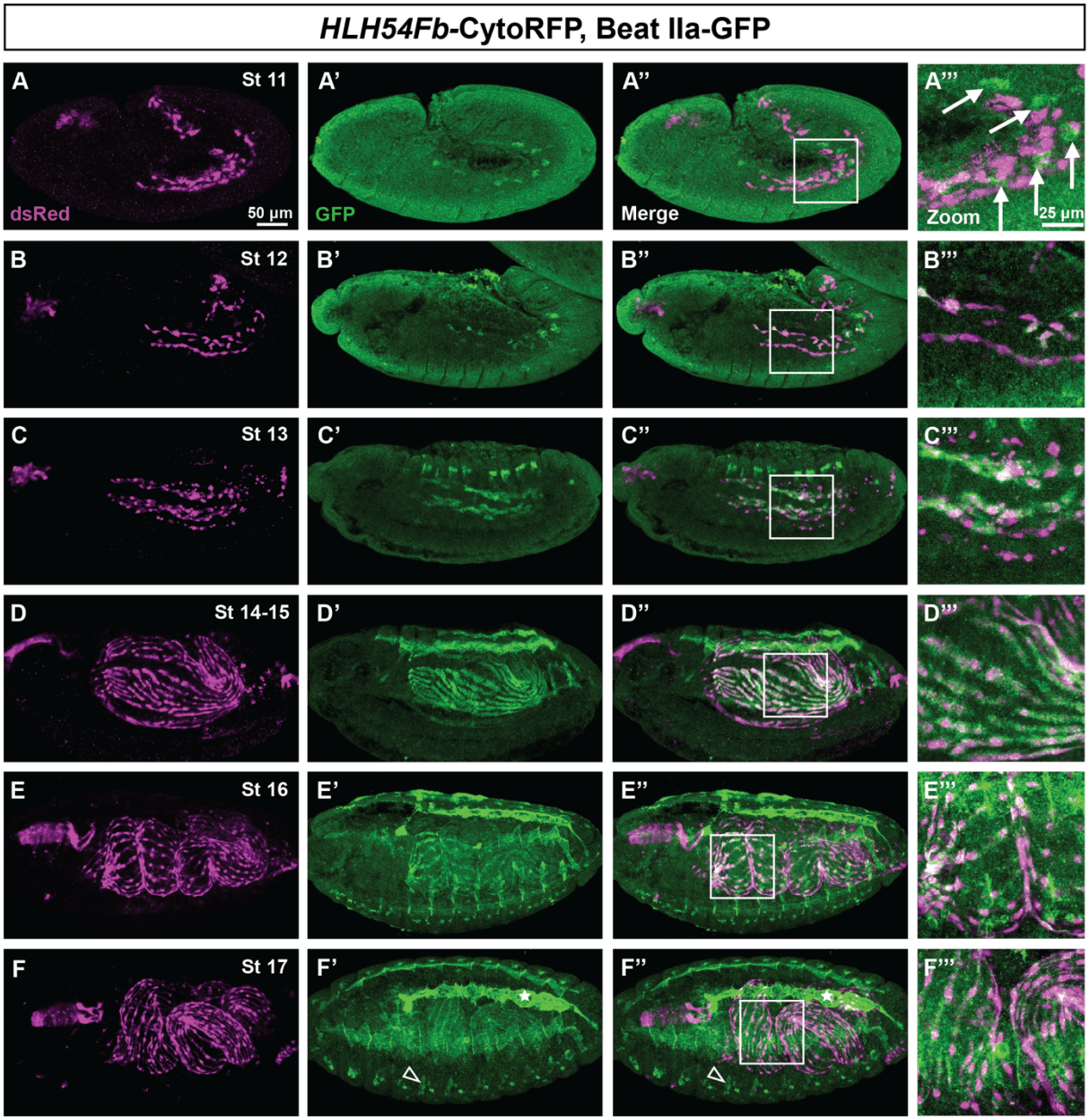

Fig. 16: Expression pattern of Beat IIa protein during embryogenesis.
Immunostainings of embryos expressing *HLH54Fb*-CytoRFP and Beat IIa-GFP. CVM and LVMP cells were marked with anti-dsRed in magenta (A-F). Beat IIa-expressing cells were marked green with anti-GFP (A'-F'). Merged images (A''-F''). At stage 11, although GFP signals are detected in cells near the migrating cohorts, most are not CVM cells due to a lack of overlap signals (arrows in A''' indicate GFP-positive cells). The Beat IIa-GFP is detectable in CVM cells from late stage 12, and its expression increases in CVM cells during stage 13 (B-C'''). At stages 14 and 15, Beat IIa is strongly expressed in the migrating LVMP cells (D-D'''). After stage 16, the signal decreases in LVM fibers but lasts until the end of the embryogenesis (E-F'''). Additionally, it seems that Beat IIa-GFP is expressed in the CNS (data not shown), some somatic muscles (empty arrowheads in F' and F''), pericardial cells (stars in F' and F''), and other unidentified tissues. Squared areas are enlarged in (A'''-F'''). The scale bar in (A) applies to (A-F''). The scale bar in (A''') applies to all enlarged images.

2.2.3 *beat IIb* is transcribed in CVM and LVMP cells

Based on previous research, Beat IIb seems also expressed in CVM cells. Thus, the detailed embryonic expression pattern of *beat IIb* was under examination.

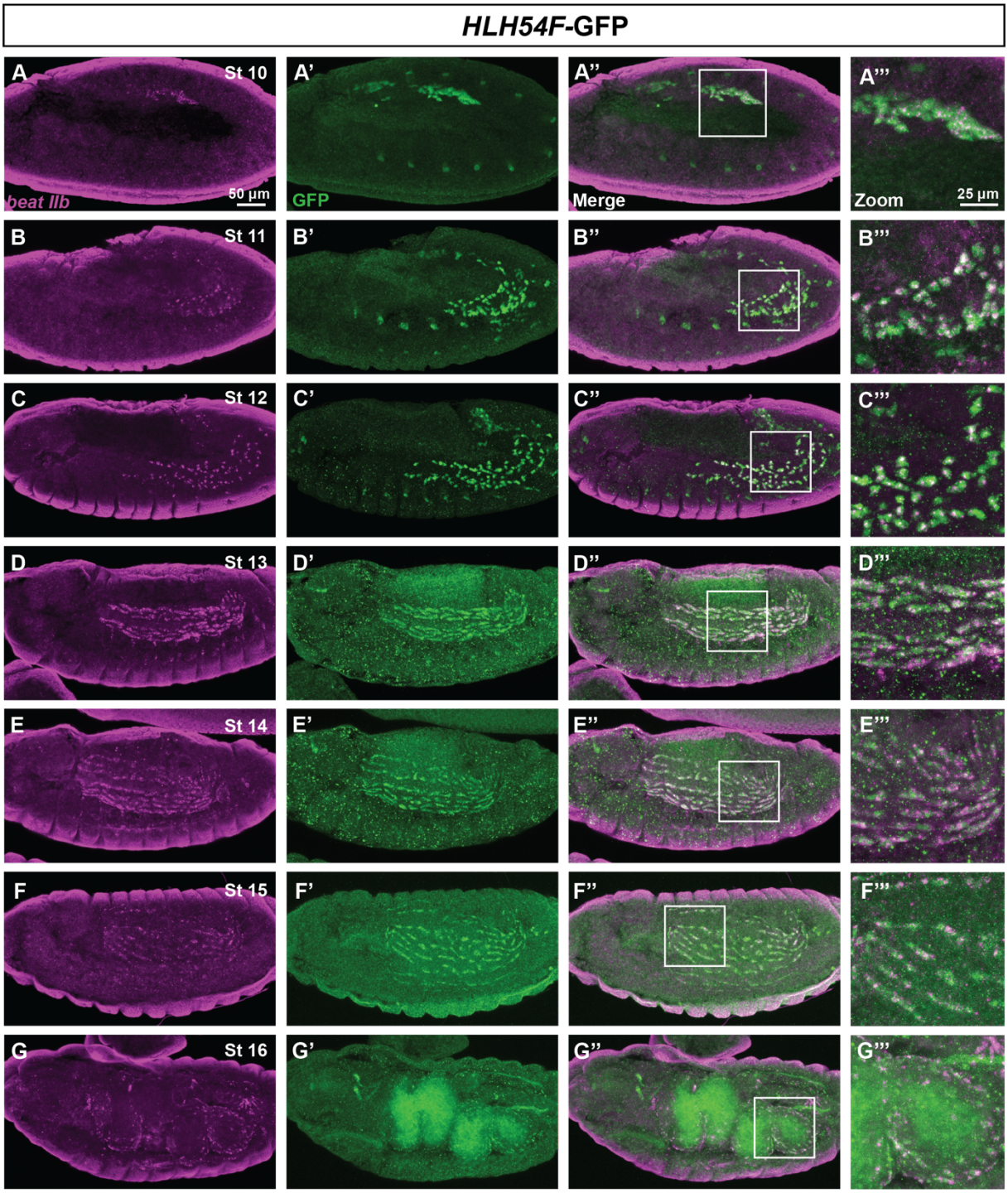

Fig. 17: Expression pattern of *beat IIb* mRNA during embryogenesis.
FISH of *beat IIb* (A-G) in *HLH54F*-GFP embryos where CVM and LVMP cells were visualized by anti-GFP staining (A'-G'). The right column shows the merged images (A''-G''). From stage 10 onward, *beat IIb* mRNA

is detected in the anteriorly migrating CVM cells (A-C’’’). At stages 13 and 14, the *beat IIb* transcription is strongly detected in the migrating LVMP cells (D-E’’’). Since stage 15, the signal in LVMP cells decreases but is still detectable at stage 16 in matured LVM cells (F-G’’’). Squares mark enlarged areas. The scale bar in (A) applies to (A-G’’). The scale bar in (A’’’) applies to all enlarged images.

HLH54F-GFP embryos were used for the FISH of *beat IIb*, followed by an anti-GFP antibody staining. As shown in **Fig. 17**, *beat IIb* mRNA in CVM cells is detectable from stage 10 (A-A’’’). Afterward, the transcription signal increases during the anterior CVM migration (B-C’’’), and the strongest signal is found at stages 13 to 15 during the dorsal-ventral migration of LVMP cells (D-E’’’). At stage 15, the *beat IIb* transcription level decreases. However, unlike *beat IIa,* which can not be detected at stage 16, *beat IIb* mRNA remains present in LVM cells (compare G’’’ in **Fig. 17** with G’’’ in **Fig. 15**).

2.2.4 Beat IIb-GFSTF is detected in CVM and LVMP cells

The GFP-tagged Beat IIb of the Beat IIb$^{MI03102\text{-}GFSTF.0}$ embryos (also known as Beat IIb-GFSTF; Nagarkar-Jaiswal, 2015) enables the investigation of the embryonic Beat IIb protein expression pattern. To define its expression in CVM and LVMP cells, Beat IIb$^{MI03102\text{-}GFSTF.0}$ were crossed with *HLH54Fb*-CytoRFP flies, and their embryos were immuno-stained.

As shown in **Fig. 18**, anti-dsRed indicates CVM and LVMP cells (A-G), and anti-GFP staining shows the Beat IIb-GFSTF expressing cells (A’-G’). According to the merged images, Beat IIb can be detected in CVM cells from stage 10 and its expression lasts throughout the migration and differentiation process until stage 17 in matured LVM fibers. Besides this, at stages 13 and 14, Beat IIb is also found in the amino serosa (**Fig. 18**C’, C’’, arrows), some somatic muscle precursor cells (**Fig. 18**C’, C’’, arrowheads), and other unidentified tissues (perhaps head mesoderm, **Fig. 18**C’, C’’, empty arrowheads). At stage 17, Beat IIb is additionally detected in the CNS (**Fig. 18** G’, G’’, arrows) and some somatic muscles (**Fig. 18** G’, G’’, arrowheads). This expression pattern is consistent with its mRNA detection (compare **Fig. 18** with **Fig. 17**).

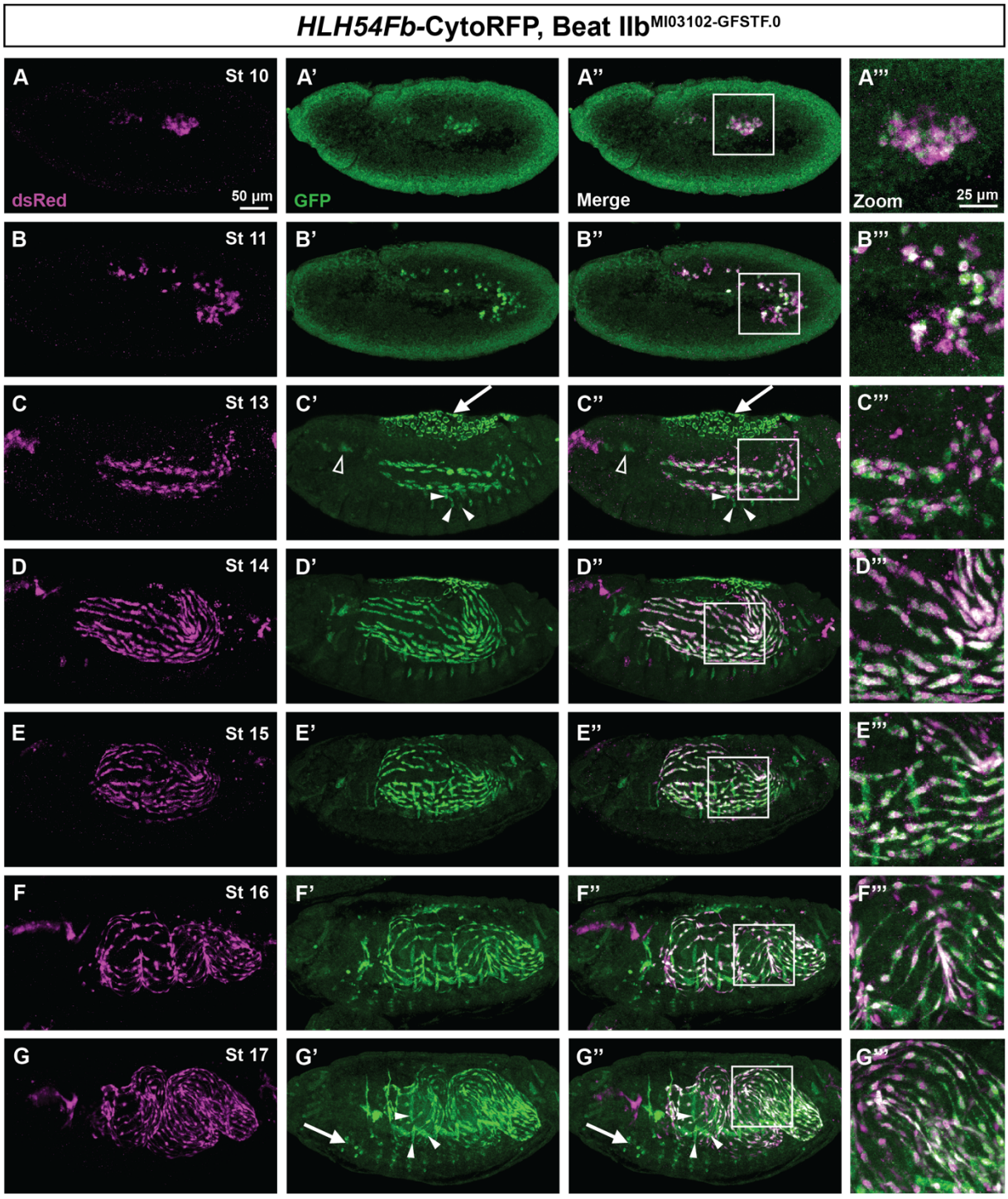

Fig. 18: Expression pattern of Beat IIb protein during embryogenesis.
Confocal microscopy of embryos carrying *HLH54Fb*-CytoRFP and Beat IIb$^{MI03102\text{-}GFSTF.0}$. CVM and LVMP cells were stained by anti-dsRed (A-G). Beat IIb-expressing cells were visualized by anti-GFP (A'-G'). Beat IIb is detectable in CVM cells at stage 10 (A-A'''). At stage 13, Beat IIb is found not only in CVM cells but also in amnio serosa (C' and C'', arrows), some somatic muscle precursor cells (C' and C'', arrowheads), and other unidentified tissues (C' and C'', empty arrowheads). Afterward, Beat IIb expression is constantly detected in the whole migration and differentiation process of LVMP cells (D-F'''). At stage 17, Beat IIb is expressed in the LVM fibers, some somatic muscles (arrowheads in G' and G''), and the CNS (arrows in G' and G''). Squares mark enlarged areas. The scale bar in (A) applies to (A-G''). The scale bar in (A''') applies to all enlarged images.

Based on the above observations, it is interesting to notice that *beat IIa* and *beat IIb* exhibit a similar embryonic expression pattern. To investigate this more closely, Beat IIb-GFSTF embryos were used to perform FISH for *beat IIa* (**Fig. 19**). As shown in the merged images, both signals are detected in CVM and LVMP cells, as well as some somatic muscle precursors (**Fig. 19**C-C", arrowheads), and some unidentified tissues (**Fig. 19**C-C", empty arrowheads). The difference is that Beat IIb is expressed in the amnio serosa (**Fig. 19**C', C", arrows), while *beat IIa* mRNA is found in other cell types (**Fig. 19**C', C", stars, probably the pericardial cells). In addition, *beat IIa* expression in the CNS is detectable in more cells than Beat IIb (**Fig. 19**, compare arrows in E and E').

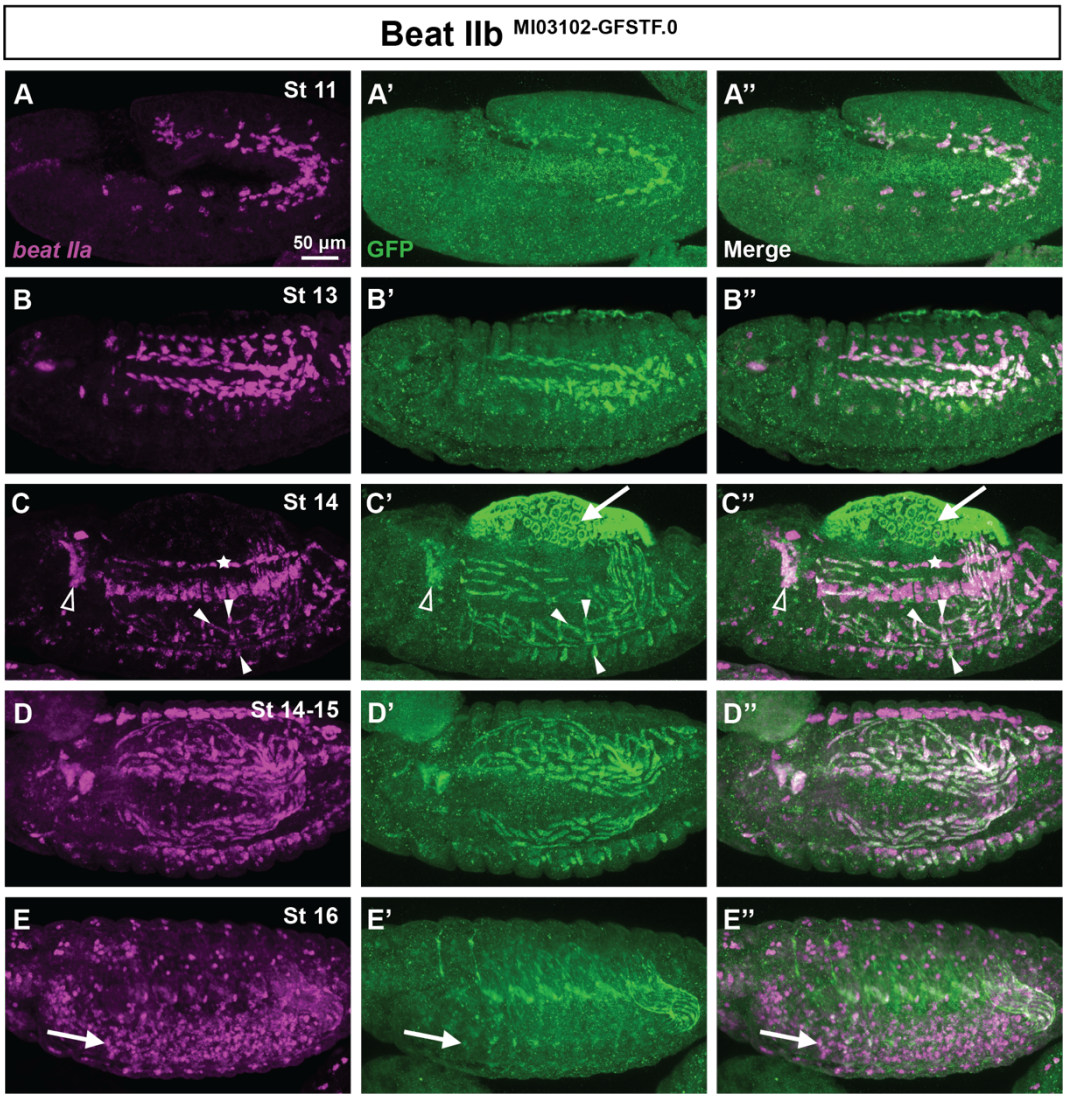

Fig. 19: Embryonic expression patterns of *beat IIa* and *beat IIb* are similar but not identical.
Microscopy images of embryos from Beat IIb$^{MI03102\text{-}GFSTF.0}$ (green) with the FISH of *beat IIa* (magenta). As shown in merged images (A''-E''), both *beat IIa* mRNA and Beat IIb are found in CVM and LVMP. Besides this, their signals co-localize in somatic muscle precursor cells (arrowheads in C-C'') and some unidentified tissues (empty arrowheads in C-C''). Additionally, *beat IIa* mRNA is found in pericardial-like cells (stars in C and C''), and Beat IIb is detected in the amnio serosa (arrows in C' and C''). The expression of *beat IIa* is broader than Beat IIb in the CNS (compare arrows in E with E'). The scale bar in (A) applies to all images.

2.3 Beat II protein structure

As both Beat II proteins are expressed in CVM and LVMP cells, it is interesting to investigate whether they exert function in the migration and differentiation processes of these cells. To this end, predicted Beat II protein structures were first analyzed, and then various generated or collected mutants and transgenic flies were under investigation.

2.3.1 Beat II protein structure prediction

Beat IIa and Beat IIb protein structures were predicted using different programs (see **Table 12**). Beat IIa consists of 431 amino acids, including two predicted transmembrane domains, through which the protein is inserted in the cell membrane, and the central part is located outside the cell (**Fig. 20**A, B). Beat IIb is composed of 404 amino acids and is predicted to be a glycosylphosphatidylinositol (GPI)-anchored protein with a signal peptide at the N-terminus and a hydrophobic signal sequence at the C-terminus (**Fig. 20**C, D). A GPI anchor is a posttranslational modification that involves the attachment of a glycolipid to the C-terminus of a protein. After processing in the endoplasmic reticulum and Golgi apparatus, the matured GPI-anchored proteins are transported to the cell membrane (Kinoshita 2016).

Additionally, the SMART (Letunic et al. 2020; de Castro et al. 2006) predict only one immunoglobulin (IG) domain in both Beat IIa and Beat IIb (**Fig. 20**A, C). However, two potential IG domains are displayed using AlphaFold (Evans et al. 2021) (**Fig. 20**B, D). The predicted IG sequences of Beat II were thus aligned with the known Beat Ia for comparison. As shown in the alignments, the IG1 domains, predicted by both the SMART and AlphaFold, are highly conserved in Beat Ia, Beat IIa, and Beat IIb. The cysteines highlighted in yellow are critical for forming an intramolecular disulfide bond to stabilize the β-sheets (**Fig. 20**E). These essential cysteines are also conserved in the second potential IG domain predicted by AlphaFold (highlighted in yellow in **Fig. 20**F). However, additional amino acids (boxed red in **Fig. 20**F) are depicted between the two cysteines in Beat IIa and Beat IIb, forming a loop between the β-strands (shown by arrowheads in **Fig. 20**B, D).

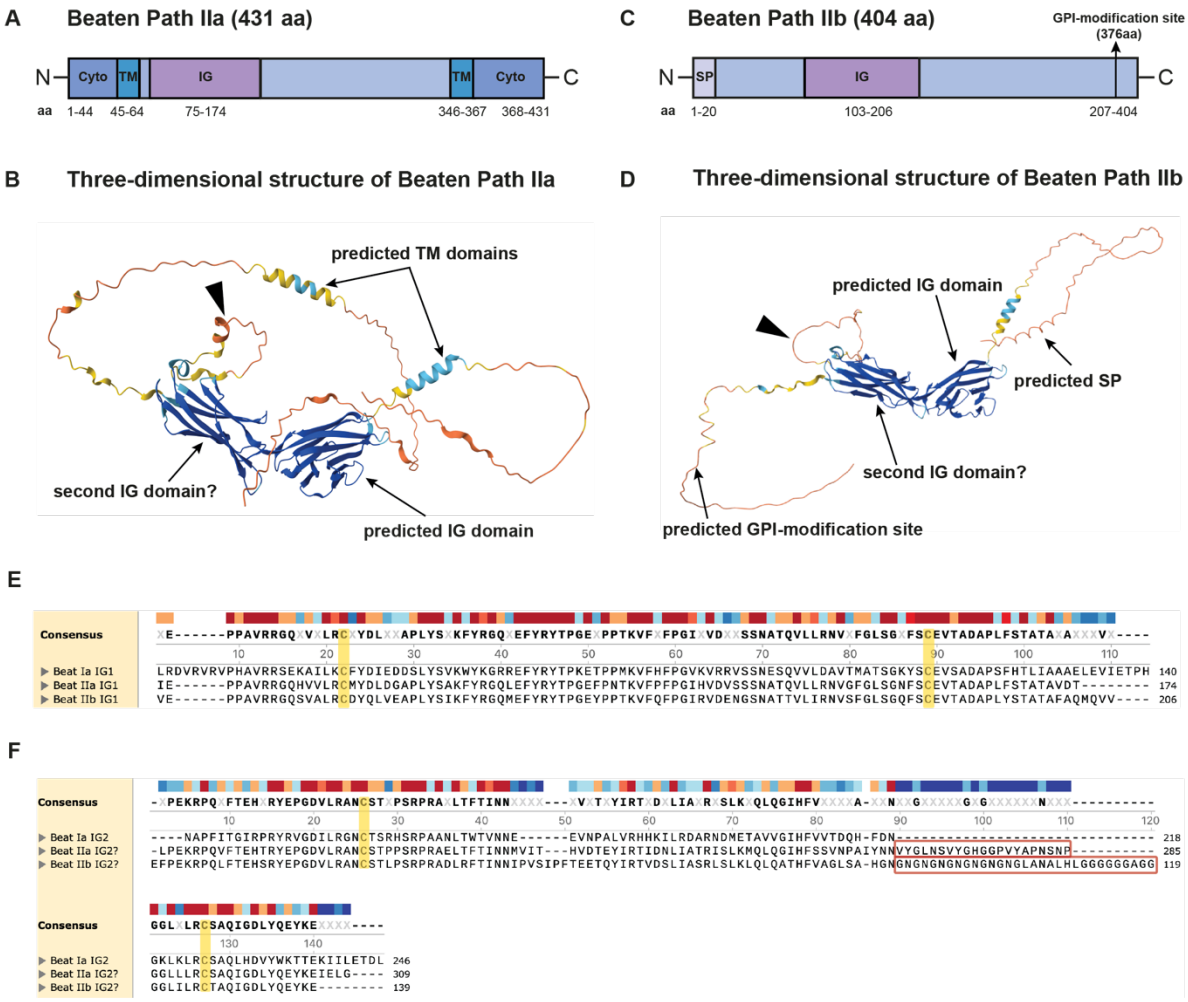

Fig. 20: Protein structural analysis of Beat IIa and Beat IIb.
(A) Beat IIa protein consists of 431 amino acids with two predicted transmembrane domains. The SMART program predicts only one IG domain, while with the three-dimensional structure shown by AlphaFold (B), there is a second potential IG domain. (C) Beat IIb contains 404 amino acids and is predicted to be a GPI-anchored protein, with a signal peptide predicted at the N-terminus and a hydrophobic signal sequence at the C-terminus, which are essential for the posttranslational processes and translocation to the cell surface. Similar to Beat IIa, only one IG domain is predicted by SMART, but another IG domain is displayed by the AlphaFold prediction (D). (E) Alignment of the IG domain (IG1) predicted by both the SMART and AlphaFold of Beat Ia and Beat II. Sequences are highly conserved, and essential cysteines are highlighted in yellow. (F) Alignment of the second IG domain (IG2) predicted by the AlphaFold of Beat Ia and Beat II. Two cysteines are conserved, while additional sequences in Beat II form a loop between the β-sheets (boxed red in F, and the loops are depicted by arrowheads in B and D). IG: immunoglobulin, TM: transmembrane, Cyto: cytoplasmic domain, aa: amino acid.

2.3.2 Creation of *beat II* mutants and fusion constructs

Different mutations and constructs were created or collected to perform a functional analysis of *beat II*. The *beat IIa*$^{+2}$ and *beat IIb*$^{\Delta 14}$ single mutants were kind gifts (Osaka et al. 2024). In the *beat IIa*$^{+2}$ mutant, two additional base pairs are inserted, which results in an earlier stop codon after 59 amino acids located in the transmembrane domain. In the *beat IIb*$^{\Delta 14}$ mutant, due to a loss of 14 base pairs, a stop codon is induced after 49 amino acids before the predicted IG

domain. In addition, as *beat IIa* and *beat IIb* have similar rates of evolution, and both are expressed in CVM and LVMP cells, their functions might be redundant. A double mutant in which both genes are knocked out is thus critical for the functional analysis. Due to their close gene locus, the double mutant was created using the CRISPR/Cas9 technique instead of recombination. A *beat IIb* gRNA, which targets the position before the predicted IG domain, was injected with a Cas9 helper into the *beat IIa*$^{+2}$ mutant embryos. After sequencing, several positive candidates were characterized, and the *beat IIa*$^{+2}$*beat IIb*^{L88*} was used in this study (**Fig. 21**A, B). Moreover, a deficiency line Df(3R)ED5780, in which both genes are deleted, was given as a gift from Manfred Frasch's group (**Fig. 21**C). Furthermore, C-terminal GFP/mCherrry-tagged constructs were cloned and used in the cell-cell aggregation assay and rescue experiments (**Fig. 21**D-F). As Beat IIb might be a GPI-anchored protein, in which the integrity of the C-terminus is crucial for the membrane attachment, a construct where GFP is inserted at the N-terminus was additionally generated (**Fig. 21**G).

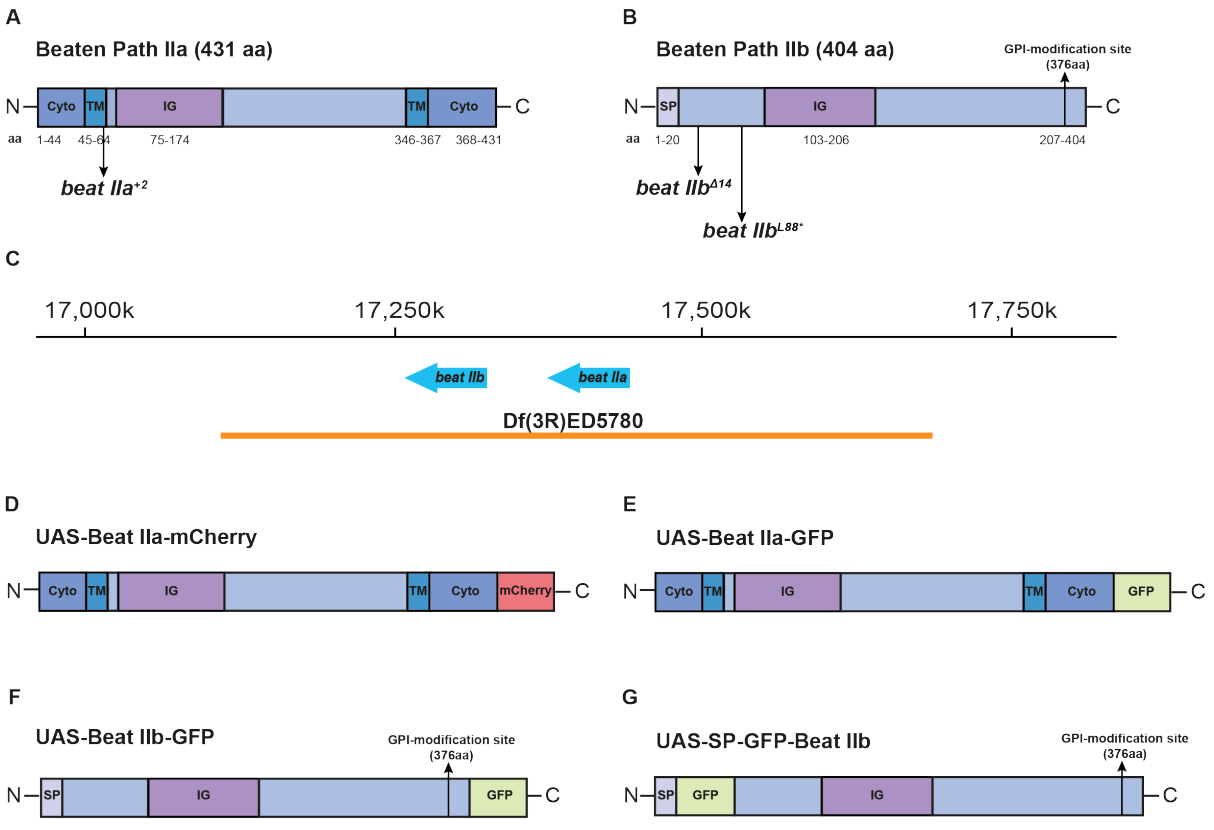

Fig. 21: Schematic overview of the *beat II* mutants and constructs.
(A) *beat IIa*$^{+2}$ used in this research exhibits an insertion with two base pairs, resulting in frameshifting and a stop codon in the first predicted transmembrane domain. (B) *beat IIb*$^{\Delta 14}$ exhibits a deletion of 14 base pairs, and its protein ends shortly after the predicted signal peptide. In this work, a *beat II* double mutant was created by injecting *beat IIb* gRNA and Cas9 helper into the *beat IIa*$^{+2}$ embryos. *beat IIb*^{L88*}, which carries an earlier stop codon at position 89, was thus combined with *beat IIa*$^{+2}$ and named *beat IIa*$^{+2}$ *beat IIb*^{L88*}. (C) Df(3R) ED5780 contains a deletion that includes both *beat IIa* and *beat IIb* genes. (D-G): Different GFP- or mCherry-tagged Beat II UAS constructs. IG: immunoglobulin, TM: transmembrane, Cyto: cytoplasmic domain, aa: amino acid.

2.4 *beat II* mutant phenotype

The *beat II* mutants and deficiency lines enable the investigation of whether *beat II* genes exert functions in the migration and differentiation processes of CVM and LVMP cells.

2.4.1 LVMP cell migration shows minor defects in *beat II* single mutants

In order to rule out potential effects of mutations in closely located genes, *beat II* single mutants were crossed over the *beat II* deficiency (Df(3R)ED5780), and their embryos were analyzed (**Fig. 22**).

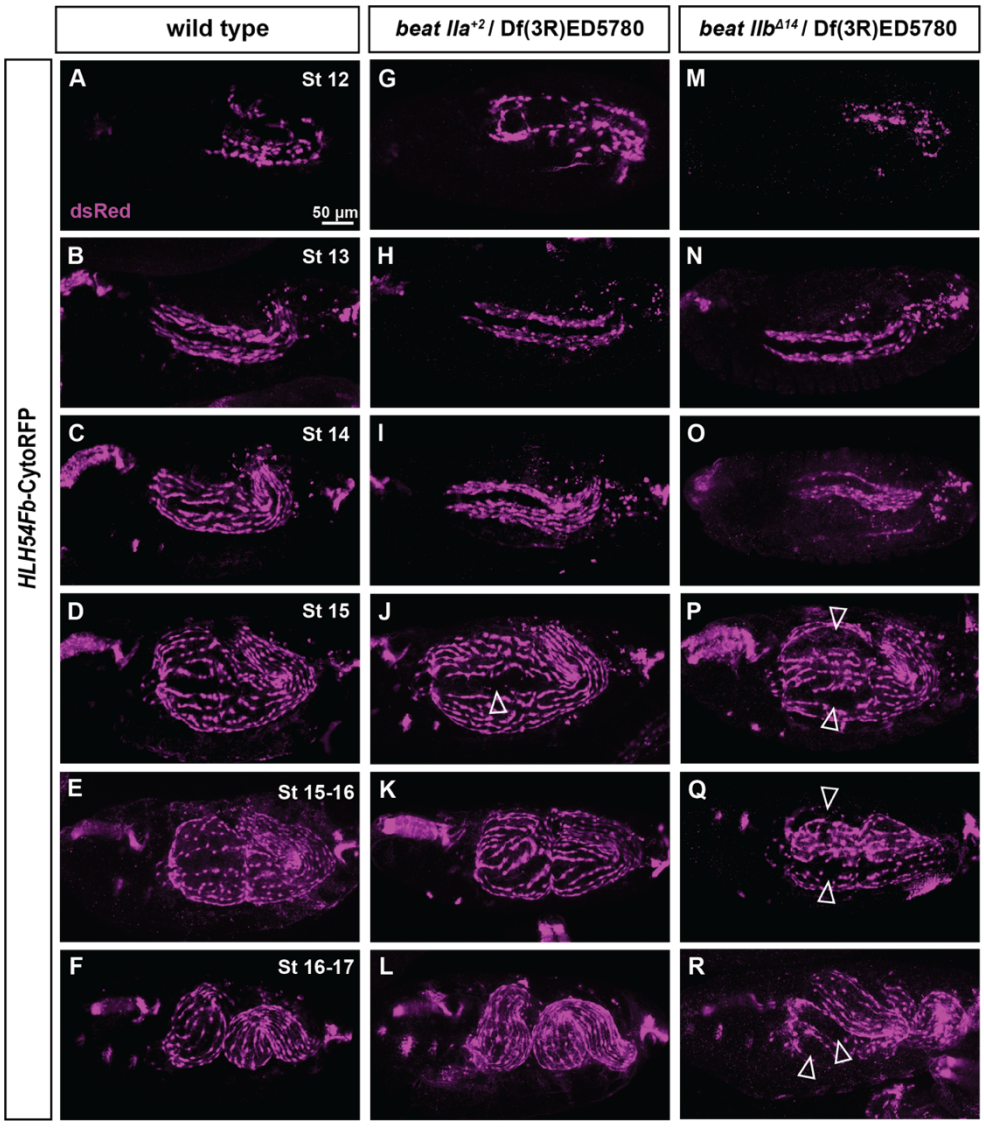

Fig. 22: The dispersal of LVMP cells in *beat II* single mutants is slightly aberrant.
Immunostainings of *Drosophila* embryos with anti-dsRed antibody. (A-F) Wild-type embryos showing the regular migration pattern of CVM and LVMP cells. At stage 15, LVMP cells are evenly dispersed around the midgut (D).

(G-R) Transheterozygous *beat IIa* or *beat IIb* mutant over *beat II* deficiency embryos. No apparent abnormalities are observed from stage 10 to stage 14. However, from stage 14 to 15, LVMP cells can not fully ensheath the whole midgut (areas lacking LVMP cells are indicated by empty arrowheads in J and P). This phenotype is more severe in the *beat IIb*$^{\Delta 14}$ (compare P with D and J). After stage 15, there are no obvious defects in the *beat IIa*$^{+2}$, but gaps without LVMP cells remain in the *beat IIb*$^{\Delta 14}$ (empty arrowheads in Q and R). The scale bar in (A) applies to all images.

Up to stage 14, no obvious defects are observed. Only until the transition phase from stage 14 to 15, the arrangement of LVMP cells is slightly aberrant. Rather than being evenly aligned to ensheath the whole midgut, LVMP cells in *beat II* single mutants can not fully cover the central gap between the dorsal and ventral stipe (**Fig. 22**J, P, gaps are indicated by empty arrowheads). Interestingly, this phenotype is more evident in the *beat IIb* mutant. At stage 16, no significant abnormalities are found in the *beat IIa*$^{+2}$ embryos, while in *beat IIb*$^{\Delta 14}$, gaps devoid of LVM fibers are still observed (**Fig. 22**Q, R). It seems that the time used for the dispersal of LVMP cells over the midgut is slightly prolonged in the absence of Beat IIa, and both the speed and distribution of the LVMP cells are affected due to a loss of Beat IIb.

2.4.2 CVM and LVMP cell migration is severely affected in *beat II* double mutant

As mentioned, the functions of *beat IIa* and *beat IIb* may be redundant. Thus, a *beat II* double mutant (*beat IIa*$^{+2}$*beat IIb*^{L88*}) and the Df(3R)ED5780 line deleting both genes were analyzed. In **Fig. 23,** embryos carrying *HLH54Fb*-CytoRFP were immunostained with anti-dsRed as a control (A-F), and the same marker was stained in transheterozygous *beat II* double mutant (G-L) and homozygous Df(3R)ED5780 (M-R) embryos.

CVM cells can initiate the anterior migration in the *beat II* double mutant embryos as in the wild type (**Fig. 23**G). At stage 13, although the CVM cells at the front do reach their destinations, cells are more densely grouped compared to the controls, where cells are aligned in a loose cell stream (**Fig. 23**, compare H with B). Beginning with stage 14, more severe migration defects are observed as long as LVMP cells initiate the dorsal-ventral migration. The morphology and orientation of LVMP cells are severely disrupted. These cells are no longer orientated in an anterior-posterior direction. Their migratory path is irregular, and many show roundish and shrunken cell shapes, typical characteristics of dying cells (**Fig. 23**I, arrows). At stage 15, when LVMP cells should have completed the dispersal around the entire midgut, there are still gaps that are not covered by LVMP cells in the *beat II* double mutant (**Fig. 23**J, empty arrowheads).

At stage 16, the midgut constrictions appear as the wild type (**Fig. 23**, compare arrows in K and E), but areas lacking LVMP cells are still present (**Fig. 23**K, empty arrowheads). By the end of embryogenesis, most longitudinal fibers are not evenly distributed, and large spaces are devoid of LVM fibers (**Fig. 23**L, empty arrowheads).

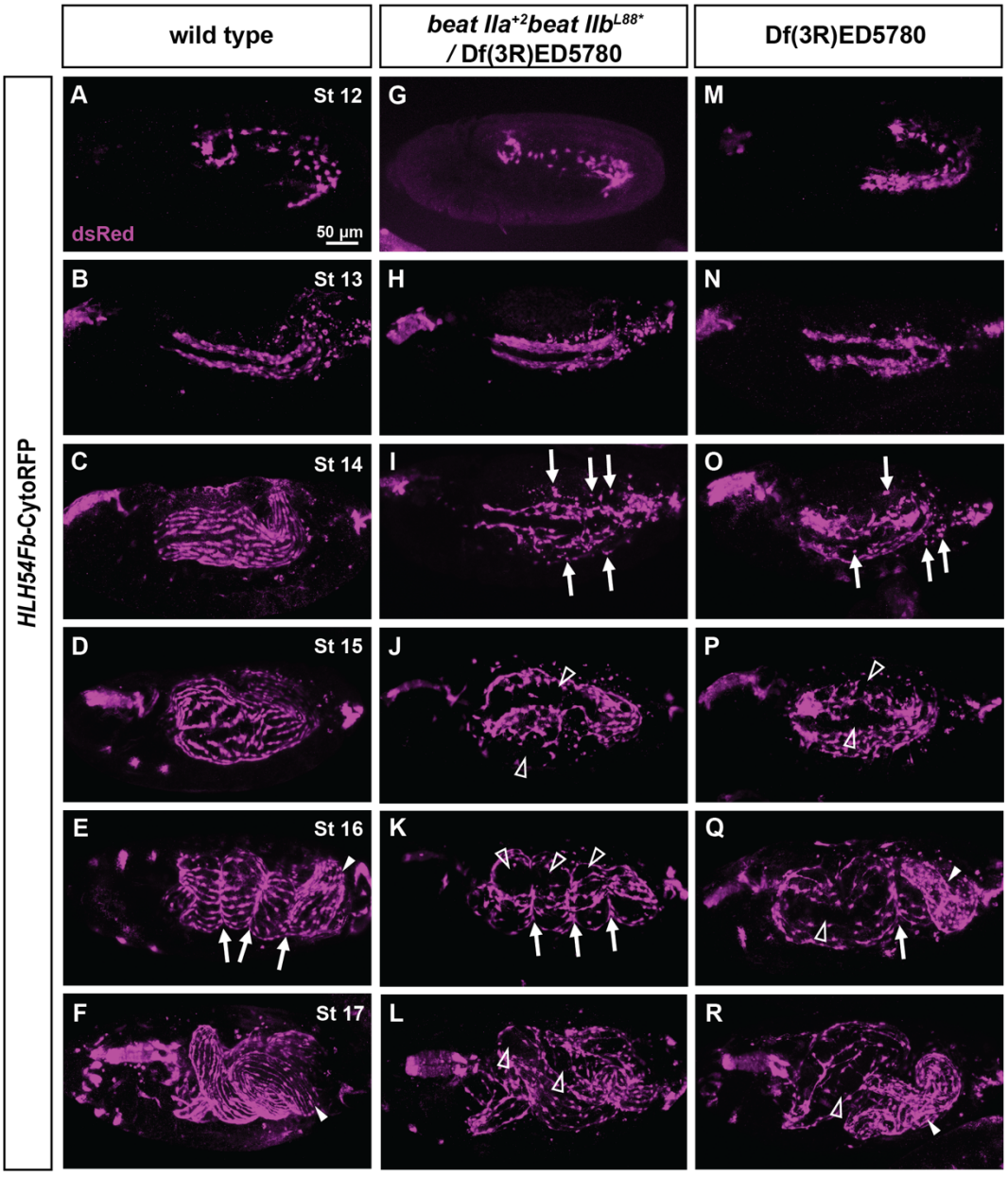

Fig. 23: Severe migration defects in *beat II* mutant and deficient embryos.
Immunostainings of *Drosophila* embryos with anti-dsRed antibody. (A-F) *HLH54Fb*-CytoRFP embryos showring regular CVM and LVMP cell migration. (G-L) Transheterozygous *beat II* double mutant over Df(3R)ED5780 embryos. Although the CVM cells can initiate the anterior migration and reach the foregut-midgut transition as in controls, cells are more densely connected instead of migrating in a loose cell stream (compare H with B). Many cells display abnormal cell morphology (arrows in I) and orientation. At stage 15, LVMP cells failed to cover the

entire midgut (the empty arrowheads in J indicate the gaps). At stage 16, the midgut constrictions form normally (compare arrows in K and E) but still contain areas lacking LVMP cells (empty arrowheads in K). By the end of embryogenesis, LVM fibers are not evenly distributed, leaving large spaces devoid of longitudinal muscles (empty arrowheads in L). (M-R) Homozygous *beat II* deficient embryos. A similar but slightly stronger phenotype is detected. At stage 16, the midgut constrictions are altered, especially in the anterior and middle regions (compare arrows in Q with E). By the end of embryogenesis, LVM cells at the posterior midgut seem denser than the control (compare arrowheads in Q and R with E and F) while leaving large spaces lacking longitudinal muscles (empty arrowheads in Q and R). The scale bar in (A) applies to all images.

The embryos carrying a homozygous *beat II* deficiency exhibit a similar but slightly stronger phenotype than the *beat II* mutant. At stage 16, constrictions in the front and middle parts of the midgut are missing (**Fig. 23**, compare arrows in Q with E). By stage 17, LVM cells at the posterior midgut seem denser than controls (**Fig. 23**, compare arrowheads in Q and R with D and F), while leaving space without LVM fibers in the front and middle midgut (**Fig. 23**R, empty arrowhead).

2.5 Restored Beat IIa rescues the *beat II* mutant phenotype

To verify the function of *beat II* in the CVM and LVMP cell migration, a UAS-Beat IIa-Cherry construct was generated and used in the rescue experiment. In this experiment, homozygous Df(3R)ED5780 embryos served as the control group, in which the CVM and LVMP migration was severely disrupted (**Fig. 24**A-F). Under the control of the *HLH54Fd*-Gal4 driver, Beat IIa-Cherry was overexpressed in CVM and LVMP cells in the homozygous Df(3R)ED5780 embryos and visualized by the anti-dsRed staining (**Fig. 24**G-L”).

With the overexpression of Beat IIa in CVM and LVMP cells, the mutant phenotype of the deficiency line is strongly rescued (**Fig. 24**, compare G-L with A-F). At stage 13, when the anterior migration is completed, cells are more organized and arranged stream-like rather than connected and grouped (**Fig. 24**, compare I with C). During stages 14-15, although there are still some gaps that are not covered, LVMP cells migrate in a more regular pattern, and fewer cells display irregular cell morphology (**Fig. 24**, compare J-K with D-E). At the later stage, more LVMP cells are differentiated, covering most of the surface of the midgut (**Fig. 24**, compare L with F). In addition, this rescued phenotype is similar to the *beat IIb* single mutant phenotype (compare G-L in **Fig. 24** with M-R in **Fig. 22**).

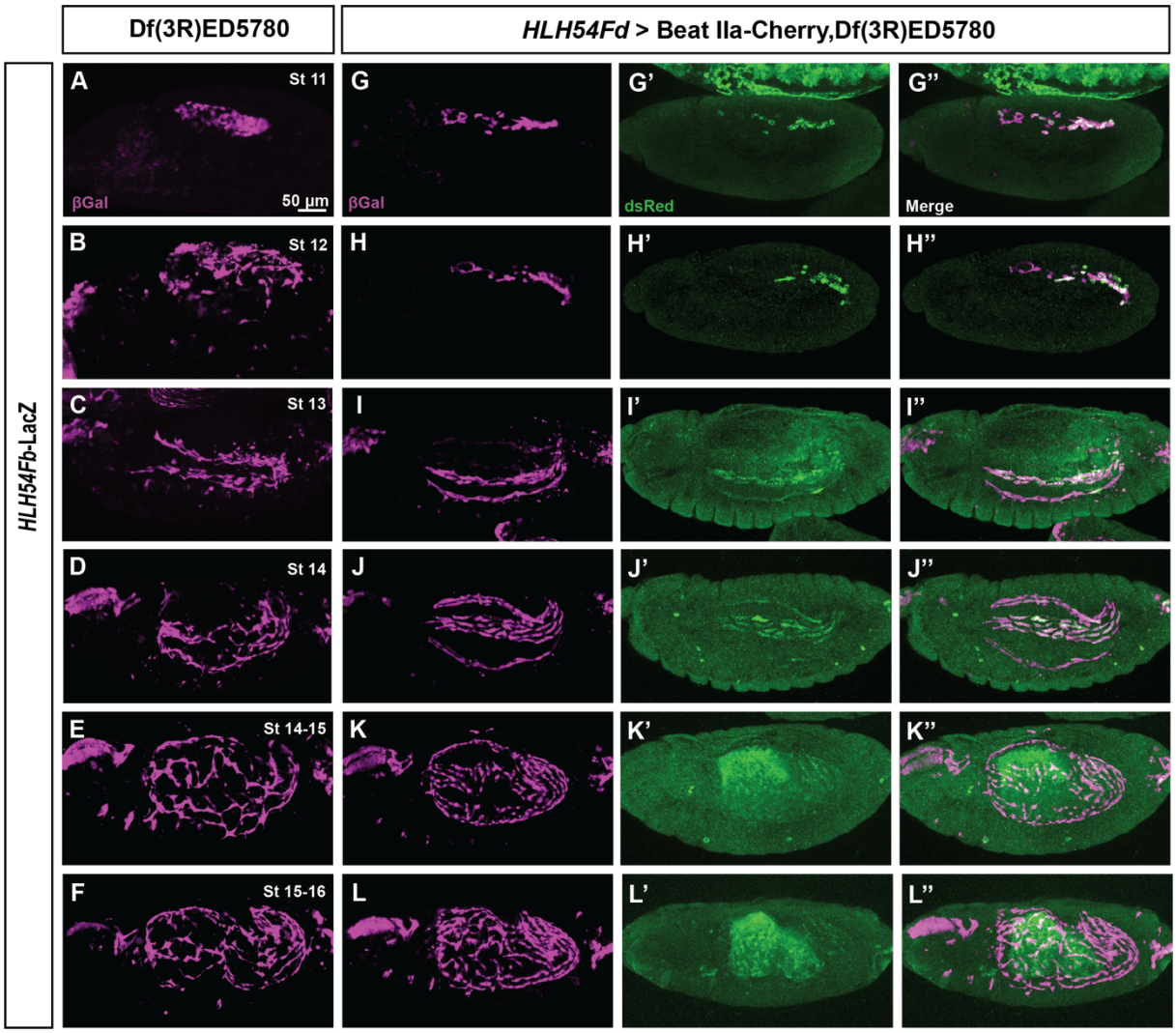

Fig. 24: Restored Beat IIa in CVM and LVMP cells rescues the *beat II* mutant phenotype.
Confocal images of CVM and LVMP cells visualized by the anti-βGal antibody staining. Homozygous Df(3R)ED5780 embryos were shown as controls (A-F). Beat IIa-Cherry was overexpressed by *HLH54Fd*-Gal4 in CVM and LVMP cells (G'-H'). When compared with the controls, the *beat II* mutant phenotype is rescued by the restored Beat IIa to a large degree (compare G-L with A-F). At stages 11-13, the migrating CVM cells are arranged stream-like, while cells are often grouped in the deficiency. Subsequently, the LVMP cells show a more regular migration pattern than the control group. At stages 15-16, most areas of the midgut are covered by LVMP cells. The scale bar in (A) applies to all images.

2.6 LVM fibers exhibit defects in *beat II* mutant L3 larvae

The viability of *beat II* mutant larvae enables examining the number and morphogenesis of LVM fibers in L3 larvae. Midgut of the L3 larvae from w^{1118} and *beat II* mutants were isolated and stained with phalloidin. As phalloidin selectively binds filamentous actin, the visceral muscle fibers were thus visualized. The number and the width of the LVM fibers were under examination.

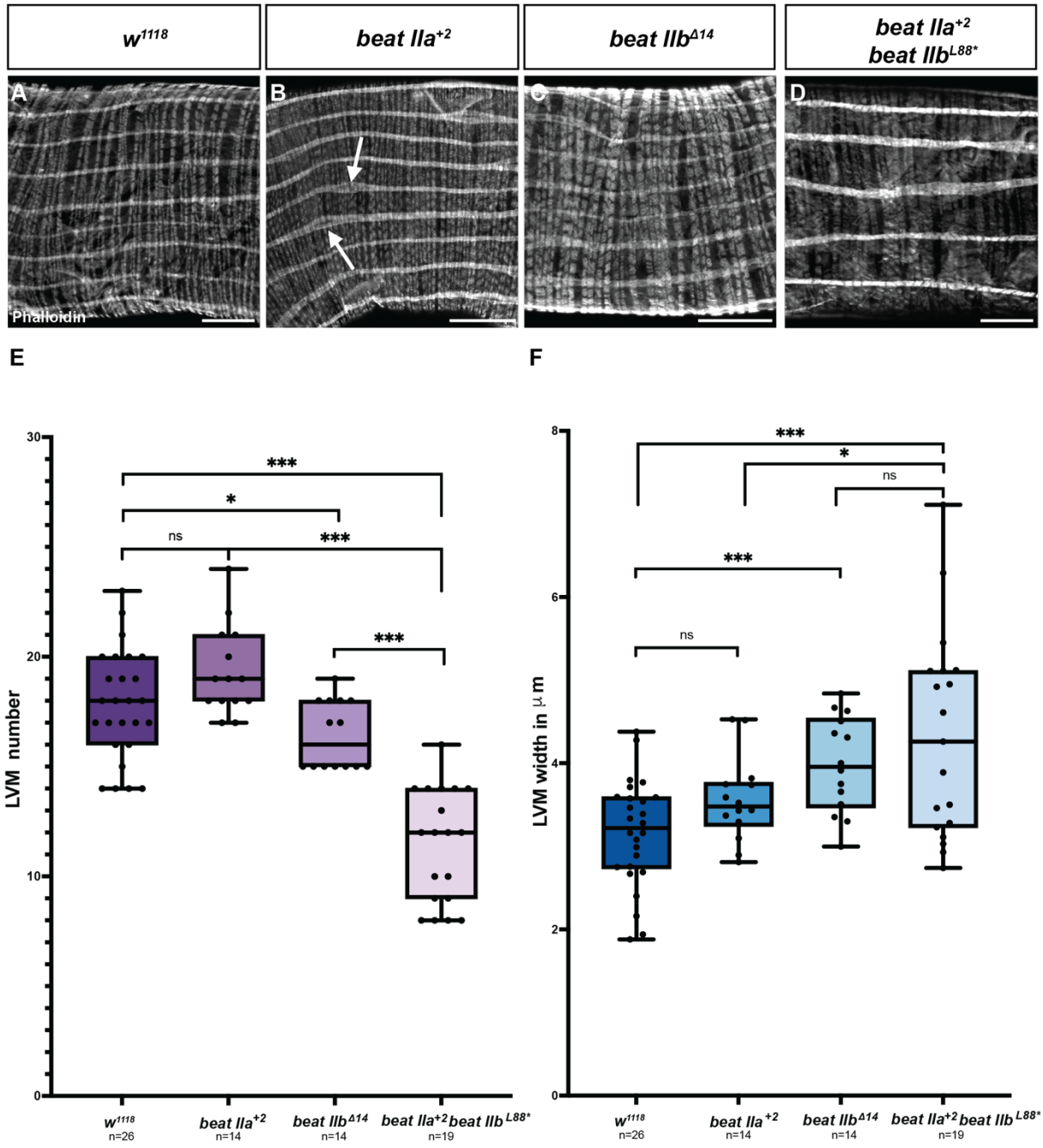

Fig. 25: LVM fibers in the L3 larvae of *w*^{1118} and *beat II* mutants.
(A-D) Confocal images of randomly picked third-instar larvae of *w*^{1118} and *beat II* mutants. LVM fibers were visualized by Phalloidin. Arrows in (B) indicate abnormal parts with enlargements and space in the center. (E) Statistic analysis of LVM fiber number. In *w*^{1118}, around 18 longitudinal fibers are observed on both sides of the midgut. The number in the homozygous *beat IIa*$^{+2}$ larvae shows no significant difference from the control. However, it decreases to 16 in the *beat IIb*$^{\Delta 14}$ and 12 in the *beat IIa*$^{+2}$*beat IIb*^{L88*} double mutant larvae. (F) Statistic analysis of LVM fiber width. There is no significant difference between the *beat IIa*$^{+2}$ and *w*^{1118}. The average width slightly increases from 3.5 µm to 3.8 µm in the *beat IIb*$^{\Delta 14}$ and 4.2 µm in the *beat IIa*$^{+2}$*beat IIb* ^{L88*} double mutant. ns: not significant, *p < 0.05, **p < 0.01, ***p < 0.001. The Kolmogorov-Smirnov test was used for the normality test, and the p-value was determined by a two-tailed T-test or a two-tailed Mann-Whitney U test in this and other analyses of this work.

As shown in **Fig. 25**, both circular and longitudinal visceral muscle fibers are detected. Whereby, longitudinal fibers are those that extend along the midgut tube. In the w^{1118} larvae, there are around 18 LVM fibers on both sides of the midgut (only one side is shown in the figure), and the average width of each fiber is around 3.5 μm. In the *beat IIa*$^{+2}$ homozygous larvae, no significant difference is detected. However, some enlarged parts with a space in the middle are more often detected (**Fig. 25**B, indicated by arrows). In contrast, in the *beat IIb*$^{\Delta 14}$ the LVM fibers are wider than the control group, and there is a slight decrease in the number. Most interestingly, when both Beat IIa and Beat IIb are absent, the fiber number drops to 12, while the average width increases to 4.2 μm.

2.7 Side IV expression pattern

Based on the observations above, Beat II proteins seem to be required for proper CVM and LVMP cell migration. To seek potential interaction partners, Side IV, which had been proven to interact with Beat II, was investigated.

2.7.1 *side IV* is transcribed in TVM cells

In situ hybridization with w^{1118} embryos was first checked for the expression pattern of *side IV*, and it showed a potential signal in the TVM (data not shown). Thus, embryos expressing GFP in TVM cells were utilized for the FISH of the *side IV* probe.

As **Fig. 26** suggests, *side IV* mRNA is transcribed in TVM cells. It is first detected in the segmental TVM clusters at stage 11 and lasts until stage 15. Afterwards, it decreases in the TVM. Additionally, *side IV* mRNA is detected in other cell types, which may be adult muscle precursor cells and a subset of ventral and lateral muscle cells (data not shown; similar observations are demonstrated in Li et al. 2017 and Lavergne et al. 2020). The specificity of the *side IV in situ* probe was confirmed by adding it to the *side IV* deficiency embryos, where no signal in the TVM could be detected (data not shown).

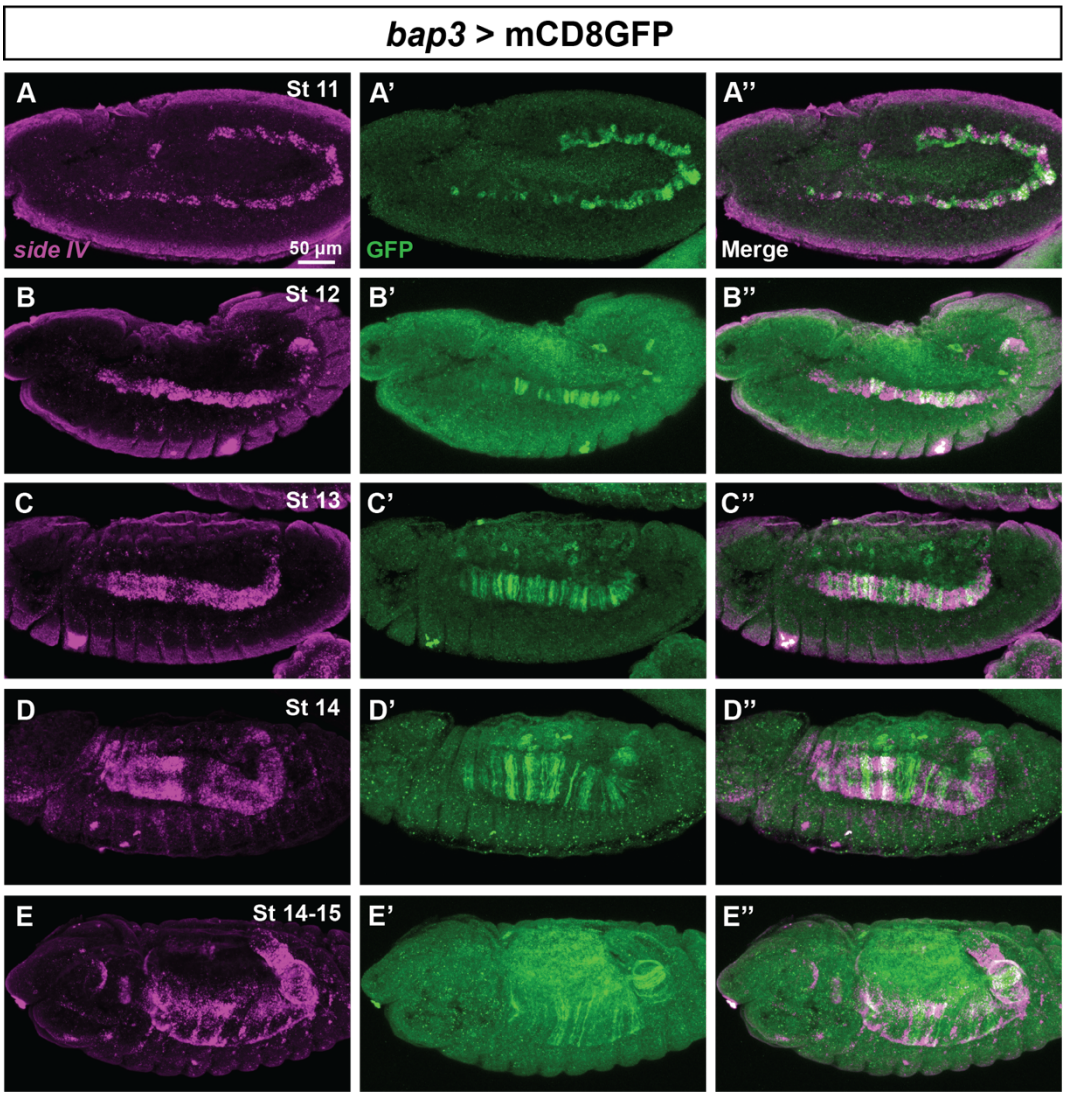

Fig. 26: Expression pattern of *side IV* mRNA during embryogenesis.
FISH of *side IV* (magenta) in *bap3* > mCD8GFP embryos where TVM cells were visualized by anti-GFP staining (green). The right column shows the merged images (A''-E''). At stage 11, *side IV* mRNA is detected in the TVM primordia. Its transcription lasts until stage 15. Afterward, the signal decreases. The scale bar in (A) applies to all images.

2.7.2 Side IV-GFP is detected in TVM cells

The Side IV-FsF-GFP line (Osaka et al. 2024) enables the examination of Side IV protein during embryogenesis. As an FRT (flippase recognition target)-flanked transcriptional stop cassette was inserted before the GFP, this line was first crossed with the hs-FLP (see **4.2.1.7**). Upon removing the stop cassette, GFP expression was active and thus could label the endogenous Side IV protein.

To verify its expression in the TVM, Fas III, a TVM marker, was co-stained with the GFP. As shown in the merged images (**Fig. 27**A''-F''), Side IV protein is expressed in the TVM. The signal is first detected at stage 12, later than the *side IV* mRNA transcription which is already visible at stage 11. However, the Side IV-GFP signal lasts throughout the embryogenesis, while the *side IV* mRNA is no longer detectable after stage 15. Worthy mentioning is that from stage 15 on, Side IV-GFP is observed in LVMP and LVM fibers (**Fig. 27**D'-F'). This expression pattern assembles the Fas III expression, which is also first detected in the TVM and then in the LVMP and LVM cells (Klapper et al. 2002).

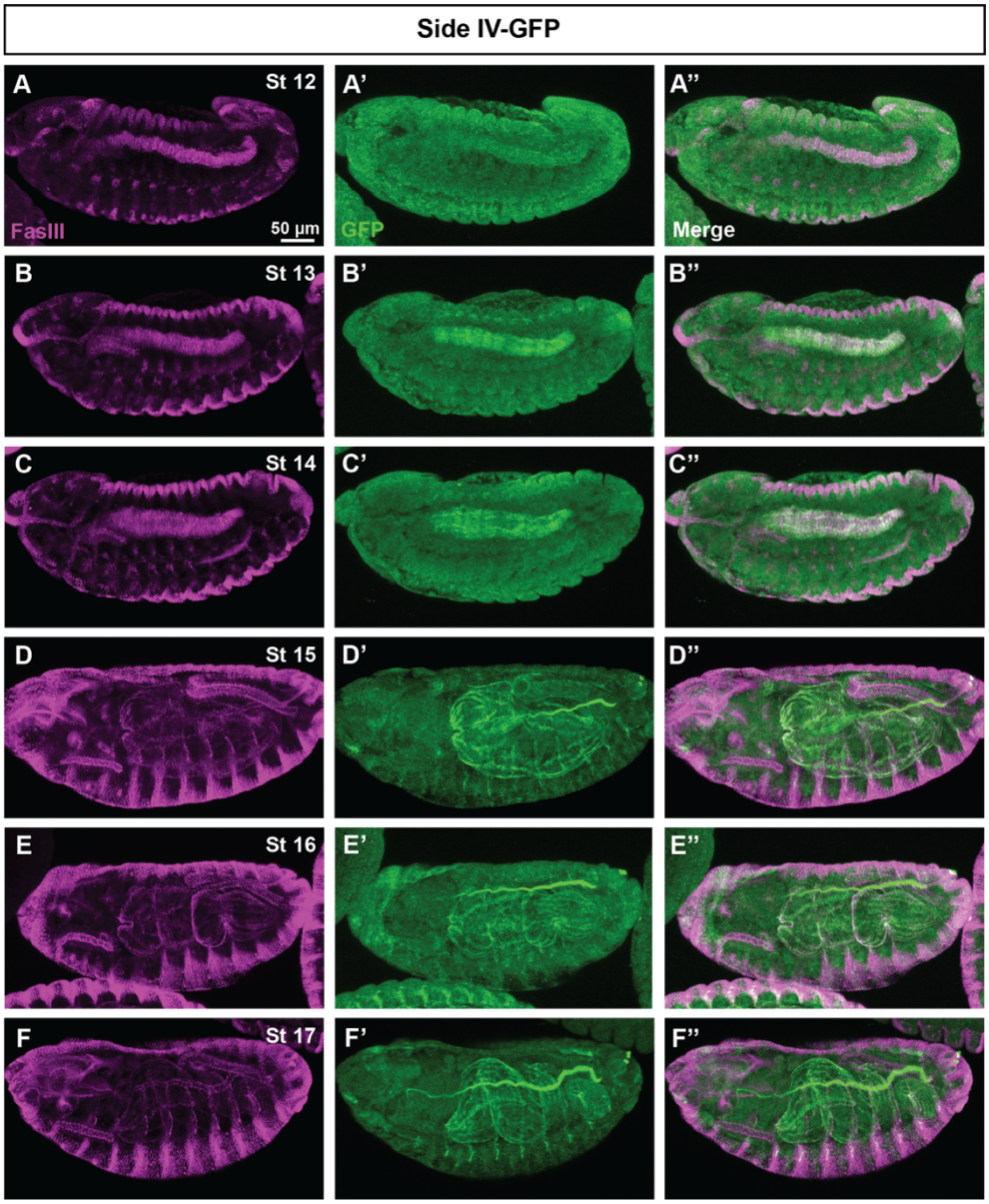

Fig. 27: Expression pattern of Side IV protein during embryogenesis.
Immunostainings of Side IV-GFP embryos. Anti-Fas III was used to mark the TVM (A-F). Side IV-GFP were stained with anti-GFP (A'-F'). Merged images suggest that Side IV protein is expressed in the TVM from stage 12 (A''-C''). After stage 15, it is detected in LVMP and LVM cells until the end of embryogenesis (D''-F''). The scale bar in (A) applies to all images.

2.7.3 Side IV is detected by anti-Side IV in TVM cells

Further results were obtained using the anti-Side IV antibody generated by the Claude Desplan group. This antibody was used to examine Side IV expression in the *Drosophila* optic lobe (Carrier et al. 2023). Together with anti-Fas III staining, the findings shown in **Fig. 28** support the conclusion that Side IV is expressed in the TVM.

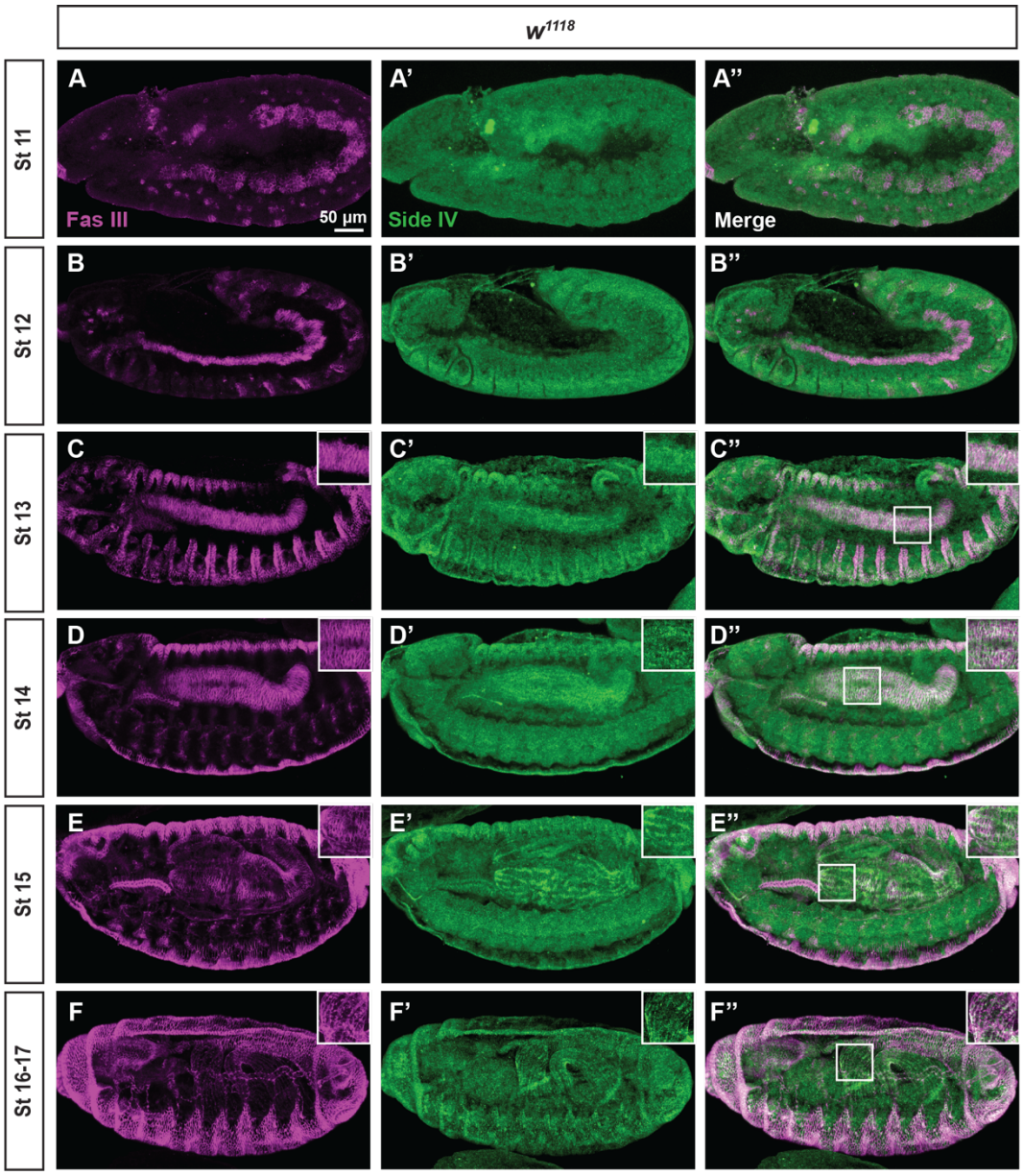

Fig. 28: Anti-Side IV antibody detection of Side IV protein during embryogenesis.
Immunostainings of w^{1118} embryos with anti-Fas III (TVM cells) and anti-Side IV. Merged images are shown as (A''-F''). Only after stage 13, Side IV is found in the TVM cells (C-C''). From stage 14 onwards, Side IV is expressed in the LVMP cells and later in the LVM fibers (D-F''). The scale bar in (A) applies to all images. Interesting areas are enlarged in the squares at the top right corner.

At stages 11 and 12, when Fas III-positive cells have formed a continuous band, Side IV-GFP is not detected in these cells (**Fig. 28**A-B''). Compared with the *in situ* results, in which the *side IV* mRNA is detectable since stage 11, there is a delay in the signal detection (compare A-B'' in **Fig. 28** with A-B'' in **Fig. 26**). This may be due to the antibody capability. Nevertheless, from stage 13 onwards, Side IV protein is identified firstly in the TVM (**Fig. 28**C-D'') and later in the LVM cells (**Fig. 28**E-E''), which aligns with the Side IV-GFP detection (compare **Fig. 28** with **Fig. 27**).

2.8 Side IV protein structure

As the FISH and IHC staining results suggest, Beat IIa and Beat IIb are expressed in CVM and LVMP cells. Meanwhile, Side IV exists in their migration track TVM. Thus, further investigations of Side IV in regulating migration and differentiation of CVM and LVMP cells were conducted.

2.8.1 Side IV protein structure prediction

Before the functional analysis, the structure of Side IV was predicted and analyzed using multiple programs (see **Table 12**). Side IV is composed of 1001 amino acids. Like its family member Side, five extracellular IG domains are predicted, followed by a fibronectin type-III (FN3) and a transmembrane domain (**Fig. 29**A, B). The IG domains in Side IV and other family members consist of two β-sheets, which typically contain seven antiparallel β-strands held together by two cysteines (highlighted in yellow, **Fig. 29** C).

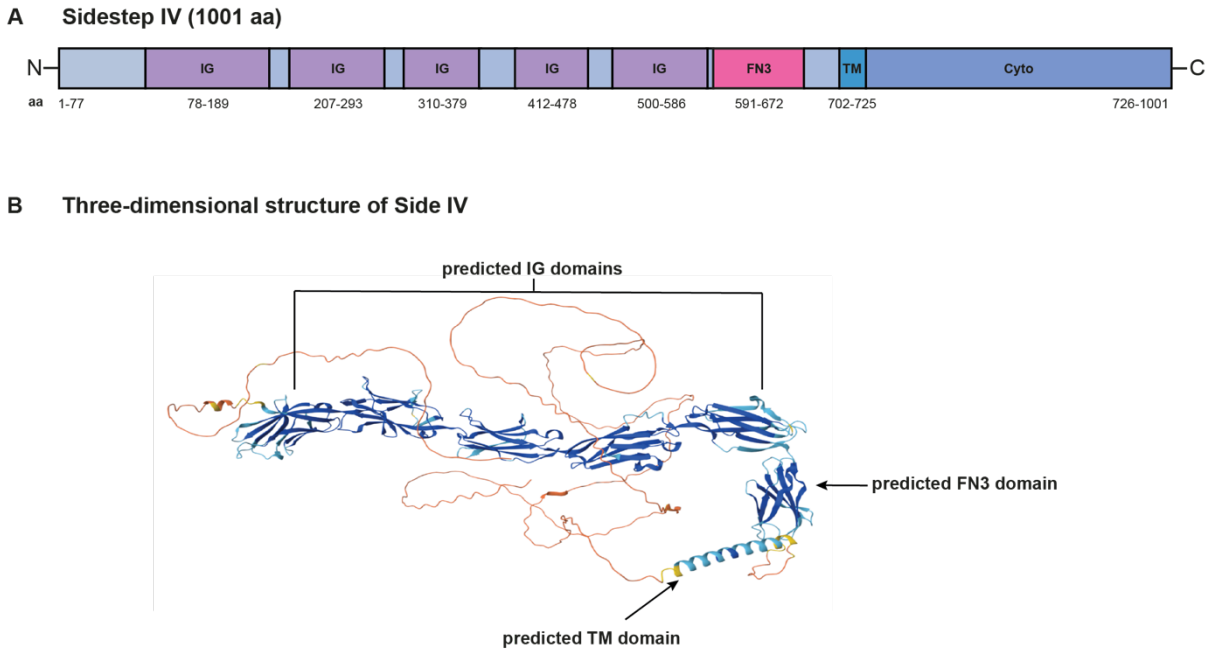

Fig. 29: Protein structure analysis for Side IV.
(A) The predicted domain structure of Side IV. It is a 1001-amino-acid (aa) transmembrane protein with five IG domains and a FN3 domain. (B) AlphaFold prediction of the three-dimensional structure of Side IV. The IG domains in Side IV typically contain two β-sheets. (C) Alignment of IG domains of Side and Side IV. Highly conserved cysteines (highlighted in yellow) are spaced forty to sixty amino acids apart, forming a disulfide bond to hold the β-sheets in the IG domains. Idential, similar, and not similar bases are indicated in black, blue and red colors, respectively. IG: immunoglobulin, TM: transmembrane, FN3: fibronectin type-III, Cyto: cytoplasmic domain, aa: amino acid.

2.8.2 *side IV* mutant alleles and fusion constructs

Dr. Jaqueline Kinold created two *side IV* mutants used in this work by crossing the *side IV* TRiP-KO line (Bloomington number #82064) with Vasa-Cas9. The TRiP-KO line was donated by the DRSC/TRiP gRNA Fly Stock Database, and it expresses sgRNA ubiquitously for Cas9-mediated mutagenesis of *side IV* (Zirin et al. 2020). In these *side IV* mutants, a frameshifting

induces an earlier stop codon in the first IG domain region at 134aa and 146aa positions, respectively (**Fig. 30**A). In addition, the Df(3R)Excel7320 was ordered from the Bloomington Center. The deletion in this deficiency line covers the *side IV* gene region (**Fig. 30**B). Furthermore, full-length or mutated Side IV with a mCherry tag was cloned into the vectors containing the UAS for the cell-cell aggregation assay (**Fig. 30**C).

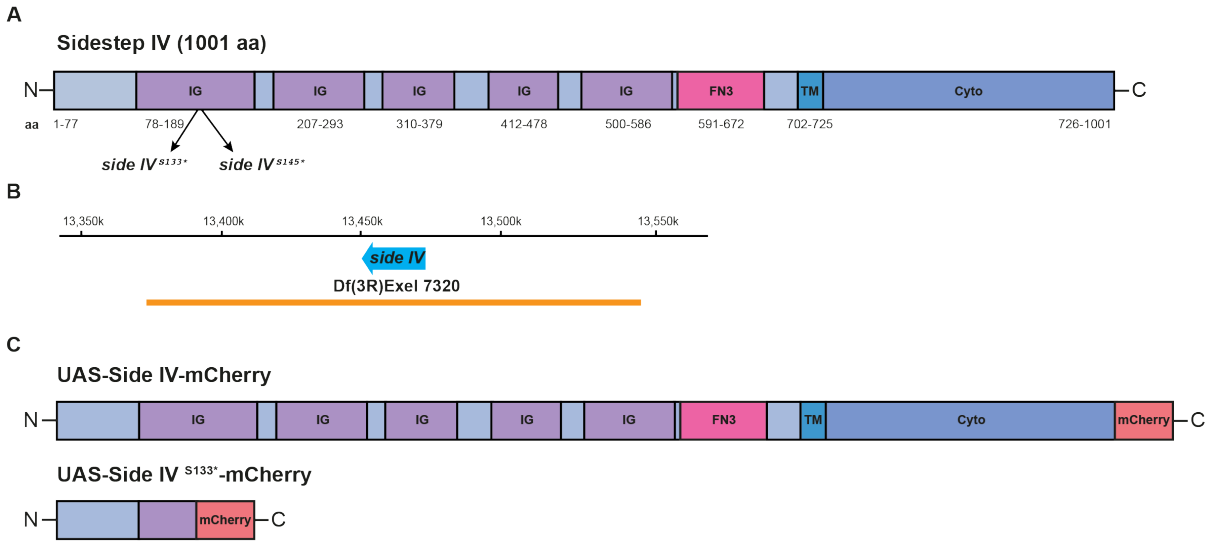

Fig. 30: Schematic overview of the *side IV* mutants and constructs.
(A) Side IV contains 1001 amino acids and is predicted as a type I transmembrane protein. *side IV*^{S133*} and *side IV*^{S145*} mutants carry a stop codon at positions 134 and 146, resulting in shorter proteins. (B) Df(3R) Exel7320 line exhibits a deletion that includes the *side IV* gene. (C) A mCherry tag is fused to the C-terminus of full-lengthed Side IV or mutated Side IV^{S133*}. The fusion constructs are inserted into UAS vectors. IG: immunoglobulin, TM: transmembrane, FN3: fibronectin type-III, Cyto: cytoplasmic domain, aa: amino acid.

2.9 CVM and LVMP cell migration shows severe defects in *side IV* mutant

To address whether Side IV influences CVM and LVMP cell migration and differentiation, *side IV* mutants and deficiency were combined with the CVM marker *HLH54Fb*-CytoRFP. Interestingly, in the transheterozygous *side IV* mutant (**Fig. 31**G-L), as well as the homozygous *side IV*^{S145*} or *side IV*^{S133*} mutants (data not shown), CVM and LVMP cells show severe migration defects.

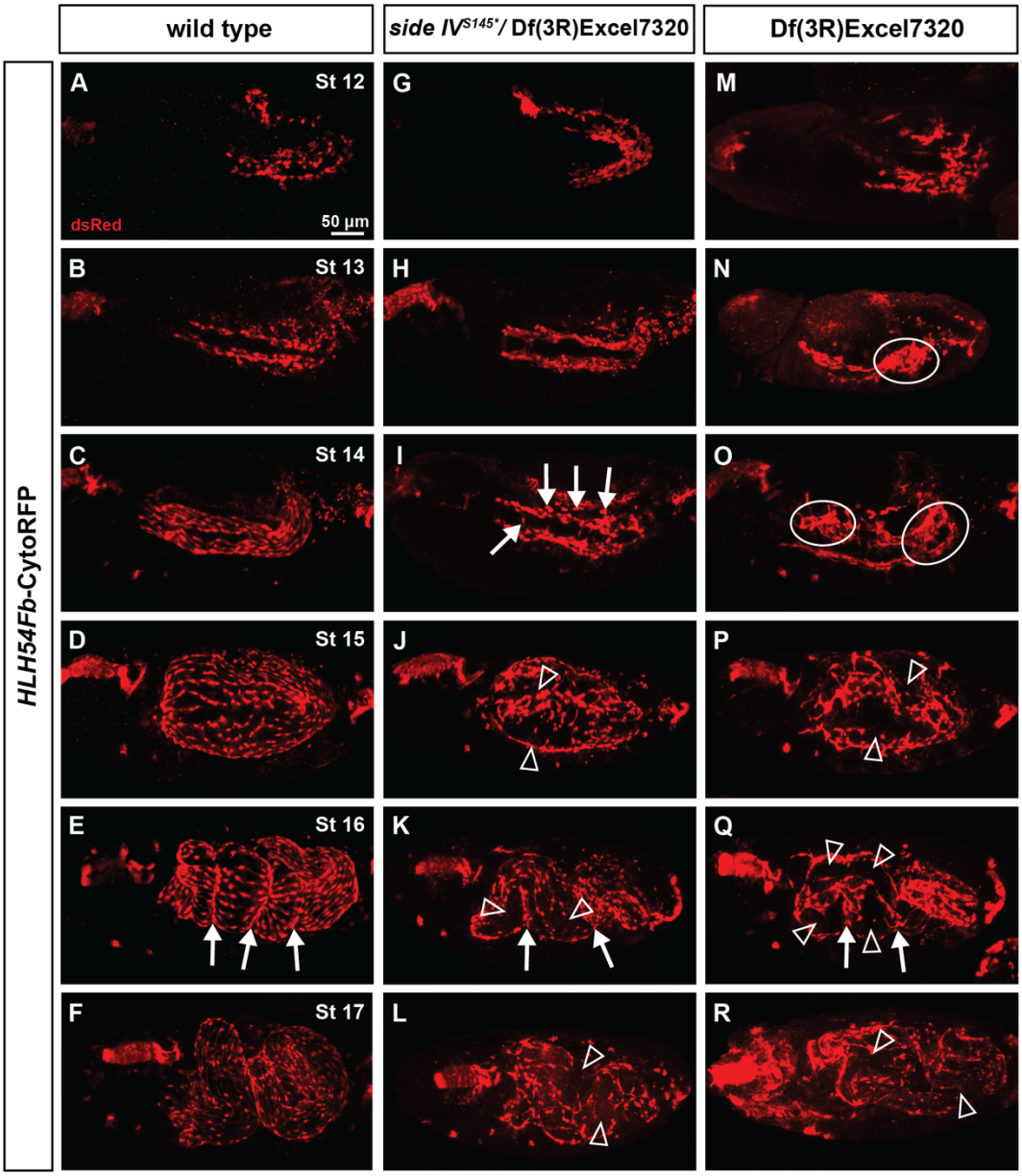

Fig. 31: Abnormal migration is observed in *side IV* mutant and deficient embryos.
Immunostained *Drosophila* embryos with anti-dsRed. (A-F) Wild-type *HLH54Fb*-CytoRFP embryos showing regular CVM and LVMP cell migration pattern. (G-L) Transheterozygous *side IV* mutant embryos. Although CVM cells can migrate anteriorly and reach their destinations, they are more densely connected. From late stage 13 on, the dorsal-ventral migration of the LVMP cells is strongly affected. Many cells are off-track and display a round cell shape (I, arrows). LVMP cells with abnormal cell shapes and distances are not properly orientated at later stages. Only a few LVM fibers are formed by the end of embryogenesis, and large spaces are not covered by LVM fibers (J-L, empty arrowheads). Additionally, midgut constrictions are altered (compare arrows in K with E). A similar and slightly stronger phenotype is observed in the *side IV* deficient embryos (M-R). The migrating CVM and LVMP cells are often clustered (circles in N and O). The midgut is not constricted as expected (compare arrows in Q and E), and LVM fibers can not be differentiated appropriately at the end (P-R, empty arrowheads). The scale bar in (A) applies to all the images.

At stages 11-13 only minor defects characterized as more densely connected cells are detected (**Fig. 31**G-H). With the beginning of stage 14, the migration pattern is progressively disrupted. Many cells are not on the correct migration track and display a roundish and shrunken cell

shape, indicating they may undergo cell apoptosis (**Fig. 31**I, arrows). At stage 15, instead of being aligned parallelly and distributed evenly around the midgut, LVMP cells in the *side IV* mutants are irregularly orientated, some cells are grouped while leaving spaces without LVMP cells (**Fig. 31**J). In the wild type, at late stage 16, midgut constrictions appear (**Fig. 31**E, arrows indicate midgut constrictions). Neighboring LVMP cells are connected and extend along the midgut tube, forming matured LVM fibers. However, in the *side IV* mutant, especially in the anterior and middle parts of the midgut, large spaces lacking LVM fibers exist. In addition, the constrictions of the midgut are also slightly affected (**Fig. 31**K, empty arrowheads indicate areas without LVMP cells, and arrows indicate midgut constrictions). Although some LVM fibers are eventually formed by the end of embryogenesis, they are often grouped and irregularly distributed (**Fig. 31**L, empty arrowheads indicate areas lacking longitudinal fibers).

The homozygous *side IV* deficient embryos show a similar phenotype as the mutants but slightly stronger (**Fig. 31**M-R). The migrating CVM and LVMP cells are grouped and show irregular cell shapes from late stage 12 (**Fig. 31**N, O, circles). As a result, large spaces devoiding of LVM fibers and altered midgut constrictions are observed (**Fig. 31**P-R, empty arrowheads indicate areas lacing LVMP and LVM cells, and arrows indicate midgut constrictions).

Most interestingly, these phenotypes are similar to the *beat II* double mutant phenotypes (compare **Fig. 31** with **Fig. 23**), indicating Side IV might function with Beat II to assist a proper migration and differentiation of CVM and LVMP cells.

2.10 LVM fibers exhibit defects in *side IV* mutant L3 larvae

The viability of *side IV* mutant larvae enables the investigation of the number and morphology of LVM fibers in larvae. After the isolation from the w^{1118} and the transheterozygous *side IV* mutants, the midguts were fixed and stained with Phalloidin conjugated with a fluorophore. Images of LVM fibers on both sides of the midgut were acquired and analyzed.

Compared with the wild type, there is a decrease in the LVM fiber number, while together, there is a significant increase in the width of the fibers. In wild-type larvae, around 18 LVM fibers with an average width of 3.5 μm are observed. In the *side IV* mutant, only 11 fibers are found, but the average width is increased to 4.8 μm (**Fig.32**).

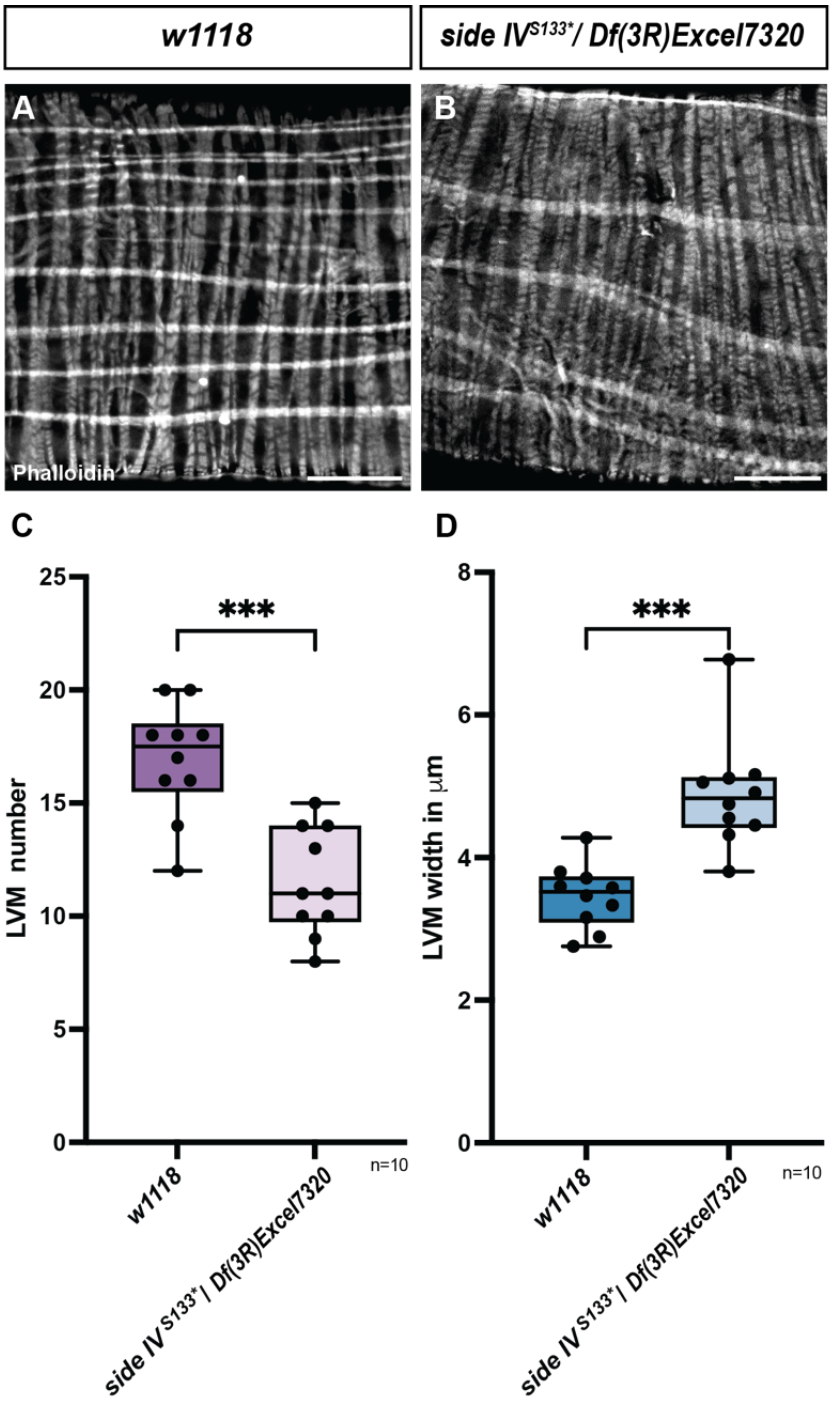

Fig. 32: LVM fibers in the L3 larvae of *w*^{1118} and *side IV* mutants.
(A and B) Confocal images of *w*^{1118} and transheterozygous *side IV* mutant larvae at the third instar stage. LVM fibers were stained with phalloidin conjugated with the fluorescent Texas Red-X dye. Genotypes are shown above. Scale bars: 50 µm. (C) Statistic analysis of LVM fiber number. LVM fibers on both sides of the midgut are counted. In *w*^{1118}, the count ranges from 12-20, and the average number is 17-18. In *side IV* mutant, the number varies from 8 to 15, and the average is 11. (D) Statistic analysis of LVM fiber width. In the control group, the average width of the fibers is around 3.5 µm, and it is significantly increased to 4.8 µm in the *side IV* mutant. ns: not significant, *p < 0.05, **p < 0.01, ***p < 0.001.

2.11 Myoblast fusion in *side IV* mutant embryos

As abnormalities in the number and width of the LVM fibers in *side IV* mutants were detected, the question was raised whether myoblast fusion between the longitudinal founder cells (FCs) and the TVM-derived fusion-competent myoblasts (FCMs) is affected. In wild-type embryos, after the fusion of the circular visceral myoblast, there are remaining unfused FCMs on the dorsal and ventral margins of the TVM. These cells are determined to fuse with longitudinal FCs to form LVM fibers (Klapper et al. 2002).

A previous work has reported that the Rolling Pebbles 7 (Rols7), the adaptor molecule that interacts with the intracellular domain of Duf/Kirre, is required for the longitudinal myoblast fusion (Rudolf et al. 2014). When Rols7 is absent, e.g. in the *rols7*^{XX117} mutant or a *rols7* deficiency (Df(3L)BK9), unfused FCMs are found between the visceral and the somatic mesoderm at late stage 12. By the end of embryogenesis, the constrictions of the first and second midgut chambers are altered due to the misformation of the LVM fibers (Rudolf et al. 2014).

To check the longitudinal myoblast fusion process, the *bagpipe 3 (bap3)*-RFP line (Reim et al. 2012), where RFP marks all the visceral myoblasts of the trunk mesoderm, was utilized. In the wild type, the fused circular visceral muscle precursors are spindle-like and extend dorsal-ventrally at stage 13 (**Fig. 33**A, A'). However, in the homozygous DF(3L)BK9 embryos, due to a disruption of the longitudinal myoblast fusion, unfused FCMs are detected (**Fig. 33**B', arrows), similar to the previous observation from Rudolf et al. 2014 (Figure 4B). By contrast, in the *side IV* mutant, no signs of unfused FCMs are observed (**Fig. 33**C, C'), indicating that the first fusion step between the FCMs with the longitudinal FCs is unaffected in the absence of Side IV.

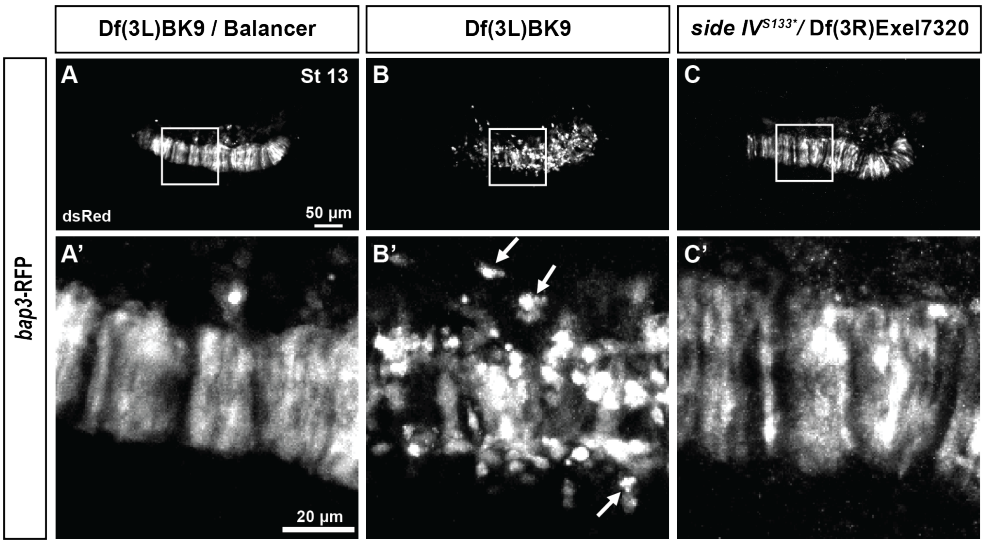

Fig. 33: Side IV is not required for the first fusion between longitudinal FCs with FCMs.
Immuno-stained *Drosophila* embryos by anti-dsRed to visualize the trunk visceral myoblasts. (A and A') Embryos from the *rols7* deficiency over a balancer. The fusion of the circular FCs with the FCMs is finished at stage 13. The fused circular visceral muscle precursors are in spindle-like shape and continue to extend dorsal-ventrally. During the expansion of the circular muscle precursors, the remaining FCMs fuse with the longitudinal FCs and differentiate into LVM cells. (B and B') Homozygous *rols7* deficient embryos. The longitudinal myoblast fusion is affected due to a loss of Rols7. Unfused FCMs are detected between the visceral and somatic mesoderm (arrows indicate unfused FCMs). (C and C') Transheterozygous *side IV* mutant embryos. No remaining unfused FCMs are observed, indicating that the visceral myoblast fusion process is unaffected. The scale bar in (A) applies to (A, B, and C). The scale bar in (A') applies to (A', B', and C'). Squares mark the enlarged areas.

In order to obtain more insights into the fusion process, RFP-tagged nuclear histone was forced to be expressed in CVM and LVMP cells of the *side IV* mutant embryos, which enabled the tracking and counting of nuclei during the migration and differentiation process. At stage 12, while most CVM cells have not initiated fusion, a small group of cells with two or even three nuclei are observed (**Fig. 34**B'''). At late stage 13, although the migration pattern is disrupted, most LVMP cells have completed two to three rounds of fusion (**Fig. 34**C'''). By the end of stage 15, five to six nuclei are observed in the LVMP cells (**Fig. 34**E''').

For a better comparison, images from **Fig. 34** (A''-G''') are aligned with the corresponding control groups from **Fig. 14** (A''-G'''). At stage 12, more cells in the *side IV* mutant have finished the first and even second fusion (**Fig. 35**, compare I' with B'). At late stage 13 the LVMP cells tend to have close contact with the neighboring cells, making it difficult to count the exact nuclear number. However, many of them own three to four nuclei, while the number is often one or two in the control group (**Fig. 35**, compare J' with C'). Afterward, the LVMP cells display abnormal distribution, orientation and migration patterns compared to the wild type. Nevertheless, most cells own five or six nuclei until stage 15, identical to the wild type (**Fig. 35**, compare L' with E').

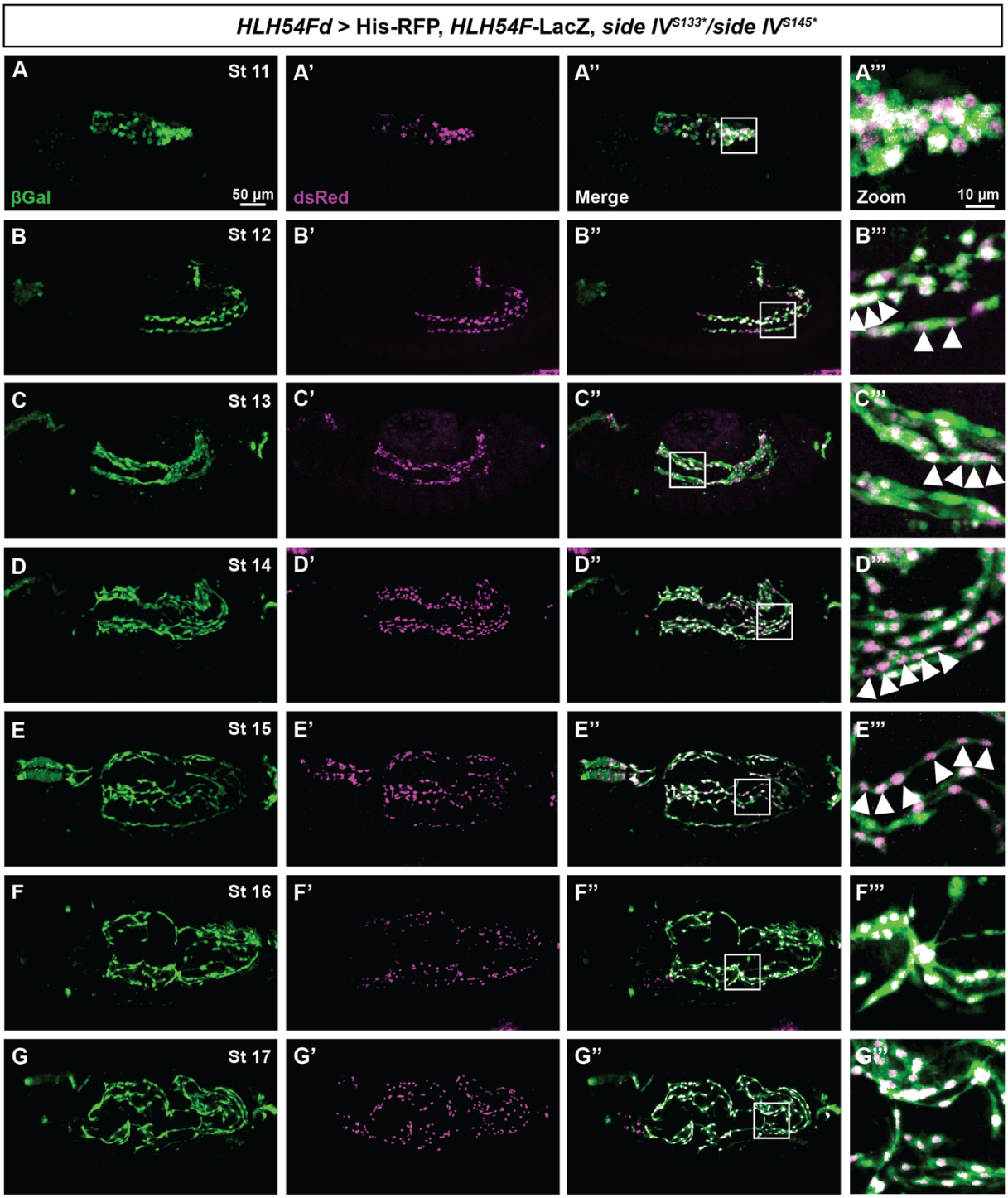

Fig. 34: Nuclei in developing LVMP cells of *side IV* mutant embryos.
Confocal images of nuclei number in the developing LVMP cells of the *side IV* mutant embryos. Nuclear Histone-RFP was expressed in CVM and LVMP cells by the *HLH54Fd*-Gal4 line. (A-G) LacZ-marked CVM and LVMP cells were visualized by anti-βGal staining. (A'-G') Histone-RFPF was visualized by anti-dsRed staining. (A''-G'') Merged images and squares mark the area enlarged in (A'''- G'''). The myoblast fusion starts at late stage 12. Until stage 15, most cells contain up to six nuclei despite abnormal distribution and orientation of the LVMP cells. The scale bar in (A) applies to (A-G''). The scale bar in (A''') applies to all enlarged images.

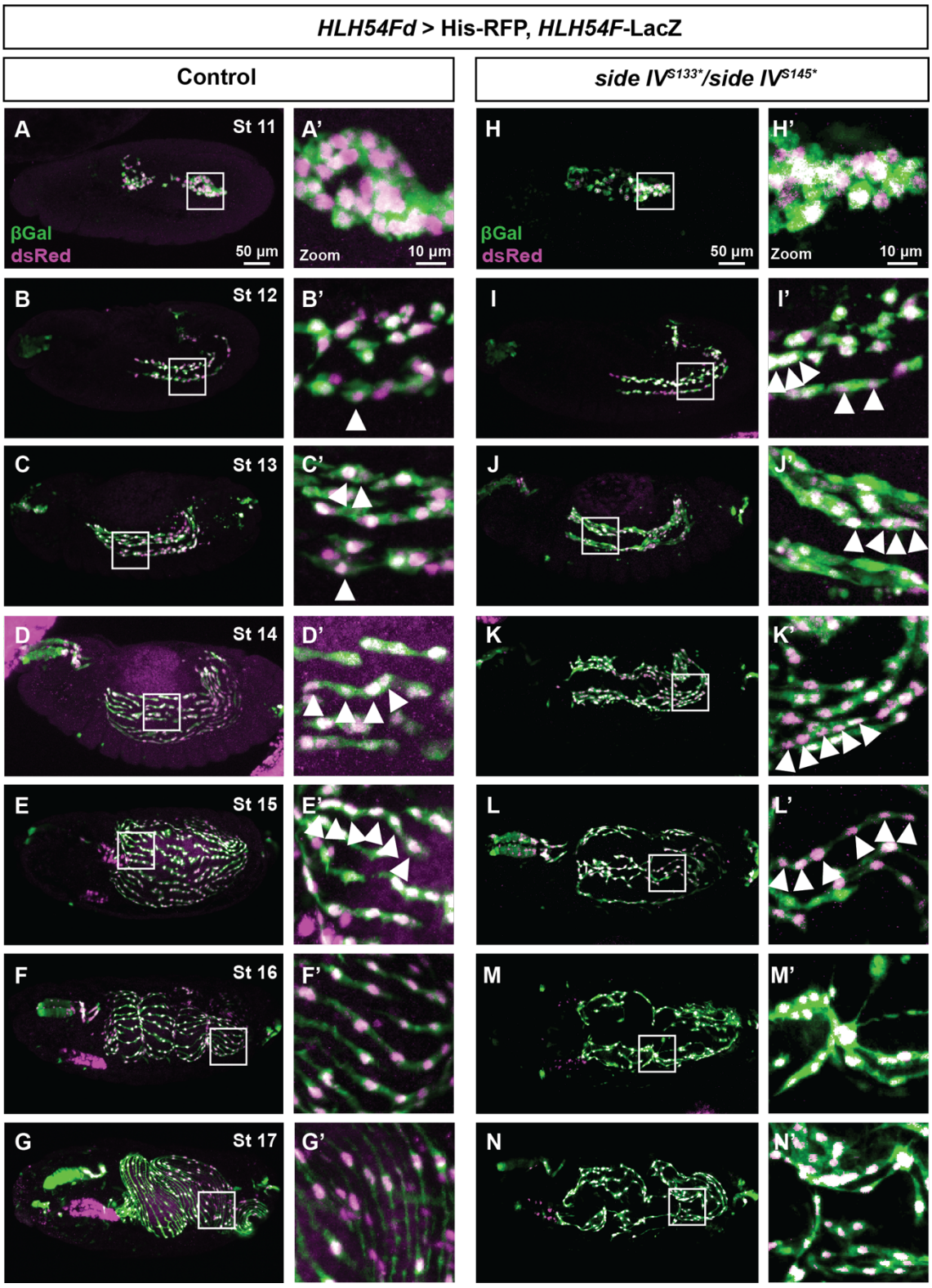

Fig. 35: Comparison of nuclei in LVMP cells in wild-type with *side IV* mutant embryos.
Merged images from **Fig. 14** (wild-type) aligned with images from **Fig. 33** (*side IV* mutant). With the disrupted distribution and orientation of LVMP cells in *side IV* mutant embryos, it is difficult to count the nuclear number. The myoblast fusion process seems either sped up or misformed in the absence of Side IV, as more nuclei are found compared to the wild-type embryos at a similar development stage (compare I'-K' with B'-D'). Nevertheless, most LVMP cells achieve six nuclei at stage 15 in both wild-type and side IV mutants. After stage 15, it is impossible to count the nuclear number in one LVM fiber as the anterior and posterior neighboring cells are connected and the gut tube is twisted.

This observation is supported by the quantitative analysis (**Fig. 36**), suggesting that the myoblast fusion capacity is not affected when Side IV is absent. Of note is that the nuclei in the *side IV* mutants are often clustered instead of aligned one by one in a row, implying that Side IV plays a role in the migration and orientation of LVMP cells.

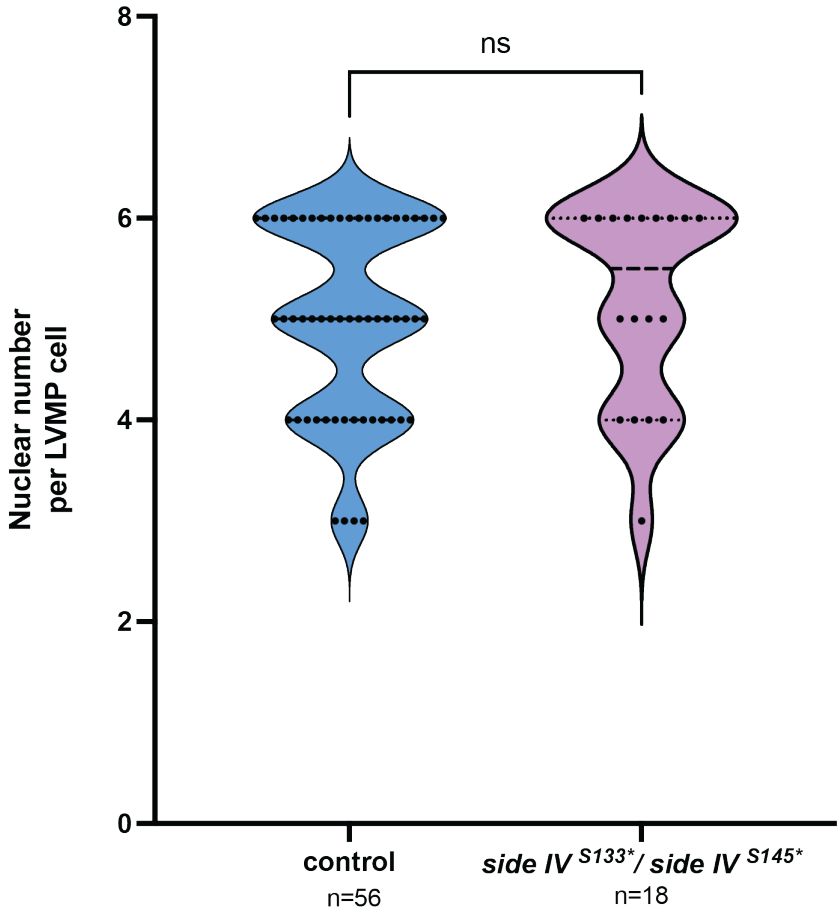

Fig. 36: Nuclear counts in LVMP cells in the control and *side IV* mutant embryos.
Nuclear counts within LVMP cells in control and transheterozygous *side IV* mutant embryos at stage 15. No significant difference is found in these groups, supporting the observation that the myoblast fusion capacity is not affected in *side IV* mutant. ns: not significant.

2.12 LVMP cells lost contact with the TVM in *side IV* mutant

Based on the observation above, Side IV is expressed in the TVM and is required for proper CVM and LVMP migration. To shed light on the underlying mechanism, the morphology of the TVM was first analyzed, but no morphological changes were observed in the *side IV* mutant. However, the contact between the TVM and the migrating cells was altered.

As described before, during the whole migration process, CVM and LVMP cells keep close contact with the TVM to promote the directional movement of the cohorts (**Fig. 37**A, B). Interestingly, in the *side IV* mutant, instead of being well-organized and migrating upon the expanding TVM, many LVMP cells lost contact with the TVM. These off-track cells are often grouped (**Fig. 37**D, circles), and display a roundish and shrunken shape (**Fig. 37**C, D, arrows), which is a typical characteristic of cells undergoing apoptosis. A similar phenomenon is also observed in the wild-type embryos but is limited to a small portion of cells (**Fig. 37**A, B, arrows). This data leads to the hypothesis that those abnormal cells are eventually dead, and a loss of them results in a decreased number of LVM fibers at the end of embryogenesis.

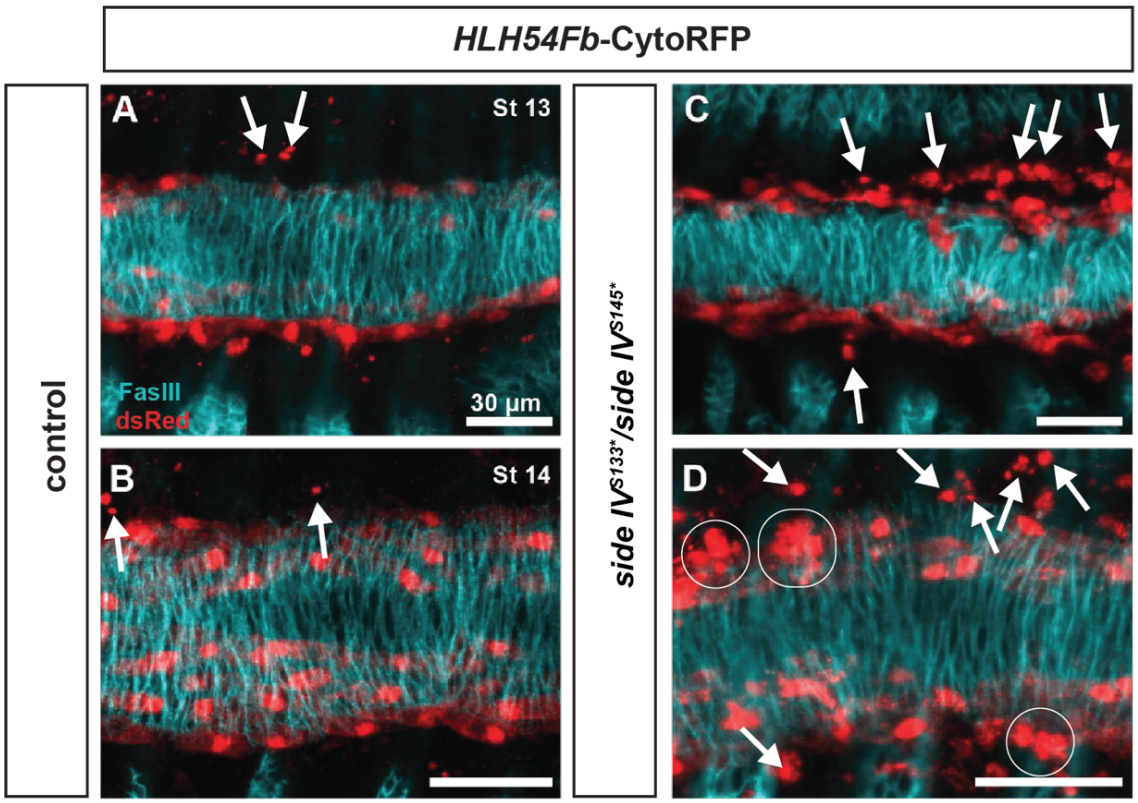

Fig. 37: LVMP cells lost contact with the TVM in *side IV* mutant.
Microscopy images of anti-dsRed and anti-Fas III stainings of *HLH54Fb*-CytoRFP embryos in the wild-typic or *side IV* mutant background. CVM and LVMP cells were marked in red and the TVM was shown in cyan. At stage 13, CVM cells migrate along the dorsal and ventral margins of the TVM (A). Along with the expansion of the TVM, LVMP cells migrate upon the TVM towards the dorsal and ventral. Only a few cells are located away from the TVM (B). In the *side IV* mutant, some cells are still in close contact with the TVM margins, but many cells lost this contact (C). Those off-track cells are often round and shrunk in shape. The dorsal-ventral migration process of the LVMP cells is severely affected (D). LVMP cells are irregularly distributed, many cells are located away from the TVM, displaying abnormal morphology, while some cells are grouped. Arrows indicate off-track cells. Circles indicate grouped cells. Scale bars: 30 µm.

2.13 Increased apoptosis in *side IV* mutant embryos

To test the hypothesis that the LVMP cells that lost contact with the TVM in the *side IV* mutant undergo cell death, multiple methods and tools were utilized.

2.13.1 Detected TUNEL signals in LVMP cells in *side IV* mutant embryos

As DNA becomes extremely fragmented in the last phases of apoptosis, the terminal deoxynucleotidyl transferase dUTP nick end labeling (TUNEL) reaction can attach a modified dUTP to the 3'-OH end of the damaged DNA. Multiple direct or indirect detecting methods can find the changed dUTP, such as adding fluorescein-dUTP. Thus, the TUNEL assay can be used to detect potential apoptosis during the dorsal-ventral migration process of the LVMP cells.

In **Fig. 38**, the wild-type *HLH54Fb*-CytoRFP reporter line was used as a control, and LVMP cells were visualized with anti-dsRed in magenta. The same reporter line combined with the *side IV* mutant was compared with the control group. The TUNEL signal in green reports on dying cells.

At stage 14, in the control group, although the TUNEL signals are detected in the epidermis, head, and ventral regions (**Fig. 38**A), no specific signal comes from the LVMP cells (as no overlapped signal in the LVMP cells in **Fig. 38**A''). As a comparison, the TUNEL signals are increased in the midgut region in the *side IV* mutant (**Fig. 38**B). The zoomed images (**Fig. 38**C-C'') show that the TUNEL signals are present in the LVMP cells with abnormal cell shape, suggesting these cells are dying. The loss of these cells may be the reason for the decreased LVM fibers at the end of embryogenesis and in the larvae.

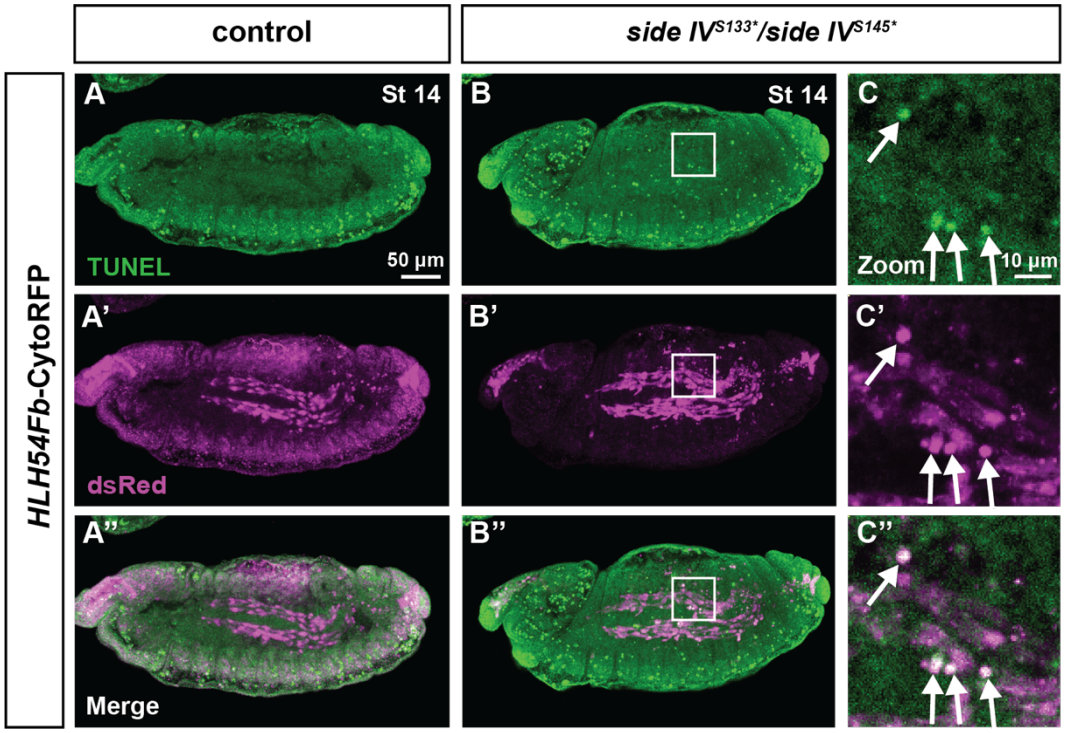

Fig. 38: TUNEL signals are detected in LVMP cells in *side IV* mutants.
Confocal images of LVMP cells visualized by anti-dsRed staining in magenta. The TUNEL signals were shown in green. White signals result from a colocalization. (A'', B'' and C'') Merged images from the corresponding images. In the control group, the TUNEL signalsare detected in the epidermis, head, and ventral region of the embryos (A). As shown in (A''), no TUNEL signals come from the migrating LVMP cells. In the transheterozygous *side IV* mutant (B-B''), the TUNEL staining is increased in the midgut region (compare B with A). As shown in the magnified images from the square region (C-C''), the TUNEL signals are present in the LVMP cells that are roundish and small (arrows). The scale bar in (A) applies to (A-B''). The scale bar in (C) applies to (C-C'').

2.13.2 Caspase activity in LVMP cells is reported by Apoliner

In addition to the TUNEL assay, a fluorescent apoptosis reporter, Apoliner, was used for apoptosis detection (Bardet et al. 2008). This reporter consists of two fluorophores, enhanced green fluorescent protein (eGFP) and monomeric red fluorescent protein (mRFP), which are connected by a specific and effective caspase-sensitive site. Under normal conditions, eGFP and mRFP are colocalized at the cytoplasm membrane. However, during the apoptosis process, the reporter is cleaved by caspase activation, causing eGFP to go into the nucleus and leave mRFP at the membrane (Bardet et al. 2008).

In **Fig. 39**, the expression of UAS-Apoliner 5 was driven by the *HLH54Fd*-Gal4 in the LVMP cells in the wild-typic or *side IV* mutant background. At stage 14, signals from the mRFP, and eGFP proteins are overlapped at the membrane in the control group (**Fig. 39**A'', A'''). By

contrast, with the *side IV* mutant background, the mRFP signal is strongly detected in the shrunken LVMP cells where the caspase activity is assumed to be active. However, the eGFP is weakly detected or absent (**Fig. 39**B’’’, arrows). The absent eGFP signal is presumably due to the high proteolytic activity after it is cleaved from the mRFP by the caspase, a similar phenomenon was previously reported (Bardet et al. 2008).

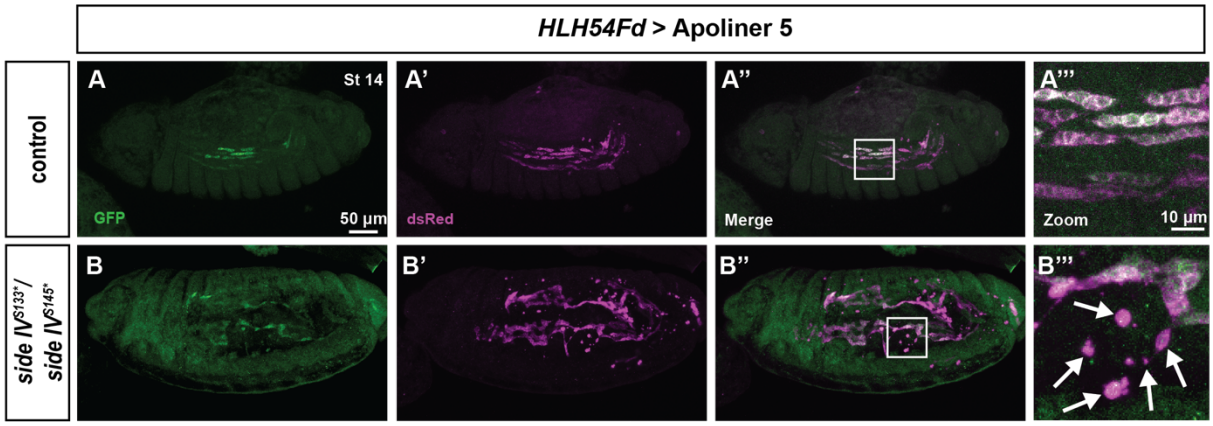

Fig. 39: Apoliner reports on increased caspase activity in the *side IV* mutant.
Microscopy of apoliner in the embryos stained with eGFP in green and mRFP in magenta. White color results from colocalization. Squares mark the zoomed area in (A’’’ and B’’’). (A-A’’’) Apoliner in control embryo at stage 14. The eGFP staining is weaker compared with the staining of the mRFP, which may be due to the anti-GFP antibody capacity. In the migrating LVMP cells, two signals colocalized at the membrane (A’’’). (B-B’’’) Apoliner in the *side IV* mutant embryos. In some cells, co-localized signals are observed on the membrane. However, in many other cells, only mRFP staining is left, while eGFP staining is weak or even absent, presumably due to the high proteolytic activity in these cells. The scale bar in (A) applies to (A-B’’). The scale bar in (A’’’) also applies to (B’’’).

To investigate the apoptosis in the *side IV* mutant more closely, the TUNEL assay was combined with the Apoliner detection. In the control group (*HLH54Fd* > Apoliner 5), more unspecific GFP signals are detected when compared with the embryos that were not performed with TUNEL detection (compare **Fig. 40** A with **Fig. 39** A). Nevertheless, the eGFP and mRFP signals from the Apoliner are largely colocalized (**Fig. 40**B, B’). Although some TUNEL signals near the midgut region are detected, mostly in RFP-negative cells that are away from the migration path (**Fig. 40**C, C’). As a comparison, in the *side IV* mutant embryos, the GFP signal is even more unspecific and largely decreases in the LVMP cells which display abnormal morphology (**Fig. 40**E, E’). Additionally, the TUNEL signal is often detected in the RFP-positive cells where the eGFP signal is absent (**Fig. 40**F, F’). Taken together, both the TUNEL assay and Apoliner report on apoptosis in the LVMP cells in the *side IV* mutant embryos.

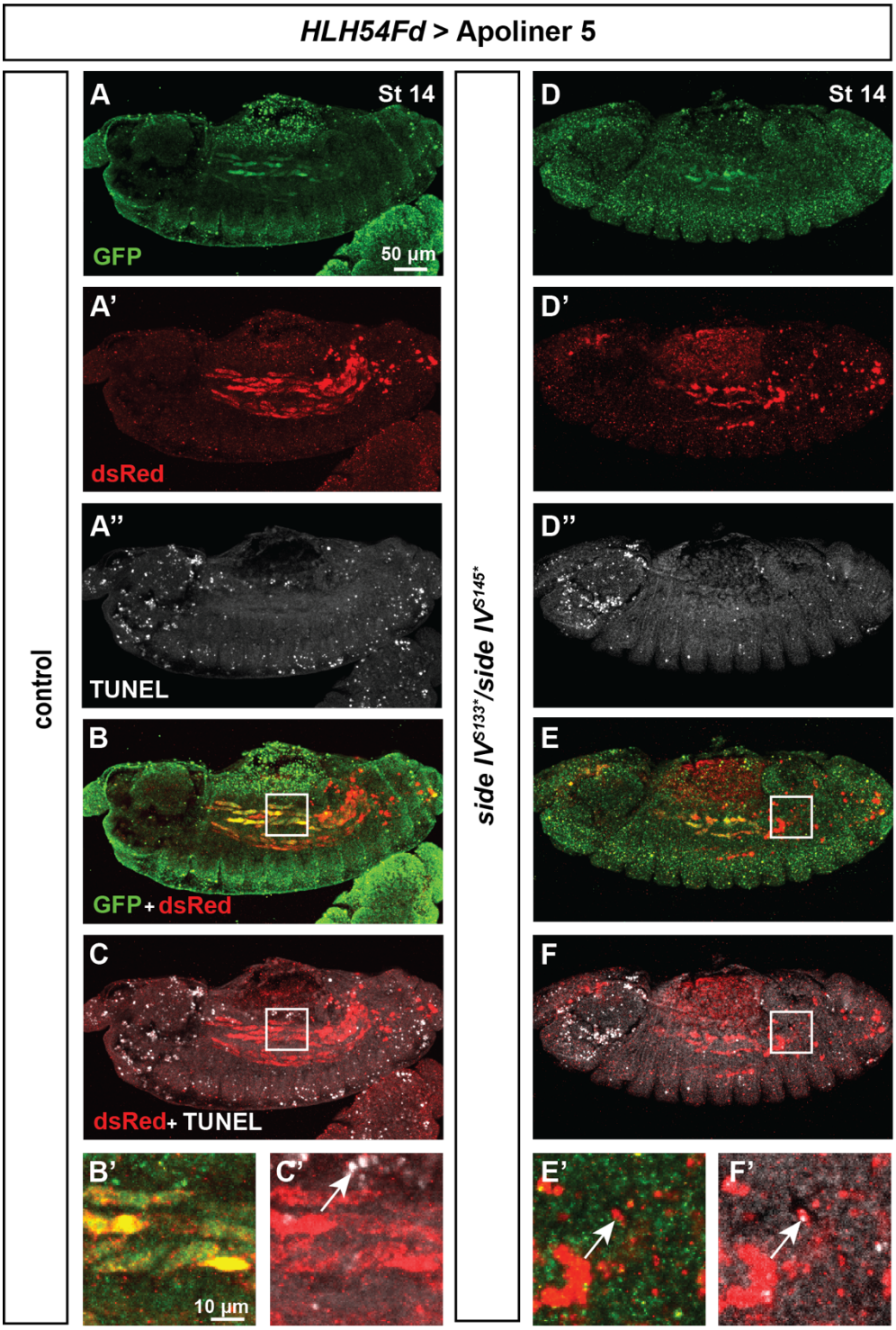

Fig. 40: LVMP cell death detected by the TUNEL assay and Apoliner in *side IV* mutant.
Microscopy of embryos stained by antibodies and TUNEL reagents. Aopliner was visualized by anti-GFP (green) and anti-dsRed (red), and the TUNEL signals were shown in grey. (A-A'') Single channels from the wild-type embryos at stage 14. (B) Merged image from (A) and (A'), square marks the enlarged area in (B'). (C) Merged image from (A') and (A''), square marks the enlarged area in (C'). As shown in (B'), signals from eGFP and RFP of the Apoliner are largely colocalized. TUNEL signals are detected in a few cells that are away from the normal migration path. They are not supposed to be LVMP cells as they are RFP- and GFP-negative (arrow in C'). (D-D'') Single channels from the *side IV* mutant embryos at stage 14. (E) Merged image from (D) and (D'), the squared area is enlarged in (E'). (F) Merged image from (D') and (D''), the squared area is enlarged in (F'). When compared with the control, the eGFP signal is largely decreased (E and E'), which may be due to the proteolytic activity during the apoptosis. Of note, the TUNEL signals are often present in cells that exhibit morphological changes (arrow in F'). The scale bar in (A) applies to (A-F). The scale bar in (B') applies to enlarged images.

2.13.3 LVMP cell death is reported by anti-Tey antibody staining

A third method to detect LVMP cell death was achieved by using the anti-Teyrha-Meyrha (Tey) antibody. Tey is a variant of the RNF220 family of ubiquitin ligases and is expressed in the CVM, LVMP, and somatic muscle 12 cells (Frasch et al. 2023; Inaki et al. 2010). As it is specifically located in the nucleus and its staining by anti-Tey is absent in cellular debris of dead cells, a loss of anti-Tey signal could indicate cell death (Macabenta et al. 2022).

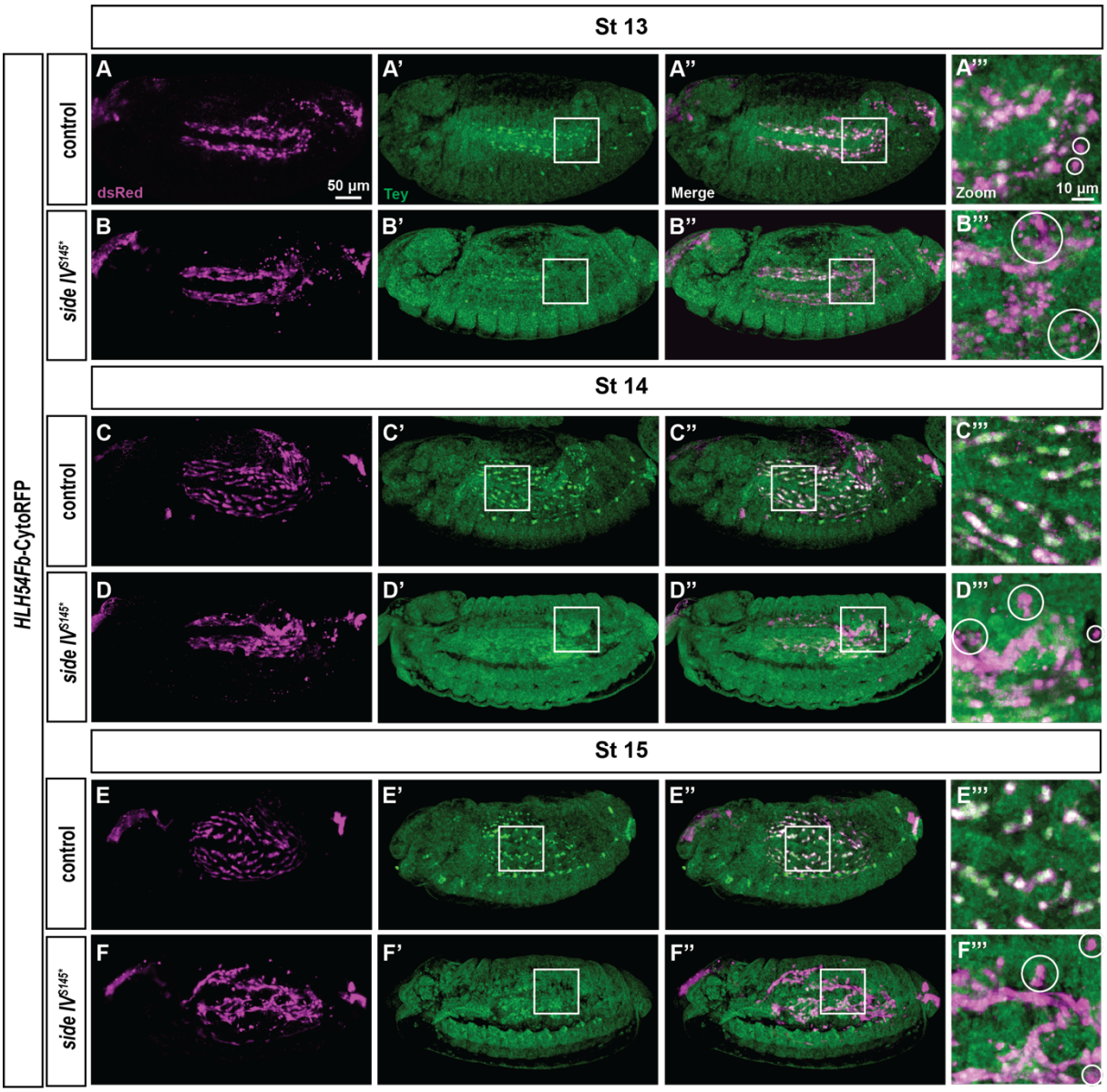

Fig. 41: Increased cell death is reported by a loss of anti-Tey staining in *side IV* mutant embryos.
Immunostainings of embryos expressing *HLH54F*-CytoRFP reporter. LVMP cells were stained with anti-dsRed. The nuclei of living LVMP cells were marked by anti-Tey. Squares indicate mignificated areas. (A-A''', C-C''', E-E'''): At stage 13, in the caudal region of wild-type embryos, some mismigrated cells that have lost contact with the TVM show no Tey signals (circles in A'''), indicating they undergo cell death. Nevertheless, during the dorsal-ventral migration, most RFP-positive cells have a Tey antibody signal. (B-B''', D-D''', F-F'''): In the *side IV* mutant embryos, LVMP cell migration is notably disrupted. The mismigrating cells often display abnormal cell

morphology with a loss of Tey antibody staining for the nuclei (circles in B’’’, D’’’, and F’’’). The increased number of Tey-negative cells indicates an increased death in the *side IV* mutant. The scale bar in (A) applies to (A-F’’), and the scale bar in (A’’’) applies to all enlarged images.

Using anti-Tey, cell death is only detected in a restricted number of cells that lost contact with the TVM in wild-type embryos (**Fig. 41**A’’’, circles). However, in the *side IV* mutant, along with the disordered LVMP cell migration, the Tey signal is notably absent in the mismigrating cells (**Fig. 41**B’’’, D’’’, and F’’’, circles). These increased Tey-negative cells indicate a higher LVMP cell death in the *side IV* mutant. In summary, all three methods for detecting cell death showed the same result and demonstrated an increased number of dying cells in *side IV* mutants.

2.13.4 Fewer LVMP cells in *side IV* mutant display abnormal morphology when apoptosis is blocked

As shown above, cell death is reported in the migrating LVMP cells that lost their contact with the TVM in *side IV* mutant by multiple methods and tools. However, these methods do not specifically report on apoptosis (Grasl-Kraupp et al. 1995; de Torres et al. 1997; Bardet et al. 2008; Nishida et al. 2024). To investigate if the death of these off-track cells is induced by apoptosis, the baculovirus p35 protein, which functions to prevent apoptotic cell death (Hay et al. 1994), was forced to express in the CVM and LVMP cells.

Firstly, to exclude the potential effects of p35 overexpression on the CVM and LVMP cell migration, p35 was expressed by *HLH54Fd*-Gal4 in the wild-type background as a control. When compared with the regular migration pattern, no significant abnormalities are observed (compare A-E in **Fig. 42** with A-H in **Fig. 12**). Then, p35 was expressed using the same driver line in the *side IV* mutant background (**Fig. 42**K-E), and the results were compared with the *side IV* mutant migration pattern without p35 overexpression (**Fig. 42**F-J).

In *side IV* mutant embryos, especially during stages 13-14, many migrating LVMP cells are off-track and display abnormal morphology (**Fig. 42**F, G). As demonstrated above, these cells were proven to undergo cell death. If their cell death is induced by apoptosis, then after inducing p35 in these cells, there should be fewer round and small cells and more surviving cells in the migrating cohorts. Attempts were first made to quantify whether more cells survived. However, due to the densely connected cells, it is hard to identify single cells. Nevertheless, the off-track cells with round and shrunken shapes are decreased (**Fig. 42**, compare K-L with F-G), and the

quantitative analysis (**Fig. 43**) supports this observation. Thus, the death of these off-track cells in the *side IV* mutant is proven to be induced by apoptosis.

Additionally, the migration patterns in the later stages were compared among these groups to check if the blocked apoptosis exerts further impact on the CVM and LVMP migration. However, as the distribution and orientation of the LVMP and longitudinal muscles are severely disrupted in the absence of Side IV, it is difficult to determine if there is a further alteration.

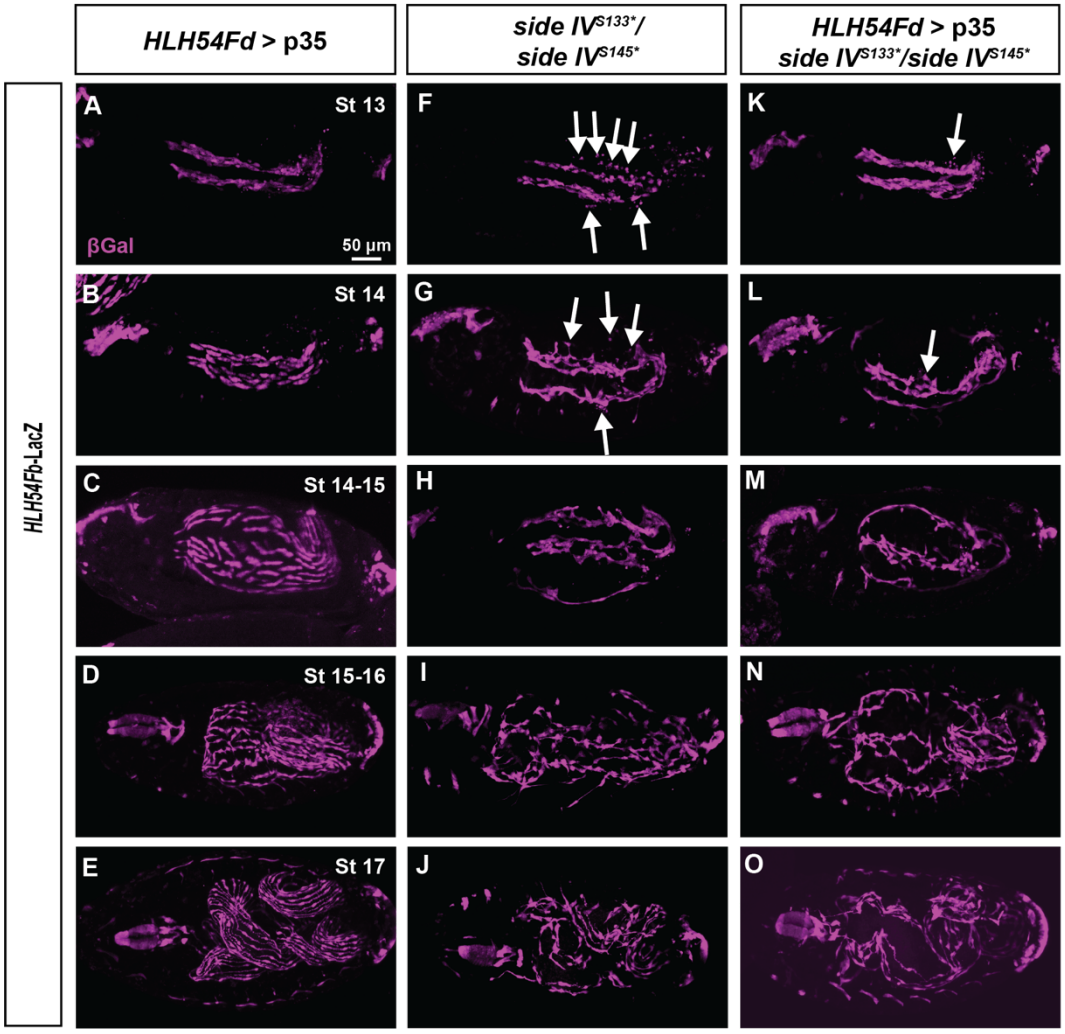

Fig. 42: Fewer LVMP cells in *side IV* mutant display abnormal morphology when apoptosis is blocked. Confocal images of CVM and LVMP cells marked by *HLH54Fb*-LacZ. (A-E) As a control, p35 was forced to express in CVM and LVMP cells by the *HLH54Fd*-Gal4 line. No abnormalities are observed in the migration and differentiation of the CVM and LVMP cells, suggesting no significant effect of overexpressed p35 on these processes. (F-J) Abnormal CVM and LVMP cell migration pattern in *side IV* mutant. During stages 13-14, many LVMP cells are away from the migration path and display round and shrunken cell shapes (arrows in F and G). (K-O) p35 was overexpressed in the CVM and LVMP cells in the *side IV* mutant background. Fewer cells with roundish and shrunken cell shapes are observed (compare K-L with F-G), which suggests that induced p35 blocks their death. In addition, more neighboring cells seem to be fused or connected (compare K with F). However, as the arrangement of LVMP cells and longitudinal fibers in the *side IV* mutant is severely disrupted, it is difficult to assess if there is a further impact of the blocked cell death on the formation of the LVM fibers during embryogenesis. The scale bar in (A) applies to all images.

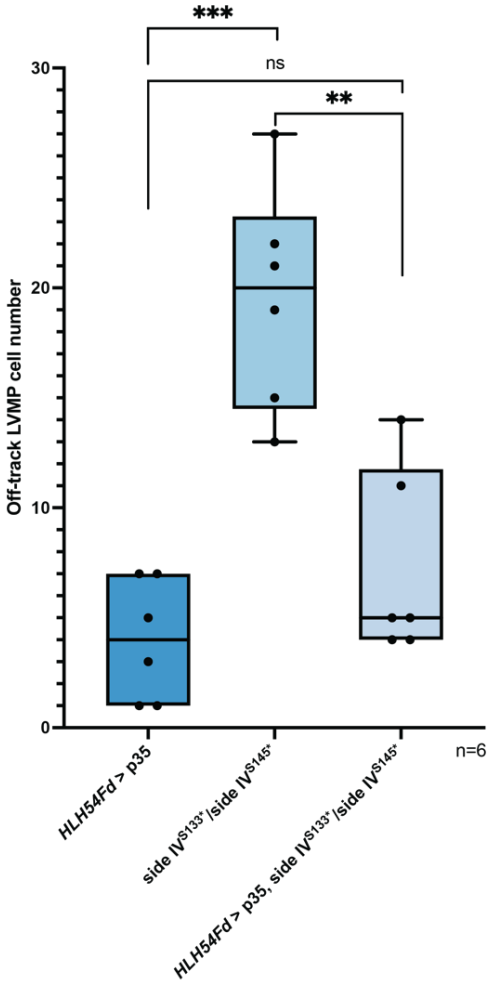

Fig. 43: Statistics of the abnormal LVMP cells in *side IV* mutant embryos.
LVMP cells that lost contact with the TVM and displayed roundish and shrunken cell shapes were counted. When p35 is overexpressed in CVM and LVMP cells in the wild-typic background, only limited cells are off-track and display abnormal morphology. In the *side IV* mutant embryos, these cells are significantly increased. However, after inducing p35 to block apoptosis, the number of these cells decreases and shows no difference with the control. Six embryos at stages 13 and 14 from each genotype were analyzed. ns: not significant, *p < 0.05, **p < 0.01, ***p < 0.001.

2.14 CVM and LVMP cells are misguided by ectopic Side IV expression

To provide additional insights into the potential guidance role of Side IV in regulating the CVM and LVMP cell migration, different driver lines were used to force a Side IV ectopic expression. Among all the tested driver lines, *btl*-Gal4, which drives the expression in the trachea, exerts the strongest impact on the CVM and LVMP cells.

During embryogenesis, the trachea system is developed as a network of epithelial tubules that supply oxygen to various target organs. For instance, from stage 12 onwards, visceral branches are extended towards the midgut to spread over the surface of the visceral mesoderm to provide oxygen to the intestine. As the filopodia activity of the migrating LVMP cells during this period is highly dynamic (Frasch et al. 2023), the ectopic expression of Side IV in the trachea visceral branches is of great possibility to be detected by the migrating cells.

To rule out the potential effect of overexpression in the trachea on the migrating CVM and LVMP cells, UAS-mCD8GFP was used as a control. Moreover, *side IV* mutant embryos were used for the ectopic expression experiments to be devoid of endogenous Side IV. As Shown in **Fig. 44**, GFP is successfully expressed in the trachea system (D'-F'), and the white dotted lines in image E' indicate the developing visceral branches extending toward the midgut. The migration pattern of the CVM and LVMP cells is similar to the *side IV* mutant phenotype where no GFP or any other protein is overexpressed (**Fig. 44**, compare D-F with A-C). In the merged images (**Fig. 44**D''-F''), some colocalized signals in white color are observed but possibly are false impressions due to the overlap location between the trachea and the migrating cells in the Z direction. No direct contact between these tissues is detected.

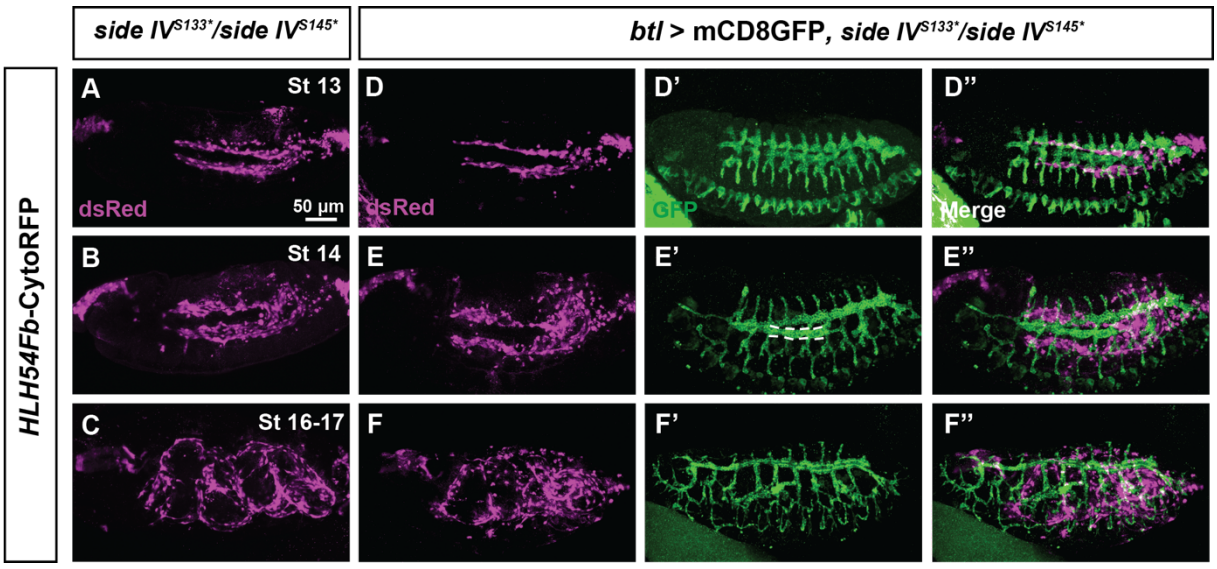

Fig. 44: Overexpressed GFP in the trachea has no impact on CVM and LVMP cell migration.
Microscopy of CVM and LVMP cells marked by *HLH54Fb*-CytoRFP. *side IV* mutant embryos devoid of endogenous Side IV in which the *btl*-Gla4 line was used to support the ectopic expression of GFP in the tracheal system. (A-C) The migration pattern of CVM and LVMP cells in *side IV* mutant serves as the control. With the GFP expression in the trachea (verified by anti-GFP staining in D'-F'), the CVM and LVMP cell migration is similar to the control group (compare D-F with A-C). Moreover, as shown in the merged images (D''-F''), there is no direct contact between the migrating CVM and LVMP cells with the GFP-positive trachea branches. Dotted lines in (E') indicate trachea visceral branches. The scale bar in (A) applies to all images.

Next, V5-tagged Side IV was expressed in the trachea system using the same driver line in the *side IV* mutant embryos, and the overexpression was verified by anti-V5 staining (**Fig. 45**D'-F'). When comparing the migration pattern with the *side IV* mutant phenotype (**Fig. 45**, compare D-F with A-C), obvious differences exist as the gap between the migrating streams is much narrower (compare the gaps indicated with arrows in B and E). Even fewer LVM fibers are formed in the front and middle parts of the midgut at stage 17, resulting in more severely altered midgut constrictions (**Fig. 45**, compare F with C). Moreover, close contact between the LVMP and LVM cells with the trachea is observed, indicating these cells are misrouted toward the Side IV-expressed trachea branches (**Fig. 45**D''-F'').

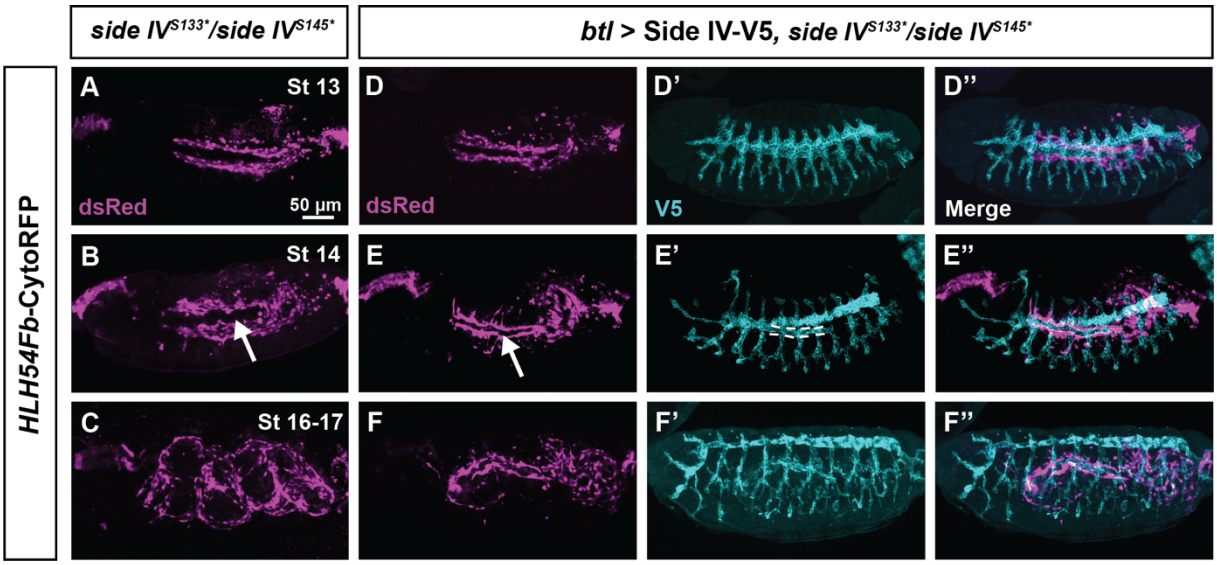

Fig. 45: Ectopic expression of Side IV in the trachea misroutes LVMP cells.
Microscopy of *side IV* mutant embryos expressing *HLH54Fb*-CytoRFP. V5-tagged Side IV was forced to be expressed in the trachea system by the *btl*-Gal4 driver line. (A-C) *side IV* mutant embryos without ectopic expression of Side IV serve as the control. (D'-F') Side IV overexpression in the trachea system is verified by anti-V5 staining. With the ectopic Side IV expression, the migration pattern of the CVM and LVMP cells is different from the control group. The gap between the two migrating streams is narrower (compare arrows in B and E), and constrictions of the midgut are more severely impacted (compare F with C). As shown in the merged images (D''-F''), LVMP and LVM cells are found closely located with the Side IV-positive trachea branches. Dotted lines in (E') indicate trachea visceral branches. The scale bar in (A) applies to all images.

For a better comparison, the overexpression of GFP (**Fig. 44**D''-F'') and Side IV (**Fig. 45**D'-F') in similar regions from the embryos at comparable developmental stages were analyzed (see **Fig. 46**). The enlarged images clearly show that the overexpressed GFP in the trachea has no significant effect on the migrating LVMP cells, as the migrating LVMP streams are away from the visceral branches next to the midgut (**Fig. 46**A-C'). In contrast, the LVMP cells are attracted to the Side IV-expressed visceral branches and have close contact with them (**Fig. 46**D-F'). It

seems that the ectopic Side IV provides chemoattraction cues to misdirect the LVMP cells, suggesting that Side IV may play a key role in guiding the CVM and LVMP cell migration.

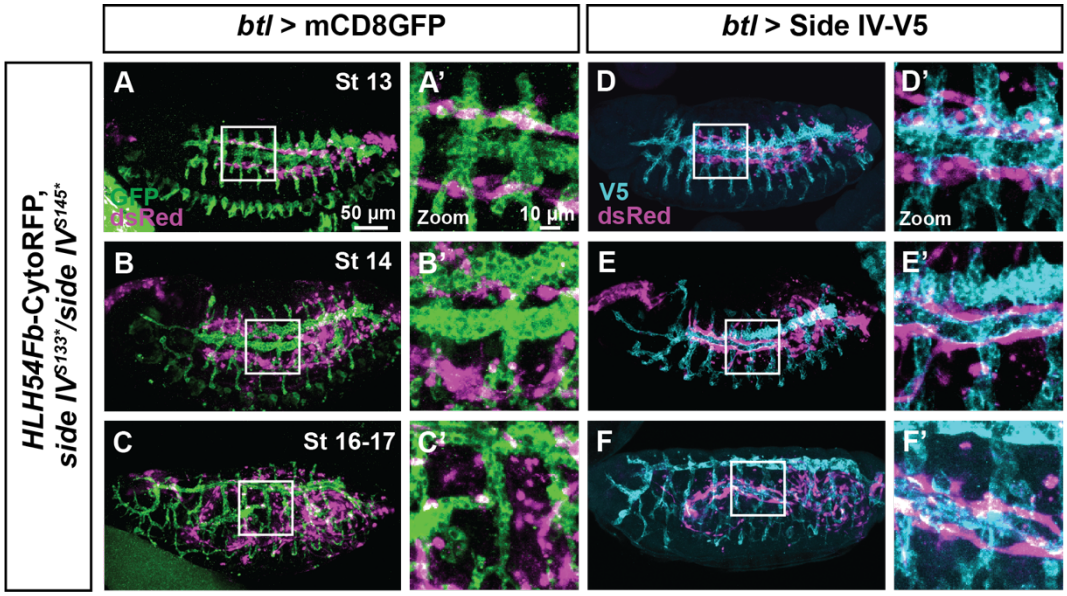

Fig. 46: Comparison of ectopic expression of GFP and Side IV in the trachea.
Confocal images of *side IV* mutant embryos where the GFP or V5-tagged Side IV was forced expressed in the trachea by the *btl*-Gal4 driver line. CVM and LVMP cells were marked in magenta, GFP staining was shown in green, and Side IV expression was visualized by anti-V5 in cyan. (A-C') No significant impact on the migrating LVMP cells is observed when GFP is expressed in the trachea system. (D-F') As a comparison, when Side IV is expressed in the trachea, the migrating LVMP cells, as well as the matured longitudinal visceral muscle fibers, are tightly attached to the Side IV-positive tracheal branches. Squares mark areas enlarged. The scale bar in (A) applies to (A-F). The scale bar in (A') applies to (A'-F').

Because the CVM and LVMP cell migration is even more severely impacted when there is an overexpression of Side IV in the trachea system, a question arises as to whether the LVM fibers in larvae are also subject to more significant damage. Therefore, the midguts of corresponding genotypes were isolated from L3 larvae to investigate the LVM fiber amount and width. As the statistics show (**Fig. 47**), in the *side IV* mutant background, there is a reduction in the LVM number and an increase in the LVM fiber width, and an additional overexpression of GFP in the trachea does not bring in further changes. However, when Side IV is expressed using the same driver line in the *side IV* mutant larvae, the average LVM amount reduces from ten to four (eighteen in the wild type) and there is also a slight increase in the width. Taken together, the observations in the embryos and the larvae demonstrate that the ectopic expression of Side IV misguides the CVM and LVMP cell migration and seriously impacts the LVM fiber formation.

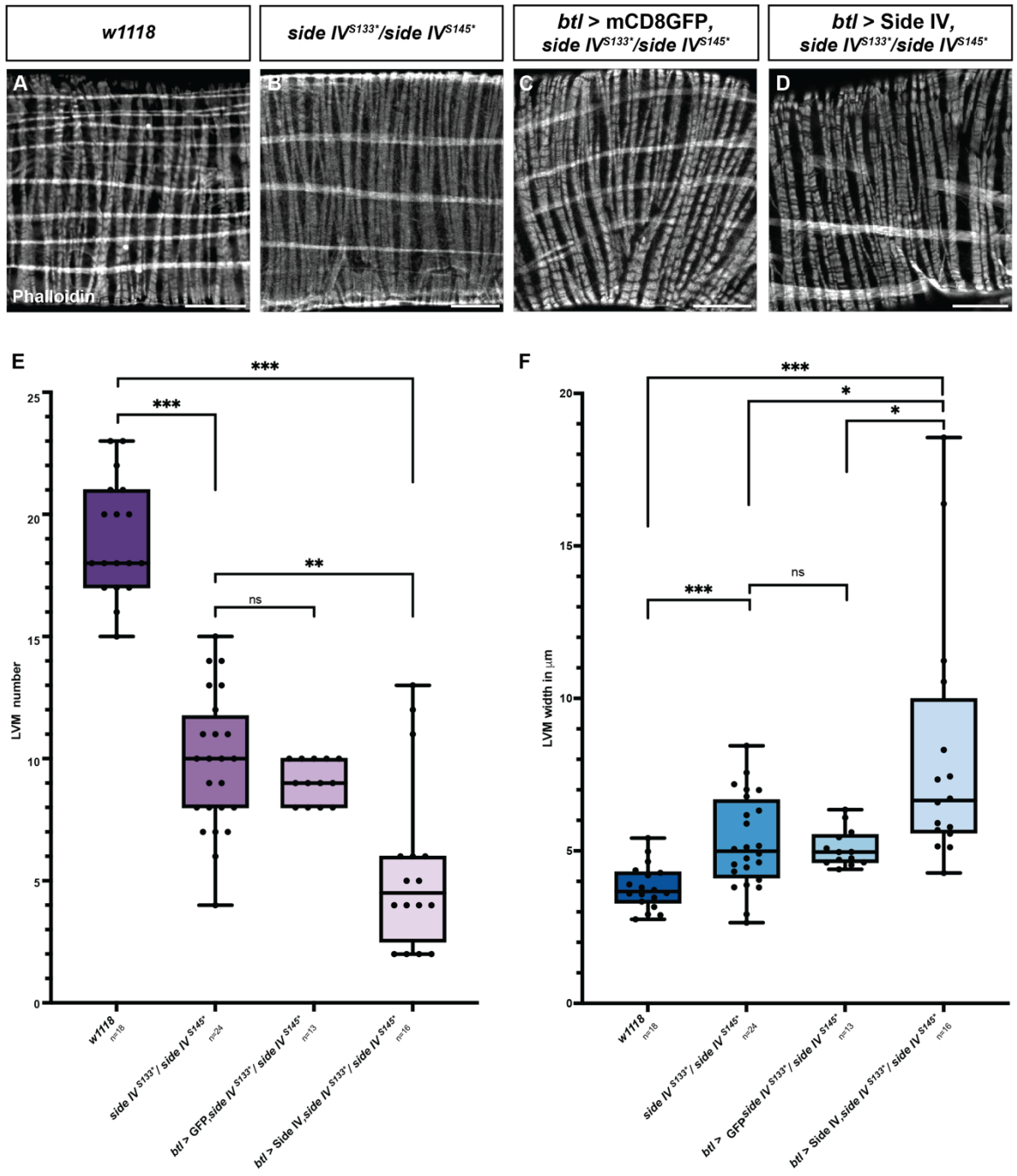

Fig. 47: Larval LVM fibers with ectopic expression of Side IV in the trachea.
(A-D) Confocal images of the midguts from *side IV* mutant larvae in which the GFP or Side IV was overexpressed in the trachea. Both circular and longitudinal visceral fibers of midguts are visualized by phalloidin. The horizontal ones are the LVM fibers. Scale bars: 50 µm. (E) Statistics of the LVM number. In the w^{1118}, the average number is 18, which drops to 10 in the *side IV* mutant. The overexpression of GFP does not lead to additional alterations, whereas the overexpression of Side IV reduces this count to 4. (F) Statistics of the LVM width. When Side IV is absent, the width of LVM fibers increases from 3.5 µm to 4.9 µm, and the overexpression of Side IV causes additional growth of the fibers (around 6.7 µm). ns: not significant, *$p < 0.05$, **$p < 0.01$, ***$p < 0.001$.

2.15 Beat II and Side IV interaction detection

Based on the above findings, one hypothesis is that Beat II proteins work together with Side IV to keep the CVM and LVMP cells on the correct migration path. As Beat IIa and Beat IIb are expressed in CVM and LVMP cells, while Side IV is expressed in TVM cells, the recognition and interaction of these proteins *in trans* should be the basis for working together to guide the migration. Previous publications have reported that Beat II proteins interact with Side IV (Li et al. 2017; Özkan et al. 2013). However, biochemical methods were used in those experiments to check the interactions. To investigate if Beat II can interact with Side IV *in trans*, suspension S2 cells were used in the cell-cell aggregation assay.

2.15.1 Beat II Interacts with Side IV *in trans*

S2 cells were first transfected with Beat IIa-GFP, SP-GFP-Beat IIb, and Side IV-mCherry. After a two-day incubation, the corresponding cells were mixed and shaken for two hours to facilitate a potential interaction. Images were taken with the confocal microscope, and the transmitted light channel (T-PMT) was recorded to show the untransfected cells. As Beat IIa and Beat IIb are both expressed in the CVM and LVMP cells, a group of Beat IIa and Beat IIb co-transfected cells was additionally included.

As shown in **Fig. 48**, cell aggregates with two colors (arrows in A”’, B”’, and C”’) indicate that both Beat IIa and Beat IIb interact with Side IV *in trans*, and the co-transfected cells behave similarly to the singly-transfected ones. Although the untransfected S2 cells also form aggregates when the density is high enough, those aggregates are often small and do not contain fluorescence (**Fig. 48**A”’, B”’ and C”’, arrowheads). Together, these results prove that Beat IIa- and Beat IIb-expressing cells can recognize and interact with the Side IV-expressing cells.

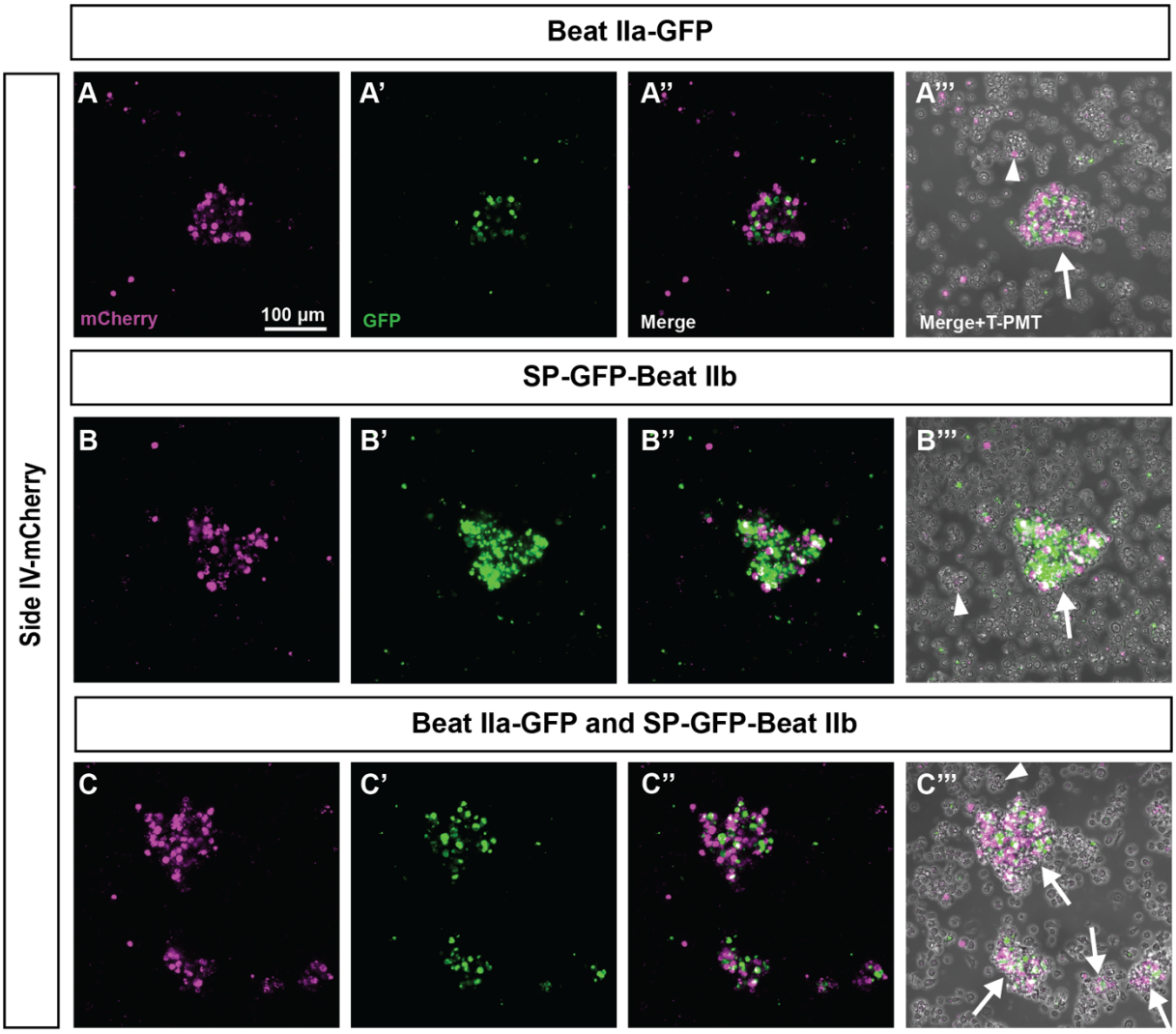

Fig. 48: Beat IIa and Beat IIb form cell aggregates with Side IV.
Confocal images acquired at the wavelength of 543nm (A-C) and 488 nm (A'-C'). The transmitted light channel (T-PMT) was recorded to show the untransfected cells. Although untransfected S2 cells form groups when the cell density is high enough, those cell groups are often small and have no fluorescence (A'''-C''', arrowheads). Notably, large cell aggregates with two fluorescent colors are detected (A'''-C''', arrows), indicating *in trans* protein-protein interactions. The scale bar in (A) applies to all images

To quantify this observation, twenty cell aggregates were randomly picked from the untransfected control and the experimental groups. The outlines of the aggregates were depicted, and the area size was measured. The statistical analysis result (**Fig. 49**) shows that the aggregates in the experimental groups are significantly larger than the untransfected cells, and there is no difference between the Beat II co-transfected cells and the singly-transfected groups.

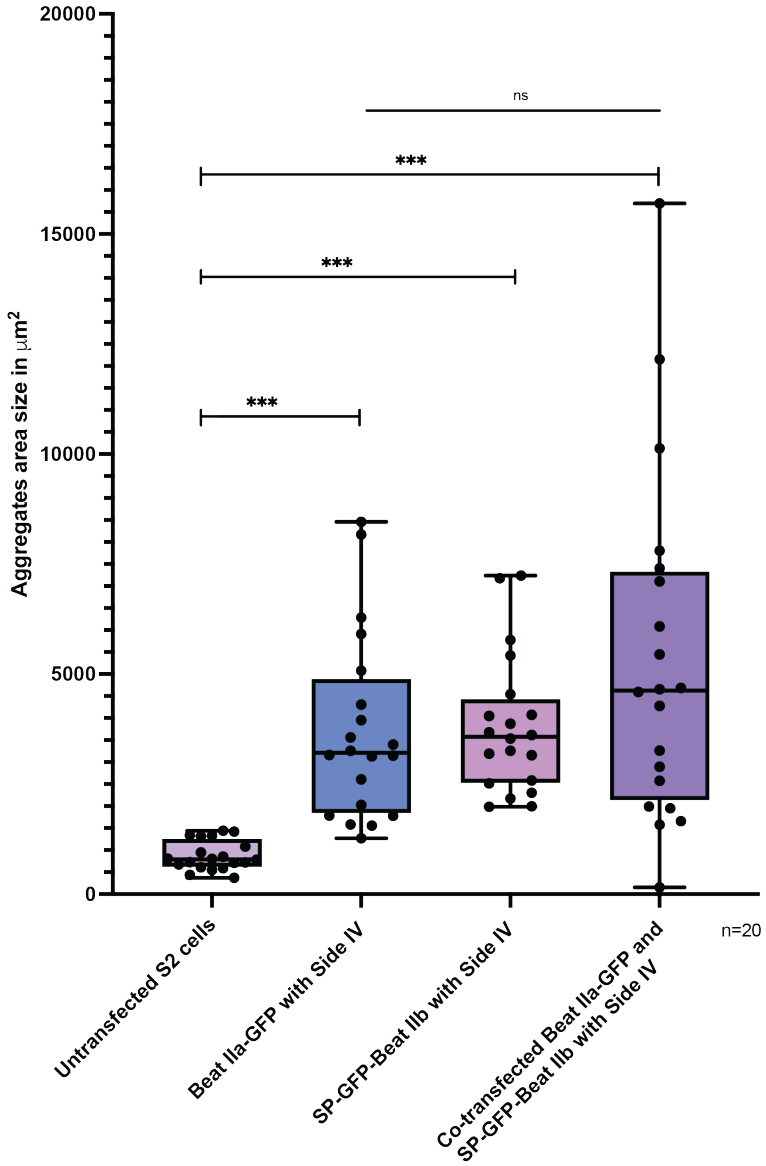

Fig. 49: Beat IIa and Beat IIb form cell aggregates with Side IV.
Statistics analysis of aggregates formed by untransfected and transfected S2 cells. The aggregates formed by Beat IIa- or Beat IIb-transfected S2 cells with the Side IV-transfected cells significantly differ from the control group. In addition, S2 cells that are co-transfected by both Beat IIa and Beat IIb show no difference from the singly-transfected cells. n=20, ns: not significant, *p < 0.05, **p < 0.01, ***p < 0.001.

2.15.2 Beat II shows no interaction with mutated Side IV

As abnormal CVM and LVMP migration patterns were observed in the *side IV^{S133*}* and *side IV^{S145*}* mutants, to test the hypothesis that mutated Side IV lost the ability to interact with Beat II, a UAS-Side IV^{S133*}-mCherry construct was cloned and used in the cell-cell aggregation assay.

With the mutated Side IV, no aggregates with two fluorescent colors are detected (**Fig. 50**). One observation of note is that there are aggregates from the cells transfected with SP-GFP-Beat IIb (**Fig. 50**B-C’’’, arrows). Although these aggregates have larger sizes than the control groups, there is only green fluorescence coming from the GFP-tagged Beat IIb, which suggests that these cell aggregates are not a result of the Beat II and Side IV ^{S133*} protein interaction.

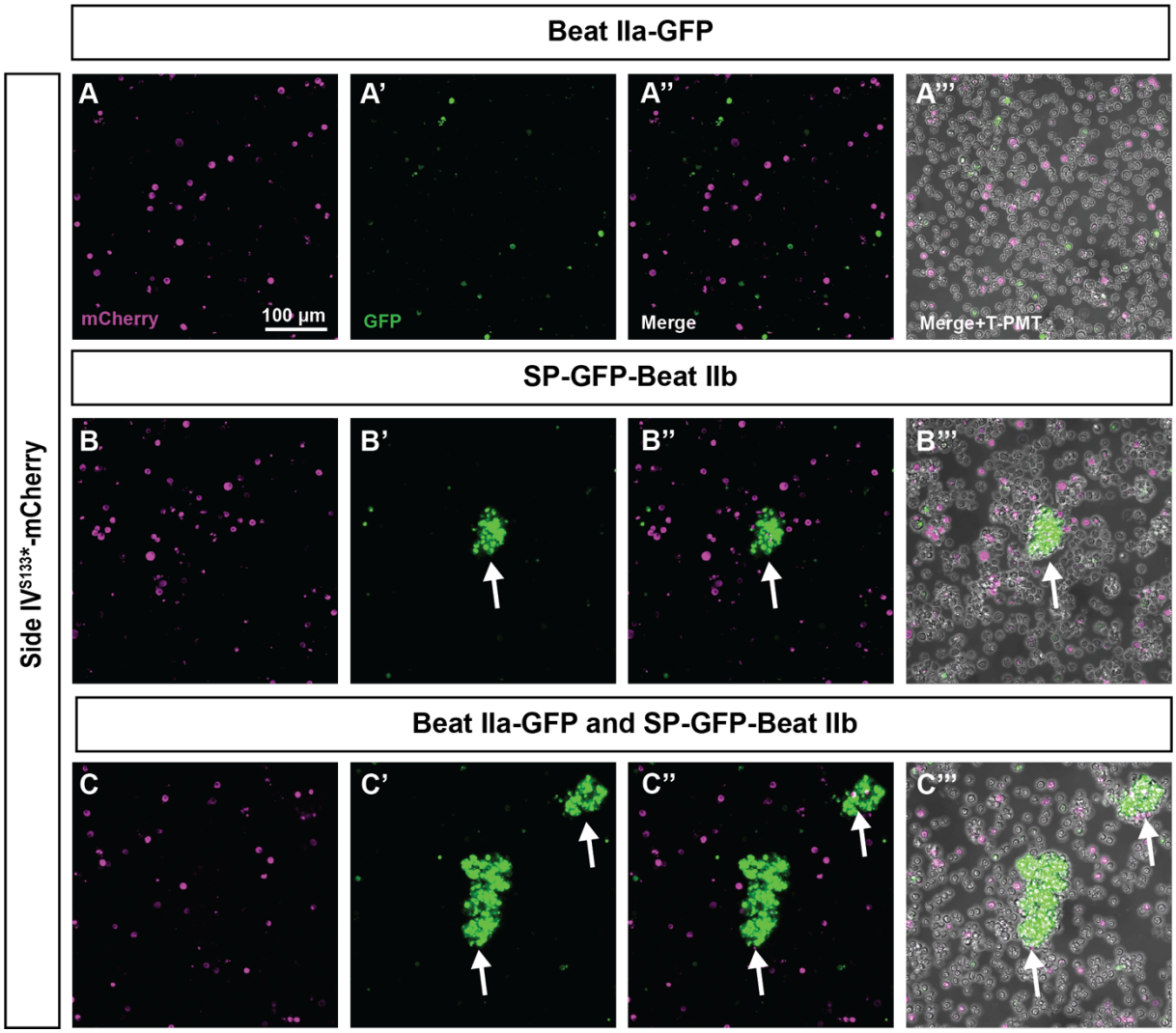

Fig. 50: Beat IIa and Beat IIb do not form cell aggregates with Side IV^{S133*}.
Confocal images acquired at the wavelength of 543nm (A-C) and 488 nm (A’-C’). The transmitted light channel (T-PMT) was recorded to show the untransfected cells. (A-A’’’) When the Beat IIa-transfected cells are mixed with Side IV^{S133*}-transfected cells, no aggregates with two fluorescence are observed. (B-B’’’) Only aggregates with green fluorescence coming from the Beat IIb-transfected cells are detected (indicated by arrows). (C-C’’’) Co-transfected cells with both Beat IIa and Beat IIb behave similarly to the Beat IIb-transfected cells. The scale bar in (A) applies to all images.

2.15.3 Beat II and Side IV interaction prediction

Beat II-Side IV interactions were independently predicted using FlyPredictome through AlphaFold-Multimer (AFM) (Evans et al. 2021; Homma et al. 2023). As shown in the three-dimensional structures (**Fig. 51**), Beat II sequences are colored in red, and Side IV is colored in blue. The potential interaction domains are highlighted. The first IG domain of Beat IIa or Beat IIb is close to the first IG domain of Side IV, indicating that they may be responsible for the interaction. Interaction of the first IG domains has previously been experimentally determined for Beat Ia and Side (Heymann et al. 2022).

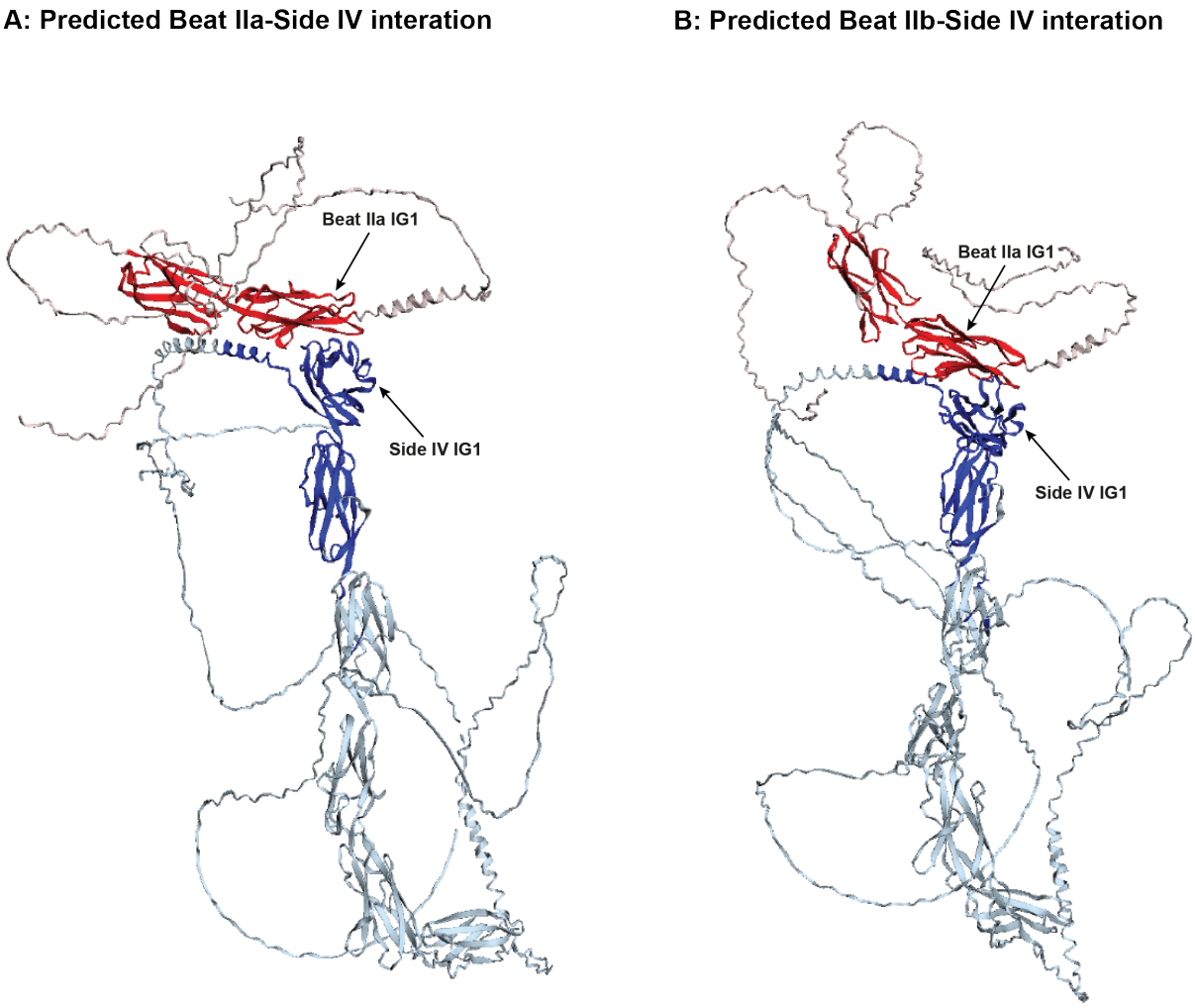

Fig. 51: Predicted Beat II/Side IV interaction by AlphaFold-Multimer.
Predicted three-dimensional structure of the complex structure of *Drosophila* Beat IIa (A) and Beat IIb (B) interacting with Side IV. The domains of Beat II are colored in red, and the domains of Sdie IV are colored in blue. Protein structures and interacting domains are determined and visualized with ChimeraX. The database is available at www.flyrnai.org/tools/fly_predictome (Kim et al. 2024).

2.16 Larval food intake assay

The midgut musculature is responsible for food transport. As the longitudinal visceral muscle fibers are decreased in the *beat II* double mutant and *side IV* mutant larvae, a raised question is whether the larval feeding behavior is affected when Beat II or Side IV is absent. To address this question, a larval food intake assay was used to test food consumption in larvae (**Fig. 52**).

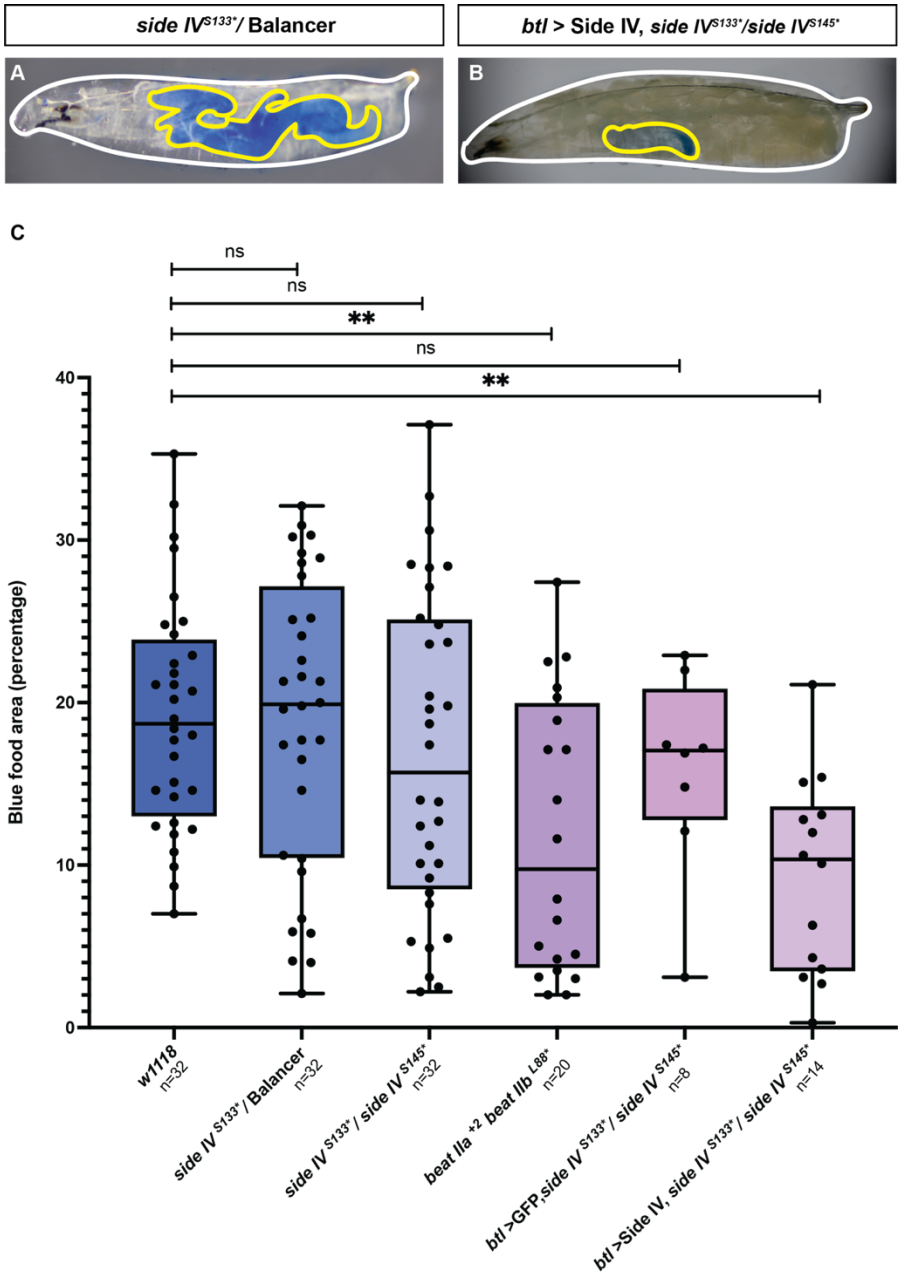

Fig. 52: Larval food intake measurements.
(A and B) Illustrations showing the procedure for measuring food consumption. The amount of food consumed is quantified by calculating the ratio of blue-stained pixels (yellow outlines) to the total number of pixels in the entire larval body (white outlines). (C) Data from the food intake assay for the control and mutant genotypes. ns: not significant, *p < 0.05, **p < 0.01, ***p < 0.001.

To ensure the tested larvae are in similar development stages, eggs were only collected for two hours and raised for 96 hours at 25°C. After being starved for 1.5 hours, the larvae were fed with fresh yeast dyed with bromphenol blue sodium salt (less than 1%) for 15 minutes. w^{1118} and *side IV* ^{S133*} over a balancer were set as control groups, no significant difference is observed between these two groups.

When compared with the controls, transheterozygous *side IV*^{S133*} over *side IV* ^{S145*} larvae show no feeding defects. Of note, when Side IV is overexpressed in the trachea system when the endogenous *side IV* is mutated, there is a significant decrease in food consumption. Taken together with the observation that LVM fibers are more severely impacted when there is an ectopic expression of Side IV than an expression of GFP in the trachea (**Fig. 47**), this phenomenon could be explained as only when the LVM fibers are reduced to a certain amount, the larval feeding behavior can then be affected. Interestingly, there is also a significant reduction in the food consumption of *beat IIa*$^{+2}$*beat IIb*^{L88*} double mutant, of which the LVM fiber number is similar to the *side IV* mutant larvae. However, although the fiber number is similar, abnormalities like splitting or merging in the LVM fibers are more often detected in the *beat II* double mutant. In addition, escapers of *beat IIa*$^{+2}$*beat IIb*^{L88*} double mutant rarely survived until the adult stage, indicating that Beat II proteins may exert further influence on the growth of LVM fibers during the larval and pupal stages.

In summary, this work has shown that Beat II-expressing CVM and LVMP cells migrate over the Side IV-expressing TVM cells. Both Beat II and Side IV are essential for the proper migration and differentiation of CVM and LVMP cells.

3 Discussion

In this work, Beat IIa and Beat IIb proteins are found expressed in the migrating caudal visceral mesoderm (CVM) and longitudinal visceral mesoderm precursor (LVMP) cells. In addition, Side IV is found in the trunk visceral mesoderm (TVM) cells, which serve as the migration substrate for CVM and LVMP cells. Similar migration and differentiation defects are observed in both the *beat II* double mutants and *side IV* mutants, characterized as irregular migration patterns with abnormal cell morphology and distribution. Apoptosis is detected in the mismigrating cells. As a result, fewer longitudinal visceral muscle (LVM) fibers are detected at the larval stage. Both Beat II proteins interact with Side IV *in trans*. Ectopically expressed Side IV in the trachea attracts CVM and LVMP cells to the visceral tracheal branches. These results suggest that Beat II and Side IV proteins are required for the CVM and LVMP cell migration and differentiation

3.1 CVM and LVMP cells use TVM as migration substratum

Migrating cells require both traction and adhesion to a substratum to move. During the anterior migration of the CVM cells and the dorsoventral migration of the LVMP cells, TVM serves as their migration substratum. At stage 10, CVM cells initiate migration over the midgut primordia, as the TVM was not specialized yet (Ismat et al. 2010). Once the TVM cells differentiate at stage 11, CVM cells adhere and maintain close contact with them until the LVM fibers are eventually differentiated. Like many other examples, the CVM and LVMP cell migration process is regulated by dynamically coupling extracellular signals from the surrounding tissues with the remodeling of polarity and adhesion complexes (Kadam et al. 2012; Reim et al. 2012; Urbano et al. 2009; Ismat et al. 2013).

During the migration course, TVM provides not only mechanical support but also survival and guidance cues for CVM and LVMP cells (Sun et al. 2020). For instance, TVM expresses αPS integrin, contributing to CVM cell movement by adhering to and signaling from the underlying ECM (Urbano et al. 2011). Moreover, the FGF ligands *pyr* and *ths* expressed in the TVM, activate their receptor *htl* in CVMs synergistically to support CVM survival and migration (Reim et al. 2012; Kadam et al. 2012). As previous studies and this work have shown, when TVM formation is disrupted, e.g. in the *bap* mutant, fewer CVM cells and irregular migration

patterns are detected (Reim et al. 2012). Even when apoptosis is inhibited, the surviving CVM cells still exhibit an abnormal migration manner, indicating that TVM is critical for guiding CVM cells on the correct path (Reim et al. 2012).

Meanwhile, the substratum TVM is influenced by the migratory CVM cells (Macabenta and Stathopoulos 2019). In FGF mutants, the midline-crossing phenotype of CVM cells strongly correlates with the abnormal contralateral merging of the TVM. Additionally, in the absence of CVM cells, TVM cells display a convoluted, looping morphology instead of a relatively linear shape (Macabenta and Stathopoulos 2019). Taken together, in the course of CVM and LVMP cell migration, TVM serves as the migration substratum, providing mechanical support, survival cues, and guidance signals for the migratory cells, and is also influenced by the migratory behaviors of the CVM cells.

3.2 Beat II proteins are expressed in CVM and LVMP cells

Among various cell surface proteins of the immunoglobulin superfamily, one subfamily is known as the “Beat family”. In this family, fourteen members are classified into seven subgroups according to their phylogenetic relationships. Proteins in the same subgroup have similar evolution rates and often show comparable embryonic expression patterns (Li et al. 2017; Pipes et al. 2001). This work focused on two Beat II members: Beat IIa and Beat IIb.

The earliest published expression pattern regarding *beat II* comes from the work of Pipes and colleagues, where *beat II* mRNAs were detected in the CNS and a subset of ventral oblique muscles (Pipes et al. 2001). This finding distinguishes Beat II proteins from other Beat members, as all the other embryonic detectable Beats are only found in neuronal tissues. However, due to the limited image quality and the ventral view of the embryo, it is difficult to identify their specific expression in other tissues.

Until 2015, a library of 400 GFP-tagged genes, including *beat IIb,* was created using MIMICs (Minos Mediated Integration Cassette) lines (Nagarkar-Jaiswal et al. 2015). As GFP is fused to the reading frames in these lines, the embryonic expression pattern of Beat IIb protein could thus be investigated using native fluorescence or immunohistochemistry staining. Using the Beat IIb$^{MIO3102\text{-}GFSTF.0}$ line, our research group found that the Beat IIb seems expressed in CVM cells (Wehner 2020). Based on this observation, *in situ* hybridization and immunohistochemical

staining experiments were performed in this work to obtain more expression details of *beat IIb*. The results show that the expression of *beat IIb* starts from stage 10 before the CVM cell migration and lasts in the CVM-derived LVMP cells. At the end of embryogenesis, Beat IIb can still be detected in the mature LVM fibers. When comparing the expression patterns of mRNA with the protein, a difference is that the mRNA levels decrease after stage 15, while the GFP-tagged Beat IIb protein can be strongly detected until stage 17 (compare **Fig. 17** with **Fig. 18**). One reason may be that the half-lifetime of the GFP is much longer than that of mRNA (Corish and Tyler-Smith 1999; Wang and Liu 2022).

In addition, as *beat IIa* mRNA was also previously found in CVM cells (Bae et al. 2017; Ismat et al. 2010), a comprehensive embryonic expression pattern of *beat IIa* was under examination. Like *beat IIb*, *beat IIa* is expressed in the CNS, some somatic muscles, and most importantly, in CVM, LVMP, and LVM cells (**Fig. 16** and **Fig. 17**). It is worth mentioning that both *beat IIa* and *beat IIb* mRNA show strong signals from stage 12 to 15, during which the CVM cells migrate anteriorly, and the LVMP cells migrate dorsal-ventrally to cover the expanding midgut. Then, both signals decrease after stage 15. This could indicate that Beat II proteins may function in the anterior migration of CVM cells and the dorsal-ventral migration of LVMP cells.

Recently, single-cell RNA sequencing was conducted to understand the transcription programs involved in the development of *Drosophila*. Both *beat IIa* and *beat IIb* were found in the longitudinal visceral mesoderm during embryonic stage 10 to stage 16 (Peng et al. 2024), which aligns with our observation. Altogether, the expression of Beat IIa and Beat IIb in the CVM and LVMP cells is confirmed, laying the foundation for the following investigations.

3.3 Side IV is expressed in TVM cells

After analyzing the expression pattern of Beat II proteins, one raised question is whether they have potential interaction partners. To address this question, this research focused on the Side family, which also belongs to the immunoglobulin superfamily. Sides often function together with Beats, for instance, Beat Ia works with Side as a ligand-receptor pair to regulate axon growth (Siebert et al. 2009). Among the eight members in the Side family, two interesting candidates are Side and Side IV because they can interact with both Beat II proteins (Li et al. 2017; Özkan et al. 2013).

Up to now, the expression and function of Side are more well-known than Side IV. Based on previous research and the examination from our institute Side is, however, not found in tissues that are in the vicinity of CVM and LVMP cells (Siebert et al. 2009; Sink et al. 2001). As for Side IV, it was previously reported to be expressed in ventral muscle precursor cells at stage 12 and then in a subset of ventral and lateral muscles by stage 14 (Li et al. 2017). In 2020, Lavergne and his colleagues found Side IV in the lateral adult muscle precursors at stage 14, which are muscle stem cells for *Drosophila* (Lavergne et al. 2020). However, a comprehensive embryonic expression pattern of Side IV still needs to be included. Thus, *in situ* hybridization was performed in this work, and the *side IV* mRNA was surprisingly found in the TVM (**Fig. 26**).

Furthermore, to gain deeper insights into its expression pattern during *Drosophila* embryogenesis, an anti-Side IV antibody and a GFP-tagged Side IV line were used (**Fig. 27** and **Fig. 28**). Firstly, the specificity of the anti-Side IV antibody was tested by using it in the wild-type as well as the *side IV* deficiency embryos. In the wild-type embryos, a signal is observed from the TVM, while it is missing in the deficiency embryos, indicating that this antibody and the staining results are reliable. Additionally, the anti-Side IV staining is consistent with the Side IV-GFP staining. Interestingly, in both experiments, Side IV is found in the TVM cells from late stage 12.

Of note, Side IV is detectable not only in the TVM but also weakly in the LVMP cells at stage 14. Afterward, Side IV decreases in the TVM while it increases in the LVMP and later LVM cells. This phenomenon is similar to the Fas III expression, first detected in the TVM cells and later in the LVM cells (Klapper et al. 2002). Considering that *side IV* mRNA is not detected in LVMP and LVM cells, a possible explanation could be that Side IV is transferred into LVMP cells during the fusion process between TVM-derived fusion-competent myoblasts and the CVM-derived founder cells. However, whether this “translocation” plays any role in the LVMP cells is still unknown. It may interact with Beat II proteins *in cis* to stop their *in-trans* interaction or participate in other signal pathways.

The results of this thesis are again supported by the work of Peng and colleagues, who used the single-cell RNA sequencing program and detected *side IV* is detected in the circular visceral mesoderm (Peng et al. 2024).

3.4 Beat II and Side IV protein structure

In 2001, Beat IIa was predicted to be a transmembrane protein (Pipes et al. 2001). Using DeepTMHMM and InterPro, two transmembrane domains are predicted in Beat IIa, one at each terminus and the majority of the protein is located outside the cytoplasm. In comparison, Beat IIb contains no predicted transmembrane domain but a GPI-modification site at position 376 aa. Together with a signal peptide at the N-terminus, Beat IIb is predicted as a GPI-anchored protein (GPI-AP). GPI-APs are generally anchored in the outer leaflet of the cell membrane through a C-terminal GPI anchor, a complex glycolipid moiety consisting of a phosphoethanolamine linker, a glycan core, and a phospholipid tail (Paulick and Bertozzi 2008). GPI-APs have been found to function in various roles, including serving as enzymes, adhesion molecules, protease inhibitors, and receptors (Kinoshita 2016).

As for the immunoglobulin (IG) domain prediction, SMART predicts only one IG domain in both Beat IIa and Beat IIb, while AlphaFold shows two potential IG repeats. This situation resembles the prediction for Beat Ia, where SMART predicts only one, but AlphaFold predicts two IG domains. According to previous studies, Beat Ia tends to have two IG repeats based on the sequence alignment analysis of Beat Ia with other known IG superfamily members, like *Drosophila* Fas III (Mushegian 1997; Bazan and Goodman 1997). The sequence alignment and the secondary structural analysis suggest that the Beat Ia IG domain is a nine-β-stranded structure held together by a disulfide link composed of two central cysteines (Bazan and Goodman 1997).

To gain more insights into the Beat II structure, the potential two IG sequences were aligned with the ones from Beat Ia. In both alignments, the essential cysteines are conserved, and the sequences in the first IG domain of Beat IIa and Beat IIb are highly similar to the Beat Ia. However, the second IG domain alignment shows fewer similarities with the Beat Ia, with additional amino acids forming a loop between the β-strands (**Fig. 20**). As this loop structure is not seen in other known IG domains, e.g. *Drosophila* Fas II, Fas III, and Side, it might be the reason for the inability of SMART to detect the second IG domain. Another explanation for the difference between these two IG domains might be that the first IG domain is responsible for the interactions with Side family proteins, while the second potential domain is less functional. This explanation will be further discussed in the next section.

Like other Side family members, Side IV is predicted as a membrane protein with a transmembrane sequence at the C-terminus. Additionally, five IG domains and an FN3 domain are predicted. Together, Beat II and Side IV are predicted as transmembrane or GPI-anchored proteins, suggesting that they are expressed on opposing cell surfaces during visceral cell migration and they may recognize each other *in trans*. This *in-trans* interaction was proven in this study using the cell-cell aggregation assay, as discussed in the next section. Further experiments like the phosphatidylinositol-specific phospholipase C cleavage assay could be used to check if Beat IIb is a GPI-AP, and other structure-function analyses could be done to confirm the rest predictions.

3.5 Beat II interacts with Side IV *in trans*

Two independent studies reported that both Beat IIa and Beat IIb can interact with Side IV in biochemical assays (Li et al. 2017; Özkan et al. 2013), but these interactions have not been proven *in vivo*. Considering that Beat II proteins are expressed in CVM and LVMP cells, while Side IV exists in TVM cells, their ability to recognize and interact with each other *in trans* would lay a foundation for the hypothesis that they work together to play a role during the CVM and LVMP cell migration.

To provide further evidence, Beat II-Side IV interactions are predicted using FlyPredictome through AlphaFold-Multimer (AFM). AFM is an expansion of AlphaFold2 to predict complex protein structures. AlphaFold2 utilizes artificial intelligence trained on multiple sequence alignments and structural information to predict protein structures. It generates a Template Modelling (pTM) score to forecast structures and visualizes the confidence in these structures using the local Distance Difference Test. Based on this, AFM calculates the interface pTM score (ipTM) and predicts protein complexes. It has been used for various predictions, e.g. to predict protein-protein interactions in yeast and cross-kingdom interactions at the plant-pathogen interface (Evans et al. 2021; Kim et al. 2024; Homma et al. 2023).

Using AFM, both Beat IIa-Side IV and Beat IIb-Side IV interactions are predicted to have a high rank (**Fig. 51**). The first IG domains of Beat II and Side IV seem responsible for the interaction, as they are arranged closely. Similar observations are described in previous work of our institute, which demonstrates that Beat Ia and Side interact through their first IG domains.

When the first IG domain of Beat Ia or Side is deleted, the attraction of motor axons and their complex formation is abolished (Heymann et al. 2022).

The cell-cell aggregation assay was then performed using S2 cells in suspension to test if Beat II proteins interact *in trans* with Side IV in cells. For transient transfections, UAS-Side IV-mCherry and UAS-Beat IIa-GFP were used. As for Beat IIb, a GFP tag was first added at the C-terminus. However, the fluorescence after transfection is much weaker than other constructs like Beat IIa-GFP. Since Beat IIb may be a GPI-anchored protein with a predicted GPI-modification sequence at the C-terminus, a GFP was then inserted at the N-terminus after the signal peptide to avoid interrupting the C-terminus.

Eventually, in either the Side IV-Beat IIa or Side IV-Beat IIb group, aggregates are significantly larger than the untransfected or singly-transfected S2 cells, indicating that Side IV-transfected cells can recognize and interact with Beat II-transfected cells. In addition, as both Beat II proteins are expressed in the CVM and LVMP cells, a well of S2 cells were co-transfected with Beat IIa and Beat IIb simultaneously and then mixed with the Side IV-transfected S2 cells. In this group, the aggregates show no difference with the Beat IIa- or Beat IIb-transfected groups (**Fig. 48** and **Fig. 49**).

Of note, as severe migration defects were found in the *side IV^{S133*}* and Side IV^{S145*} mutants, the full-length Side IV is then replaced with Side IV^{S133*} to check if the interaction with Beat II is lost. Within expectations, in the Side IV^{S133*}-Beat II experimental groups, aggregate formation is abrogated. Cell clusters are only found in the groups with SP-GFP-Beat IIb transfected cells, but these clusters only contain Beat IIb but not Side IV (**Fig. 50**). The reason may be that the GFP insertion in this construct induces adhesions among themselves. These findings provide strong experimental evidence that Side IV and Beat II proteins can interact *in trans*.

3.6 *beat IIa* and *beat IIb* function redundantly during CVM and LVMP cell migration

As Beat II proteins are expressed in CVM and LVMP cells, *beat IIa* and *beat IIb* single and double mutants were first checked for the embryonic CVM and LVMP cell migration and differentiation processes.

When *beat IIa* or *beat IIb* is mutated, only minor defects with empty spaces having no LVMP cells are detected at stage 15. These defects are more evident in the *beat IIb* single mutant, in which areas lacking longitudinal fibers are still present by the end of embryogenesis (**Fig. 22**). Most interestingly, if both *beat IIa* and *beat IIb* are mutated or deleted, CVM and LVMP cell migration show severe defects, which can be characterized as disordered cell migration and misshapen cell morphology with fewer LVM fibers that can be formed at the end (**Fig. 23**). These observations reflect a redundant function of *beat IIa* and *beat IIb* in regulating the CVM and LVMP cell migration.

Similar redundant phenotypes were previously described for *Big brother (Bgb)* and *Brother (Bro)*. Bgb is a nuclear protein that co-localizes with Lozenge (Lz) and Runt (Run) in *Drosophila*. During the ds-RNA-mediated genetic interference analyses, another protein called Bro exhibited a redundant role for Bgb (Kaminker et al. 2001). Both Bgb and Bro can physically interact with Run to enhance its affinity for DNA (Fujioka et al. 1996; Golling et al. 1996). In a null allele of *run*, segmentation defects are observed, which can be characterized by deletions of denticle belts. However, when only *Bgb* is knocked down, there are no significant effects on the segmentation. In comparison, when *Bro* is knocked down, minor defects in the segmentation pattern are identified, which partially resemble the *run* mutant phenotype. Striking, the disruption of both *Bro* and *Bgb* results in strong segmentation defects, which are identical to the defects in *run* mutants, suggesting that the functions of *Bro* and *Bgb* are compensatory in regulating the segmentation (Kaminker et al. 2001).

Taken together, these data indicate that *beat IIa* and *beat IIb* function redundantly during the CVM and LVMP cell migration. Although the disruption of *beat IIa* or *beat IIb* alone does not induce severe defects, the function of *beat II* in cell migration becomes evident when both partner genes are disrupted.

3.7 Expression of Beat IIa in CVM and LVMP cells rescues *beat II* mutant phenotype

Having observed that CVM and LVMP cell migration show severe defects in the *beat II* double mutant and the *beat II* Df(3R)ED5780 line, it is interesting to investigate whether restoring Beat II in CVM and LVMP cells could rescue the mutant phenotype. To this end, *HLH54Fd*-Gal4 was used for driving the UAS-Beat IIa-Cherry expression in CVM and LVMP cells.

Firstly, UAS-Beat IIa-Cherry was crossed with *HLH54Fd*-Gal4 in the wild-typic background to check if it could be successfully expressed within the target cells. With the anti-dsRed staining, Beat IIa-Cherry is strongly detected in the CVM cells at stages 11 and 12. However, the signal decays after stage 13 and almost can not be detected at stage 16. This observation is contractionary with the findings from the antibody staining for the Beat IIa-GFP line, where the expression of Beat IIa is still detected by the end of embryogenesis. A possible explanation is that the *HLH54Fd*-Gal4 line may not support the expression of Beat IIa-GFP at later stages. Further screening should be performed to seek an ideal driver line that reflects the time- and tissue-specific expression of Beat II. Similar identifications of driver lines for Side have been done in previous work of our institute (Kinold 2016).

Nevertheless, the restored Beat IIa expression using this Gal4 line greatly rescues the *beat II* mutant phenotype, as a more regular migration pattern of CVM and LVMP cells is observed. It is worth mentioning that when only the Beat IIa expression is restored, the phenotype looks very similar to the *beat IIb* single mutant phenotype, where the dispersion of the LVMP cells around the midgut chamber is delayed and some areas can not be fully covered by LVMP cells (compare **Fig. 24** with **Fig. 22**). This successful rescue proves again that Beat II plays a role in regulating the CVM and LVMP cell migration.

Meanwhile, the rescue experiment with Beat IIb is still ongoing. An UAS-Beat IIb-GFP line in which the GFP tag was joined at the C-terminus was already created. However, its expression under the control of the *HLH54Fd*-Gal4 driver line is fragile. The signal is only detectable at stage 11. Afterward, no Beat IIb-GFP is detected in the CVM or LVMP cells. Thus, another UAS-SP-GFP-Beat IIb line, where GFP is at the N-terminus, is under preparation.

3.8 Beat II functions with Side IV to regulate CVM and LVMP cell migration

As Side IV is expressed in the migration substratum for CVM and LVMP cells, the migration pattern of these cells in the *side IV* mutant and deficiency lines was also analyzed. Interestingly, the *side IV* mutant phenocopies the *beat II* double mutant (compare **Fig. 31** with **Fig. 23**). Given the fact that Side IV can recognize and interact with Beat II *in trans*, Side IV and Beat II might function as a ligand-receptor pair to assist the cell migration.

Based on previous research, a similar guidance function is exerted by the FGF signals. In *Drosophila* embryos, two FGF ligands, Pyramus (Pry) and Thisbe (Ths) are expressed in the TVM cells, and their receptor Heartless (Htl) exists in CVM cells. In both FGFs or *htl* mutants, there are severe defects in CVM migration, including a disordered migration pattern with midline crossing of the bilateral cell streams. Together with a series of genetic experiments, it has been demonstrated that FGF signaling is essential for ensuring the survival of the CVM cells and keeping them on the correct migration path (Mandal et al. 2004; Kadam et al. 2012; Reim et al. 2012; Macabenta and Stathopoulos 2019).

Recently, the Beat II-Side IV interaction has attracted more and more attention. In 2024, Osaka and his colleagues used the *Drosophila* visual system as the model and showed that Beat IIb and Side IV regulate the specificity of synapse formation (Osaka et al. 2024). They examined the function of Beat II proteins in the visual system and found that Beat II was expressed in the M1-M2 and M9-M10 layers of the medulla. To test if misexpressed Side IV could induce synapse formation, Side IV was ectopically introduced in R7 photoreceptors. Consequently, additional synapses were formed in the layers where Beat II proteins exist, and these layers were not the usual targets for R7. In addition, over-expressed Side IV caused the GFP-tagged Beat IIb to become punctate, a common phenomenon when synapse-organization transmembrane proteins were clustered. Most interestingly, around 70% of Side IV/Beat IIb co-localized with ectopic synapses, strongly suggesting that Beat II-expressing neurons could attract Side IV-expressing axons to trigger synapse formation. Furthermore, they showed that the Side IV/Beat IIb recruits Kirre and Dsyd-1, and the Side IV/Beat IIb/Kirre/Dsyd-1 complex formation restricts synaptic specificity and inhibits miswiring. Notably, they also performed cell-cell aggregation assays, confirming that Beat II-transfected S2 cells aggregate with Side IV-transfected cells (Osaka et al. 2024). Altogether, the findings from this work and other groups allowed the demonstration whereby the migrating cell-expressing Beat II interacts with the substratum-expressing Side IV to regulate the cell migration.

3.9 Abnormal LVM fibers in *side IV* and *beat II* mutant larvae

Due to the twisted tube-like gut, which can hardly be isolated from the embryo, it is difficult to examine the details of the LVM fibers at the embryonic stage. Fortunately, the viability of

beat II and *side IV* mutant third-instar larvae enables the isolation of the midgut and investigation of the number and morphologies of the LVM fibers.

The number and width of the LVM fibers of *beat II* mutants were first compared with the w^{1118} larvae. In the *beat* IIa^{+2} mutant, there is no difference concerning the number or width, however, split myofibrils with a gap in the center are often detected. In the *beat* $IIb^{\Delta 14}$ mutant, the width of the fibers is slightly increased, and there is a minor reduction in the numbers (from 18 to 16). By contrast, in the *beat* IIa^{+2}*beat* IIb^{L88*} double mutant, there is a further reduction in the number (from 18 to 12) and an increase in the width of LVM fibers (**Fig. 25**). Interestingly, similar defects are observed in the *side IV* mutant, where the LVM number drops to 12, and the average width increases to 4.8 μm (**Fig.32**).

The increased fiber width may result from the distorted and abnormal distribution of LVM cells during embryogenesis or due to potential functions of Beat II and Side IV in the further growth of longitudinal fibers during the larval stage. Regarding the decreased number of fibers, one hypothesis is that there is a loss of CVM or LVMP cells in the mutants, which leads to fewer cells that can differentiate into LVM fibers. The loss of cells may be caused by uncoordinated cell migration, which triggers anoikis. Another assumption is that the longitudinal visceral myoblast fusion is disrupted, resulting in fewer LVM muscles being formed. These two hypotheses will be discussed in the next sections.

3.10 Longitudinal myoblast fusion capacity is not affected in *side IV* mutant embryos

As discussed above, one possible explanation for the aberrant shape of syncytia and decreased LVM fibers is that the myoblast fusion process is affected. Thus, the TVM-derived fusion-competent cells and the nuclear number in the developing LVMP cells were examined. Because the *side IV* mutants were generated much earlier than the *beat II* double mutant, most of the following experiments were performed with the *side IV* mutants.

During the formation of the embryonic midgut musculature, the FCMs for both circular and longitudinal visceral muscles arise from the TVM. At stage 12, each FCM fuses with one circular FC to differentiate into a binucleated circular muscle precursor cell. Upon the end of this circular myoblast fusion, the remaining fusion-competent cells migrate to both ventral and

dorsal margins of the TVM band, fusing with the longitudinal FCs arising from the CVM to form the longitudinal muscle precursors (Klapper et al. 2002). According to a previous study, the fusion-restricted myogenic adhesive structure (FuRMAS)-like complex containing Dumbfounded/Kin of Irre (Duf/Kirre), F-actin, Blow, and Rolling pebbles (Rols) is required in the longitudinal myoblast fusion at the fusion sites (Rudolf et al. 2014). When this structure is affected, the formation of LVM fibers is disrupted. For instance, in the *rols7* mutant embryos, unfused fusion-competent cells are detected at late stage 12, indicating a fusion defect. This defect results in fewer LVM fibers containing fewer nuclei (Rudolf et al. 2014). However, no signs of unfused fusion-competent cells are observed in the *side IV* mutant embryos, indicating that the fusion process is not affected (**Fig.32**).

The nuclei numbers in the developing LVMP cells were also counted to obtain more details. In wild-type embryos, the initial longitudinal myoblast fusion starts at stage 13. Most LVMP cells have two to four nuclei at the early stage 14 and three to five at the late stage 14. At the end of the migration, before lining up at late stage 15, cells generally contain five or six nuclei (Frasch et al. 2023 , and this work). Nuclear counting is more difficult in the *side IV* mutant embryos due to the aberrant morphology and arrangement of the syncytia. Nevertheless, some cells with clear boundaries shown by the *HLH54Fb*-LacZ marker enable nuclear counting. In the *side IV* mutant, even at stage 12, cells with two nuclei are detected. At stage 13, the migrating cells tend to cluster in groups, and many contain up to four nuclei, implying that they already finished two to three rounds of fusion. During stages 14 to 15, the spreading process of the LVMP cells around the midgut chamber is problematic for nuclei counting. The spaces between the cell streams are still devoid of cells. However, most of them own five or six nuclei, suggesting that they are able to finish the fusion process even though their migration is affected (**Fig. 35**).

Based on those observations, the absence of Side IV does not affect the longitudinal myoblast fusion capacity. However, it may trigger some signal pathways to bring forward the initial fusion to stage 12 and speed up the continuous fusion processes. As mentioned above, a FuRMAS-like structure containing Duf/Kirre is found in the longitudinal FC and FCM cells, which may act as the adhesive signaling center that mediates myoblast fusion (Rudolf et al. 2014). In a recent publication, Side IV and Beat IIb can form a complex with Kirre to regulate synaptic specificity (Osaka et al. 2024). These findings hint that Side IV or the interaction between Side IV and Beat II may get involved in the temporal regulation of the myoblast fusion via the FuRMAS-like adhesion centers.

3.11 Increased cell death in *side IV* mutant embryos

Because the myoblast fusion capacity is not affected when Side IV is absent, the reduced LVM fibers may result from increased cell death in the *side IV* mutant embryos. In migrating collectives, maintaining tissue homeostasis by eliminating abnormal or mismigrating cells is critical for embryonic development, as disordered collective migration features chronic inflammation and metastatic cancer. Anoikis, a type of apoptosis induced by substratum de-adhesion, is often involved in the quality control mechanism to promote homeostasis. A recent publication has demonstrated that collectively migrating CVM and LVMP cells use both FGF and bone morphogenetic protein signaling to eliminate mismigrated cells via anoikis, for which the cell-cycle-regulated expression of the cell death gene *hid* (*head involution defective*) is responsible (Macabenta et al. 2022). Therefore, the observation that many migrating LVMP cells lost contact with the TVM leads to the hypothesis that the de-attachment from the substratum triggers the anoikis program in those cells to prevent adhesion-independent growth.

Terminal deoxynucleotidyl transferase-mediated d-UTP Nick End Labeling (TUNEL) assay was thus utilized to detect cell death. In apoptotic cells, activated endonucleases cleave chromosomal DNA into a large number of DNA double-strand breaks, which can be labeled with fluorochromes and identified by fluorescence microscopy (Darzynkiewicz et al. 2008). In the control group, the TUNEL signal is detected in the head region, CNS, and epidermis, indicating cell death occurs in these regions or tissues. As a comparison, in the *side IV* mutant embryos, the TUNEL signal is additionally detected in the abdominal region. The co-staining with a CVM/LVMP cell marker proves some of these signals specifically come from the CVM and LVMP cells. Of note, cells detected with the TUNEL signal are often on the incorrect migration path and display abnormal morphology with shrunken and roundish cell shape, a hallmark of dying cells (**Fig. 38**). Hence, it is concluded that in the *side IV* mutant, cells lose the attachment with the substratum and undergo cell death.

Additionally, cell death detection using Apoliner was performed. Apoliner is a caspase sensor containing two fluorophores, mRFP and eGFP, connected by a specific caspase-sensitive site. When caspases are activated, the two fluorophores are cleaved, and eGFP is then transported into the nucleus while mRFP stays on the membrane (Bardet et al. 2008). This sensor is tested in different tissues and conditions. S2 cells induced to die by a 10-min exposure to ultraviolet show a clear separation of two fluorescence. In live embryos, with a time-lapse movie imaging

of the epidermis, caspase activity can be tracked by the presence of GFP in the nucleus and the red membrane. However, in the dying cells of fixed *Drosophila* embryos, only the mRFP is robust, and the eGFP signal is often missing, presumably due to the high proteolytic activity in the dying cells (Bardet et al. 2008).

In this work, the Apoliner was expressed in CVM and LVMP cells using the *HLH54Fd*-Gal4 driver line. In the control group, overlap signals from both eGFP and mRFP are predominant. However, in the *side IV* mutant embryos, the eGFP signal disappears to a large degree. Especially in the cells that show abnormal cell shape and TUNEL signal, only the mRFP is observed while the eGFP is no longer detectable, indicating these cells are dying (**Fig. 40**). Moreover, this conclusion is strengthened by the anti-Tey staining, of which the nuclear signal is missing in the dead LVMP cells (**Fig. 41**).

However, given that the TUNEL assay, Apoliner, and anti-Tey are not specific in detecting apoptosis (Grasl-Kraupp et al. 1995; de Torres et al. 1997; Bardet et al. 2008; Nishida et al. 2024) , no direct evidence shows that anoikis is responsible for the dying cells. Therefore, the p35, which can specifically block apoptotic cell death was utilized. If the dying cells are induced by apoptosis, then more cells should survive and fewer cells with abnormal cell shapes should be detected after the expression of p35 in the *side IV* mutants. However, due to the highly dense cell groups, it is hard to count the exact number of surviving cells. Fortunately, the quantification of the off-track cells is possible. Align with the observation, the statistics show a significant decrease in these cells that were proven to undergo cell death (**Fig. 42** and **Fig. 43**).

Taken together, these findings show that the LVMP cells that lost their contact with the TVM undergo apoptosis, perhaps anoikis to prevent an adhesion-independent growth. A loss of these cells is likely the reason for the reduction of LVM fiber numbers.

3.12 Ectopic expression of Side IV misroutes CVM and LVMP cell migraiton

Suppose a protein provides a chemoattractive signal for the ligand-expressing migrating cells, in that case, it should be possible to reroute the migration path when it is ectopically expressed in a defined tissue. Previous studies showed that Side and Beat Ia work as a receptor/ligand pair to guide axon growth. Side is dynamically expressed in neurons and muscles during

embryogenesis, and its ligand Beat Ia is expressed in motor axons. In wild-type embryos, motor axons follow a Side-labeled pathway that defines their growth directions. Interestingly, when the Side is forced to be expressed in the tracheal system of the *side* mutant where the endogenous Side is absent, motor axons are attracted to the tracheal branches and are tightly attached to them. As a comparison, in the *side* mutant, motor axons grow out into the periphery, but none of them are located close to the trachea branches. These facts provide strong evidence that the Side-expressing substrate guides Beat Ia-expressing axons to reach their target muscle fields (Siebert et al. 2009).

Similarly, if Side IV acts as an instructive molecule to guide the migration of Beat II-expressing CVM and LVMP cells, it should also be possible to reroute the migration path by creating an ectopic attraction. *breathless*-Gal4 (*btl*-Gal4) is thus used to drive misexpression of Side IV in the tracheal system. During embryogenesis, the tracheal primordia appear as 10 sets of placodes and undergo predictable branching and merging processes to create a network of tubular epithelium. During stages 11 to 16, six primary branches are extended and branched to spread over various target organs to supply oxygen. Among them, the visceral branches migrate toward the midgut and distribute over the surface of the visceral mesoderm (Hayashi and Kondo 2018). Meanwhile, at these stages, the filopodia activity of the LVMP cells is highly dynamic (Frasch et al. 2023), which means that when there is an overexpression of Side IV in the tracheal system, it should be detected by the active filopodia of the migrating LVMP cells.

Although the LVMP cell migration is disordered in the *side IV* mutant embryos, it shows no direct connection with the GFP-expressing trachea (**Fig. 44**). However, the Side IV-expressing tracheal branches can attract the migrating LVMP cells, as many cells are observed migrating along the tracheal tubes. At the same time, large spaces, especially in the anterior region of the midgut, are devoid of LVMP cells. As a result, most surviving LVMP cells are clustered along with the visceral trachea, and only a few can form LVM fibers at the end of stage 16 (**Fig. 45**). It seems that when Side IV is misexpressed, even much fewer LVM fibers are differentiated. Therefore, the LVM fibers of the L3 larvae were analyzed to confirm this observation. The statistical data shows that when GFP is expressed in the trachea, there is no difference with the *side IV* mutant. In comparison, there is a further reduction of the LVM number when Side IV is misexpressed in the trachea (**Fig. 47**). These findings strongly suggest that Side IV plays a guidance role in regulating the CVM and LVMP cell migration process.

3.13 *beat II* and *side IV* mutant larvae in food intake assay

The *Drosophila* intestine is built by a monolayered epithelium of enterocytes, surrounded by the visceral musculature, an interwoven contractile network consisting of a layer of circular muscles and longitudinal fibers. The visceral musculature is primarily responsible for the movement of the digestive tract, thereby playing a crucial part in digestion and growth (Sink and Hartenstein 2006; Aghajanian et al. 2016; Schröter et al. 2006).

Because decreased longitudinal fibers were observed in the *side IV* and *beat II* double mutant larvae, this work aimed to examine whether their food intake ability is affected. To this end, a food intake assay using blue-dyed yeast was performed. Unexpectedly, the statistical data shows no significant difference between the control group and the s*ide IV* mutant larvae (**Fig. 52**). This suggests that the food-consuming ability is unaffected when Side IV is absent. However, if Side IV is ectopically expressed in the trachea in the *side* IV mutant background, the larvae intake much less food than the control group in a period of 15 min.

Considering that the longitudinal fibers are notably reduced in the *side IV* mutant with ectopic expression of Side IV in the trachea (see **Fig. 47**), one possible explanation is that the food intake ability is only influenced when the LVM fibers are reduced to a specific threshold. In the *side IV* mutant larvae, more than half of the longitudinal muscle fibers eventually form. These conserved muscles, together with the circular muscles, might provide enough strength for the peristaltic movement of the intestine. However, when the fibers further decrease to one-fourth of the normal amount, the movement of the gut is significantly hindered, and thus the food intake ability is affected. Another possibility is that the reduced peristaltic movement of the *side IV* mutant is compensated by the passive movement of the intestine along with the body movement, therefore no significant difference is detected between the control and the *side IV* mutant.

Of note, one interesting finding is that although the longitudinal fiber amount in the *beat II* double mutant is similar to the *side IV* mutant (compare **Fig. 25** with **Fig.32**), there is a significant reduction of food consumption in the *beat II* double mutant larvae but not in the *side IV* mutant. Together with the observations that more morphological defects like myofibril splitting are detected in the *beat II* mutant; almost all homozygous *beat II* double mutants die during pupation, while homozygous *side IV* mutated adults often escape, the difference in the

food intake ability could be explained as *beat II* may exert additional functions in the larval development. To examine these assumptions, further experiments like detailed morphological and quantitative analysis of the visceral muscle fibers, real-time 3D microscopy for gut movement, and other feeding and excretion assays should be performed.

Altogether, the findings in this work suggest that Beat II and Side IV function as a ligand-receptor pair to guide the migrating CVM and LVMP cells on the TVM. It is the first time that a guidance function of Beat and Side family members has been revealed in non-neural cells.

4 Materials and Methods

4.1 Materials

4.1.1 Chemicals, reagents, and kits

Table 1: Chemicals and reagents

Chemicals and Reagents	Manufacturer
Agar-Agar	BD (Becton, Dickinson and Company), Sparks, MD, USA
Agarose low EEO	AppliChem, Darmstadt, Germany
Ampicillin	AppliChem, Darmstadt, Germany
Apple juice (Hohes C)	Eckes-Granini Deutschland, Nieder-Olm, Germany
Bacto™ Yeast Extract	Thermo Fisher Scientific, Schwerte, Germany
Bromphenol blue sodium salt	Carl Roth, Karlsruhe, Germany
Chloramphenicol	AppliChem, Darmstadt, Germany
Chlor bleach	Colgate-Palmolive, Hamburg, Germany
Corn grits	Küper, Oberhausen, Germany
Denhardt's Solution (50x)	Thermo Fisher Scientific, Schwerte, Germany
DIG RNA Labeling Mix	Roche, Basel, Switzerland
Disodium hydrogen phosphate (Na_2HPO_4)	Grüssing, Filsum, Germany
1,4-Dithiothreit (DTT) ($C_4H_{10}O_2S_2$)	Carl Roth, Karlsruhe, Germany
Dimethyl sulphoxide (DMSO)	Carl Roth, Karlsruhe, Germany
dNTPs (dATP, dTTP, dGTP, dCTP)	Thermo Fisher Scientific, Schwerte, Germany
Ethanol absolute	VWR International, Leuven, Belgium
Ethylenediaminetetraacetic acid (EDTA)	Carl Roth, Karlsruhe, Germany
Fetal bovine serum (FBS)	PAN-Biotech, Aidenbach, Germany
Ficoll 400	Sigma Aldrich Chemic, Steinheim, Germany
Formamide	AppliChem, Darmstadt, Germany
Formaldehyde 37%	Merck, Darmstadt, Germany
Gene Ruler 1kb DNA-Ladder	Thermo Fisher Scientific, Schwerte, Germany
Glycerol	Thermo Fisher Scientific, Schwerte, Germany
Heparin	Merck, Darmstadt, Germany
Heptane	Sigma Aldrich Chemic, Steinheim, Germany
H_2O_2 (30%)	Merck, Darmstadt, Germany
Hydrochloric acid (HCl)	VWR International, Leuven, Belgium
Kanamycine	AppliChem, Darmstadt, Germany
Malt extract	Lindenmeyer, Öhringen, Germany
Meganesium chloride ($MgCl_2$)	Carl Roth, Karlsruhe, Germany
Methanol	Thermo Fisher Scientific, Schwerte, Germany
Nail polish	cosnova, Sulzbach, Germany
Nipagin	Merck, Darmstadt, Germany
Normal donkey serum (NDS)	Jackson Immunoresearch, West Grove, PA, USA
Normal goat serum (NGS)	Jackson Immunoresearch, West Grove, PA, USA
Nonidet P-40	AppliChem, Darmstadt, Germany
Oligo d(T) 18 mRNA Primer	New England Bio Labs, Frankfurt a. Main, Germany

Penicillin-Streptomycin-Glutamine 100x	Thermo Fisher Scientific, Schwerte, Germany
Potassium acetate (CH_3COOK)	Carl Roth, Karlsruhe, Germany
Potassium chloride (KCl)	AppliChem, Darmstadt, Germany
Potassium dihydrogen phosphate (KH_2PO_4)	AppliChem, Darmstadt, Germany
Propionic acid	Sigma Aldrich Chemic, Steinheim, Germany
Q5 High-Fidelity DNA Polymerase	New England Bio Labs, Frankfurt a. Main, Germany
RNase Inhibitor, Murine	New England BioLabs, Frankfurt a. Main, Germany
Schneider's *Drosophila* medium	PAN-Biotech, Aidenbach, Germany
Sodium chloride (NaCl)	VWR International, Leuven, Belgium
Sodium citrate ($C_6H_5Na_3O_7$)	Carl Roth, Karlsruhe, Germany
Sodium dodecyl sulfate (SDS), ultra pure	Carl Roth, Karlsruhe, Germany
Sodium dihydrogen phosphate (NaH_2PO_4)	Grüssing, Filsum, Germany
di-Sodium hydrogen phosphate (Na_2HPO_4)	Grüssing, Filsum, Germany
Sodium hydroxide-Pellets (NaOH)	AppliChem, Darmstadt, Germany
Soy flour	Heirler Cenovis, Radolfzell, Germany
Sheared Salmon Sperm DNA	Thermo Fisher Scientific, Schwerte, Germany
SuperScript™ III Reverse Transcriptase	Thermo Fisher Scientific, Schwerte, Germany
SYBR Safe DNA Gel Stain	Thermo Fisher Scientific, Schwerte, Germany
Texa Red™ Phalloidin	Thermo Fisher Scientific, Schwerte, Germany
Treacle	Grafschafter Krautfabrik, Meckenheim, Germany
Tris(hydroxymethyl)aminomethane (Tris/Tris base)	Carl Roth, Karlsruhe, Germany
TRIS blotting-grade	Carl Roth, Karlsruhe, Germany
TRIS-hypochloride	Carl Roth, Karlsruhe, Germany
Tryptone	BD (Becton, Dickinson and Company), Sparks, MD, USA
Trypan Blue Stain, 0.4%	Aligned Genetics, Villeneuve d'Ascq, France
TritonX-100	Carl Roth, Karlsruhe, Germany
Tween 20	Carl Roth, Karlsruhe, Germany
Tyramide Cy3	AAT Bioquest, Pleasanton, CA, USA
Tyramide Cy5	AAT Bioquest, Pleasanton, CA, USA
Yeast powder	Heirler Cenovis, Radolfzell, Germany

Table 2: Kits

Kits	Manufacturer
BP Clonase Enzyme Mix and Reagents	Thermo Fisher Scientific, Schwerte, Germany
DNeasy Blood & Tissue Kit	QIAGEN, Hilden, Germany
Effectene® Transfection Reagent	QIAGEN, Hilden, Germany
Mix2Seq Kit	Eurofins Genomics, Ebersberg, Germany
NucleoSpin® Gel and PCR Clean-up kit	MACHEREY-NAGEL, Düren, Germany
One-step TUNEL Assay Kit (Red, AF594)	Elabscience Biotechnology, Houston, TX, USA
pENTR/D-TOPO Cloning Kit	Thermo Fisher Scientific, Schwerte, Germany
Plasmid DNA Purification Kit	MACHEREY-NAGEL, Düren, Germany
RNeasy Mini Kit	QIAGEN, Hilden, Germany

4.1.2 Buffers and medium

All buffers, mediums, and solutions are dissolved in ultrapure water unless otherwise indicated.

Table 3: Buffers and mediums

Fly breeding	
Standard *Drosophila* medium	10l Demineralized water 50g Agar 168g Yeast powder 450g Malt extract 95g Soy flour 712g Corn grits 400g Treacle cook 25min, cool to ~ 65°C, then add: 45ml Propionic acid 15g Nipagin
Apple juice agar	3l Demineralized water 1l Apple juice 100g Sugar 70g Agar
Agarose gel electrophoresis	
50x TAE buffer	2M Tris-base 0.05M EDTA, pH=8.2
1% Agarose gel	1% (w/v) Agarose in 1x TAE buffer, boil, cool down to 50°C, add: SYBR Safe (7µl per 100ml of gel)
6x DNA loading buffer	0.25% (w/v) Bromophenol blue 15% (w/v) Ficoll in 1x TAE Store at 4°C
Immunohistochemistry	
10x PBS	1.37M NaCl 27mM KCl 100mM Na_2HPO_4 20mM KH_2PO_4, pH=7.4
PTX	1x PBS with 0.1% Triton X-100
PTX + 5% NGS	1x PTX with 5% (v/v) Normal goat serum, store at 4°C
70% Glycerol	70% (v/v) Glycerol in PBS
***In situ* hybridization**	
10x SSC buffer	4.41g Sodium citrate 8.77g NaCl 1l Deionized water pH=7.2
Probe buffer	50% Formamid 50% TE, pH=7.5 0.1% Tween 20
AP buffer	100mM Tris, pH=9.5 100mM NaCl 50mM $MgCl_2$ 0.1% Tween 20
Hybridization buffer	50% Formamid 4x SSC 1x Dehnhardt's Solution 250µg/ml Sheared Salmon Sperm DNA 50µg/ml Heparin 0.1% Tween

Wash buffer	50% Formamid 2x SSC 0.1% Tween 20
Tyramide Cy3 working solution	1µl Tyramide stock solution (5mM) in 1ml PBT with 0.003% H_2O_2
Tyramide Cy5 working solution	1µl Tyramide stock solution (5mM) in 1ml PBT with 0.003% H_2O_2
Molecular cloning	
LB medium	10g NaCl 10g Tryptone 5g Yeast powder add 1l Ultrapure H_2O pH=7.0, autoclave, add desired antibiotics
LB agar plates	10g NaCl 10g Tryptone 5g Yeast extract 20g Agar add 1l H_2O, pH=7.0 autoclave, cool to ~50°C, add desired antibiotics cast petri dishes
Ampicillin stock solution	60mg/ml Ampicillin, store at -20°C
Chloramphenicol stock solution	Ethanol with 34mg/ml Chloramphenicol, store at -20°C
Kanamycin stock solution	50mg/ml Kanamycin, store at -20°C
Cell culture	
Complete Schneider's Drosophila medium	Schneider's *Drosophila* medium 10% (v/v) heat-inactived FBS 1x Penicillin-Streptomycin-Glutamine
Freezing medium	45% conditioned complete Schneider's medium 45% fresh complete Schneider's medium 10% DMSO

4.1.3 Antibodies

Table 4: Primary antibodies

Immunohistochemistry			
Antibodies	**Host animals**	**Dilution**	**Manufacturer**
anti-βGal	mouse	1:100	DSHB (40-1a), Iowa City, IA, USA
anti-dsRed	rabbit	1:400	Takara Bio, Kusatsu, Japan
anti-GFP	rabbit	1:1000	Acris Antibodies (TP401), Herford, Germany
anti-GFP	mouse	1:100	DSHB (1D2), Iowa City, IA, USA
anti-GFP	rat	1:1000	NACALAI TESQUE, Kyoto, Japan
anti-Side IV	mouse	1:100	(Carrier et al. 2023)
anti-Tey	mouse	1:400	(Frasch et al. 2023)
anti-V5	mouse	1:200	Thermo Fisher Scientific, Schwerte, Germany
anti-Fas III	mouse	1:40	DSHB (7G10), Iowa City, IA, USA
***In situ* hybridization**			
Antibodies	**Host animals**	**Dilution**	**Manufacturer**
anti-Digoxigenin-POD, Fab fragemnts	goat	1:100	Roche, Basel, Switzerland

Table 5: Secondary antibodies

Immunohistochemistry				
Antibodies	**Host animals**	**Dilution**	**Fluorophores**	**Manufacturer**
anti-Mouse	goat	1:500	Alexa 488	Jackson Immunoresearch, West Grove, PA, USA
anti-Mouse	goat	1:500	Alexa 647	
anti-Mouse	goat	1:500	Cy3	
anti-Rabbit	goat	1:500	Alexa 488	
anti-Rabbit	goat	1:500	Cy3	
anti-Rat	donkey	1:500	Alexa 488	
anti-Rat	donkey	1:500	Alexa 647	

4.1.4 Primers

Table 6: Primers

Primers	5'-3' Sequence	Usage
U63 Fwd	ACGTTTTATAACTTATGCCCCTAAG	Sequencing
Cherry ORF Fwd	CCGACCCAGCTTTCTTGTAC	
Cherry ORF Rev	CCATAGGTTGGAATCTAAAATACACAAAC	
Cherry Express Seq Fwd	CGGCTCGAGGTCGAC	
Cherry Express Seq Rev	GCTCACCATTCTAGCAGA	
Destination Seq 1 Fwd	GATGCATCTCAAAAAAATGGTGG	
Destination Seq 2 Rev	CTTCACGTAGGCCTTGGAGC	
Destination Seq 3 Rev	CGATTCATTAATGCAGCTGGCACG	
Cherry Seq 2 Rev	CTTCACGTAGGCCTTGGAGC	
GFP ORF Fwd	CCCAGCTTTCTTGTACAAAGTGG	
GFP Seq 2 Rev	GGTAGCGGCTGAAGCACTGC	
GFP Seq 3 Rev	CATCACTAGATGGCATTTCTTCTGAGC	
Beat IIa Fwd	CACCATGCTGGAGTTGCAACTTTG	Used for TOPO cloning
Beat IIa Rev	GGCCAGACGCAGACTTTC	
BeatIIb Fwd	CACCATGTGGCAGACACTATCAACTTTTAGCAC	
Beat IIb Rev	GCTACCAGTAATTAGTTGGGCCAACG	
Side IV Fwd	CACCATGCATCACGAGGAGACATACC	
Side IV^{S133*} Rev	GCTGAGCGCCTGTCCAAACTGC	
Side IV CDS 1 Fwd	AAAAAAGCTTATGCATCACGAGGAGACATACCAAG	Insertion of Side IV into the pBS vector
Side IV CDS 2978 Rev	AAAATCTAGATATACAACTTTCCTGTATGCGATTCG	
T3 primer	ATTAACCCTCACTAAAG	Used for *in situ* hybridization
T7 primer	AATACGACTCACTATAGG	
beat IIa M-Seq-Fwd	CCCCAAAAAGTGCCAAGAAACAGACAG	Used for sequencing *beat II* double mutants
beat IIa M-Seq-Rev	CTAAACAAATGGCAGACTTACCCATGCTC	
beat IIb M-Seq-Fwd	CCAAGCGCGTTGACAATGTG	
beat IIb M-Seq-13off-Rev	CCCAGCGTTTTTTGTGCGAG	

Table 7: Oligonucleotides used for OE-PCR and Topo-cloning

Fragments	DNA templates	Primers	5'-3' Sequence
Beat IIb SP-Spacer	pENTR_Beat IIb	Frag1(SP+Spacer) Fwd	CACCATGTGGCAGACACTAT CAACT
		Frag1(SP+Spacer) Rev	CCTTGCTCACCATACCGCTTC CTGCCACTGCTGCTGCTGCTG
GFP	pUAST*attB*_rfA _eGFP	Frag2(Spacer+GFP) For	GCAGCAGTGGCAGGAAGCGGT ATGGTGAGCAAGGGCGAGGAG
		Frag2(Spacer+GFP) Rev	TGCTGGTTGTGCCTTGTACAGCT CGTCCATGC
Beat IIb 21-404	pENTR_Beat IIb	Frag3 (BIIb_21-404) For	GAGCTGTACAAGGCACAACCAG CAGCAACTTG
		Frag3 (BeatIIb_21-404) Rev	GCTACCAGTAATTAGTTGGGCC AAC

4.1.5 Plasmids

Table 8: Plasmids

Entry Vectors			
Plasmids	**Inserts**	**Resistance**	**Source**
pENTR/D-Topo-Empty	---	kanamycin	Thermo Fisher Scientific, Schwerte, Germany
pENTR_Beat IIa	Beat IIa full length	kanamycin	N. Huang, this work
pENTR_Beat IIb	Beat IIb full length	kanamycin	N. Huang, this work
pENTR_Beat IIb-SP-Spacer-GFP-21-404aa (SP-GFP-Beat IIb)	Beat IIb-SP-Spacer-GFP-21-404aa	kanamycin	N. Huang, this work
pENTR_Side IV ^{S133*}	Side IV 1-133aa	kanamycin	N. Huang, this work
Expression Vectors			
Plasmids	**Inserts**	**Resistance**	**Source**
pUAST*attB*_rfA	---	chloramphenicol ampicillin	Gift from C. Klämbt, Universität Münster
pUAST*attB*_rfA_eGFP	---	chloramphenicol ampicillin	Gift from C. Klämbt, Universität Münster
pUAST*attB*_rfA_mCherry	---	chloramphenicol ampicillin	Gift from C. Klämbt, Universität Münster
pUAST*attB*_Beat IIa_eGFP	---	ampicillin	N. Huang, this work
pUAST*attB*_Beat IIa_mCherry	---	ampicillin	N. Huang, this work
pUAST*attB*_Beat IIb_eGFP	---	ampicillin	N. Huang, this work
pUAST*attB*_ Beat IIb-SP-Spacer-GFP-21-404aa (SP-GFP-Beat IIb)	---	ampicillin	N. Huang, this work
pUAST*attB*_Side IV_mCherry	---	ampicillin	Gift from, T. Suzuki, Tokyo Institute of Technology
pUAST*attB*_ SideIV^{S133*}_mCherry	---	ampicillin	N. Huang, this work
Other Vectors			
Plasmids	**Inserts**	**Resistance**	**Source**
pBS-SK	---	ampicillin	Gift from C. S. Goodman, U.C. Berkeley
pBS-SK_Side IV	Side IV full length	ampicillin	N. Huang, this work

pCFD3-dU6:3	---	ampicillin	addgene, Watertwon, MA, USA
pFLC-I_Beat IIa	Beat IIa cDNA	ampicillin	DGRC, RE17794
pBPGUw-Act5C-Gal4	Act5C-Gal4	ampicillin	Gift from S. Bogdan, Philipps-University Marburg

4.1.6 Fly stocks

Table 9: Fly stocks

General flies	
Genotype	**Source**
w^{1118}	AG Aberle, Stock collection
$w^-; \frac{If}{CyO}$	AG Aberle, Stock collection
$w^-; \frac{Gla, wg^{laz}}{CyO,twi>GFP}$	AG Aberle, Stock collection
$w^-;; \frac{Dr}{TM6c}$	AG Aberle, Stock collection
$w^-;; \frac{Ly}{TM3,twi>GFP}$	AG Aberle, Stock collection
$w^-; \frac{If}{CyO,act::GFP}; \frac{Ly}{TM3,twi>GFP}$	AG Aberle, Stock collection
$w^-; \frac{If}{CyO,act::GFP}; \frac{Dr}{TM3,twi>GFP}$	AG Aberle, Stock collection
$w^-; \frac{If}{CyO,act::GFP}; \frac{Ly}{TM6C}$	AG Aberle, Stock collection
Gal4 flies	
Genotype	**Source**
w^-; *bap3*-Gal4	Gift from I. Reim, Philipps-University Marburg
w^-; *btl*-Gal4	Gift from M. Krasnow, Stanford University
$y^-w^-; \frac{HLH54Fd-Gal4}{CyO}$	Bloomington Drosophila Stock Center #91633
UAS flies	
Genotype	**Source**
w^-; UAS-Apoliner 5	Gift from I. Reim, Philipps-University Marburg
y^-w^-; UAS-mCD8-GFP	(Lee and Luo, 1999)
w^-;; UAS-Histon-RFP	Gift from I. Reim, Philipps-University Marburg
$w^-; \frac{UAS-p35.H}{CyO, Wg^{LacZ}}; \frac{MKRS}{TM6B}$	Gift from T. Klein, Heinrich Heine University Duesseldorf Bloomington Drosophila Stock Center #5072
Beat IIa- and Beat IIb-related flies	
Genotype	**Source**
$w^-;; \frac{Beat\ IIa::FlpTag}{TM6B}$	Gift from F. Pinto-Teixeira, University of Toulouse
$y^-w^-;;$ Beat $IIb^{MI03102\text{-}GFSTF.0}$	Bloomington Drosophila Stock Center #59406
w^-; *HLH54Fb*-LacZ; $\frac{Df\ (3R)ED5780}{TM3,LacZ}$	Gift from M. Frasch, Friedrich-Alexander-University Erlangen-Nürnberg
$y^-w^-; \frac{GMRFsF-Gal4,BrpFSFGFP}{CyO,\ y^+}; \frac{beat\ IIa^{+2}}{TM6B,y^+}$	Gift from T. Suzuki, Tokyo Institute of Technology
$y^-w^-; \frac{SP}{CyO,y^+}; \frac{beat\ IIb^{\Delta 14}}{TM6B,y^+}$	Gift from T. Suzuki, Tokyo Institute of Technology
$w^-;; \frac{beat\ IIa^{+2}\ beat\ IIb^{L88*}}{TM6c}$	N. Huang, this work
$w^-; \frac{UAS-Beat\ IIa-mCherry}{CyO}$	N. Huang, this work
$w^-; \frac{UAS-Beat\ IIb-eGFP}{CyO}$	N. Huang, this work

Side IV-related flies	
Genotype	**Source**
$y^{-}w^{-};; \frac{\text{Side IV}-\text{FSF}-\text{GFP}}{\text{TM6B},y^{+}}$	Gift from T. Suzuki, Tokyo Institute of Technology
$w^{-};; \frac{\text{side } IV^{S133*}}{\text{TM3},twi>GFP}$	J. Kinold, Heinrich Heine University Duesseldorf
$w^{-};; \frac{\text{side } IV^{S145*}}{\text{TM3},twi>GFP}$	J. Kinold, Heinrich Heine University Duesseldorf
$w^{-};; \frac{\text{Df (3R)}Excel\ 7320}{\text{TM6B}}$	Bloomington Drosophila Stock Center #7975
$y^{-}w^{-}; \frac{\text{UAS}-\text{Side IV}-\text{V5}-\text{PDZ}}{\text{CyO},y^{+}}$	Gift from T. Suzuki, Tokyo Institute of Technology
Other flies	
Genotype	**Source**
$y^{-}w^{-}; \frac{\text{hs}-\text{Flp}}{\text{CyO},y^{+}}$	Gift from T. Suzuki, Tokyo Institute of Technology
$y^{-}w^{-}$; *HLH54Fb*-CytoRFP	Bloomington Drosophila Stock Center #92001
$w^{-};;$ *HLH54F*-GFP	Bloomington Drosophila Stock Center #55841
w^{-}; *HLH54Fb*-LacZ	Gift from M. Frasch, Friedrich-Alexander-University Erlangen-Nürnberg
$y^{-}w^{-}$; *bap3*-RFP	Bloomington Drosophila Stock Center #92967
$w^{-};; \frac{bap^{208}}{\text{TM3}}$	Bloomington Drosophila Stock Center #91539
$w^{-};; \frac{\text{Df(3L)BK9}}{\text{TM3,Sb}}$	Bloomington Drosophila Stock Center #2991

4.1.7 Equipments

Table 10: Equipments

General equipments	
Equipments	**Manufacturer**
Cell strainer, pore size: 100µm	SARSTEDT, Nümbrecht, Germany
Centrifuge 5425R	Eppendorf Corporate, Hamburg, Germany
Centrifuge 5430R	Eppendorf Corporate, Hamburg, Germany
Dissection plates	Roland Vetter Laborbedarf OHG, Ammerbuch, Germany
Dry bath FB15101	Thermo Fischer Scientific, Schwerte, Germany
Eppendorf Tubes® 5.0ml	Eppendorf Corporate, Hamburg, Germany
GFL Paraffin Streckbad 1052	GFL Gesellschaft für Labortechnik, Burgwedel, Germany
Insect Pins Minutiens (Austerlitz, 0.10mm)	Fine Science Tools, Heidelberg, Germany
Isotemp Water Bath	Thermo Fischer Scientific, Schwerte, Germany
Marienfeld Superior™ Precision Cover Glass, 18 x 18mm	Electron Microscopy Sciences, Hatfield, PA, USA
Microcentrifuge tubes with graduations, 0.5ml, 1.5ml, 2ml	VWR International, Leuven, Belgium
Microplate shakers Orbit™ P4	Labnet Oy, Vantaa, Finland
Microscope slides 76 x 26 x 1mm	Paul Marienfeld, Lauda-Koenigshofen, Germany
NanoPhotometer® NP80	Implen , München, Germany
NITRILE Gloves (S, M, L)	VWR International, Leuven, Belgium
Parafilm® M Laboratory Wrapping Film	Thermo Fischer Scientific, Schwerte, Germany
pH-Meter pH300	Hanna Instruments, Vöhringen, Germany
Pipette Controler accu-jet® pro	BRAND, Wertheim, Germany
PIPETMAN® P20, P200, P1000	Gilson, Middleton, WI, USA

Pipette tip 20µl, 200µl, 1000µl	SARSTEDT, Nümbrecht, Germany
Rocking Platform Shaker	Avantor, Radnor, PA, USA
Scale (instrument for weighing)	Denver Instrument, Denver, CO, USA
Scientific Industries SI™ Vortex-Genie™ 2	Thermo Fischer Scientific, Schwerte, Germany
Serological Pipette 5ml, 10ml, 25ml	SARSTEDT, Nümbrecht, Germany
TC-Insert 24-well, 8.0µm	SARSTEDT, Nümbrecht, Germany
Thermomixer compact	Eppendorf Corporate, Hamburg, Germany
Tissue culture testplates 24-well	TPP Techno Plastic Products AG, Trasadingen, Switzerland
Tube 15ml, 50ml	SARSTEDT, Nümbrecht, Germany
Tweezer (#4)	Fine Science Tools, Heidelberg, Germany
Ultrapure water system	Veolia Water Technologies & Solutions, Trevose, PA, USA
Uni Shaker 2	Lab Logistics Group, Meckenheim, Germany
Urine cup	SARSTEDT, Nümbrecht, Germany
Water bath Julabo 6A	JULAB, Seelbach, Germany
Cell culture and Molecular cloning	
Equipments	**Manufacturer**
Cell culture flask, T-25, 25ml	SARSTEDT, Nümbrecht, Germany
Centrifuge 3-16 PK	Sigma Laborzentrifugen, Osterode am Harz, Germany
CryoPure Tubes	SARSTEDT, Nümbrecht, Germany
Cryo-Safe™ Cooler -1°C Freeze Controller	Thermo Fischer Scientific, Schwerte, Germany
Falcon® Tissue culture dish (35mm, 60mm, 100mm)	Corning, Glendale, AZ, USA
Heratherm Compact Microbiological Incubator	Thermo Fischer Scientific, Schwerte, Germany
Incubator Hood TH30	Edmund Bühler, Bodelshausen, Germany
Incubator	Memmert, Schwabach, Germany
Luna™ Automated Cell Counter	Aligned Genetics, Villeneuve d'Ascq, France
Luna™ Cell Counting Slides	Aligned Genetics, Villeneuve d'Ascq, France
Precision™ Shaking Water Bath SWB 15	Thermo Fischer Scientific, Schwerte, Germany
TC Plate 6 Well, Suspension, F	SARSTEDT, Nümbrecht, Germany
Thermo Scientific™ Safe 2020 Class II Biological Safety Cabinet	Thermo Fischer Scientific, Schwerte, Germany
µ-Dish 35mm high (Imaging chamber)	ibidi, Gräfelfing, Germany
Water Bath Aqualine AL 18	LAUDA DR. R. WOBSER, Lauda-Königshofen, Germany
PCR and Gel electrophoresis	
Equipments	**Manufacturer**
Biometra® PCR thermal cycler	Analytik Jena, Jena, Germany
Biometra® Standard Power Pack P25	Analytik Jena, Jena, Germany
Biorad ChemiDoc™	Bio-Rad Laboratories, Feldkirchen, Germany
IBI A Kodak Company Gel Reader	Carestream Health, Rochester, NY, USA
Imaging	
Equipments	**Manufacturer**
Axio Imager M2	Zeiss, Jena, Germany
Axio Vert A1	Zeiss, Jena, Germany
Laser Scanning Micriscope (LSM 710)	Zeiss, Jena, Germany
Laser Scanning Micriscope (LSM 880)	Zeiss, Jena, Germany
LEICA M165 FC Fluorescent Stereo	Leica Microsystems, Wetzlar, Germany
Microscope body stemi 508	Zeiss, Jena, Germany
Nikon D580	Nikon Europe B.V., Amstelveen, The Netherlands
Stereo Stemi 2000	Zeiss, Jena, Germany

4.1.8 Software

Table 11: Software

Software	Manufacturer
Adobe Illustrator	Adobe Systems, San Jose, CA, USA
(Fiji is just) ImageJ	GNU General Public License
Image Lab Software	Bio-Rad Laboratories, Feldkirchen, Germany
Microsoft Excel	Microsoft Corporation, Redmond, WA, USA
Microsoft Word	Microsoft Corporation, Redmond, WA, USA
Prism 9	GraphPad Software, Boston, MA, USA
SnapGene	GSL Biotech LLC, Boston, MA, USA
Zen Blue	Carl Zeiss Microscopy, Jena, Germany

Table 12: Programs used for protein domain prediction

Programs	Predicted domains
AlphaFold	three-dimensional strucuture
big PI-Predictor	GPI anchor
DeepTMHMM	transmembrane domain
InterPro	multiple domains
PredGPI	GPI anchor
Phobius	signal peptide
ScanProsite	IG domain
SMART	IG domain

4.1.9 Gene and protein information

Further information about the genes and proteins described in this thesis can be found in NCBI (The National Center for Biotechnology) as the following names: *beat IIa* (gene ID: 42086; protein name: CG14334-PA), *beat IIb* (gene ID:42082; protein name: CG4135-PC), *side IV* (gene ID:41657; protein name: CG14372-PC).

4.2 Methods

4.2.1 Fly maintenance, genetics, and behavior analysis

Flies were cultivated on a standard *Drosophila* medium within plastic tubes sealed with plugs and maintained at 18°C, 25°C, or room temperature (RT). Virgin female flies (hatched at 18°C

for less than ten hours) were paired with male flies of the corresponding genotypes to conduct crosses.

4.2.1.1 *Drosophila* embryo collection

The intended genotypes of *Drosophila* were mated in small plastic cages on apple juice agar plates. A small amount of fresh yeast was added to promote egg-laying. Plates of apple juice agar were replaced twice per day. Embryos were collected from the agar plates and transferred to a filter using a soft brush and 1x PBS. Collected embryos were then dechorionized with 2% hypochlorite for four minutes and rinsed with PBS.

4.2.1.2 *Drosophila* embryonic development stage subdivision

Drosophila embryonic development has been subdivided into seventeen stages (Campos-Ortega and Hartenstein 1985). This work focuses on stages 10 to 17. The appearance of the stomodeum identifies the onset of stage 10, which lasts about one hour. Once the germ band retraction starts, embryos are developed into stage 11. The shortening of the germband is completed by the end of stage 12. The beginning of head involution characterizes the end of stage 13. During stage 14, the midgut dorsal closure proceeds. At stage 15, the midgut forms a closed tube and fully encloses the yolk sac. The constrictions appear in the midgut during stage 16. The last stage is characterized by the air-filled tracheal tree and retracted ventral cord.

4.2.1.3 Germline transformation

Through germline transformation via the ΦC31 integrase technique, which allows for site-specific integration, transgenic fly lines were generated (Bischof et al. 2007). Plasmids containing a UAS-enhancer and promoter, the coding sequence for the target protein, an *attB* integration site, and a *white*$^{+}$ marker gene were first produced using the Gateway system. Then, the isolated plasmids were injected into early-stage embryos containing the *attP* site and *w*$^{-}$. Thus, the target protein coding sequence can be inserted into the fly genome via the recombination of *attB* and *attP* sites, and the *white*$^{+}$ marker could confirm the insertion. The details of plasmids are in **Table 8**. FlyORF (University of Zurich, Switzerland) performed the injection process. *attP*40:2L,25C6, and *attP*3:3L, 68A4 strains were used for injections targeted at the second or third chromosome, respectively.

4.2.1.4 Establishment of transgenic fly lines

In single crossings, hatchened male flies (F0) originating from the injected embryos (see chapter **4.2.1.3**) were crossed to w^- virgins. Because successful transformation results in integrating the injected DNA into the germline of the fly genome in F1 offspring and, consequently, the expression of the *white*$^+$ marker gene. The eye color could be used to screen the F1 offspring flies that emerged from these various crossings. Positive transformants were crossed to w^-; If/CyO or w^-; Dr/TM6C. Using dominant marker segregation, the transgenic fly line could be established over a balancer chromosome.

4.2.1.5 CRISPR/Cas9

Clustered regularly interspaced short palindromic repeats (CRISPR) sequence together with CRISPR-associated 9 (Cas9) protein are used for editing genes in *Drosophila* (Gratz et al. 2013; Kondo and Ueda 2013; Jinek et al. 2012). CRISPR/Cas9 system contains the Cas9 and a gRNA (guide RNA) that guides Cas9 to recognize and destroy the target DNA sequence. Cas9, initially characterized as a part of the CRISPR bacterial innate immune system, has been discovered to encode a specific type of sequence-specific endonuclease. The specificity of its target is determined by the gRNA. Reprogramming Cas9 to target a different sequence is a straightforward process that involves designing a 20-base pair sequence of the gRNA. The primary criterion for selecting acceptable 20-bp targets is the presence of an "NGG" sequence known as the protospacer adjacent motif (PAM). The simplicity and flexibility of the design, make CRISPR/Cas9 technique an optimal approach for genome-scale applications (Kondo and Ueda 2013; Jinek et al. 2012; Gratz et al. 2013).

CRISPR/Cas9 was used in this work to create *beat II* double mutants. The *beat IIb* gRNA was designed (5'-3': GGCACAGTAGCAGTAGCCAC) and inserted into the pCFD3-dU6:3 vector. Then, it was injected with a Cas9 helper (offered by FlyOrf) into the *beat IIa*$^{+2}$ mutant embryos. FlyORF performed the injection (University of Zurich, Switzerland). The hatched flies were balanced with w^-; Dr/TM6C, and the offspring were sequenced using the corresponding primers listed in **Table 6**.

4.2.1.6 Tissue-specific gene expression

Using the Gal4/UAS system, gene expression in *Drosophila* can be regulated in a spatiotemporal manner (Brand and Perrimon 1993). The gene encoding the yeast transcription factor Gal4 is introduced in the *Drosophila* driver line driven by a time- and tissue-specific promoter. In the *Drosophila* effector line, the genome is inserted with an upstream activating sequence (UAS) before the target gene. After mating, Gal4 proteins from the driver line can bind to the UAS region of the effector line in their offspring. As gene expression relies upon the upstream activating sequence being activated by the time- and tissue-specific Gal4 proteins, the target gene expression is thereby regulated.

4.2.1.7 Removal of stop cassette from Side IV-FsF-GFP

Side IV-GFP expression was activated by combining the Side IV-FsF-GFP with the hs-FLP line. Side IV-FsF-GFP males and hs-FLP virgins were mated in a vial for 2-3 days. Then, they were transferred into a fresh vial at 25°C. After two hours, the adults were removed, and the embryos were incubated in a 37°C water bath for one hour to activate the flippase. Afterward, the embryos were kept at 25°C, and the desired flies were sorted out with corresponding markers on the balancers.

4.2.1.8 Food intake assay for L3 larvae

To ensure the tested larvae were at the same developing stage, embryos were collected for 2 hours and raised for 96 hours at 25°C. Then, the larvae (L3 stage) were picked and sorted by GFP-marked balancers using a UV-bino. After rinsing with tap water, larvae were starved on a moistened filter paper in a 35 mm petri dish for one and a half hours. Following this, they were brought to an agar plate (35 mm) filled with the dyed yeast (containing less than 1% Bromophenol Blue sodium salt) for 15 minutes at RT. After a heat shock, larvae were mounted in 70% glycerol in PBS on a slide. The photos were taken with a Nikon D850.

4.2.2 Molecular biological methods

4.2.2.1 Genomic DNA isolation

Drosophila genomic DNA was extracted from larvae or adults utilizing the DNeasy Blood & Tissue Kit (QIAGEN, Hilden, Germany). Larvae (around 10) or adults (1-20 flies) were gathered and frozen at -20°C overnight in 1.5 ml reaction tubes to enable cell disruption. After adding 180 µl PBS, samples were meticulously homogenized with a clean plastic micro pestle. Then 20 µl proteinase K and 200 µl buffer AL (lysis buffer) were added to the sample mixture, followed by incubation at 56°C for 10 minutes. RNA contamination is eliminated by adding 4 µl RNase A and incubating at RT for two minutes. The sample mixture was then combined with 200 µl of 100% ethanol, put into DNeasy columns, and centrifuged at 8000 rpm for one minute. After discarding the filtrate and adding 500 µl of buffer AW1 (wash buffer) to the column, the mixture was centrifuged at 8000 rpm for an additional minute. Again, the filtrate was discarded, followed by adding 500 µl of buffer AW2 (wash buffer) and a three-minute centrifugation at 14,000 rpm to dehydrate the membrane. When the column was transferred to a new reaction tube, 25-100 µl of buffer AE (elution buffer) was introduced, followed by incubation at RT for one minute and centrifugation at 8000 rpm for another minute. Photometric estimation of the DNA concentration was performed, and the DNA was maintained at -20°C.

4.2.2.2 RNA isolation

RNA was isolated from *Drosophila* embryos using the NucleoSpin® RNA kit from Macherey-Nagel. About 50 mg embryos were collected and dechorionated as described above (see **4.2.1.1**) in a 1.5 ml reaction tube. Collected embryos were then homogenized in 350 µl lysis buffer RA1 with a clean plastic micro pestle, followed by an addition of 35 µl 150 mM DTT (dithiothreithol). To reduce viscosity, the lysate was filtrated through the NucleoSpin® Filter (violet ring) by centrifuging for 1 min at 11,000 x g at RT (all the following centrifuge steps were at RT). Then, the flowthrough was transferred to a new 1.5 ml reaction tube and mixed with 350 µl 70% ethanol by pipetting up and down five times. Afterward, the lysate was loaded into a NucleoSpin® Filter (light blue ring), placed in a fresh collection tube, and centrifuged for 30 s at 11,000 x g. 350 µl of membrane desalting buffer was added to the lysate, followed by 1-minute centrifugation at 11,000 x g to dry the membrane. The DNA was digested by incubating the lysate with a DNase reaction mixture comprising 90 µl Reaction buffer for rDNase and 10 µl

reconstituted rDNase at RT for 15 minutes. Three washes were performed to clean and dry the membrane. The initial washing was conducted using 200 µl of wash buffer RAW2 at 11,000 x g for 30 seconds at a centrifuge. The second wash used 600 µl of wash buffer RA3 at a centrifuge at 11,000 x g for 30 seconds. The final wash was conducted using 250 µl of buffer RA3 and centrifuged at 11,000 x g for two minutes. The RNA was eluted in 60 µl of DNase-free water via a one-minute centrifugation at 11,000 x g and was stored at -80°C.

4.2.2.3 Reverse transcription

Complementary DNA (cDNA) was produced from a total RNA template via reverse transcription. This approach provides the ability to subject transcribed gene sequences to PCR amplification. 7.5 µg RNA was incubated in a total of 17.55 µl water in a heat block at 90°C for two minutes, followed immediately by an incubation of two to five minutes on ice. The samples were subsequently incubated in a PCR cycler set at 50°C for one hour after adding the master mix (see **Table 13**). The probes were heat-inactivated at 95°C for two minutes and were transferred directly onto ice. At -20°C, the cDNA was preserved.

Table 13: Reverse transcription components

Components	30µl reaction	Final concentration
5x First Strand Buffer	6µl	1x
10mM dNTP Mix (2.5mM each)	1.2µl	400µM
Oligo-dT (18) Primer	1.2µl	0.5µg/µl
0.1M DTT	1µl	0.1M
Murine RNase Inhibitor (40U/µl)	1µl	1.3U/µl
Super Script III Reverse Transcriptase (200U/µl)	1µl	6.7U/µl
Total volume	12.45µl	

4.2.2.4 Polymerase chain reaction (PCR)

Polymerase chain reaction (PCR) is used to amplify specific DNA fragments. The reaction requires template DNA, a pair of primers, dNTPs, a heat-stable polymerase, and the polymerase-specific reaction buffer (see **Table 14**). All the PCR reactions in this work was performed using the Biometra® PCR thermal cycler (Analytik Jena, Jena, Germany).

Table 14: 50µl PCR reaction components

Components	50 µl Reaction	Final concentration
5x Q5 Reaction buffer	10µl	1x
10mM dNTP	1µl	200µM
10µM Forward primer	2.5µl	0.5µM
10µM Reverse primer	2.5µl	0.5µM
Template DNA	DNA genomic: 200ng-1µg Plasmid: 1pg-10ng	< 1, 000ng
Q5 polymerase	0.5µl	0.02U/µl
Ultrapure H_2O	Up to 50µl	---

A PCR cycle consists of denaturing, annealing, and elongation steps. When double-stranded DNA is heated to 95-98°C during the denaturing process, it undergoes melting, forming single-stranded DNA molecules. Afterward, the primers can undergo hybridization with the single-stranded DNA by reducing the temperature to approximately 55-65°C. The assembly of nucleotides from 5' to 3' begins with the primers and the addition of nucleotides to the free 3'-hydroxyl group of the growing DNA strand at a reaction temperature of 72°C (see **Table 15**). After each PCR cycle, the amount of the DNA is doubled.

Table 15: Standard PCR cycle

Processes	Temperature	Duration	Repeat
Initial denaturation	98°C	30s	---
Denaturation	98°C	10s	32 cycles
Annealing	50-72°C	30s	
Elongation	72°C	20-30s/Kb	
Final extension	72°C	120s	---
Hold	4°C	---	---

4.2.2.5 Overlap extension PCR (OE PCR)

The overlap extension PCR (OE PCR) method facilitates the assembly of DNA fragments from various sources *in vitro*. Thus, artificial fusion constructs and site-directed mutagenesis can be generated without employing serial cloning procedures or linker components for restriction enzymes (Ho et al. 1989).

The following four steps are necessary to perform OE PCR. First, Primers were designed to generate fragments with overlapping endings. Then, individual fragments were prepared using

standard PCR. Afterward, an overlap PCR reaction joined all the fragments with equal molar amounts (see **Table 16** and **Table 17**).

Table 16: Overlap PCR components

Components	50µl Reaction	Final concentration
5x Q5 Reaction buffer	10µl	1x
10 mM dNTP	1µl	200µM
Fragment 1	variable	50-800ng
Fragment 2	variable	50-800ng
(Fragment 3)	variable	50-800ng
Q5 polymerase	0.5µl	0.02U/µl
Ultrapure H_2O	Up to 50µl	---

Table 17: Thermocycling conditions for an overlap PCR

Processes	Temperature	Duration	Repeat
Initial denaturation	98°C	30s	
Denaturation	98°C	10s	15 cycles
Annealing	60°C	30s	
Elongation	72°C	20-30s/Kb	
Final extension	72°C	120s	---
Hold	4°C	---	---

Finally, 3 µl of the above overlap PCR reaction was utilized as a DNA template and subsequently amplified with an extension PCR using the end primers (**Table 18** and **Table 19**).

Table 18: Extension PCR components

Components	50 µl Reaction	Final concentration
5x Q5 Reaction buffer	10µl	1x
10mM dNTP	1µl	200µM
10µM Forward primer	2.5µl	0.5µM
10µM Reverse primer	2.5µl	0.5µM
Overlap PCR product	3µl	< 1, 000ng
Q5 polymerase	0.5µl	0.02U/µl
Ultrapure H_2O	Up to 50µl	

Table 19: Thermocycling conditions for an extension PCR

Processes	Temperature	Duration	Repeat
Initial denaturation	98°C	30s	
Denaturation	98°C	10s	20 cycles
Annealing	72°C	30s	
Elongation	72°C	20-30s/Kb	
Final extension	72°C	120s	
Hold	4°C		

The final PCR product was purified by gel extraction.

4.2.2.6 Agarose gel electrophoresis

Gel electrophoresis was employed to segregate nucleic acids. The negatively charged DNA strands migrated to the positive pole of the agarose gel due to the applied voltage. Thus, the fragments were separated based on their respective sizes.

The size of the DNA fragments to be analyzed determines the agarose concentration utilized for the gel. A low agarose concentration was employed to isolate large DNA fragments (see **Table 20**).

Table 20: Agarose gel electrophoresis concentrations

Agarose concentration	DNA fragment range (Kb)
0.5%	1-30
1%	0.5-10
2%	0.1-2

Before being applied to the gel, the samples were combined with 1x loading buffer to increase their density and allow electrophoresis tracking. A 1 kb DNA ladder was also used to determine fragment size. The Bio-Rad ChemiDoc™ (Feldkirchen, Germany) was utilized to conduct the analyses.

4.2.2.7 PCR clean-up

The NucleoSpin Gel and PCR Clean-up kit (Machery-Nagel, Düren, Germany) were used to purify DNA fragments from PCR.

One sample volume was mixed with two volumes of binding buffer NTI to adjust the DNA binding condition. Then, up to 700 µl sample mixture was loaded into a NucleoSpin® Gel and PCR Column placed in a collection tube, followed by a centrifuge at 11,000 x g for 30 seconds (all the centrifuge steps were at RT). After discarding the flowthrough, the column was returned to the collection tube. Afterward, 700 µl of wash buffer NT3 was added into the column and centrifuged at 11,000 x g for 30 seconds. Another one-minute centrifuge at 11,000 x g was performed to dry the membrane completely. Then, the column was placed into a new 1.5 ml reaction tube, adding 15-30 µl elution buffer NE or water. After one minute of incubation at RT, the column was centrifuged for 1 minute at 11,000 x g to elute the DNA. The purified PCR product can be used for cloning, sequencing or stored at -20°C.

4.2.2.8 Gel extraction

PCR can generate by-products of varying band sizes; in such cases, the intended product can be isolated and cut out after gel electrophoresis. The gel extraction was conducted using the NucleoSpin Gel and PCR Clean-up kit (Machery-Nagel, Düren, Germany).

To ascertain the volume of binding buffer NTI to use, the weight of the excised gel fragment was measured. After combining the gel fragment with two times the volume of the binding buffer NTI, it was incubated at 50°C for ten minutes or until complete dissolution. Then, up to 700 µl sample was transferred to a column, followed by 30 s centrifugation at 11,000 x g at RT. Following the addition of 700 µl wash buffer NT3, an additional 30 s centrifugation at 11,000 x g at RT was conducted. Further centrifugation at 11,000 x g for one minute was performed at RT to dry the membrane completely. After transferring the column to a fresh 1.5 ml reaction tube, 15–30 µl elution buffer NE or water was added. Following an initial minute of incubation at ambient temperature, the column was subsequently centrifuged at 11,000 x g at RT for one minute to elute the DNA. The purified PCR product can be used for further analysis or stored at -20°C.

4.2.2.9 Sanger sequencing

Sanger sequencing was utilized to ascertain the precise nucleotide order of DNA probes (performed by Eurofins Genomics, Ebersberg, Germany). In accordance with the product's purity and size, DNA was diluted and prepared as follows:

Table 21: Sanger sequencing using Mix2Seq kit

Sample type	Product length	Sample concentration	Volume
Plasmid DNA	< 15kbp	50-100ng/µl	5µl
Purified PCR products	150-300bp	1ng/µl	5µl
	300-1000bp	5ng/µl	5µl
	1000-3000bp	10ng/µl	5µl
Primer	16-25 bases	5pmol/µl	5µl

The sequencing results were analyzed using SnapGene software (GSL Biotech LLC, Boston, MA, USA).

4.2.3 Microbiological methods

4.2.3.1 TOPO cloning

A blunt-ended PCR product can be directionally inserted into a target vector by employing TOPO cloning. The forward primer, which incorporates the topoisomerase I-induced CACC sequence, undergoes ligation using the GTGG overhang of the vector. The pENTR/DTOPO kit from Invitrogen (Thermo Fischer Scientific, Schwerte, Germany) was utilized for TOPO cloning.

After transferring the components (see **Table 22**) via pipette into a reaction tube, they were incubated at RT for 30 minutes. For optimal TOPO® Cloning efficiency, a freshly purified PCR product with a molar ratio ranging from 0.5:1 to 2:1 was employed for the vector TOPO®.

Table 22: TOPO reaction components

Components	6µl reaction
TOPO® vector	1µl
Salt solution	1µl
Fresh purified PCR product	0.5-4µl
Ultrapure water	Up to 6µl

Afterward, a 2 µl of the TOPO reaction was used to transform 50 µl One Shot TOP10 *E. coli* cells (Thermo Fischer Scientific, Schwerte, Germany), which were cultured on plates containing LB agar medium with 50 ng/ml kanamycin. The individual colonies were picked to

prepare liquid culture using the LB medium containing 50 ng/ml kanamycin to isolate plasmids. The isolated plasmids were checked by restriction enzyme digestion and Sanger sequencing.

4.2.3.2 Gateway LR reaction

Multiple DNA fragments may be cloned in parallel using the same enzymes in a standardized manner with the Gateway recombinational cloning method (Hartley et al. 2000; Walhout et al. 2000). The process of gateway cloning relies on the bacteriophage λ's exact integration and excision reactions to enter and exit the genome of *E.* coli (Hartley et al. 2000). Thus, the Invitrogen® Gateway™ LR Clonase™ II enzyme mix (Thermo Fisher Scientific, Schwerte, Germany) generated *attB* and *attP* sites by recombining *attL* sites with *attR* sites. Due to the extremely specific recognition of *att* sites, each recombination reaction produces a unique set of derivatives.

Table 23: Gateway LR reaction components

Components	Concentration	10µl reaction
Entry clone	50-150ng/µl	1µl
Destination clone	150ng/µl	1µl
LR Clonase™ II enzyme mix	---	2µl
TE buffer (pH=8)	---	6µl

Following a two-hour to overnight incubation at 25°C, the reaction was terminated by adding 1 µl Proteinase K and a subsequent incubation at 37°C for ten minutes. The obtained samples were subsequently transformed into 50 µl One Shot TOP10 *E. coli* (Thermo Fischer Scientific, Schwerte, Germany). For each sample, 50 µl and 200 µl were transferred to LB plates supplemented with 60 ng/ml ampicillin.

4.2.3.3 Plasmid isolation

The Macherey-Nagel (Düren, Germany) NucleoSpin® Plasmid kit was employed for the rapid mini-preparation of plasmid DNA. Following transferring the bacterial liquid culture into a 5 ml reaction tube, the sample was pelleted at 11,000 x g for one minute via centrifugation (all the centrifuges were conducted at RT). The supernatant was discarded, and the pellet was resuspended in 250 µl resuspension buffer A1 by vortexing or pipetting. 250 µl of lysis buffer A2 was then introduced and agitated via inversion. After five minutes of incubation at RT,

300 µl of buffer A3 was added to achieve neutralization. By inverting the samples, the blue color change was eliminated. Then, a ten-minute centrifugation at 11,000 x g was conducted, thus proteins were precipitated and removed. After transferring the supernatant to a 2 ml reaction tube containing a column, it was centrifuged at 11,000 x g for one minute to bind the vector DNA on the membrane of the column. If required, a second centrifugation step was repeated to utilize the complete supernatant. The flow-through was discarded, and the membrane was washed with 600 µl of wash buffer A4 and subsequently discarded, following one-minute centrifugation at 11,000 x g. Afterward, a two-minute centrifugation at 11,000 x g was performed to dry the membrane completely. The column was placed in a new 1.5 ml reaction tube, and 30-50 µl of water or elution buffer AE was added, followed by one minute of incubation at RT. The plasmid DNA was finally eluted via centrifuge at 11,000 x g for one minute and stored at -20 °C.

4.2.3.4 Restrict enzyme digestion

As the restriction digestion can validate the successful cloning of the target sequence into the vector, enzymes from New England Biolabs (Frankfurt a. Main, Germany) were utilized.

Table 24: Restrict enzyme digestion components

Components	25µl reaction
DNA	0.5µg
10x NEBuffer	2.5µl
Restriction enzyme	0.5µl
Nuclease-free water	Up to 25µl

The isolated DNA was digested within a 25 µl reaction volume, and the reaction mixture was incubated for 15 minutes at 37 °C. After that, a 10 µl reaction mix was mixed with 2 µl 6x loading buffer and loaded on an agarose gel to undergo electrophoresis. The results were visualized using ChemiDoc™ from Bio-Rad.

4.2.3.5 Chemically competent *E. coli* bacteria transformation

Plasmids and other exogenous DNA are incorporated into bacteria via transformation. For this purpose, bacteria should be competent, and the plasmid should possess a so-called origin of

replication, which enables replication independently from the replication of its host's genome. Additionally, antibiotic-resistance genes encoded within the plasmid facilitate the selection of positive transformants.

Firstly, Invitrogen® One Shot TOP10 (Thermo Fisher Scientific, Schwerte, Germany) or self-made XL1 Blue competent cells were defrosted on ice. Approximately 1-2 µl of the intended plasmid was introduced into 25-50 µl cells. After 30 minutes of incubation on ice, the bacteria were heat-shocked for 30 seconds in a water bath at 42°C before being re-incubated on ice for 2 minutes. 250 µl pre-warmed S.O.C medium was introduced, followed by horizontal shaking of the bacteria at 37°C for one hour at 300 rpm using a thermo mixer (Eppendorf, Hamburg, Germany). 50–200 µl transformed cells were incubated overnight at 37°C on selective agar plates. The following day, several single colonies were selected and cultured into 10-20 ml of LB medium containing the corresponding antibiotic. Following overnight incubation at 37°C on a thermo shaker (Edmund Buehler, Bodelshausen, Germany), 2-5 ml cultures were utilized to isolate plasmid. To prepare glycerol stocks of the specialized bacteria, 500 µl of glycerol was added to 500 µl of bacterial culture; the resulting stocks were then stored at -80°C.

4.2.3.6 Cell culture

The Schneider 2 (S2) cells were kept in culture flasks (25 ml) with a complete medium at 26°C. After three to four days, until the cell density reaches 6-20 x 10^6 cells/ml, the cells could be split at 1:2-1:10 to achieve a 2-4 x 10^6 cells/ml concentration.

To freeze S2 cells, 12 ml cell suspension at a density of 1 x 10^7 was centrifuged at 150 x g for 10 min at 4°C. The cell pellet was resuspended in 10 ml PBS and then centrifuged at 150 x g for 10 min at 4°C. After that, cells were resuspended at a density of 1.1 × 10^7 cells/mL in the freezing medium and were aliquoted into 2 ml pre-cooled cyro tubes (1 ml cell suspension/tube). Tubes were first placed in a control rate freezer (Mr. Frosty™, Thermo Fisher Scientific, Schwerte, Germany) at -80°C, and after 24 hours, they were stored in liquid nitrogen.

To initiate cell culture from frozen stock, the vial of S2 cells was removed from liquid nitrogen and thawed quickly at 30°C. Then, the whole content was transferred into a sterile conical tube containing 4 ml pre-warmed Complete Schneider's *Drosophila* medium and centrifuged at

150 x g for 10 min at RT. Afterward, the supernatant was removed, and cells were gently resuspended in 5 ml fresh Complete Schneider's *Drosophila* medium.

4.2.3.7 Transient transfection of S2 cells

The Effectene® Transfection Reagent (QIAGEN, Hilden, Germany) was utilized to transfect S2 cells transiently. S2 cells were counted by LUNA™ Automated Cell Counter (Aligned Genetics, Villeneuve d'Ascq, France) and diluted to 8 x 10^5 to 1 x 10^6 cells/ml. Then, 1.5 ml cells were transferred into one well of a 6-well plate. The Caspr and expression vectors were diluted to 100 ng/µl. A volume of 90 µl of DNA-condensation EC buffer, 5 µl act5C-Gal4, 5 µl expression vector, and 8 µl of enhancer were pipetted into an autoclaved reaction tube. Vibrating briefly following an incubation at RT for five minutes. 10 µl of Effectene was subsequently introduced. Ten seconds of vortexing, followed by 15 minutes of incubation at RT. Then, 600 µl Schneider's medium was added dropwise to the cells using a pipette. After homogenizing the cells with a gentle shaking of the plate, cells were incubated at 26°C for two days.

4.2.3.8 Cell-cell aggregation assay

The protein-protein interaction was analyzed by cell-cell aggregation assay. After two-day incubation of the S2 cells transfected by specific expression vectors, cell clumps were disrupted by pipetting up and down 20-30 times. Then, 300 µl of two distinct cell suspensions from the 6-well plate were transferred to one imaging chamber (µ-Dish 35mm high, ibidi, Gräfelfing, Germany). The imaging chamber was incubated in the dark for two hours while rocking using Rocking Platform (VWR, Leuven, Belgium) at RT at 100 rpm. This incubation period facilitated the potential interaction of the cells. Afterward, the cell suspensions were subjected to LSM 710 analysis to identify possible cell aggregates.

4.2.4 Biochemical methods

4.2.4.1 Immunohistochemistry of *Drosophila* embryos

Immunohistochemistry was used to investigate the distribution and location of specific expressed proteins in *Drosophila* embryos. The procedure includes preparing the embryos and the labeling process.

Sample preparation (Fixation of embryos)

Embryos that had been dechorionized were transferred into a reaction tube containing 600 µl heptane and 600 µl PBS containing 3.7% formaldehyde. The tube was then placed on a nutator for 20 minutes. Following removing the formaldehyde (lower phase), 600 µl methanol was introduced, and the vitelline membrane was eliminated by vigorously shaking the embryos for 1-2 minutes. In contrast to the embryos, which descend to the bottom, the membrane debris remains in the interphase. After the removal of the upper phase and interphase, the embryos underwent three five-minute washes with 500 µl methanol. Embryos may then be used for labeling or preserved in methanol at -20°C for several months.

Sample labeling

The fixed embryos underwent three 10-minute washes in 500 µl PTX using a nutator. They were incubated for 30 minutes in 500 µl PTX supplemented with 5% normal goat serum (NGS) to block non-specific binding sites. Following the addition of primary antibodies, the embryos were incubated at 4°C overnight on the nutator. After four 10-minute washes in 500 µl PTX, fluorescently labeled secondary antibodies were added. These antibodies were diluted in 500 µl PTX containing 5% NGS. The embryos were then incubated in the dark on the nutator at RT for two hours. The embryos were washed four times in 500 µl PTX for ten minutes and then were rinsed in PBS. Afterward, they were covered in 400 µl 70% glycerol in PBS at 4°C.

Sample mounting

Once the embryos had settled to the bottom of the reaction tube, they were mounted for further imaging. A 200 µl pipette tip was cut to allow embryos to traverse it without being subjected to excessive shearing forces. 37 µl glycerol-containing embryos were added to an object slide. The slide was then covered with an 18 x 18 mm cover slide and sealed with nail polish.

4.2.4.2 Immunohistochemistry of *Drosophila* larval gut

The immunohistochemistry application was utilized to analyze the number and width of the longitudinal visceral muscle fibers of the *Drosophila* larval midgut.

Sample preparation

To ensure the larvae that were analyzed were at the same developing stage, embryos were collected for two hours and raised at 25°C. After five days, larvae (L3 stage) were radomly picked. Interesting genotypes were sorted by GFP-tagged balancers using a UV bino. Under a stereo microscope, the larval guts were carefully isolated and placed on an 8.0 µm TC-insert in a well of a 24-well plate containing PBS. The well was then placed on a nutator and the larvae were fixed in 800 µl PBS containing 3.7% formaldehyde for 15 minutes. Afterward, the larvae were washed with 800 µl PTX for 3 x 10 minutes.

Sample labeling

The fixed larval guts were first incubated in 800 µl PTX + 5% NGS for 30 minutes to block unspecific binding sites. Then, 2 µl Texas Red™-X Phalloidin was added for labeling. After incubation in the dark for two hours, the guts were washed with 800 µl PTX for 10 minutes three times and rinsed one time with PBS. The fluorescently labeled guts were preserved in 800 µl 70% glycerol in PBS at 4°C.

Sample mounting

After the guts descended to the bottom, they could be mounted for imaging. First, 20 µl 70% glycerol in PBS was placed on a slide. The guts were then carefully transferred using forceps onto the slide under a stereo microscope. The guts were covered with an 18 x 18 mm cover slide and sealed with nail polish.

4.2.4.3 *In situ* hybridization of *Drosophila* embryos

Fluorescent *in situ* hybridization (FISH) enables the detection of mRNA in *Drosophila* embryos. The major steps include probe preparation, sample preparation, hybridization, and signal labeling.

Probe preparation (*in vitro* transcription)

PCR was used to amplify the desired DNA sequence regulated by T3, T7, or SP6 promoters. Following the purification of the PCR products, *in vitro* transcription was conducted, which allows the generation of RNA transcripts from DNA sequences. Digoxigenin-labeled nucleotides, which permit immunochemical labeling, were used for subsequent probe detection.

Table 25: *In vitro* transcription components

Components	Volume
Purified PCR product	10µl
DIG RNA labeling mix	2µl
Polymerase reaction buffer	Depends on the polymerase
RNA polymerase	2µl
RNase inhibitor	1µl
ddH_2O	Up to 20µl

The reaction mixture was incubated at 37°C for four hours. The probe was precipitated overnight at -20°C by adding 30 µl ddH2O, 20 µl 7.5 M ammonium acetate, and 75 µl 96% ethanol. After a 15-minute centrifugation at 4°C and 14,000 rpm, the supernatant was discarded, and the pellet was resuspended in 30 µl sample buffer.

Sample preparation

The fixed *Drosophila* embryos stored in methanol were used in the FISH. First, methanol was discarded and substituted with 600 µl PBS containing 3.7% formaldehyde and 300 µl methanol. After that, the embryos were placed on a shaker at RT for ten minutes. Then, 300 µl PBS with 3.7% formaldehyde and 600 µl methanol were utilized to replace the liquid. After 10 minutes of incubation on a shaker at RT, a second fixation was conducted for 10 minutes using 500 µl PBS containing 3.7% formaldehyde. The embryos were then washed three times for ten minutes with 500 µl PBT.

Hybridization

Following a 30-minute pre-hybridization of the samples in 500 µl hybridization buffer in a water bath at 52°C with circulation, non-specific binding sites were blocked. After adding 1-

5 µl of the DIG-labeled probe, the samples were incubated in a water bath at 52°C overnight. Four washing steps were conducted the following day using 500 µl of pre-warmed wash buffer. The samples were rinsed twice with 500 µl PBT and washed for 30 minutes with 500 µl PBT on the shaker on the third day.

Signal labeling

Cyanine 3 tyramide was used to develop the signal for the labeled probe. At first, 500 µl PBT containing 5% NGS supplemented with the anti-Digoxigenin-POD was added. Following a 2-hour incubation at RT, three washing steps were completed using 500 µl PBT for five minutes while shaking. Afterward, a 100 µl tyramide working solution was added to the embryos. The samples were incubated for 10 minutes in the dark at RT on the shaker. Then, they were washed thrice for five minutes with 500 µl PBT and rinsed once with PBS. After the embryos sank in 400 µl 70% glycerol in PBS, they could be mounted for microscopy. If an antibody staining was intended to be included, a standard staining protocol was conducted after the last washing step of the above cyanine 3 tyramide staining.

4.2.4.4 TUNEL assay

Terminal deoxynucleotidyl transferase dUTP nick end labeling (TUNEL) is used to identify DNA fragmentation in apoptosis-induced double-strand DNA breaks by labeling their 3′-hydroxyl termini (Gorczyca et al. 1993).

Freshly fixed (less than two weeks) *Drosophila* embryos were used to detect apoptosis using the One-Step TUNEL assay kit (Elabscience Biotechnology, Houston, TA, USA). After three 10-minute washes with 500 µl PTX, unspecific binding sites of embryos were blocked by incubating with 500 µl PTX+5% NGS at RT for 30 min. Following three 10-minute washes with 500 µl PTX, the primary antibodies were introduced, and the embryos were incubated at 4°C overnight (or at RT for two hours). The embryos were then washed with 500 µl PTX three times (every time 10 minutes). Afterward, 100 µl TdT equilibration buffer was added. The embryos were incubated on a shaker at 37°C for 30 min, followed by adding the reaction mixture containing the secondary antibodies (see **Table 26**).

Table 26: TUNEL assay components

Components	Positive control / Experimental group	Negative control
TdT equilibration buffer	35ul	40ul
Labeling solution	10ul	10ul
TdT enzyme	5ul	0ul
Secondary antibody	0.1ul	0.1ul

The embryos with the reaction mixture were incubated in the dark on a shaker at 37°C for two hours and washed with 500 µl PBS three times (every time 5 minutes). Then, the PBS was replaced with 400 µl 70% glycerol in PBS, and when the embryos were sunk to the bottom, they could be mounted for imaging.

4.2.5 Microscopy and Image Processing

Confocal images were acquired using the Zeiss LSM 710 or LSM 880 confocal microscope. When acquired, Z-stacks sections were of 1-2 µm intervals. Images were processed with Fiji (ImageJ) software. The process was limited to correct global brightness and background subtraction. The maximum intensity projections of Z-stacks were utilized for all figures (unless the use of a single stack is mentioned). The anterior end of the embryo is oriented to the left, while the dorsal portion is positioned upwards. Images were compiled in Illustrator (CC2022).

4.2.6 Quantification and Statistical Analysis

For each experimental or control group, specimens were randomly chosen from at least three independently repeated experiments. Data sets were tested for normal distribution using the Kolmogorov-Smirnov test with Lilliefors correction. p-values were determined by the T-test or two-tailed Mann-Whitney U test, *$p \leq 0.05$, **$p \leq 0.01$, ***$p \leq 0.001$. Data analysis was performed and presented with Prism 9 software (GraphPad Software, Boston, MA, USA).

4.2.6.1 Food intake assay for L3 larvae

To quantify the food intake assay, L3 larvae of the same developing stage were picked for each experimental or control group. The outlines of the whole larval body and the blue-food-filled area were depicted and measured with the “freehand selections” and “Measure” tools of the Fiji (ImageJ) program.

4.2.6.2 LVM fibers of L3 larval midgut

L3 larvae of the same developing stage were selected and dissected for each experimental or control group. The number of LVM fibers was counted by hand. The width of the LVM fibers was measured using the "straight selections" and "Measure" tools of the Fiji (ImageJ) software.

4.2.6.3 Cell-cell aggregation assay

For the quantification analysis of the cell-cell aggregation assay, 20-30 aggregates were randomly chosen. The size of the cell aggregates was measured using Fiji (ImageJ). Outlines of the aggregates were first depicted with the "freehand selections" and then determined by the "Mesure" tool.

4.3 Contributions

I supervised several bachelor students who contributed to this thesis during this work.

Table 27: Contributions

Experiments	Partly performed by	References
Fig. 13	Yakun Li	Bachelor thesis: Li, 2024
Fig. 14	Yakun Li	Bachelor thesis: Li, 2024
Fig. 15	Nina Magewirth	Bachelor thesis: Magewirth, 2023
Fig. 33	Johanna Engeln	---
Fig. 34	Yakun Li	Bachelor thesis: Li, 2024
Fig. 40	Yakun Li	Bachelor thesis: Li, 2024
Fig. 40	Yakun Li	Bachelor thesis: Li, 2024
Fig. 52	Yakun Li	Bachelor thesis: Li, 2024

References

Aberle H. 2009. 'Searching for guidance cues: follow the Sidestep trail', *Fly (Austin)*, 3: 270-3.

Aghajanian P., Takashima S., Paul M., Younossi-Hartenstein A., and Hartenstein V. 2016. 'Metamorphosis of the *Drosophila* visceral musculature and its role in intestinal morphogenesis and stem cell formation', *Dev. Biol.*, 420: 43-59.

Alberts B., Johnson A. , Lewis J. , Raff M., Roberts K., and Walter P. 2002. *Molecular Biology of the Cell* (Garland Science: New York).

Aman A., and Piotrowski T. 2010. 'Cell migration during morphogenesis', *Dev. Biol.*, 341: 20-33.

Ananthakrishnan R., and Ehrlicher A. 2007. 'The forces behind cell movement', *Int. J. Biol. Sci.*, 3: 303-17.

Azpiazu N., and Frasch M. 1993. '*tinman* and *bagpipe*: two homeo box genes that determine cell fates in the dorsal mesoderm of *Drosophila*', *Genes Dev.*, 7: 1325-40.

Badolato R. 2013. 'Defects of leukocyte migration in primary immunodeficiencies', *Eur. J. Immunol.*, 43: 1436-40.

Bae Y. K., Macabenta F., Curtis H. L., and Stathopoulos A. 2017. 'Comparative analysis of gene expression profiles for several migrating cell types identifies cell migration regulators', *Mech. Dev.*, 148: 40-55.

Bardet P. L., Kolahgar G., Mynett A., Miguel-Aliaga I., Briscoe J., Meier P., and Vincent J. P. 2008. 'A fluorescent reporter of caspase activity for live imaging', *Proc. Natl. Acad. Sci. USA*, 105: 13901-5.

Bazan J. F., and Goodman C. S. 1997. 'Modular structure of the *Drosophila* Beat protein', *Curr. Biol.*, 7: R338-9.

Beiman M., Shilo B. Z., and Volk T. 1996. 'Heartless, a *Drosophila* FGF receptor homolog, is essential for cell migration and establishment of several mesodermal lineages', *Genes Dev.*, 10: 2993-3002.

Bischof J., Maeda R. K., Hediger M., Karch F., and Basler K. 2007. 'An optimized transgenesis system for *Drosophila* using germ-line-specific phiC31 integrases', *Proc. Natl. Acad. Sci. USA*, 104: 3312-7.

Bökel C., and Brown N. H. 2002. 'Integrins in development: moving on, responding to, and sticking to the extracellular matrix', *Dev. Cell.*, 3: 311-21.

Brand A. H., and Perrimon N. 1993. 'Targeted gene expression as a means of altering cell fates and generating dominant phenotypes', *Dev.*, 118: 401-15.

Cabernard C., Neumann M., and Affolter M. 2004. 'Cellular and molecular mechanisms involved in branching morphogenesis of the *Drosophila* tracheal system', *J. Appl. Physiol.* , 97: 2347-53.

Campos-Ortega J. A., and Hartenstein V. 1985. *The embryonic development of Drosophila melanogaster* (Springer Berlin: Heidelberg).

Carrier Y., Rio L., Formicola N., de Sousa-Xavier V., Tabet M., Chen Y. D., Wislez M., Orts L., and Teixeira F. P. 2023. 'Biased cell adhesion organizes a circuit for visual motion integration', *bioRxiv*: 2023.12.11.571076.

Corish P., and Tyler-Smith C. 1999. 'Attenuation of green fluorescent protein half-life in mammalian cells', *Protein Eng.*, 12: 1035-40.

Darzynkiewicz Z., Galkowski D., and Zhao H. 2008. 'Analysis of apoptosis by cytometry using TUNEL assay', *Methods*, 44: 250-4.

Davis J. R., Huang C. Y., Zanet J., Harrison S., Rosten E., Cox S., Soong D. Y., Dunn G. A., and Stramer B. M. 2012. 'Emergence of embryonic pattern through contact inhibition of locomotion', *Dev.*, 139: 4555-60.

de Castro E., Sigrist C. J., Gattiker A., Bulliard V., Langendijk-Genevaux P. S., Gasteiger E., Bairoch A., and Hulo N. 2006. 'ScanProsite: detection of PROSITE signature matches and ProRule-associated functional and structural residues in proteins', *Nucl Acids Res.*, 34: W362-5.

de Torres C., Munell F., Ferrer I., Reventós J., and Macaya A. 1997. 'Identification of necrotic cell death by the TUNEL assay in the hypoxic-ischemic neonatal rat brain', *Neurosci. Lett.*, 230: 1-4.

Dorey K., and Amaya E. 2010. 'FGF signalling: diverse roles during early vertebrate embryogenesis', *Dev.*, 137: 3731-42.

Engelhardt B., and Ransohoff R. M. 2012. 'Capture, crawl, cross: the T cell code to breach the blood-brain barriers', *Trends Immunol*, 33: 579-89.

Englund C., Lorén C. E., Grabbe C., Varshney G. K., Deleuil F., Hallberg B., and Palmer R. H. 2003. 'Jeb signals through the Alk receptor tyrosine kinase to drive visceral muscle fusion', *Nat.* , 425: 512-6.

Evans R., O'Neill M., Pritzel A., Antropova N., Senior A., Green T., Žídek A., Bates R., Blackwell S., Yim J., Ronneberger O., Bodenstein S., Zielinski M., Bridgland A., Potapenko A., Cowie A., Tunyasuvunakool K., Jain R., Clancy E., Kohli P., Jumper J., and Hassabis D. 2021. "Protein complex prediction with AlphaFold-Multimer." In.: bioRxiv.

Fambrough D., and Goodman C. S. 1996. 'The *Drosophila beaten path* gene encodes a novel secreted protein that regulates defasciculation at motor axon choice points', *Cell*, 87: 1049-58.

Fendl S., Vieira R. M., and Borst A. 2020. 'Conditional protein tagging methods reveal highly specific subcellular distribution of ion channels in motion-sensing neurons', *eLife*, 9: e62953.

Frasch M., Ismat A., Reim I., and Raufer J. 2023. 'The RNF220 domain nuclear factor Teyrha-Meyrha (Tey) regulates the migration and differentiation of specific visceral and somatic muscles in *Drosophila*', *Dev.*, 150: dev201457.

Fujioka M., Yusibova G. L., Sackerson C. M., Tillib S., Mazo A., Satake M., and Goto T. 1996. 'Runt domain partner proteins enhance DNA binding and transcriptional repression in cultured *Drosophila* cells', *Genes Cells*, 1: 741-54.

Golling G., Li L., Pepling M., Stebbins M., and Gergen J. P. 1996. 'Drosophila homologs of the proto-oncogene product PEBP2/CBF beta regulate the DNA-binding properties of Runt', *Mol Cell Biol*, 16: 932-42.

Gorczyca W., Traganos F., Jesionowska H., and Darzynkiewicz Z. 1993. 'Presence of DNA strand breaks and increased sensitivity of DNA in situ to denaturation in abnormal human sperm cells: analogy to apoptosis of somatic cells', *Exp. Cell Res.*, 207: 202-5.

Gorfinkiel N., and Arias A. M. 2007. 'Requirements for adherens junction components in the interaction between epithelial tissues during dorsal closure in *Drosophila*', *J. Cell Sci.*, 120: 3289-98.

Grasl-Kraupp B., Ruttkay-Nedecky B., Koudelka H., Bukowska K., Bursch W., and Schulte-Hermann R. 1995. 'In situ detection of fragmented DNA (TUNEL assay) fails to discriminate among apoptosis, necrosis, and autolytic cell death: a cautionary note', *Hepatol.*, 21: 1465-8.

Gratz S. J., Cummings A. M., Nguyen J. N., Hamm D. C., Donohue L. K., Harrison M. M., Wildonger J., and O'Connor-Giles K. M. 2013. 'Genome Engineering of *Drosophil*a with the CRISPR RNA-Guided Cas9 Nuclease', *Genet.*, 194: 1029-35.

Gupta P. B., Kuperwasser C., Brunet J. P., Ramaswamy S., Kuo W. L., Gray J. W., Naber S. P., and Weinberg R. A. 2005. 'The melanocyte differentiation program predisposes to metastasis after neoplastic transformation', *Nat. Genet.*, 37: 1047-54.

Hamilton W. C., Stolarska M. A., and Ismat A. 2022. 'Simulation and in vivo experimentation predict AdamTS-A location of function during caudal visceral mesoderm migration in *Drosophila*', *Dev. Dyn.*, 251: 1123-37.

Hartley J. L., Temple G. F., and Brasch M. A. 2000. 'DNA cloning using in vitro site-specific recombination', *Genome Res.*, 10: 1788-95.

Hay B. A., Wolff T., and Rubin G. M. 1994. 'Expression of baculovirus P35 prevents cell death in *Drosophila*', *Dev.*, 120: 2121-9.

Hayashi S., and Kondo T. 2018. 'Development and Function of the *Drosophila* Tracheal System', *Genet.*, 209: 367-80.

Heymann C., Paul C., Huang N., Kinold J. C., Dietrich A. C., and Aberle H. 2022. 'Molecular insights into the axon guidance molecules Sidestep and Beaten path', *Front. physiol.*, 13: 1057413.

Ho S. N., Hunt H. D., Horton R. M., Pullen J. K., and Pease L. R. 1989. 'Site-directed mutagenesis by overlap extension using the polymerase chain reaction', *Gene*, 77: 51-9.

Hollfelder D., Frasch M., and Reim I. 2014. 'Distinct functions of the laminin β LN domain and collagen IV during cardiac extracellular matrix formation and stabilization of alary muscle attachments revealed by EMS mutagenesis in *Drosophila*', *BMC Dev. Biol.*, 14: 26.

Homma Felix, Huang Jie, and van der Hoorn Renier A. L. 2023. 'AlphaFold-Multimer predicts cross-kingdom interactions at the plant-pathogen interface', *Nat. Commun.*, 14: 6040.

Inaki M., Shinza-Kameda M., Ismat A., Frasch M., and Nose A. 2010. '*Drosophila* Tey represses transcription of the repulsive cue Toll and generates neuromuscular target specificity', *Dev.*, 137: 2139-46.

Ismat A., Cheshire A. M., and Andrew D. J. 2013. 'The secreted AdamTS-A metalloprotease is required for collective cell migration', *Dev.*, 140: 1981-93.

Ismat A., Schaub C., Reim I., Kirchner K., Schultheis D., and Frasch M. 2010. 'HLH54F is required for the specialization and migration of longitudinal gut muscle founders from the caudal mesoderm of *Drosophila*', *Dev.*, 137: 3107-17.

Jaglarz M. K., and Howard K. R. 1995. 'The active migration of *Drosophila* primordial germ cells', *Dev.*, 121: 3495-503.

Jinek M., Chylinski K., Fonfara I., Hauer M., Doudna J. A., and Charpentier E. 2012. 'A programmable dual-RNA-guided DNA endonuclease in adaptive bacterial immunity', *Sci.*, 337: 816-21.

Kadam S., Ghosh S., and Stathopoulos A. 2012. 'Synchronous and symmetric migration of *Drosophila* caudal visceral mesoderm cells requires dual input by two FGF ligands', *Dev.*, 139: 699-708.

Kaminker Joshua S., Singh Rajan, Lebestky Tim, Yan Huajun, and Banerjee Utpal. 2001. 'Redundant function of Runt Domain binding partners, Big brother and Brother, during *Drosophila* development', *Dev.*, 128: 2639-48.

Kim A.R., Hu Y., Rodiger J, Mohr S. E., and Perrimon N. 2024. 'Enhanced Protein-Protein Interaction Discovery via AlphaFold-Multimer', *bioRxiv*: 2024.02.19.580970.

Kinold J. C. 2016. 'Function and regulation of the axon guidance molecules Sidestep and Beaten path Ia in *Drosophila melanogaster*', Ph.D. Thesis, Heinrich Heine University Duesseldorf.

Kinoshita T. 2016. 'Glycosylphosphatidylinositol (GPI) anchors: biochemistry and cell biology: introduction to a thematic review eeries', *J. Lipid Res.*, 57: 4-5.

Klapper R., Stute C., Schomaker O., Strasser T., Janning W., Renkawitz-Pohl R., and Holz A. 2002. 'The formation of syncytia within the visceral musculature of the *Drosophila* midgut is dependent on *duf*, *sns* and *mbc*', *Mech. Dev.*, 110: 85-96.

Kondo S., and Ueda R. 2013. 'Highly improved gene targeting by germline-specific Cas9 expression in *Drosophila*', *Genet.*, 195: 715-21.

Kozlov M. M., and Chernomordik L. V. 2015. 'Membrane tension and membrane fusion', *Curr Opin Struct Biol.*, 33: 61-7.

Kunwar P. S., Sano H., Renault A. D., Barbosa V., Fuse N., and Lehmann R. 2008. 'Tre1 GPCR initiates germ cell transepithelial migration by regulating *Drosophila* melanogaster E-cadherin', *J. Cell Biol.*, 183: 157-68.

Kusch T., and Reuter R. 1999. 'Functions for *Drosophila* brachyenteron and forkhead in mesoderm specialization and cell signalling', *Dev.*, 126: 3991-4003.

Lauffenburger D. A., and Horwitz A. F. 1996. 'Cell Migration: A Physically Integrated Molecular Process', *Cell*, Volume 84, Issue 3: 359-69.

Lavergne G., Zmojdzian M., Da Ponte J. P., Junion G., and Jagla K. 2020. '*Drosophila* adult muscle precursor cells contribute to motor axon pathfinding and proper innervation of embryonic muscles', *Dev.*, 147: dev.183004.

Lee H. H., Norris A., Weiss J. B., and Frasch M. 2003. 'Jelly belly protein activates the receptor tyrosine kinase Alk to specify visceral muscle pioneers', *Nat. Commun.*, 425: 507-12.

Letunic I., Khedkar S., and Bork P. 2020. 'SMART: recent updates, new developments and status in 2020', *Nucl Acids Res.*, 49: D458-D60.

Li H., Watson A., Olechwier A., Anaya M., Sorooshyari S. K., Harnett D. P., Lee H. P., Vielmetter J., Fares M. A., Garcia K. C., Özkan E., Labrador J. P., and Zinn K. 2017. 'Deconstruction of the Beaten Path-Sidestep interaction network provides insights into neuromuscular system development', *eLife*, 6: e28111.

Macabenta F., and Stathopoulos A. 2019. 'Migrating cells control morphogenesis of substratum serving as track to promote directional movement of the collective', *Dev.*, 146: dev. 177295.

Macabenta F., Sun H. T., and Stathopoulos A. 2022. 'BMP-gated cell-cycle progression drives anoikis during mesenchymal collective migration', *Dev. Cell*, 57: 1683-93.e3.

Mandal L., Dumstrei K., and Hartenstein V. 2004. 'Role of FGFR signaling in the morphogenesis of the *Drosophila* visceral musculature', *Dev. Dyn.*, 231: 342-8.

Martin B. S., Ruiz-Gómez M., Landgraf M., and Bate M. 2001. 'A distinct set of founders and fusion-competent myoblasts make visceral muscles in the *Drosophila* embryo', *Dev.*, 128: 3331-8.

Martin D., Zusman S., Li X., Williams E. L., Khare N., DaRocha S., Chiquet-Ehrismann R., and Baumgartner S. 1999. '*wing blister*, a new *Drosophila* laminin alpha chain required for cell adhesion and migration during embryonic and imaginal development', *J. Cell Biol.*, 145: 191-201.

Montell D. J. 2003. 'Border-cell migration: the race is on', *Nat. Rev. Mol. Cell Biol.*, 4: 13-24.

Moreira S., Stramer B., Evans I., Wood W., and Martin P. 2010. 'Prioritization of competing damage and developmental signals by migrating macrophages in the *Drosophila* embryo', *Curr. Biol.*, 20: 464-70.

Mowat D. R., Croaker G. D., Cass D. T., Kerr B. A., Chaitow J., Adès L. C., Chia N. .L, and Wilson M. J. 1998. 'Hirschsprung disease, microcephaly, mental retardation, and characteristic facial features: delineation of a new syndrome and identification of a locus at chromosome 2q22-q23', *J. Med. Genet.*, 35: 617-23.

Mushegian A. R. 1997. 'The *Drosophila* Beat protein is related to adhesion proteins that contain immunoglobulin domains', *Curr. Biol.*, 7: R336-8.

Nagarkar-Jaiswal S., Lee P. T., Campbell M. E., Chen K., Anguiano-Zarate S., Cantu Gutierrez M., Busby T., Lin W., He Y., Schulze K. L., Booth B. W., Evans-Holm M., Venken K. J. T., Levis R. W., Spradling A. C., Hoskins R. A., and Bellen H. J. 2015. 'A library of MiMICs allows tagging of genes and reversible, spatial and temporal knockdown of proteins in *Drosophila*', *eLife*, 4: e05338.

Nguyen D. X., and Massagué J. 2007. 'Genetic determinants of cancer metastasis', *Nat. Rev. Genet.*, 8: 341-52.

Nguyen H. T., and Xu X. 1998. '*Drosophila* mef2 expression during mesoderm development is controlled by a complex array of cis-acting regulatory modules', *Dev. Biol.*, 204: 550-66.

Niewiadomska P., Godt D., and Tepass U. 1999. 'DE-Cadherin is required for intercellular motility during *Drosophila* oogenesis', *J. Cell Biol.*, 144: 533-47.

Nishida H., Albero A. B., Onoue K., Ikegawa Y., Sulekh S., Sakizli U., Minami Y., Yonemura S., Wang Y. C., and Yoo S. K. 2024. 'Necrosensor: a genetically encoded fluorescent sensor for visualizing necrosis in *Drosophila*', *Biol. Open*, 13: bio060104.

Norman M. U., and Hickey M. J. 2005. 'Mechanisms of lymphocyte migration in autoimmune disease', *HLA*, 66: 163-72.

Osaka J., Ishii A., Wang X., Iwanaga R., Kawamura H., Akino S., Sugie A., Hakeda-Suzuki S., and Suzuki T. 2024. 'Complex formation of immunoglobulin superfamily molecules Side-IV and Beat-IIb regulates synaptic specificity', *Cell Rep.*, 43: 113798.

Özkan E., Carrillo R. A., Eastman C. L., Weiszmann R., Waghray D., Johnson K. G., Zinn K., Celniker S. E., and Garcia K. C. 2013. 'An extracellular interactome of immunoglobulin and LRR proteins reveals receptor-ligand networks', *Cell*, 154: 228-39.

Paulick M. G., and Bertozzi C. R. 2008. 'The glycosylphosphatidylinositol anchor: a complex membrane-anchoring structure for proteins', *Biochem.*, 47: 6991-7000.

Peng D., Jackson D., Palicha B., Kernfeld E., Laughner N., Shoemaker A., Celniker S. E., Loganathan R., Cahan P., and Andrew D. J. 2024. 'Organogenetic transcriptomes of the *Drosophila* embryo at single cell resolution', *Dev.*, 151: dev202097.

Pipes G. C., Lin Q., Riley S. E., and Goodman C. S. 2001. 'The Beat generation: a multigene family encoding IgSF proteins related to the Beat axon guidance molecule in *Drosophila*', *Dev.*, 128: 4545-52.

Pocha S. M., and Montell D. J. 2014. 'Cellular and molecular mechanisms of single and collective cell migrations in *Drosophila*: themes and variations', *Annu. Rev. Genet.*, 48: 295-318.

Popichenko D., Hugosson F., Sjögren C., Dogru M., Yamazaki Y., Wolfstetter G., Schönherr C., Fallah M., Hallberg B., Nguyen H., and Palmer R. H. 2013. 'Jeb/Alk signalling regulates the Lame duck GLI family transcription factor in the *Drosophila* visceral mesoderm', *Dev.*, 140: 3156-66.

Reim I., Hollfelder D., Ismat A., and Frasch M. 2012. 'The FGF8-related signals Pyramus and Thisbe promote pathfinding, substrate adhesion, and survival of migrating longitudinal gut muscle founder cells', *Dev. Biol.*, 368: 28-43.

Renault A. D., Kunwar P. S., and Lehmann R. 2010. 'Lipid phosphate phosphatase activity regulates dispersal and bilateral sorting of embryonic germ cells in *Drosophila*', *Dev.*, 137: 1815-23.

Renault A. D., Sigal Y. J., Morris A. J., and Lehmann R. 2004. 'Soma-Germ Line Competition for Lipid Phosphate Uptake Regulates Germ Cell Migration and Survival', *Sci.*, 305: 1963-66.

Rørth P. 2009. 'Collective Cell Migration', *Annu. Rev. Cell Dev. Biol.*, 25: 407-29.

Rout P., Preußner M., and Önel S. F. 2022. '*Drosophila melanogaster*: A model system to study distinct genetic programs in myoblast fusion', *Cells*, 11: 321.

Rudolf A., Buttgereit D., Jacobs M., Wolfstetter G., Kesper D., Pütz M., Berger S., Renkawitz-Pohl R., Holz A., and Önel S. F. 2014. 'Distinct genetic programs guide *Drosophila* circular and longitudinal visceral myoblast fusion', *BMC Cell Biol.*, 15: 27.

Schröter R. H., Buttgereit D , Beck L , Holz A , and Renkawitz-Pohl R. 2006. 'Blown fuse regulates stretching and outgrowth but not myoblast fusion of the circular visceral muscles in *Drosophila*', *Differentiation*, 74: 608-21.

Siebert M., Banovic D., Goellner B., and Aberle H. 2009. '*Drosophila* motor axons recognize and follow a Sidestep-labeled substrate pathway to reach their target fields', *Genes Dev.*, 23: 1052-62.

Sink H., and Hartenstein V. 2006. 'The muscle pattern of *Drosophila*', *Muscle development in Drosophila*: 8-27.

Sink H., Rehm E. J., Richstone L., Bulls Y. M., and Goodman C. S. 2001. 'sidestep encodes a target-derived attractant essential for motor axon guidance in *Drosophila*', *Cell*, 105: 57-67.

Stathopoulos A., Tam B., Ronshaugen M., Frasch M., and Levine M. 2004. '*pyramus* and *thisbe*: FGF genes that pattern the mesoderm of *Drosophila* embryos', *Genes Dev.*, 18: 687-99.

Stepanik V., Dunipace L., Bae Y. K., Macabenta F., Sun J., Trisnadi N., and Stathopoulos A. 2016. 'The migrations of *Drosophila* muscle founders and primordial germ cells are interdependent', *Dev.*, 143: 3206-15.

Stramer B., Moreira S., Millard T., Evans I., Huang C. Y., Sabet O., Milner M., Dunn G., Martin P., and Wood W. 2010. 'Clasp-mediated microtubule bundling regulates persistent motility and contact repulsion in *Drosophila* macrophages *in vivo*', *J. Mol. Biol.*, 189: 681-9.

Stute C., Schimmelpfeng K., Renkawitz-Pohl R., Palmer R. H., and Holz A. 2004. 'Myoblast determination in the somatic and visceral mesoderm depends on Notch signalling as well as on milliways(mili(Alk)) as receptor for Jeb signalling', *Dev.*, 131: 743-54.

Sun J., Macabenta F., Akos Z., and Stathopoulos A. 2020. 'Collective migrations of *Drosophila* embryonic trunk and caudal mesoderm-derived muscle precursor cells', *Genet.*, 215: 297-322.

Tepass U., Fessler L. I., Aziz A., and Hartenstein V. 1994. 'Embryonic origin of hemocytes and their relationship to cell death in *Drosophila*', *Dev.*, 120: 1829-37.

Tulin S., and Stathopoulos A. 2010. 'Analysis of Thisbe and Pyramus functional domains reveals evidence for cleavage of *Drosophila* FGFs', *BMC Dev. Biol.*, 10: 83.

Urbano J. M., Domínguez-Giménez P., Estrada B., and Martín-Bermudo M. D. 2011. 'PS integrins and laminins: key regulators of cell migration during *Drosophila* embryogenesis', *PLoS One*, 6: e23893.

Urbano J. M., Torgler C. N., Molnar C., Tepass U., López-Varea A., Brown N. H., de Celis J. F., and Martín-Bermudo M. D. 2009. '*Drosophila* laminins act as key regulators of basement membrane assembly and morphogenesis', *Dev.*, 136: 4165-76.

Walhout A. J., Temple G. F., Brasch M. A., Hartley J. L., Lorson M. A., van den Heuvel S., and Vidal M. 2000. 'GATEWAY recombinational cloning: application to the cloning of large numbers of open reading frames or ORFeomes', *Methods Enzymol.*, 328: 575-92.

Wang C., and Liu H. 2022. 'Factors influencing degradation kinetics of mRNAs and half-lives of microRNAs, circRNAs, lncRNAs in blood in vitro using quantitative PCR', *Sci. Rep.*, 12: 7259.

Wehner B. M. 2020. 'Analyse von Exon-Trap-Linien der sidestep und beaten path Genfamilien in *Drosophila* melanogaster', Bachelor Thesis, Heinrich Heine Universtiy Duesseldorf.

Xu F., Zhang C., and Graves D. T. 2013. 'Abnormal cell responses and role of TNF-α in impaired diabetic wound healing', *Biomed Res. Int.*, 2013: 754802.

Yamada K. M., and Sixt M. 2019. 'Mechanisms of 3D cell migration', *Nat. Rev. Mol. Cell Biol.*, 20: 738-52.

Yoo J., Dombrovski M., Mirshahidi P., Nern A., LoCascio S. A., Zipursky S. L., and Kurmangaliyev Y. Z. 2023. 'Brain wiring determinants uncovered by integrating connectomes and transcriptomes', *Curr. Biol.*, 33: 3998-4005.e6.

Zaffran S., Küchler A., Lee H. H., and Frasch M. 2001. '*biniou* (FoxF), a central component in a regulatory network controlling visceral mesoderm development and midgut morphogenesis in *Drosophila*', *Genes Dev.*, 15: 2900-15.

Zirin J., Hu Y., Liu L., Yang-Zhou D., Colbeth R., Yan D., Ewen-Campen B., Tao R., Vogt E., VanNest S., Cavers C., Villalta C., Comjean A., Sun J., Wang X., Jia Y., Zhu R., Peng P., Yu J., Shen D., Qiu Y., Ayisi L., Ragoowansi H., Fenton E., Efrem S., Parks A., Saito K., Kondo S., Perkins L., Mohr S. E., Ni J., and Perrimon N. 2020. 'Large-scale transgenic *Drosophila* resource collections for loss- and gain-of-function studies', *Genet.*, 214: 755-67.

Index of Abbreviations

aa	amino acid
ADP	adenosine diphosphate
AFM	AlphaFold-Multimer
ATP	adenosine triphosphate
bap	*bagpipe*
beat	*beaten path*
bin	*biniou*
blow	*blow fuse*
BMP	bone morphogenetic protein
bnl	*branchless*
btl	*breathless*
°C	centigrade
Cas9	CRISPR-associated protein 9
cDNA	copy/complementary DNA
CIL	contact inhibition of locomotion
CNS	central nervous system
CRISPR	clustered regularly interspaced short palindromic repeats
CVM	caudal visceral mesoderm
CirVM	circular visceral muscle
DIG	digoxigenin
DMSO	dimethyl sulphoxide
DNA	deoxyribonucleic acid
dNTP	deoxyribonucleotide triphosphate
DTT	dithiothreitol
Duf/Kirre	Dumbfounded/Kin-of-irre
dUTP	deoxyuridine triphosphate
ECM	extracellular matrix
EDTA	ethylenediaminetetraacetic acid
EGFR	epidermal growth factor receptor
et al.	*et alii*, and other
Fas III	Fasciclin III
FC	founder cell

FCM	fusion-competent myoblast
FGF	fibroblast growth factor
FISH	fluorescence *in situ* hybridization
FN3	fibronectin type III domain
FRT	flippase recognition target
FuRMAS	fusion-restricted myogenic-adhesive structure
GFP	green fluorescent protein
GFSTF	EGFP-FlAsH-Strep-TEV-3xFlag
GPI-AP	glycosylphosphatidylinositol-anchored protein
gRNA	guidance RNA
h	hour
hid	*head involution defective*
His	Histone
HRP	horse radish peroxidase
htl	*heartless*
ICH	immunohistochemistry
IG	immunoglobulin domain
IgSF	immunoglobulin superfamily
ISH	*in sit*u hybridization
l	liter
kb	kilobase
L3	third instar larvae
LVM	longitudinal visceral muscle
LVMP	longitudinal visceral muscle precursor
M	molar
min	minute
MIMICs	minos mediated integration cassette
ml	milliliter
mRNA	messenger RNA
MSA	multiple sequence alignments
n	number
NDS	normal donkey serum
ng	nanogram
NGS	normal goat serum

nm	nanometer
n.s.	not significant
OE PCR	overlap extension polymerase chain reaction
PAM	protospacer adjacent motif
PBS	phosphate-buffered saline
PBT	phosphate-buffered saline with 0.1% tween 20
PCR	polymerase chain reaction
PGC	primordial germ cell
plDDT	local distance difference test
PMG	posterior midgut primordium
pTM	template modeling
PTX	phosphate-buffered saline with 0.1% triton X-100
PVR	PDGF/VEGF-related receptor
pyr	*pyramus*
RFP	red fluorescent protein
RNA	ribonucleic acid
RNase	ribonuclease
rols	*rolling pebbles*
rpm	rounds per minute
RT	room temperature
S2 cells	Schneider 2 cells
sec	second
SGP	somatic gonad precursor
side	*sidestep*
sna	*snail*
S.O.C	super optimal broth
TAE	Tris-acetate EDTA buffer
TBS	This-buffered saline
TBST	Tris-buffered saline with 0.1% triton X-100
TdT	terminal deoxynucleotidyl transferase
TE	Tris EDTA buffer
TEMED	tetramethylethylenediamine
tey	*teyrha-meyrha*
TM	transmembrane doman

TRiP-KO	Transgenic RNAi Project-Knockout
Tris	tris-(hydroxymethyl)amoniummethan
TSA	tyramide signal amplification
TUNEL	terminal deoxynucleotidyl transferase-mediated d-UTP nick end labeling
TVM	trunk visceral mesoderm
ths	*thisbe*
twi	*twist*
U	unites
UAS	upstream activating sequence
µl	microliter
wun	*wunen*

Index of Figures

Index of Tables

Eidesstattliche Versicherung

Ich versichere an Eides statt, dass die Dissertation von mir selbstständig und ohne unzulässige fremde Hilfe unter Beachtung der „Grundsätze zur Sicherung guter wissenschaftlicher Praxis an der Heinrich-Heine-Universität Düsseldorf“ erstellt worden ist.

Des Weiteren erkläre ich hiermit, dass die Dissertation bisher noch nicht an einer anderen Fakultät eingereicht worden ist und es somit noch keinen bisherigen Promotionsversuch gegeben hat.

Düsseldorf, den 2024

(Na Huang)

Acknowledgments

This thesis was only possible because of the abundant support, help, and love provided by many people, to whom I would like to acknowledge and extend my heartfelt gratitude.

My deepest appreciation goes first and foremost to Prof. Hermann Aberle. Thank you for supervising me through my academic journey, for always being available and present, and for being a constant source of inspiration. We had many great talks about experiments, and also mountains, trips, and cooking recipes. You have taught me so much more than research skills. I especially thank you for being so patient and careful going through my writing and for supporting my plans. Knowing I have your support means a lot to me, thank you.

I would like to thank Prof. Christine Rose. Six years ago, you offered me the chance to do the master's thesis in your lab and then agreed to be the second supervisor for my Ph.D. study. I am incredibly grateful for the kindness and wisdom you have shared with me. Many great thanks to Dr. Wolfgang Karl Kafitz, a dream supervisor and friend in every way, for cheering me on, proofreading my thesis, and all the warm wishes on each Spring Festival.

To all the members of our institute, this thesis would not have happened without you all. Thank you, Alina, Iris, and Eva, for your support and all the nice moments we had during the trips and lunch breaks. Thank my students Nina, Alice, Niklas, Antonia, Yakun, and Johanna. Thank you for helping me and sharing new perspectives with me. Extra special thanks to my former colleagues. Marcel, you can always energize us with sweets, the mooncakes you make are the best in the world. Christine, you know exactly how I feel and give me the nicest comfort. I also thank you for teaching me a lot when I was a beginner. Jaqueline, I can not count how much help I got from you. You inspire me in every aspect of my life and thank you so much for your time and effort in correcting my thesis, you saved all the "Scheider Medium".

Writing this thesis has been a challenging yet rewarding journey. I am extremely thankful to Yanfei, Jing, Sihan, and Kun for giving me emotional support, encouragement, and helpful advice. You know the best how to save me from the struggles and cheer me up.

My last tribute is to my family and friends. 2020 年初至今，我度过了迄今为止意义最为深刻的人生五年。感谢爸妈给了我生命中最重要的两样东西，即爱与自由。除此之外，最重要的理解与陪伴来自于我的好友和丹年。我曾无数次想要放弃，却又无数次放弃了放弃。因为在你们身上我看到了那么多的美好，因为透过你们的眼睛，我看到了一个比我想象中更好的自己。人生海海，和你们的相遇是随机中的必然。我给予你们我最深切的祝福，愿你们平安，健康与幸福。最后，我还想感谢我自己，感谢自己在哭过后依然没有忘记微笑：）

Appendix